

# **Development of Electrochemical Biosensor for Ageing Biomarkers**

*by*

**Yanan Wu**

A thesis submitted for the degree of  
*Doctor of Philosophy*



School of Engineering

Newcastle University, UK

February 2022



## Abstract

The ageing population is now a serious problem around the world resulting in healthy ageing is the global goal to address this issue. To effectively control the incidence of ageing diseases caused by the high-level concentration of reactive oxygen species in the human body, the electrochemical biosensor is one of the most common ways for detection. However, the lack of easy operation, high selectivity, and quick response is still the challenge of the quantitative measurement for superoxide anion ( $O_2^{\cdot-}$ ) in the blood environment.

This study is aimed to develop an  $O_2^{\cdot-}$  biosensor that could fit in a hand-held device to provide quick and accurate results. The generation methods of  $O_2^{\cdot-}$  were first discussed due to their characteristics of poor stability. Compared with the chemical generation, the biological method showed a 10 % higher activity of enzymes and good stability of generated  $O_2^{\cdot-}$  for at least 5.5 hours.

This study was focused on two biosensors, the superoxide dismutase (SOD)-based biosensor due to the high selectivity for  $O_2^{\cdot-}$ , and a coupled SOD- horseradish peroxidase (HRP) biosensor for the high accuracy of the  $O_2^{\cdot-}$  quantitative measurements. The immobilization of the enzyme SOD and HRP were achieved by layer-by-layer adsorption and cross-linking technique respectively. The calibration curves for these two biosensors were generated and the effect of interferences was discussed subsequently. Results showed both biosensors had good linearity between the detection range of 0 to 0.5 mM  $O_2^{\cdot-}$ , with the sensitivity and limit of detection for the SOD-based biosensor as 67.13  $\mu A/(mM \cdot cm^2)$  and 5.6  $\mu M$  and for coupled SOD-HRP biosensor as 23.8  $\mu A/(mM \cdot cm^2)$  and 6  $\mu M$  respectively. Only glucose showed a positive bias on SOD-based biosensor but no effect on coupled SOD-HRP biosensor.

The  $O_2^{\cdot-}$  detection in blood samples was achieved by both two biosensors and the bias from glucose was considered in the calibration for the SOD-based biosensor. The blood sample was diluted at different multiples to demonstrate the accuracy of the results. Compared with the chemiluminescence method, the biosensors showed the advantages of a quick response in 100 seconds, high selectivity for  $O_2^{\cdot-}$  and successful  $O_2^{\cdot-}$  quantitative measurement of around 0.2 mM in volunteer blood samples.

## **Covid-19 Impact statement**

It is unfortunate that the serious outbreak of COVID-19 has affected everyone in the world to some degree in recent years. For me, covid-19 has had the greatest impact on the progress of my research.

First of all, the lab experiments were affected during and after the lab closure. The experiments had to stop because of the lab closure during COVID-19 lock down from early March to end of July 2020. Data gathering was seriously delayed because of the lock down and time-limited access since school reopen.

Also, due to the half-year lock down, the prepared enzymes could not be used anymore which caused additional delays. New batch of the enzymes need to be purchased and there were large delays on delivery of these enzymes after the school reopened. Besides, new sensors need to be prepared and fabricated.

Additionally, limited access to collaborating institutions was also a large effect on my research. During COVID-19, face-to-face contact becomes impossible making it extremely difficult to obtain blood samples. The use of instruments in Medical School is restricted by limited access control. Unfortunately not much work can be done for the validity of biosensors due to this limited access.

## Acknowledgement

First of all, I would like to express my sincere gratitude to my supervisors, Dr. Mohamed Mamlouk and Prof. Eileen Hao Yu, for their consistent support, guidance and encouragement at every stage of the research project. I would like to thank them for constructive criticism of the paper manuscripts, reports and thesis. Throughout my Ph.D. study, I have met so many challenges and difficulties, and they are the persons who can help me to solve those problems.

Secondly, I would like to thank Newcastle University for the academic and student services supports, especially my research group (based in Merz Court, C318 and Bedson, G10). I gratefully acknowledge all CEAM family; technicians, administrative staff and academic staff especially those who had to deal with me: Mr. Paul Sterling for the safe storage of the enzymes I purchased; Mr. Neville Dickman for the helping with the lab issues and mechanical checking; and Mr. James Rose for his help in the mechanical lab.

Thirdly, I would like to express my gratitude and appreciation to Professor Mack Birch-Machin, Profassor Georg Lietz, Dr. Amy Bowman and Ms. Gewei Zhu from the Faculty of Medical Sciences, for their kindly providing blood samples and the chemiluminescence facilities and detection techniques. All the blood sample tests were finished with their help.

Fourthly, I am deeply grateful to Professor Michael Catt, Dr. Samet Şahin, Dr. Hang Xiang and Dr. Da Li for bringing me academic help for the operation of potentiostat and the discussion in electrochemical analysis. I would also like to thank Dr. Yucheng Wang for the 3D printing and cutting of my designed enzyme-fabrication box. They gave me many academic supports and valuable input in my Ph.D. study.

Finally, I would like to thank everyone who has inspired me to do a Ph.D. abroad. They are the ones who made my Ph.D. life memorable forever.

## Table of Contents

Abstract .....	i
Covid-19 Impact statement .....	ii
Acknowledgement .....	iii
List of Figures .....	ix
List of tables.....	xvi
Symbols and abbreviations .....	xx
Symbols.....	xx
Abbreviations .....	xxii
Chapter 1    Introduction.....	1
1.1    Background .....	1
1.2    Overview of the reactive oxygen species (ROS).....	3
1.3    Overview of the biosensors .....	5
1.4    Aims and objectives .....	8
1.4.1    Aim.....	8
1.4.2    Objectives.....	8
1.5    Structure of thesis .....	9
Chapter 2    Literature review .....	10
2.1    Detection techniques used for superoxide detection .....	10
2.2    Enzymes used for superoxide detection .....	11
2.2.1    Cytochrome c .....	12
2.2.2    Superoxide dismutase .....	14

2.2.3	Horseradish peroxidase combined with superoxide dismutase .....	19
2.3	Enzyme immobilizing methods .....	22
2.3.1	Overview of immobilized enzymes .....	22
2.3.2	Enzyme immobilization for SOD .....	25
2.3.3	Enzyme immobilization for HRP .....	27
2.4	Review of methods for analysis .....	30
2.4.1	Ultraviolet-visible spectroscopy .....	30
2.4.2	Electrochemical characterization .....	32
2.4.3	Chemiluminescence methods .....	38
Chapter 3	Methodology .....	41
3.1	Experimental preparation .....	41
3.1.1	Solution preparation .....	41
3.1.2	Modification of carbon nanotube by acid cutting .....	42
3.2	Enzyme-based biosensor fabrication .....	43
3.2.1	Layer-by-layer immobilization for SOD and XOD .....	43
3.2.2	Cross-linking immobilization for HRP .....	45
3.3	Biosensor set-up and electrochemical measurement .....	46
3.3.1	Biosensor set-up .....	46
3.3.2	Electrochemical measurement .....	49
3.4	Calculations for the calibrations of superoxide .....	50
Chapter 4	Superoxide generation .....	52
4.1	Introduction .....	52

4.2	Experimental .....	55
4.2.1	Materials.....	55
4.2.2	The method of superoxide preparation .....	56
4.2.3	Ultraviolet-visible spectroscopy .....	56
4.2.4	Electrochemical measurements.....	57
4.3	Results and discussions .....	58
4.3.1	The determination of control variable for chemical superoxide preparation.....	58
4.3.2	The pH effect on SOD enzyme activity .....	59
4.3.3	The stability of different superoxide preparations .....	62
4.4	Conclusions .....	64
Chapter 5	Development of the electrochemical biosensor based on oxidation reaction of hydrogen peroxide.....	65
5.1	Introduction .....	65
5.2	Experimental .....	68
5.2.1	Materials and Equipment Used .....	68
5.2.2	Layer-by-layer enzyme fabrication on SPE .....	69
5.2.3	Electrochemical Measurements .....	70
5.3	Results and discussions .....	70
5.3.1	Performance of SOD towards H <sub>2</sub> O <sub>2</sub> and superoxide detection.....	70
5.3.2	Comparison for four systems of biosensor for H <sub>2</sub> O <sub>2</sub> detection.....	74
5.3.3	Calibration of the biosensor based on the oxidation reaction .....	79
5.3.4	Interference detection.....	82

5.4	Conclusions.....	86
Chapter 6 Development of the electrochemical biosensor based on reduction reaction of hydrogen peroxide .....		
6.1	Introduction.....	88
6.2	Experimental .....	92
6.2.1	Materials .....	92
6.2.2	The fabrication of the biosensor .....	92
6.2.3	The design of the enzyme-fabrication box for duo-SPE .....	94
6.2.4	Electrochemical measurements .....	95
6.3	Results and discussions.....	96
6.3.1	Performance of HRP for H <sub>2</sub> O <sub>2</sub> detection.....	96
6.3.2	Fabrication of the superoxide biosensors .....	100
6.3.3	Calibration of the biosensor based on the reduction reaction.....	104
6.3.4	Interference tests.....	106
6.4	Conclusions.....	107
Chapter 7 Application of biosensor in blood tests .....		
7.1	Introduction.....	108
7.2	Experimental .....	109
7.2.1	Chemiluminescence spectroscopy .....	109
7.2.2	Electrochemical measurements .....	110
7.3	Results and discussions.....	111
7.3.1	The calibration of chemiluminescence for superoxide detection .....	111

7.3.2	The blood sample tests by chemiluminescence .....	114
7.3.3	The blood sample tests by electrochemical biosensor .....	115
7.4	Conclusions .....	118
Chapter 8	Conclusion and recommendations for future work.....	119
8.1	Conclusion.....	119
8.2	Recommendations for future work.....	121
8.2.1	Biosensor optimisation and refinement.....	121
8.2.2	Biomimic materials instead of enzymes .....	122
8.2.3	Materials for Electrode Fabrication .....	123
8.2.4	“Superoxide anion + hydrogen peroxide” detection.....	124
Appendix	.....	125
Appendix A	.....	125
Appendix B	.....	126
Appendix C	.....	133
Appendix D	.....	136
References	.....	141

## List of Figures

Figure 1.1 Life expectancy and disability-free life expectancy at birth and at 65, England, 2001 to 2019. (Summary   State of Ageing in 2020, 2022).....	2
Figure 1.2 Electron structures of common reactive oxygen species. (Yogranjan et al. 2017)...	3
Figure 1.3 The conversion of ROS in the self-control system via enzymes (Racila et al. 2009). .....	4
Figure 1.4 Schematic diagram of typical biosensors consisting of bioreceptor, transducer and electronic system and the types of bioreceptor and transducer (Meskher et al. 2023).....	6
Figure 1.5 Types of biosensors (Vargas-Bernal et al. 2012).....	7
Figure 2.1 The principle of (a) direct detection and (b) enzyme-catalysed detection of superoxide.....	11
Figure 2.2 (a) The structure of Cyt. c enzyme and heme (Manickam et al. 2017). (b) The principle of Cyt. c-based detection of superoxide. ....	13
Figure 2.3 (a) The principle of SOD-based catalytic dismutation of superoxide (Younus 2018). (b) The structure of SOD enzyme (Tainer et al. 1983).....	15
Figure 2.4 The mechanism of $O_2^{\cdot-}$ catalysed by SOD (a) the reduction reaction (b) the oxidation reaction (Tian et al. 2004).....	16
Figure 2.5 (a) The principle of the SOD-based biosensor using a surface-confined mediator for superoxide determination. The experiment setup for (b) the batch cell and (c) the flow cell. (Endo et al. 2002) .....	18
Figure 2.6 The structure of HRP which contains heme as its active site (Veitch 2004). .....	19
Figure 2.7 Scheme of the coupled reaction system (Pastor et al. 2004).....	21
Figure 2.8 The reaction intermediates formed from HRP in the presence of excessive $H_2O_2$ . (Vlasits et al. 2010).....	22
Figure 2.9 Some of the commonly used enzyme immobilization methods (Homaei et al. 2013). .....	24

Figure 2.10 Schematic representation of SOD immobilization on PDADMAC-functionalized TNS. TNS: titania nanosheets, PDADMAC: poly(diallyldimethylammonium chloride) polyelectrolyte (Rouster et al. 2018).....	25
Figure 2.11 Schematic representation of SOD biosensor based on PEDOT and CNT. CNT: carbon nanotubes, PEDOT: poly(3,4-ethylenedioxythiophene). (Braik et al. 2016).....	26
Figure 2.12 Schematic representation of SOD/CAT couple immobilization based on covalent bond and electrostatic force respectively. CAT: catalase. (Mahlicli et al. 2015) .....	27
Figure 2.13 Schematic diagram of immobilization of HRP on GO@Fe <sub>3</sub> O <sub>4</sub> @6arm-PEG-NH <sub>2</sub> . (Rong et al. 2019).....	28
Figure 2.14 Schematic diagram of cut single-walled carbon nanotube electrode preparation. PBSE: 1-Pyrenebutyric acid N-hydroxysuccinimide ester, SPE: screen-printed electrodes. (Şahin 2020).....	29
Figure 2.15 Schematic diagram of MIP/P(β-CD)/GCE (biosensor) preparation. GCE: glassy carbon electrode, MIP: molecularly imprinted polymers, P(β-CD): poly beta-cyclodextrin. (Sardaremelli et al. 2021).....	30
Figure 2.16 Schematic diagram of UV-vis spectrophotometer (Mohanta 2017).....	31
Figure 2.17 Schematic diagram of the principle of electrochemical biosensor .....	32
Figure 2.18 (a) CV potential sweep waveform (Bard and Faulkner 1983) and (b) typical resulting cyclic voltammogram (Zhang et al. 2013).....	34
Figure 2.19 Schematic of pulse voltammetry. Applied waveform for (a) NPV, (b) DPV and (c) SWV; typical voltammogram for (d) NPV, (e) DPV and (f) SWV. Recreated from literature (Deffo et al. 2023, Simões and Xavier 2017, Venton and DiScenza 2020).....	35
Figure 2.20 (a) Waveform for single-step experiment; (b) typical resulting current flow vs. time. (Bard and Faulkner 1983) .....	37
Figure 2.21 Schematic diagram of the principle and category of luminescence (Shimadzu, 2022). .....	39
Figure 2.22 The chemiluminescence reaction of luminol (Hayashi et al. 2019). .....	39

Figure 3.1 (a) Schematic reactions and the layer-by-layer structure on the working electrode of SPEs (left) and the steps of the layer-by-layer self-assembly for the biosensor (right); (b) The SEM of surface of SPE (Şahin 2020). .....	44
Figure 4.1 (a) The principle of the chromogenic assay for superoxide detection. (b) The structure of the dye (WST-1).....	55
Figure 4.2 The spectrometer-based absorbance microplate reader used for the chromogenic assay. ....	56
Figure 4.3 The absorption spectrum of WST-1 formazan (from Product Information of SOD Assay Kit).....	57
Figure 4.4 The change of concentration of dissolved oxygen with the time of air bubbling. (b) CA of the alkaline solution for superoxide preparation (0 or 5 mM Na <sub>2</sub> S <sub>2</sub> O <sub>4</sub> ) at 1.64 V for 100 seconds in the presence and absence of 10-min air bubbling.....	59
Figure 4.5 (a) Absorbance for the solutions with different pH in the presence and absence of SOD enzyme. (b) The calculated superoxide concentration and SOD activity in solutions with different pH.....	62
Figure 4.6 The concentration changes of superoxide anion prepared from different generations in 5.5 hours. Error bars are the sample standard deviation of measurements from repetitions (n = 3).....	64
Figure 5.1 The structure of the four systems for the biosensor. ....	70
Figure 5.2 Voltammogram for the electrochemical performance of each layer immobilized by layer-by-layer enzyme self-assembly technique.....	71
Figure 5.3 CV scans of the fully enzyme-immobilised C-SPE (containing both SOD and XOD) in PBS (pH = 7.4) with 0 mM and 0.5 mM H <sub>2</sub> O <sub>2</sub> . ....	73
Figure 5.4 The calibration curve for H <sub>2</sub> O <sub>2</sub> detection of the biosensor with the fully enzyme-immobilised (both SOD and XOD) C-SPE (surface area of working electrode: 0.126 cm <sup>2</sup> )...	74
Figure 5.5 CV scans of four different systems of the biosensor (left: C-SPE/enzymes and CPC-SPE/enzymes; right: C-SPE/SWCNT/enzymes and CPC-SPE/SWCNT/enzymes) with the full enzyme immobilization (including both SOD and XOD). ....	75

Figure 5.6 The calibration curve for H <sub>2</sub> O <sub>2</sub> detection of the four different systems of the biosensor with the fully enzyme-immobilised (both SOD and XOD).....	77
Figure 5.7 The calibration curve for superoxide detection of the three different systems of the biosensor with the fully enzyme-immobilised (both SOD and XOD).....	78
Figure 5.8 The linear relationship between the concentration of xanthine (0.01 to 0.5 mM) and the calculated H <sub>2</sub> O <sub>2</sub> concentration (from Figure 5.6) based on the same charge transfer (i.e. the current response in Figure 5.7). .....	79
Figure 5.9 (a) The calibration curve for H <sub>2</sub> O <sub>2</sub> detection of the biosensor with the SOD-only and full-enzyme (SOD and XOD) immobilised on SWCNT-coated C-SPE; (b) The relationship between the detected current and the calibrated current. ....	80
Figure 5.10 The overall calibration curve for the developed SOD-based biosensor for superoxide. ....	82
Figure 5.11 The interference tests for H <sub>2</sub> O <sub>2</sub> detection of the biosensor with the SOD-immobilised SWCNT-coated C-SPE. ....	83
Figure 5.12 The current response of the biosensor with the SOD-immobilised SWCNT-coated C-SPE for H <sub>2</sub> O <sub>2</sub> detection against the potential interferences (a) AA and (b) BSA with a large concentration range. ....	84
Figure 5.13 The current response of the biosensor with the SOD-immobilised SWCNT-coated C-SPE for (a) H <sub>2</sub> O <sub>2</sub> detection against glucose as the interference with a large concentration range and (b) oxidation detection by changing glucose concentration in the solution with and without H <sub>2</sub> O <sub>2</sub> . ....	85
Figure 6.1 Scheme of the normal catalytic cycle for HRP enzyme in the H <sub>2</sub> O <sub>2</sub> reduction reaction. ....	90
Figure 6.2 The structure of the biosensor using C-SPE with both SOD and HRP enzymes immobilized on SWCNT coated WE (XOD & SOD/ HRP/ SWCNT/ C-SPE). ....	93
Figure 6.3 The structure of the biosensor using duo-SPE with both SOD and HRP enzymes immobilized on SWCNT coated WEs. ....	94
Figure 6.4 (a)The set-up for the enzyme-fabrication box; (b) the detailed structure of the lid	

which contains “pig nose”; (c) the assembled enzyme-fabrication box.....	95
Figure 6.5 (a) & (b) Experimental set-up for electrochemical experiments; (c) the assembled cell for the electrochemical analysis.....	96
Figure 6.6 Voltammogram for the electrochemical performance of each layer immobilised by cross-linking technique: (a) SWCNT coated C-SPE; (b) PBSE / SWCNT / C-SPE; (c) HRP / PBSE / SWCNT / C-SPE. Tested in PBS (pH = 7.4) in the presence and absence of 1 mM H <sub>2</sub> O <sub>2</sub> . Where, 0 and 1 represent the electrolyte without and with 1 mM H <sub>2</sub> O <sub>2</sub> respectively. Scan rate: 50 mV/s. ....	97
Figure 6.7 Voltammogram for the electrochemical performance of HRP-immobilised biosensor tested in PBS (pH = 7.4) which containing increasing concentration of H <sub>2</sub> O <sub>2</sub> (0, 0.1, 0.2, 0.3, 0.4, 0.5 and 1 mM). Scan rate: 5 mV/s.....	99
Figure 6.8 The calibration curve for H <sub>2</sub> O <sub>2</sub> reduction of the HRP-immobilized C-SPE (surface area of working electrode: 0.126 cm <sup>2</sup> ).....	100
Figure 6.9 (a) The electrochemical performance for the biosensor using direct immobilization of three enzymes (HRP, SOD and XOD). (b) The enlarge vision of the current response for superoxide detection. ....	102
Figure 6.10 The electrochemical performance for the biosensor on enzyme-immobilized duo-SPE (containing all three enzymes: HRP, SOD and XOD). ....	103
Figure 6.11 The linear relationship between the concentration of xanthine (0.01 to 0.5 mM) and the calculated H <sub>2</sub> O <sub>2</sub> concentration based on the same charge transfer (i.e. the current response in Figure 6.10). ....	104
Figure 6.12 The overall calibration curve for the superoxide biosensor (enzyme-immobilized duo-SPE, the surface area of the working electrode: 0.059 cm <sup>2</sup> , SWCNT loading: 0.15 mg/cm <sup>2</sup> ). ....	105
Figure 6.13 The current response of the biosensor with the SOD & HRP-immobilised duo-SPE for H <sub>2</sub> O <sub>2</sub> detection against (a) glucose, (b) uric acid, (c) ascorbic acid and (d) bovine serum albumin as the interference.....	106
Figure 7.1 The equipment used for chemiluminescence: Tecan infinite <sup>®</sup> 200 multifunctional	

microplate reader.....	110
Figure 7.2 Results of chemiluminescence technique for superoxide detection with different concentration of xanthine from 0.05 mM to 0.5 mM in buffer. SO: superoxide produced from xanthine in the presence of xanthine oxidase.....	112
Figure 7.3 Results of chemiluminescence technique for superoxide detection with various high concentration level in buffer. SO: superoxide produced from xanthine in the presence of xanthine oxidase.....	112
Figure 7.4 Calibration curve for high concentration detection of superoxide. ....	113
Figure 7.5 Results of chemiluminescence technique for superoxide detection in blood samples diluted with blood buffer.....	114
Figure 7.6 Results of the blood test for superoxide detection by the developed SOD-based biosensor .....	115
Figure 7.7 Results of the blood test for superoxide detection by the developed coupled SOD-HRP biosensor.....	116
Figure 8.1 Schematic diagram of (a) RGO-Pt modified GCE for oxygen reduction (Zhang et al. 2014) and (b) dumbbell-like PtPd-Fe <sub>3</sub> O <sub>4</sub> nanoparticles for enhanced electrochemical detection of H <sub>2</sub> O <sub>2</sub> (Sun et al. 2012). Where RGO is reduced graphene oxide and GCE is the glassy carbon electrode. ....	123
Figure 8.2 Schematic diagram of the structure of graphene-multi-walled CNTs for oxygen reduction by laccase (Lalaoui et al. 2015). ....	124
Figure S1. 1 The calibration curve for absorbance changes with various concentrations of superoxide (0, 0.1, 0.5, 1, 5, 10, 15, 20 mM). ....	125
Figure S2. 1 The amperometry diagram for H <sub>2</sub> O <sub>2</sub> detection of the XOD/ PDDA/ SOD/ PDDA/ C-SPE at 0.6V vs Ag/Ag <sup>+</sup> (~ 0.074 V vs SHE) at 100 s. ....	126

Figure S2. 2 The electrochemical responses for different detection time in different concentration of  $H_2O_2$  and xanthine solutions on XOD & SOD/ PDDA/ SWCNT/ C-SPE by CA at 0.6V vs  $Ag/Ag^+$  at 100 s..... 127

## List of tables

Table 2.1 The categories of enzyme immobilization methods and their advantages and disadvantages .....	24
Table 4.1 The components and the adding order (from top to bottom) for pH effect on SOD activity by UV at 37 °C (Unit: $\mu\text{L}$ ; where, O and S present the generated superoxide without and with SOD enzyme respectively).....	60
Table 4.2 The components and the adding order (from top to bottom) for the stability of the prepared superoxide by UV .....	63
Table 6.1 The isoelectric point and charge carried by enzymes in solution. ....	101
Table S1. 1 The concentration changes of dissolved oxygen (DO) in solution with air bubbling in 30 minutes.....	125
Table S1. 2 The data of absorbance, calibrated superoxide concentration and calculated SOD activity in superoxide chemical-generation solutions with different pH in the absence and presence of SOD enzyme. ....	125
Table S1. 3 The superoxide concentration changes with time by different preparation methods in different pH.....	125
Table S2. 1 The data for three repeats of the current responses with various $\text{H}_2\text{O}_2$ concentrations on XOD/ PDDA/ SOD/ PDDA/ C-SPE by CA at 0.6V vs Ag/Ag <sup>+</sup> at 100 s.....	126
Table S2. 2 The data for three repeats of the current responses with various $\text{H}_2\text{O}_2$ concentrations on XOD & SOD/ PDDA/ CPC-SPE by CA at 0.6V vs Ag/Ag <sup>+</sup> at 100 s. ....	127
Table S2. 3 The data for three repeats of the current responses with various $\text{H}_2\text{O}_2$ concentrations on XOD & SOD/ PDDA/ SWCNT/ C-SPE by CA at 0.6V vs Ag/Ag <sup>+</sup> at 100 s. ...	127
Table S2. 4 The data for three repeats of the current responses with various $\text{H}_2\text{O}_2$ concentrations on XOD & SOD/ PDDA/ SWCNT/ CPC-SPE by CA at 0.6V vs Ag/Ag <sup>+</sup> at 100 s.	128

Table S2. 5 The data for three repeats of the current responses with various xanthine concentrations on XOD & SOD/ PDDA/ CPC-SPE by CA at 0.6V vs Ag/Ag <sup>+</sup> at 100 s.....	128
Table S2. 6 The data for three repeats of the current responses with various xanthine concentrations on XOD & SOD/ PDDA/ SWCNT/ C-SPE by CA at 0.6V vs Ag/Ag <sup>+</sup> at 100 s.....	129
Table S2. 7 The data for three repeats of the current responses with various xanthine concentrations on XOD & SOD/ PDDA/ SWCNT/ CPC-SPE by CA at 0.6V vs Ag/Ag <sup>+</sup> at 100 s.	129
Table S2. 8 The data for the concentration of H <sub>2</sub> O <sub>2</sub> calculated from the current detected with various concentrations of xanthine based on the current-concentration(H <sub>2</sub> O <sub>2</sub> ) curve for SOD-based biosensor.....	129
Table S2. 9 The data for three repeats of the current responses with various H <sub>2</sub> O <sub>2</sub> concentrations on SOD/ PDDA/ SWCNT/ C-SPE by CA at 0.6V vs Ag/Ag <sup>+</sup> at 100 s. ....	130
Table S2. 10 Summary of the current response changes of SOD/ PDDA/ SWCNT/ C-SPE and XOD & SOD/ PDDA/ SWCNT/ C-SPE with various H <sub>2</sub> O <sub>2</sub> concentrations by CA at 0.6V vs Ag/Ag <sup>+</sup> at 100 s. ....	131
Table S2. 11 The data for the calculated concentration of superoxide from current reading from SOD/ PDDA/ SWCNT/ C-SPE. ....	131
Table S2. 12 The data for current changes with different concentration of H <sub>2</sub> O <sub>2</sub> on SOD/ PDDA/ SWCNT/ C-SPE in the presence of additional interferences. ....	132
Table S2. 13 The data for current changes with different concentrations of H <sub>2</sub> O <sub>2</sub> on SOD/ PDDA/ SWCNT/ C-SPE in the presence of the additional various concentrations of interferences (ascorbic acid and bovine serum albumin). ....	132
Table S2. 14 The data for current responses with different concentrations of H <sub>2</sub> O <sub>2</sub> and additional glucose on SOD/ PDDA/ SWCNT/ C-SPE.....	132
Table S2. 15 The data for current responses with different concentrations of glucose on SOD/ PDDA/ SWCNT/ C-SPE in the absence and presence of 0.5 mM H <sub>2</sub> O <sub>2</sub> .....	133

Table S3. 1 The data for three repeats of the current responses with various H <sub>2</sub> O <sub>2</sub> concentrations on HRP/ PBSE/ SWCNT/ C-SPE by CA at 0.1V vs Ag/Ag <sup>+</sup> at 100 s. ....	133
Table S3. 2 The data for the current responses with various H <sub>2</sub> O <sub>2</sub> or xanthine concentrations on three enzymes-immobilized C-SPE by CA at 0.1V vs Ag/Ag <sup>+</sup> at 100 s (n = 3 repeats). ....	134
Table S3. 3 The data for the current responses with various H <sub>2</sub> O <sub>2</sub> or xanthine concentrations on three enzymes-immobilized duo-SPE by CA at 0.1V vs Ag/Ag <sup>+</sup> at 100 s (n = 3 repeats)..	134
Table S3. 4 The data for the calculated concentration of superoxide from the current reading for coupled SOD-HRP biosensor. ....	135
Table S3. 5 The data for three repeats of the current responses in the absence and presence of XOD with various H <sub>2</sub> O <sub>2</sub> concentrations on three enzymes-immobilized duo-SPE by CA at 0.1V vs Ag/Ag <sup>+</sup> at 100 s. ....	135
Table S3. 6 The data for current changes with different concentration of H <sub>2</sub> O <sub>2</sub> on three enzymes-immobilized duo-SPE by CA at 0.1V vs Ag/Ag <sup>+</sup> in the presence of additional interference.....	135
Table S4. 1 The fluorescence changes with time in solutions with different concentrations of superoxide, (SO: superoxide anion).....	136
Table S4. 2 The fluorescence changes with time in solutions with the different high-level concentrations of superoxide, (SO: superoxide anion). ....	137
Table S4. 3 The corrected fluorescence at detection time of 15 ~ 22 minutes with different concentrations of superoxide in solution. ....	138
Table S4. 4 The fluorescence changes with time in the blood which was diluted at different multiples for superoxide detection by chemiluminescence method. ....	138
Table S4. 5 The current responses of the blood at different dilution levels for superoxide detection by the developed SOD-based biosensor. ....	139
Table S4. 6 The current responses of the blood at different dilution levels for superoxide	

detection by coupled SOD-HRP biosensor. .... 140

## Symbols and abbreviations

### Symbols

$\varepsilon$	molar absorption coefficient
$\Delta E_p$	difference between peak anodic and cathodic potentials
A	the surface area of the working electrode
Ag	Silver
AgCl	silver chloride
c	the concentration of the substrates
CaCl <sub>2</sub>	calcium chloride
Cu	Copper
Cys	L-cysteine
Cyt. c	cytochrome c
d	the path length of the measuring beam
D <sub>0</sub>	diffusion coefficient
E <sup>0</sup>	standard electrode potential
E <sub>pa</sub>	peak anodic potential
E <sub>pc</sub>	peak cathodic potential
Fe	Iron
H <sub>2</sub> O <sub>2</sub>	hydrogen peroxide
H <sub>2</sub> SO <sub>4</sub>	sulfuric acid
HCl	hydrochloric acid
HNO <sub>3</sub>	nitric acid
HO <sub>2</sub> ·	hydroperoxyl

$I$	the intensity of incident light
$I_0$	the intensity of transmitted light
$i_{pa}$	peak anodic current
$i_{pc}$	peak cathodic current
$i(t)$	current detected at a certain time $t$
$K$	reaction equilibrium constant
$K_2HPO_4$	potassium phosphate dibasic
$KH_2PO_4$	potassium phosphate monobasic
$KO_2$	potassium superoxide
$M$	metal cofactors
$Mg$	manganese
$MgCl_2$	magnesium chloride
$MoS_2$	molybdenum disulfide
$n$	the number of electrons in the oxidation or reduction process
$NaCl$	sodium chloride
$NaO_2$	sodium superoxide
$NaOH$	sodium hydroxide
$NaNO_2$	sodium nitrite
$Na_2S_2O_4$	sodium dithionite
$Ni$	nickel
$NO$	nitric oxide
$O_2$	dioxygen
$O_2^-$	superoxide anion

$O_2^{\bullet 2-}$	peroxide dianion
$\cdot OH$	hydroxyl radicals
$ONOO^-$	peroxynitrite
PMA	phorbol 12-myristate 13-acetate
Pt	Platinum
$SO_3^{2-}$	sulfite ion
$S_2O_4^{2-}$	Dithionite
T	transmittance
$TiO_2$	titanium dioxide
Zn	Zinc

## Abbreviations

$\beta$ -CD	$\beta$ -Cyclodextrin
AA	ascorbic acid
ARE	alkaline reference electrode
AuNp	gold nanoparticles
BSA	bovine serum albumin
C-SPE	screen-printed carbon electrode
CA	chronoamperometry
CeNPs	cerium nanoparticles
CL	chemiluminescence
CNTs	carbon nanotubes
CP	cobalt-phthalocyanine
CPC-SPE	screen-printed cobalt-phthalocyanine/carbon electrode

CV	cyclic voltammetry
DMF	dimethylformamide
DMSO	dimethyl sulfoxide
DPV	differential pulse voltammetry
duo-SPE	dual screen-printed carbon electrode
ESR	electron spin resonance
GCE	glassy carbon working electrode
HPA	hypothalamic-pituitary axis
HRP	horseradish peroxidase
LoD	limit of detection
LSV	linear sweep voltammetry
NPV	normal pulse voltammetry
PBS	phosphate-buffered solution
PBSE	1-pyrenebutyric acid N-hydroxysuccinimide ester
PDADMAC or PDDA	poly(diallyldimethylammonium chloride)
PEDOT	poly(3,4-ethylenedioxythiophene)
PEG	polyethylene glycol
PVP	polyvinylpyrrolidone
RGO	reduced graphene oxide
RHE	Reversible Hydrogen Electrode
ROS	reactive oxygen species
SAM	self-assembled monolayer

SCE	saturated calomel electrode
SEM	scanning electron microscope
SHE	Standard Hydrogen Electrode
SNS	sympathetic nervous system
SOD	superoxide dismutase
SPEs	screen printed electrodes
SWCNT	single-wall carbon nanotube
SWV	square wave voltammetry
TNS	titania nanosheets
UA	uric acid
UV-Vis	ultraviolet–visible
XOD	xanthine oxidase
WE	working electrode

## Chapter 1 Introduction

The incidence of ageing diseases caused by the high-level concentration of reactive oxygen species, especially superoxide in the human body increased over years and reached its highest level nowadays, and the electrochemical biosensor, as an analytical device, is one of the most common ways to detect superoxide. In this chapter, reactive oxygen species, which are closely related to age-related diseases, were introduced in detail. The various biosensors were described in terms of composition, categories and advantages. Then aim and objectives were proposed based on the lack of research on the quantitative measurement of superoxide by electrochemical biosensors.

### 1.1 Background

The global population is entering an ageing stage. The number and the proportion of the elderly population in almost every country in the world are increasing. The ageing population may become one of the most important social trends in the 21st century (United Nations 2018). Almost all social areas are affected by it, including labour and financial markets, demand for goods and services such as housing, transportation and social security, family structure, and generation relationship.

According to the United Nations (2018), in 2017, the global population aged over 60 years is about 962 million, accounting for 13% of the global population and growing at a rate of around 3% every year. The share of the global population that is 65 years or older has increased significantly over the years from 6% in 1990 to 9% in 2019. It is expected to reach 16% by 2050, which means one in six of the population will be older than 65 years globally (CentreforAgeingBetter 2022). At present, Europe has the largest proportion of people aged 60 and above (25%). The number of elderly people in the world will reach 1.4 billion in 2030, 2.1 billion in 2050, and 3.1 billion in 2100.

Because it would make population balance difficult to recover and a population decline hard to avoid, the ageing population becomes a serious problem nowadays. As shown in Figure 1.1, life expectancy for both men and women at age 65 stopped improving and the disability-free life expectancy dropped by years from 2012, which is linked to various factors such as the mortality rates for stroke and cardiovascular disease (Health | The State of Ageing 2020 2021).

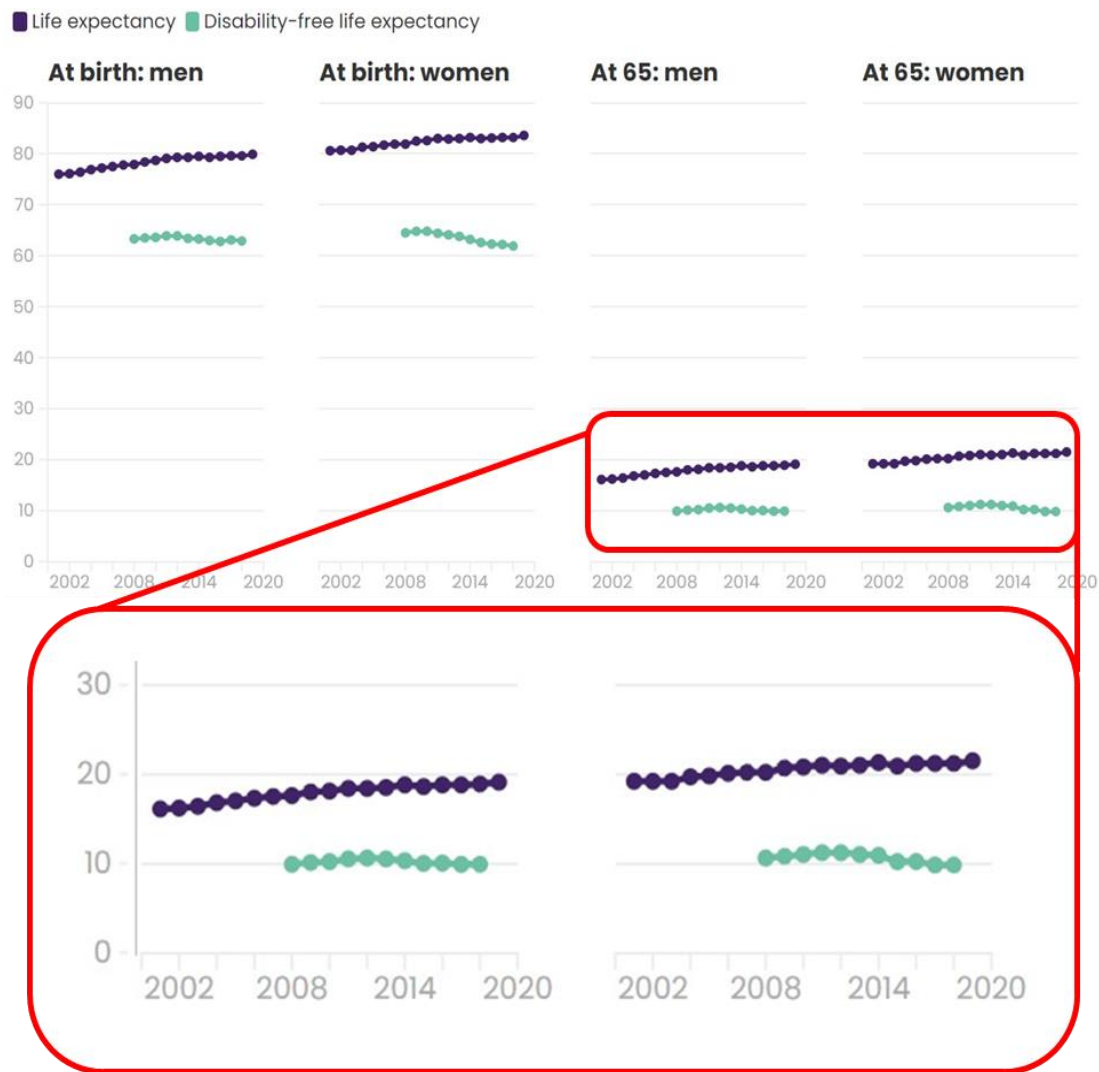


Figure 1.1 Life expectancy and disability-free life expectancy at birth and at 65, England, 2001 to 2019. (Summary | State of Ageing in 2020, 2022)

The United Nations proposed that healthy ageing be the global goal of ageing for solving this problem (Organization 2001). Healthy ageing refers to humans can still maintain a good condition in physical, psychological, intellectual, social, and economic aspects when they are old (Song et al. 2005). If a large proportion of the elderly in a country or region belongs to healthy ageing, the due role of the elderly can be fully played, and the negative impact of ageing is restricted or alleviated.

Therefore, the timely prevention of age-related diseases contributes to the maintenance of healthy ageing, and how to detect disease factors easily, quickly and efficiently is increasingly attracting the attention of the researchers. This can be achieved by establishing a handheld sensor that let seniors regularly finish the self-test at home.

## 1.2 Overview of the reactive oxygen species (ROS)

It is widely reported that the reactive oxygen species (ROS) is one of the essential balanced factors in the human body, which is related to more than 100 ageing diseases, such as cardiovascular diseases, diabetes mellitus, neurodegenerative diseases, stroke, etc (Organization 2012).

As the electron reduction product of the oxygen species in the human body, ROS has many species including superoxide anion ( $O_2^{\cdot-}$ , one-electron reduction products), hydrogen peroxide ( $H_2O_2$ , two-electron reduction products), hydroxyl radicals ( $\cdot OH$ , three electron reduction product) and nitric oxide (NO), etc. (Shah et al. 2001). The reactions of these ROS in an aqueous or vascular environment are extremely complicated, resulting in the complex components including the oxidation states of oxygen ( $(O_2)_n$  (dioxygen,  $O_2$ ,  $n=0$ ; superoxide ion,  $O_2^{\cdot-}$ ,  $n=-1$ ; and peroxide dianion,  $O_2^{\cdot 2-}$ ,  $n=-2$ ), other oxygen radicals (hydroxyl,  $OH\cdot$ ) and nonradical oxidizing agents ( $H_2O_2$ )(shown in Figure 1.2), etc. (Bayr 2005, Hayyan et al. 2016, Jie et al. 2022).

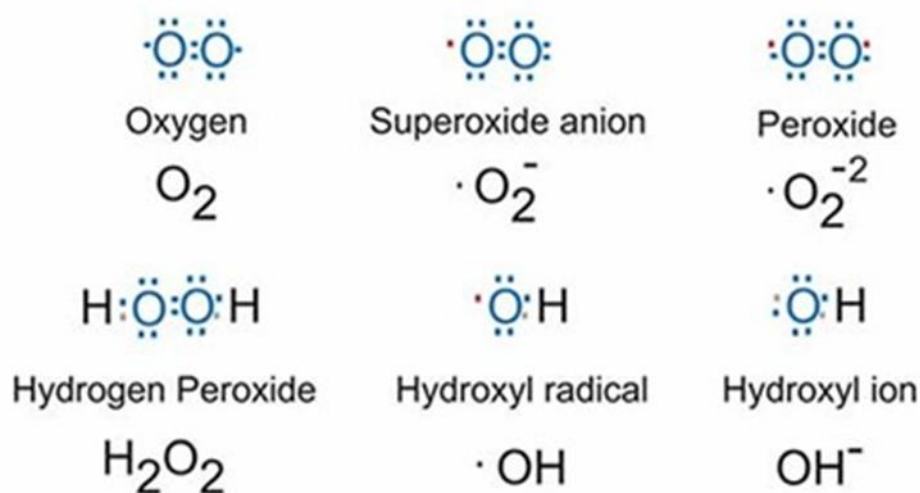


Figure 1.2 Electron structures of common reactive oxygen species. (Yogranjan et al. 2017)

There are many ways of ROS generation in the human body. In the baseline physiological state of the human organism, the main way is the side reactions of respiration of the mitochondria in cells, which is inevitable. The low concentration of ROS in the human body, normally below 1 mM, is the main medium for phagocytosis and killing by phagocytic cells, which is good for health. In this concentration, ROS could reach an equilibrium with the self-control system, as shown in Figure 1.3, to eliminate some ROS by enzymes, including superoxide dismutase (SOD), catalase, glutathione peroxidase and peroxidase.

## Formation and Elimination of Reactive Oxygen Species (ROS)

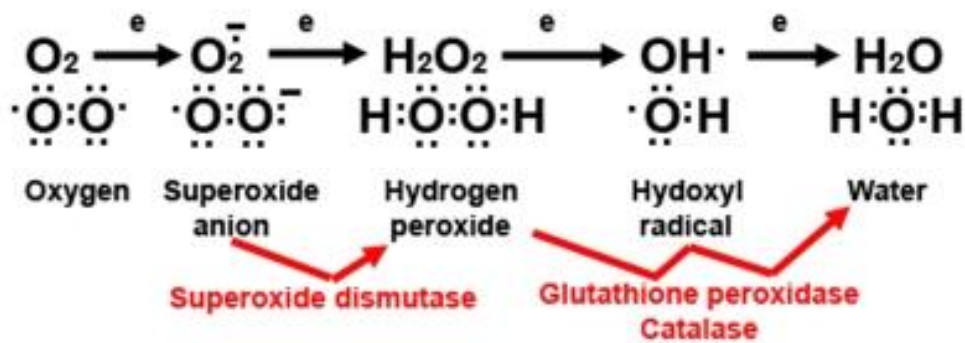


Figure 1.3 The conversion of ROS in the self-control system via enzymes (Racila et al. 2009).

ROS usually has a good effect on cell signalling and homeostasis, and the low concentration of ROS can promote the activation of transcription factors and cell proliferation and differentiation. However, it will destroy the cell structure if the concentration increases significantly. It is reported that medium and high concentrations of ROS induce cellular damage, apoptosis or even necrosis by cellular oxidative stress depending on severity and duration of exposure (Anne 2017, Held 2012). It is worth noting that the threshold concentration for excessive ROS accumulation can vary depending on several factors, including the type of ROS, the cell or tissue type, and the individual's antioxidant defence capacity. Only few reports reported the basal level of ROS concentration in human blood, e.g. superoxide anion in the order of 100s of  $\mu\text{M}$  and  $\text{H}_2\text{O}_2 \leq 10 \mu\text{M}$  (Gaikwad et al. 2021). Some studies have suggested that an increase in ROS levels greater than ten-fold above the basal levels can lead to oxidative stress and cellular damage (Theyagarajan and Kim 2023). Therefore, the daily monitoring of concentration of ROS in the human body would be one of the most simple and efficient ways to predict the formation of many ageing diseases.

Among the various species of ROS, hydrogen peroxide and superoxide anion are recognized as two major factors causing ageing diseases. Although  $\text{O}_2^{\cdot -}$  is not very stable, it has a longer react distance through the blood transmission because of its relatively long life as its half-life in hours, which results in obvious damage to the body (Yang 2013).  $\text{H}_2\text{O}_2$  is the most stable species so that it can cause larger damaged areas.

The detection of  $\text{H}_2\text{O}_2$  has been reported in numerous studies and is now well established, but the detection of superoxide anion is still not particularly effective due to the extremely low stability and concentration, especially the detections down to micromolar in the human body

(Emregul et al. 2013). Although many superoxide biosensors were described and established by various methods, the existing biosensor still lacks easy operation, high sensitivity, quantitative measurement, and quick response (Jie et al. 2022). Some of biosensors showed the sensitivity lower than  $1 \mu\text{A}/\text{cm}^2$  (Di et al. 2007, Ye et al. 2014), some of them required response time of 30 minutes or longer (Xu et al. 2007), other sensors were hard to be applied on handheld devices scale (Qin et al. 2015, Shu et al. 2021).

As one of the major species of ROS, the superoxide anion is produced in various biological systems as an intermediate in the massive reduction of molecular oxygen. The increase of  $\text{O}_2^{\cdot-}$  activity occurs in response to ischemia-reperfusion and hypoxia in traumatic brain injury, which could be associated with the etiology of cancer and progressive neurodegenerative diseases (Tian et al. 2006). The poor stability of  $\text{O}_2^{\cdot-}$  in aqueous solutions, especially acidic solutions, causes the lack of commercial samples with certain concentrations and difficulties in  $\text{O}_2^{\cdot-}$  electrochemical studies in aqueous environments.

Many methods for  $\text{O}_2^{\cdot-}$  generation were reported, including electrochemical reduction of oxygen, enzymatic methods, chemical generation from superoxide salts, electrochemical methods in strong alkaline solutions, photochemical photocatalytic methods,  $\text{O}_2^{\cdot-}$  generation at oxide surfaces and singlet oxygen one-electron reduction (Hayyan et al. 2016, Sheng et al. 2014). For the characteristics of easy operation, long-term stability, fast reaction and potential industrial application, some of the methods were discussed and compared in this project.

### **1.3 Overview of the biosensors**

Researchers found that the use of biomarker models could help predict the ageing process of a person and the risk of suffering elderly disease when they were getting older (Sebastiani et al. 2017). Recently, biomarkers are involved in the cardiovascular system, metabolic processes, inflammation, the activity between the hypothalamic-pituitary axis (HPA) and sympathetic nervous system (SNS), and visceral function (including kidney, lung and heart) (Ziech et al. 2010).

Biosensors are based on the detection of those biomarkers, and they are defined as analytical tool or system that contains immobilized biological materials, such as enzymes, antibodies, whole cells, organelles, or combinations, and binds to a suitable transducer, which converts biochemical signals into quantitative electrical signals (Li and Dai 2004). Due to their high sensitivity and selectivity, biosensors have great value in biomedicine, environmental

monitoring, food, medicine and military medicine and are being used for deep research and development (Ansari et al. 2010). Recently, the pharmaceutical industry has driven the continuous innovation of protein purification and biosensor technology and the development of nano-technology makes biosensors become a promising tool for the diagnosis and treatment of some diseases (Lu 2016).

Biosensors generally consist of two major components (as shown in Figure 1.4), one is the biomolecule recognition element, also called a bioreceptor, and the other is the signal converter, also called a transducer (Wu et al. 2004). Bioreceptors are biologically active substances, such as enzymes, antibodies, tissue sections, cells, organelles, cell membranes, nucleic acids, organic molecules, etc. (Grieshaber et al. 2008); and transducers include electrochemical electrodes, optical detection components, thermistors, field-effect transistors, piezoelectric quartz crystal and surface plasmon resonance devices. When the analyte is specifically combined with the molecular recognition element, the resulting complex, which is transformed into an electrical signal and an optical signal, can be output by the signal converter, to achieve the purpose of analysis and detection (Li and Dai 2004).

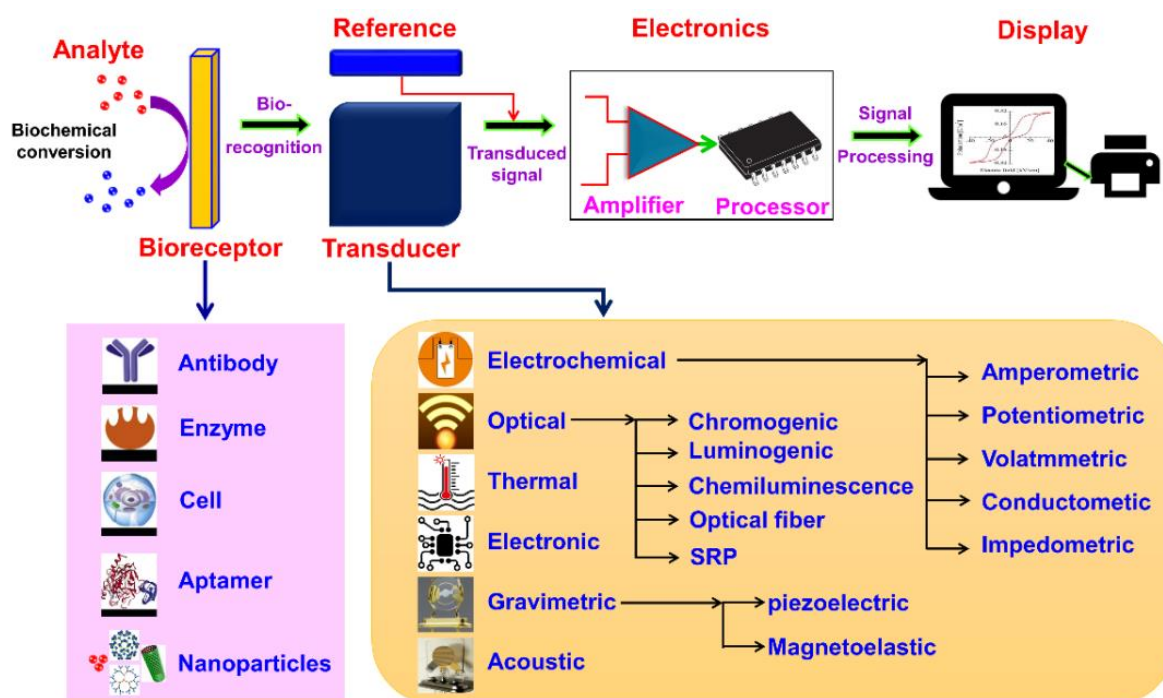


Figure 1.4 Schematic diagram of typical biosensors consisting of bioreceptor, transducer and electronic system and the types of bioreceptor and transducer (Meskher et al. 2023).

As shown in Figure 1.5, there are many species of biosensors, according to the different transducers, they can be classified as electrochemical biosensors, bioluminescent biosensors,

optical biosensors, thermistor biosensors and piezoelectric biosensors, etc. (Byrne et al. 2009).

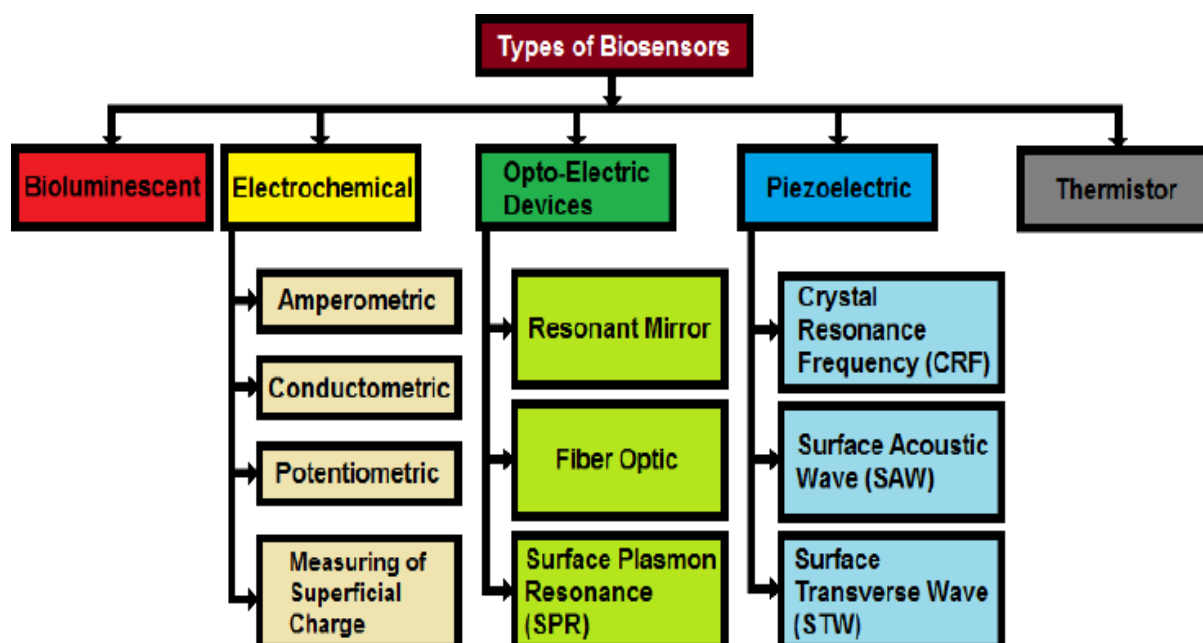


Figure 1.5 Types of biosensors (Vargas-Bernal et al. 2012)

In 1967, Updick and Hicks immobilized glucose oxidase on a hydrophobic membrane and combined it with an oxygen electrode to assemble the first enzyme electrode, a glucose electrode, for the detection of glucose in the serum (Sun et al. 2011). Since then, the enzymatic electrochemical biosensor has attracted the attention and extensive research of scientists from all fields in science and has been rapidly developed.

As a widely used tool of detection, enzymatic electrochemical biosensors have many advantages (AZoSensors.com, 2018):

- (1) Immobilized bioactive substances are used as catalysts, and valuable reagents can be used repeatedly, which overcomes the disadvantages of the high cost of enzymatic analysis and complicated chemical analysis.
- (2) Strong in specificity and high selectivity, responding only to specific substrates.
- (3) Fast analysis speed, and results can be obtained in several minutes.
- (4) High accuracy, sensitivity and good reproducibility.
- (5) Relatively simple operating system and easy to analyse automatically.
- (6) Low cost due to the continuous use, and long-term durability.

## (7) Simple electrode manufacturing

In addition, electrochemical biosensors also have other advantages, such as low energy consumption, easy to carry, no damage to the test sample, no influence from the colour of the solution and easy miniaturization (Mao et al. 2009). Therefore, using enzyme-immobilized electrochemical biosensors to detect ageing factors in the human body is one of the effective ways to predict and prevent ageing diseases, which would be a hot issue of ageing research.

### 1.4 Aims and objectives

#### 1.4.1 Aim

As mentioned in section 1.1, there is a desire to predict the impact of ROS on ageing related diseases through regular self-test at home without any pre-treatment of samples. Given the daily need of testing, this will not only save healthcare resources especially staff resources but also avoid delaying in testing and receiving the results.

The aim of the project is to establish a high-efficiency electrochemical biosensor that can achieve the quantitative measurement of superoxide concentration, that can be implemented in home operated handheld devices that helps patients to detect finger-prick blood samples at their homes. The investigation will focus on the development of enzyme immobilization on the electrode to improve the sensitivity, selectivity and accuracy of the biosensor.

#### 1.4.2 Objectives

(1) Different generation methods will be compared and discussed, to ensure that the superoxide anion is prepared in an environment suitable for high-efficiency electrochemical analysis, given the poor stability of superoxide in an aqueous solution.

(2) To assess the high-sensitivity towards superoxide of dismutase-based biosensor for the quantitative measurement of superoxide and generate a calibration curve that is bias-corrected to remove the effect of interference on the electrochemical signal.

(3) To reduce the interference of other species in blood on the electrochemical signal and minimization of the calibration bias of the sensor, the coupled-enzyme biosensor using both superoxide dismutase (SOD) and horseradish peroxidase (HRP) should be designed.

(4) Different immobilization methods will be investigated to assess the sensitivity of the

biosensor utilizing different enzymes and the structure of the enzyme-immobilized electrode will be optimized for the improvement of accuracy.

(5) To validate the developed biosensors for superoxide detection in human blood samples and calculate superoxide concentration based on the calibration curve.

## **1.5 Structure of thesis**

The serious situation of ageing population, reactive oxygen species which is the cause of the most ageing diseases and the various biosensors for the detections are introduced in Chapter 1. Chapter 2 includes the literature review of detection techniques, the use of enzymes, the enzyme immobilizing methods and the analysis methods for superoxide anions. The main methodology including experimental preparation, enzyme-based biosensor fabrication, biosensor set-up, electrochemical analysis and calculations are described in Chapter 3. The superoxide generations based on different methods are compared and discussed depending on the activity of the enzyme and stability of superoxide in Chapter 4. The SOD-based superoxide biosensor is established and the enzyme immobilization by using the lay-by-layer self-assembly method is introduced and improved with carbon nanotubes (CNTs) in Chapter 5, followed by the interference tests and bias correction of the calibration curve. Chapter 6 covers the electrochemical performance of biosensors with coupled SOD-HRP system, different enzyme immobilization methods are provided and the separation of two enzyme-catalyzed reactions is performed. The calibration curve for coupled SOD-HRP biosensor is generated subsequently. Chapter 7 shows the electrochemical behaviour of two biosensors in the detection of human blood samples, and detection based on chemiluminescence is described for comparison. The concentration of superoxide in blood samples is calculated based on the corrected calibration curve from Chapter 5 and Chapter 6. Chapter 8 summarises the main data and conclusion of this project, and suggests some further research directions based on the available data and findings in this project.

## Chapter 2 Literature review

In this chapter, different detection techniques used for superoxide detection were summarised. The challenges for the requirements of the commercial applications for these techniques were mentioned. The enzyme used for the superoxide biosensor was summarised systematically, including the structure, mechanism and applications. The benefit of immobilized enzymes and immobilizing methods were discussed and the challenges in the research area were addressed. The methods for analysis, including Ultraviolet-visible spectroscopy, electrochemical analysis and chemiluminescence were overviewed. Both the principle of these detecting methods and the data interpretation obtained from the recorder were mentioned.

### 2.1 Detection techniques used for superoxide detection

The incidence of aging diseases caused by the high-level concentration of reactive oxygen species (ROS) in the human body increased by years and reached its highest level nowadays, and the biosensor, as an analytical device, is one of the most common ways to detect ROS due to the advantages of fast detection, low cost and easy operation (Balamurugan et al. 2018, Nauseef 2014). Among all kinds of reactive oxygen species, the detection of H<sub>2</sub>O<sub>2</sub> and superoxide anion attract at present major attention of the researchers. Much research systematically demonstrated the detection of H<sub>2</sub>O<sub>2</sub> which is now well established, but the research of superoxide anion detection still requires to be explored and developed (Bayr 2005, Şahin 2020).

Many analytical detection techniques are available for superoxide detection, such as fluorescent probes, spectrophotometry, electron spin resonance (ESR), fluorescent proteins, chemiluminescent probes and electrochemical biosensors (Głód et al. 2000, Greenwald 2018, Münzel et al. 2002, Zhao et al. 2005). Yang et al. (2020) presented a developed spectrophotometric method for superoxide detection by using the ferric iron solution as the colour agent and hydroxylamine hydrochloride as a probe in a visible-light system and showed the detection range of 0 ~ 15 µM and the limit of detection of 0.8 µM. He et al. (2014) described a direct and chemically specific method to detect superoxide by using electron spin resonance via identifying the free radicals in biological environment and discussed the development of the technique by spin trapping and spin labelling to enhance the stability of free radicals. Warwar et al. (2011) provided an ESR imaging resonator by combining fluorescent probes and ESR to specifically detect superoxide in a plant root with a high reaction rate constant. Wang et al.

(2006) compared three techniques including cytochrome c spectrophotometric, hydroethidine fluorescence and lucigenin-enhanced chemiluminescence for superoxide detection in human embryonic kidney cells, and highlighted the higher sensitivity of chemiluminescence than the other two techniques.

However, for the requirements of the commercial applications, these methods have some obvious drawbacks: (a) requiring expensive equipment, complex pre-treatment and analysis procedure; (b) low selectivity, sensitivity and specificity; (c) the unstable intermediates resulting in the slow in reactions and complex products (Zhang et al. 2018). Thus, due to the advantage of simple pre-treatment processing, inexpensive instruments, fast analysis, high sensitivity, easy operation and quantitative detection, the electrochemical biosensor has been widely used as a quantitative monitoring method for superoxide detection (Balamurugan et al. 2018).

## 2.2 Enzymes used for superoxide detection

It is reported that the direct detection of the  $O_2 / O_2^{\cdot -}$  couple (Figure 2.1 (a)) was available due to the reversible electrochemical behaviour in various media at the potential of -1 V vs SCE (Hayyan et al. 2016). However, the results could easily be affected by many parameters, including humidity, electrolyte changing and the state of the electrodes. In addition, the application of direct detection in blood tests was also limited because of the poor selectivity (Tian et al. 2006). The problem could be solved by using the enzyme that specifically recognises superoxide anion. Figure 2.1 (b) showed the principle of enzyme on the selectivity of superoxide anion, which could specifically oxidase the superoxide to oxygen by self-reduction at the activate site of enzymes.

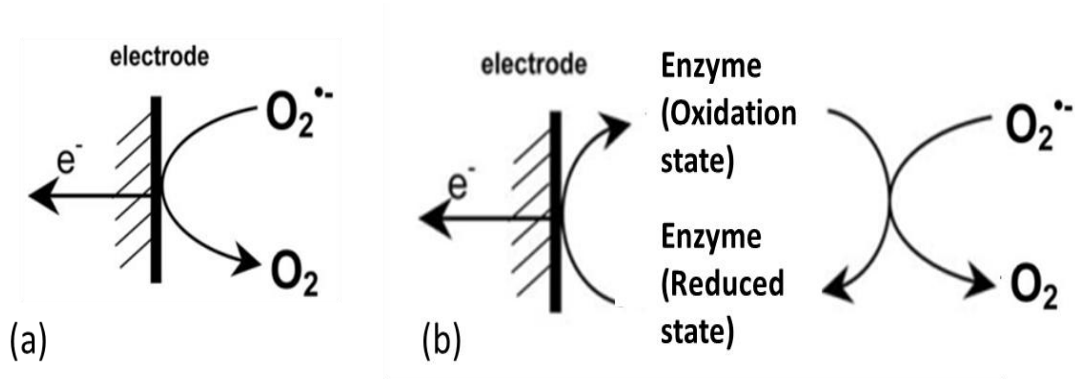


Figure 2.1 The principle of (a) direct detection and (b) enzyme-catalysed detection of superoxide.

Due to the property of specific recognition, enzymes play more and more important roles in biosensors. Enzymatic electrochemical biosensors are generally based on the catalytic action of enzymes on the generation of ions (Enomoto et al. 2013).

Several enzymes could be involved in the superoxide detection by electrochemical biosensors, such as hemin, galactose oxidase, tyrosinase, cytochrome c (Cyt. c) and superoxide dismutase (SOD) (Campanella et al. 1997, Chen et al. 2000, Xiaojun J Chen et al. 2008, Endo et al. 2002). Among all these enzymes, the study of cyt. c and SOD attracted attention because of the high selectivity and efficiency for the determination of superoxide (Tian et al. 2006).

### 2.2.1 *Cytochrome c*

The earlier studies often used Cyt. c to detect  $O_2^{\cdot-}$ . Cyt. c is a highly water-soluble protein and contains a protein-linked heme, as shown in Figure 2.2 (a), which could transmit electrons by the oxidation and reduction between the ferrous and ferric forms (Abel et al. 2010, Sanders et al. 2010). The principle of the Cyt. c-based superoxide biosensor is using the enzyme as the electron transfer mediator to oxidise superoxide anion to oxygen (shown in Figure 2.2 (b)). In this method, The  $O_2^{\cdot-}$  reduce Cyt. c while itself was oxidized to  $O_2$ ; at the same time, the reduced Cyt. c ( $Fe^{2+}$ ) is rapidly oxidized to an oxidized state ( $Fe^{3+}$ ) at a positive potential on the surface of the electrode. (Ho et al., 1995). As expected, the Cyt. c -based  $O_2^{\cdot-}$  sensor avoids the interference of ascorbic acid and uric acid and can detect  $O_2^{\cdot-}$  at low potential (Fleury et al., 2002).

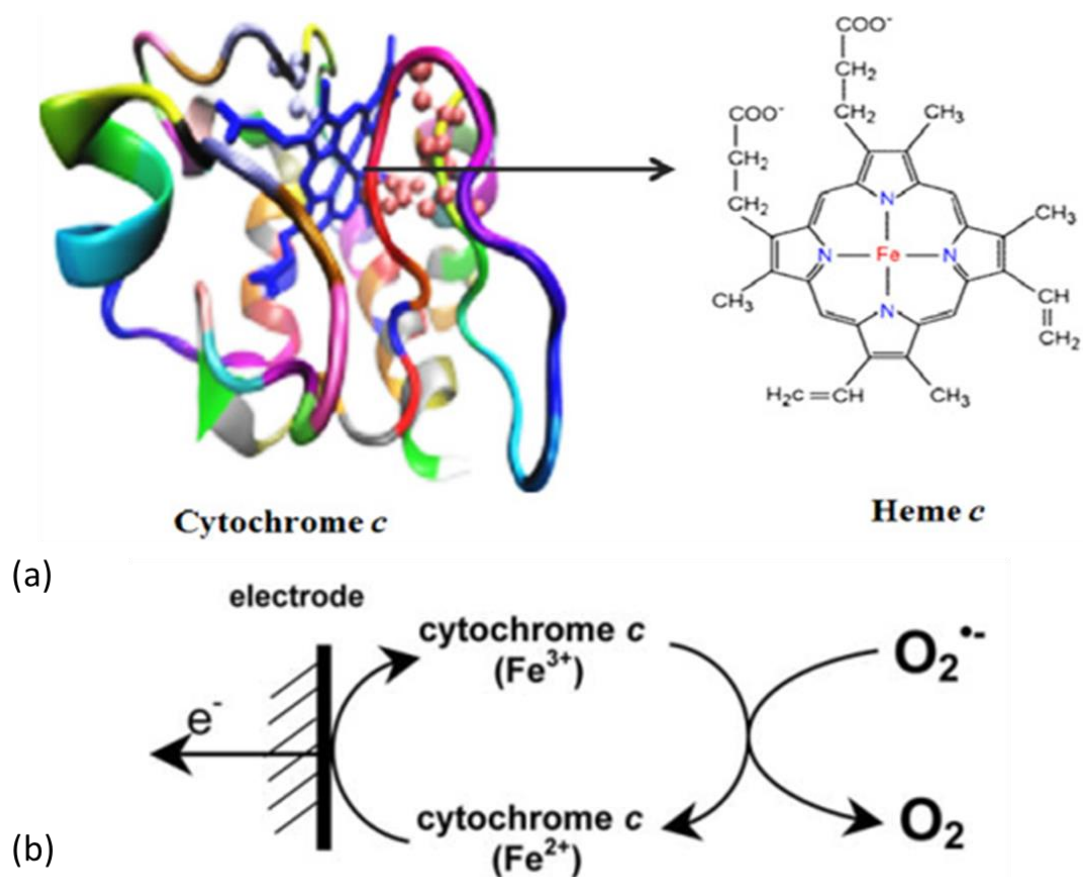


Figure 2.2 (a) The structure of Cyt. c enzyme and heme (Manickam et al. 2017). (b) The principle of Cyt. c-based detection of superoxide.

The superoxide determination by Cyt. c was mostly demonstrated on gold or platinised activated carbon electrodes. Cooper et al. (1995) self-assembled L-cystine onto the surface of a bare gold electrode and immobilized Cyt. c through a carbodiimide condensation reaction to test the electron transfer between Cyt. c and the electrode. The  $\text{O}_2^{\bullet -}$  was produced by the enzymatic reaction of the xanthine/xanthine oxidase system. The results showed that Cyt. c achieves direct electron transfer on the surface of the electrode and the apparent potential was 2mV (vs. SCE), indicating that this  $\text{O}_2^{\bullet -}$  sensor has practical application feasibility.

To enhance the sensitivity of superoxide detection, alkanethiol was applied as the promoter for the electron transfer of Cytochrome c. Ge and Lisdat (2002) described a superoxide sensor by immobilizing Cyt. c on a mixed thiol (mercaptoundecanoic acid / mercaptoundecanol) modified gold electrode. The sensor showed an obvious electrochemical redox behaviour, and the interaction of superoxide and enzyme was characterized. The long alkanethiol monolayers could be contributed to the orientation of the enzyme without denaturation, resulting in the improvement of the electrons transfer. The mixed thiol-modified sensor was also provided to protect the electrode from the fouling of the other interferences in solution, such as  $\text{H}_2\text{O}_2$  and

uric acid.

However, as a peroxidase, Cyt. c can also oxidise  $\text{H}_2\text{O}_2$  and  $\text{ONOO}^-$  in the human body or from the enzymatic reaction, which can interfere with the results of superoxide detection (Tian et al. 2006). To increase the accuracy, the enzyme with specific characteristics would be one of the alternatives.

### 2.2.2 *Superoxide dismutase*

To solve the problem of low selectivity of Cyt. c-based biosensor, as one of the ROS eliminating enzymes, SOD is widely used for detecting  $\text{O}_2^{\cdot-}$  (Endo et al., 2002; Prieto-Simón et al., 2008; Salem et al., 2014; Braik et al., 2016).

As the first line of defence against ROS damage in the life motions of cells, superoxide dismutase could catalyse disproportionation reactions of toxic superoxide anion radical into both non-toxic oxygen and hydrogen peroxide so that decrease the excessive concentration level of superoxide which causes oxidative stress in the human body (Kangralkar et al. 2010, Yasui and Baba 2006). As shown in Figure 2.3, with the characteristics of metalloenzymes, SOD achieves its catalysis on disproportionation reaction by alternate oxidation-reduction of metal ions on its active site (McCord and Fridovich 1969, Tainer et al. 1983). SODs have many species based on the metal cofactors on their active sites, such as copper-SOD (Cu-SOD), zinc-SOD (Zn-SOD), iron SOD (Fe-SOD), manganese SOD (Mn-SOD), and nickel-SOD (Ni-SOD) which are unequally distributed within the whole organism (Younus 2018). Different forms of SOD are located in different subcellular compartments, Mn-SOD usually located in the mitochondrial matrix and Cu/Zn-SOD located in the inner membrane space of mitochondria (Kitada et al. 2020).

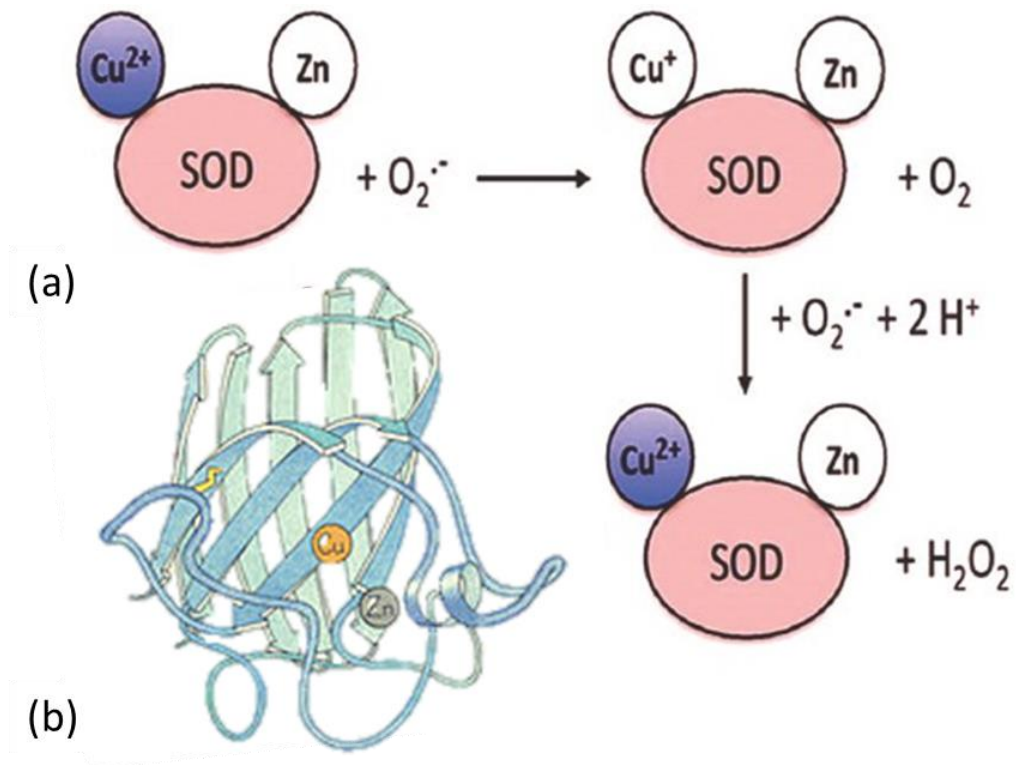


Figure 2.3 (a) The principle of SOD-based catalytic dismutation of superoxide (Younus 2018). (b) The structure of SOD enzyme (Tainer et al. 1983).

Ohsaka's research group (2002) first discovered that O<sub>2</sub><sup>•-</sup> can be simultaneously oxidized and reduced on SOD-modified electrodes, and the comparative experiments confirmed that O<sub>2</sub><sup>•-</sup> can be detected bi-directionally at both oxidation and reduction voltages. This result achieved the analysis of O<sub>2</sub><sup>•-</sup> and the long-term and reliable detection of O<sub>2</sub><sup>•-</sup> free radicals in biological systems.

The principle of SOD-catalyzed disproportionation reaction is based on a secondary reaction, in which the rate of the reaction is proportional to the product of the double substrates. The total reaction is shown in equation 2.1 (Emregul et al. 2013):



This conversion is accomplished by two steps as shown in equation 2.2 & 2.3 (Figure 2.3 (a)):





where M represents the metal cofactors present in the active site, including Cu / Zn (n = 1), Mn; Fe; and Ni (n=2). In these two steps, the electrostatic attraction of metal cofactors is preserved by the proton, and the energy released from the first step could be used to support the second step (Melo et al. 2011).

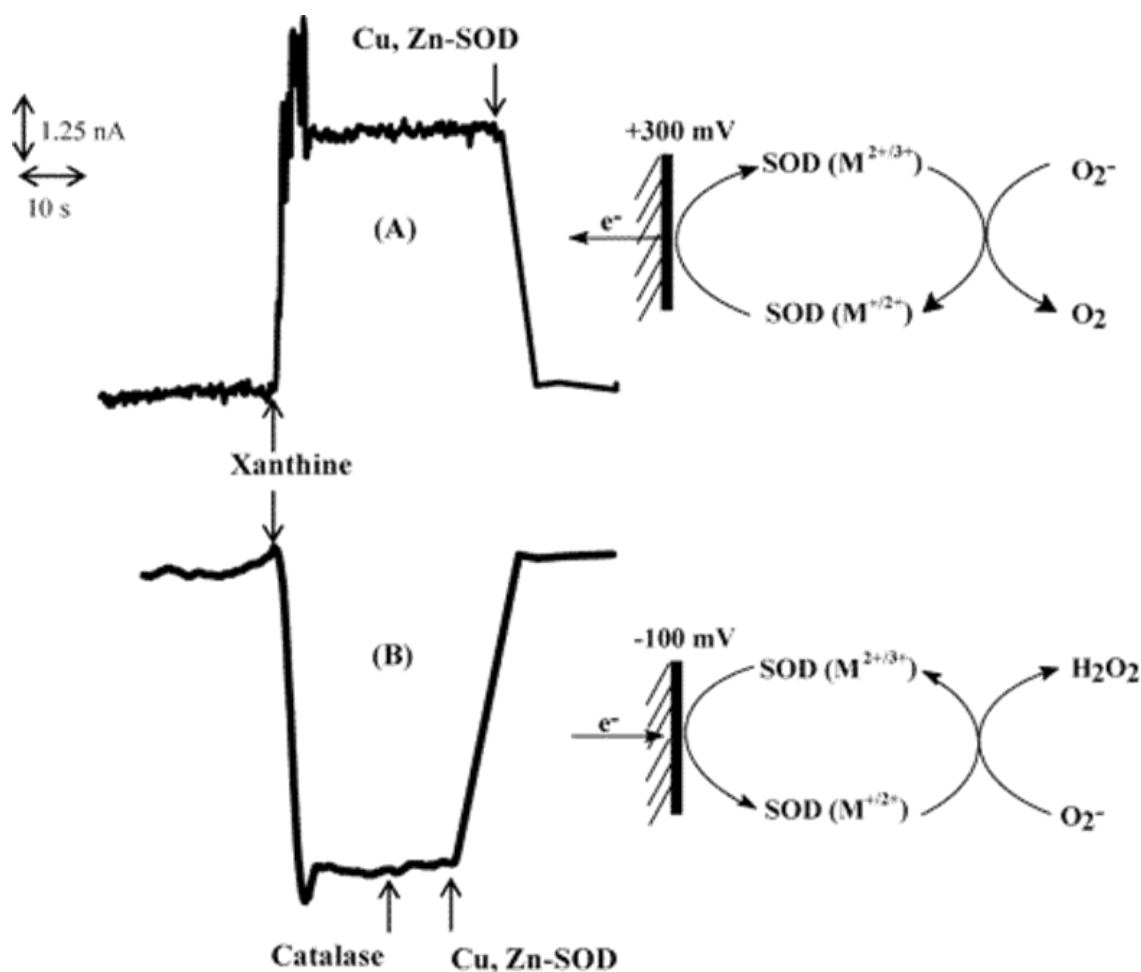


Figure 2.4 The mechanism of  $O_2^-$  catalysed by SOD (a) the reduction reaction (b) the oxidation reaction (Tian et al. 2004).

Many SOD-based superoxide biosensors separated two steps respectively on anode and cathode and detected superoxide by determining the electron transfer directly from SOD on electrode surface area. Tian et al. (2004) established a superoxide biosensor to determine the electron transfer of different kinds of SODs on a self-assembled monolayer (SAM) of 3-mercaptopropionic acid-modified gold electrode. As shown in Figure 2.4, the biosensor was proved a successful recognition of the SOD redox cycle of the active sites. Both the reduction

reaction of  $O_2^{\cdot-}$  to  $H_2O_2$  and oxidation reaction of  $O_2^{\cdot-}$  to  $O_2$  showed a significant increase in the current response at the anode and cathode, which represented that SOD has a bi-functional electro-catalytic activity for  $O_2^{\cdot-}$ .

The detection based on the direct electron transfer of SOD on the surface of the electrode required the promotor to achieve the rapid electron transfer, resulting in the electron transfer promotor becoming an important part of this kind of biosensor. Cysteine and nanomaterials showed good performance to promote electron transfer. Peng et al. (2005) used SOD, L-cysteine (Cys), sol-gel and gold nanoparticles (AuNp) to prepare three self-assembled SOD electrodes, SOD/Cys/sol-gel, SOD/Cys/AuNp and SOD/Cys/AuNP/sol-gel, by combining self-assembly method, nanotechnology and sol-gel method. Experiments showed that the SOD electron transferred faster in the electrode surface membrane by adding L-cysteine, which resulted in greatly increasing the sensitivity of the enzyme electrode. The AuNp further improved the sensitivity of the enzyme electrode because it made the catalytic effect obvious. Sol-gel could not only immobilize the enzyme efficiently but also retain its activity well.

Besides using the electron transfer promotor, another efficient way to determine the electron transfer of SOD is using a surface-confined mediator that contains metal factors. Figure 2.5 (a) shows the principle of this kind of superoxide biosensor. Instead of directly detecting the electron transfer of SOD, the mediator could efficiently mediate the oxidation reaction of superoxide and transferred the electron from SOD to the electrode. Endo et al. (2002) established a SOD-based superoxide biosensor using ferrocene-carboxaldehyde as the mediator and successfully applied in organism tests. They built two cells (shown in Figure 2.5 (b) and (c)) to respectively detect the amount of superoxide produced from the oxidation reaction with xanthine oxidase (in the batch cell) and superoxide released from the heart of an endotoxin-administered rat (in the flow cell for continuous monitoring). Results showed high sensitivity and reproducibility for superoxide detection and obtained a linear relationship between the electronic response and hypoxanthine concentration at 0 to 100  $\mu$ M, which represented that the SOD-based biosensor was available for superoxide detection in a complex organism-environment.

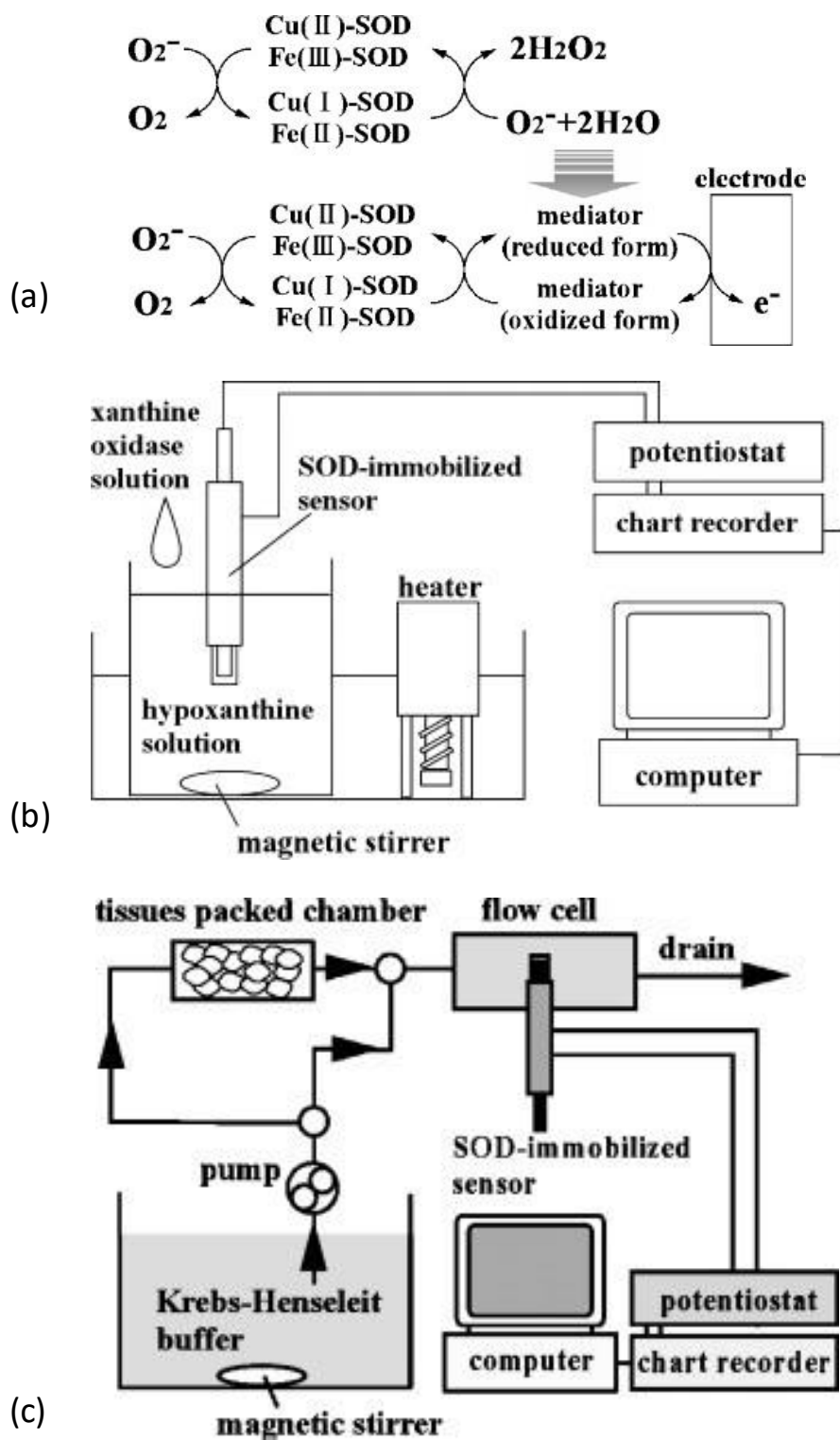


Figure 2.5 (a) The principle of the SOD-based biosensor using a surface-confined mediator for superoxide determination. The experiment setup for (b) the batch cell and (c) the flow cell. (Endo et al. 2002)

Although the biosensor based on direct electron transfer of SOD showed the advantage of convenient detection, high sensitivity and reproductivity for superoxide determination, the quantitative measurement towards the concentration of superoxide still is a challenge nowadays.

To solve this problem, the quantitative measurement of the produced hydrogen peroxide from superoxide was described in this project.

### 2.2.3 Horseradish peroxidase combined with superoxide dismutase

The direct quantitative measurement of  $\text{H}_2\text{O}_2$  is based on the electron transfer of oxidation reaction from  $\text{H}_2\text{O}_2$  to oxygen, which required high potential. This measurement was widely described because of the short response time, easy operation, good temperature stability and low detection limits (Tian et al. 2006). However, the electrical signal response at such a high potential could be easily affected by the simultaneous oxidation reactions of other electroactive species in vitro. To enhance the sensitivity of the superoxide biosensor, detecting the reduction reaction of produced  $\text{H}_2\text{O}_2$  with the specific enzyme would be an alternative way.

Horseradish peroxidase (HRP) is an important heme-containing enzyme which widely used to oxidase the various substrates in the presence of  $\text{H}_2\text{O}_2$  as the oxidizing agent (Veitch 2004). It is structured by a large alpha-helical glycoprotein binding heme as the redox factor present in the active site (Akkara et al. 1991, Veitch 2004) (shown in Figure 2.6). Due to the characteristic of the ability to reduce  $\text{H}_2\text{O}_2$  in an aqueous environment, HRP has commonly reported the utilization of the electrochemical detection of  $\text{H}_2\text{O}_2$  (Xu Chen et al. 2008, Ferapontova et al. 2001, Razola et al. 2002, Shin et al. 2020, Wu et al. 2011).

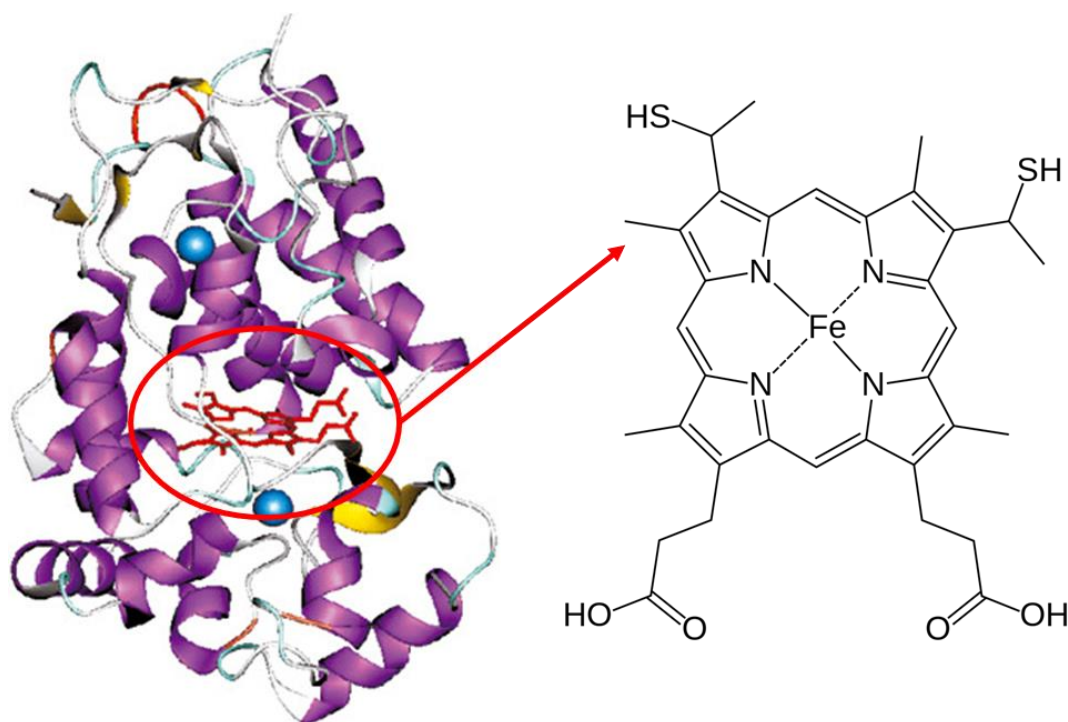


Figure 2.6 The structure of HRP which contains heme as its active site (Veitch 2004).

The principle of the HRP-catalytic reduction reaction of H<sub>2</sub>O<sub>2</sub> could be described as the following equation (Lvovich and Scheeline 1997) :



the reduction process of the HRP-catalysed reaction is (Malomo et al. 2011, Razola et al. 2002):



With the presence of H<sub>2</sub>O<sub>2</sub>, the Ferric HRP that is immobilized on the surface of the electrodes can be fully converted to its oxidized compound I. Then, the HRP compound I can be reduced to the Ferric HRP through the *HRP compound II* (the intermediate compound) in the presence of the exogenous electron donor.

The HRP-catalyzed H<sub>2</sub>O<sub>2</sub> reduction was proved to be successfully applied on H<sub>2</sub>O<sub>2</sub> biosensors. Feng et al. (2011) established an H<sub>2</sub>O<sub>2</sub> based biosensor by immobilizing HRP on a new type of chitosan/polyvinylpyrrolidone (PVP) composite membrane, with glyoxal as crosslinking agent and ferrocene as mediator. The cyclic voltammetry results showed that the sensor had good linearity in the range of H<sub>2</sub>O<sub>2</sub> concentration of 3.00 × 10<sup>-8</sup> ~ 3.00 × 10<sup>-4</sup> mol/L. Zhan et al. (2011) prepared a biosensor with polyaniline as electronic media and HRP immobilized on nano-TiO<sub>2</sub>. The results showed that the sensor had good electro catalytic reducibility for both H<sub>2</sub>O<sub>2</sub> and NaNO<sub>2</sub>.

Therefore, the quantitative measurement of superoxide anion is possibly be achieved by determining the concentration of H<sub>2</sub>O<sub>2</sub> reduced from superoxide anion in the presence of coupled SOD-HRP system. This coupled-enzyme system for superoxide determination was utilized successfully on a fluorescent biosensor. Based on the coupled reaction with superoxide dismutase–peroxidase enzymes, Mateo etc. (2004) developed a highly sensitive fluorescent biosensor in a single sol-gel matrix, which is shown in Figure 2.7. The results showed that this kind of biosensor had full activity and could be used repeatedly for at least one month. The

good performance of this fluorescent biosensor proved that the enzyme-catalyzed reactions of XOD, SOD and HRP could be performed simultaneously in the same system. However, the limitation of the fluorescent biosensor is not ignorable, such as time-consuming for the sample detection, and could be easily interfered with by the environment and compounds themselves.

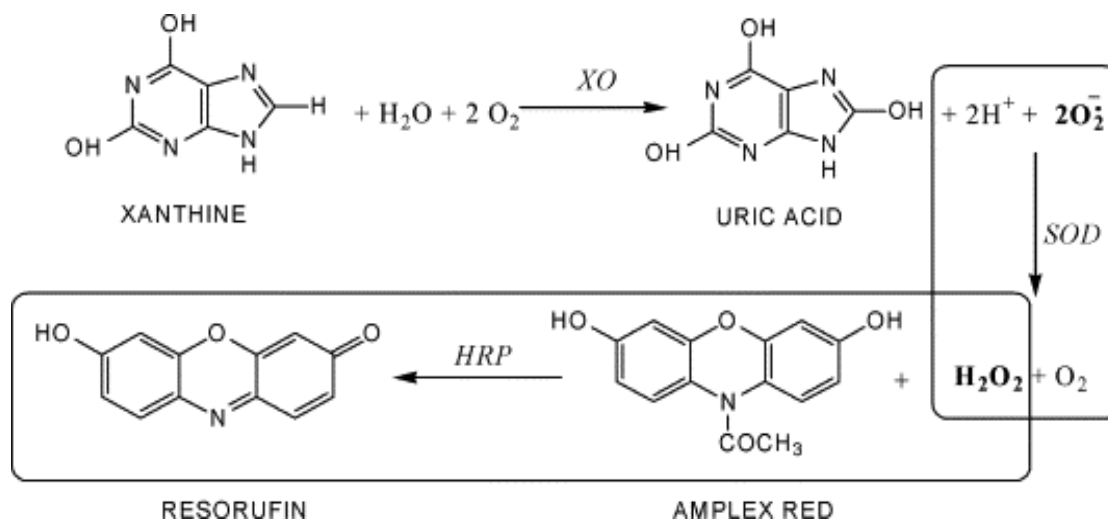


Figure 2.7 Scheme of the coupled reaction system (Pastor et al. 2004)

In an electrochemical system, the concentration of  $\text{H}_2\text{O}_2$  is distributed unequally due to the solution diffusion and electrode adsorption. Therefore, the coupled-enzyme system might be complex when the local concentration of  $\text{H}_2\text{O}_2$  reached a high level. Vlasits et al. (2010) discussed the mechanisms of catalase activity of HRP and described a series of complex enzyme reactions and various reaction intermediates formed in the presence of excessive  $\text{H}_2\text{O}_2$  (shown in Figure 2.8). In this case, the oxygen produced from superoxide could be involved in the HRP (compound III) enzymatic reactions, the efficiency of HRP might decrease and the reaction rate of the  $\text{H}_2\text{O}_2$  reduction reaction could drop resulting in the decrease of the current signal followed by the effect on the accuracy of the electrochemical biosensor.

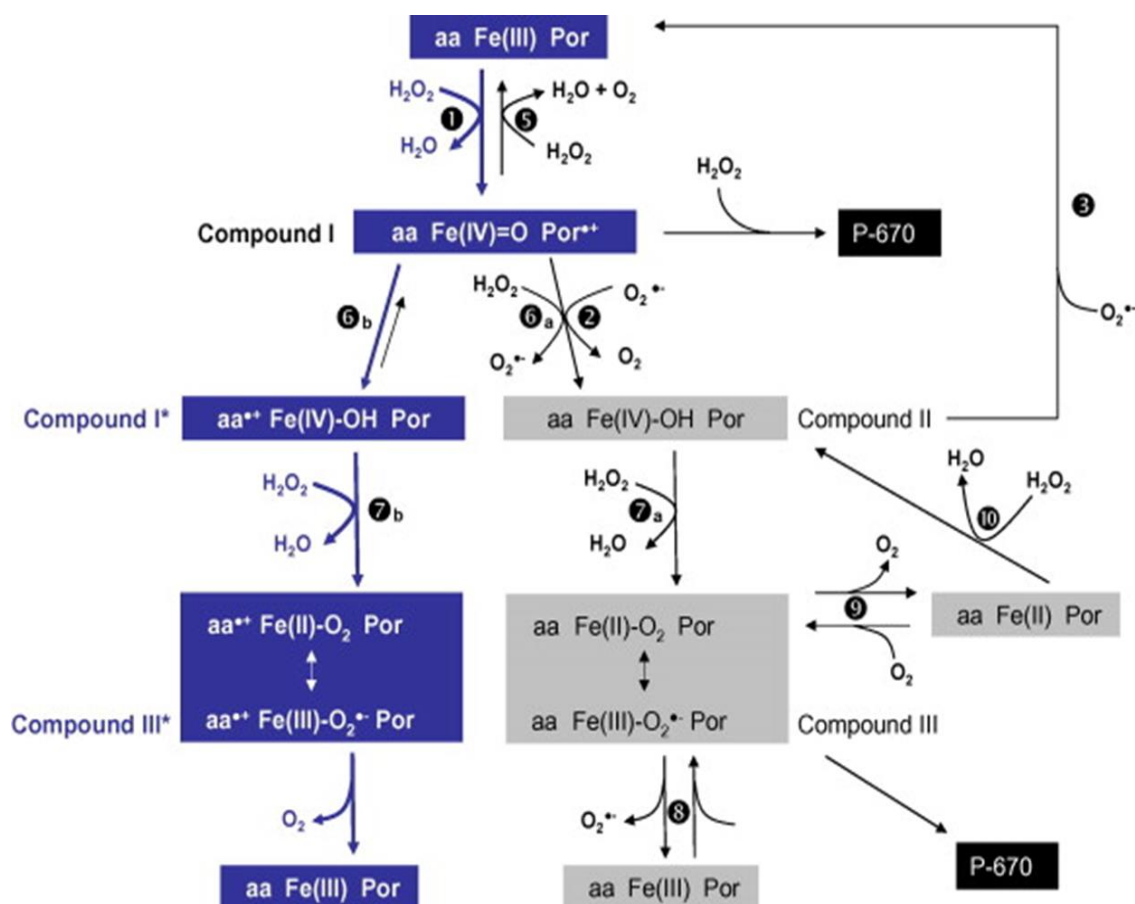


Figure 2.8 The reaction intermediates formed from HRP in the presence of excessive  $\text{H}_2\text{O}_2$ . (Vlasits et al. 2010)

In addition,  $\text{H}_2\text{O}_2$  could inhibit the activity of the SOD enzyme because of the product inhibition and the changes of the conformation of the enzyme that could affect the enzyme activity (Ambarsari and Lindawati 2017). Besides, excess  $\text{H}_2\text{O}_2$  can be converted to  $\text{OH}^\cdot$ , resulting in the denaturation of the enzyme proteins, the mutations of the nucleic acids, and the reduced activity of the enzyme. To avoid the effect of the excess  $\text{H}_2\text{O}_2$  on the electrical signal response, the separation of  $\text{H}_2\text{O}_2$  reduction reaction and the disproportionation reaction of superoxide anion on the different electrode was discussed in this project.

## 2.3 Enzyme immobilizing methods

### 2.3.1 Overview of immobilized enzymes

As catalysts with high specificity and catalytic efficiency, enzymes play an important role in many research areas, especially in the detections of various substrates. The immobilized enzyme was first described in 1916, but enzyme loadings were challenged by the limitation of available surface areas (Cao 2005). As research into the structure and function of enzyme

molecules in the 1960s, this situation has been improved by the covalent method (Homaei et al. 2013).

Compared with free enzymes, immobilized enzymes have a series of advantages such as high storage stability, easy separation and recovery, multiple reusability, continuous and controlled operation and simplicity of the process, while maintaining their efficient and specific properties (Zhang and Xing 2011).

Besides, immobilized enzymes are more suitable for use in multi-enzyme systems than free enzymes (Jia et al. 2014). Immobilized enzymes can not only increase the rate of enzyme-catalysed reactions by the multi-enzyme synergism, but control reactions proceed in a certain sequence.

It is reported that many methods have been used for enzyme immobilization. Enzyme immobilization can be divided into two main types, physical methods (non-covalent adsorption and deposition, entrapment) and chemical methods (covalent bonding, cross-linking) (Basso and Serban 2019).

The principle of four immobilization methods is shown in Figure 2.9 (Homaei et al. 2013). The carrier-bound enzyme is the immobilization of the enzyme on the carrier by physical adsorption, in which the bound is based on intermolecular interaction forces. Entrapment methods usually immobilize the enzyme in a fine gel grid of polymers or a polymeric semi-permeable membrane. Enzyme inclusion and microcapsule are both entrapment-based methods, which use gel or other organic-inorganic hybrid materials to form internal polymeric networks as the substrates (Rother and Nidetzky 2009). Cross-linking method is based on the formation of covalent bonds or relatively short sequences of chemical bonds by combining two polymer chains. Covalent bonding is a method combining enzyme and support matrix by the strong binding between the functional groups that can be covalently coupled (Vijayalakshmi et al. 2020).

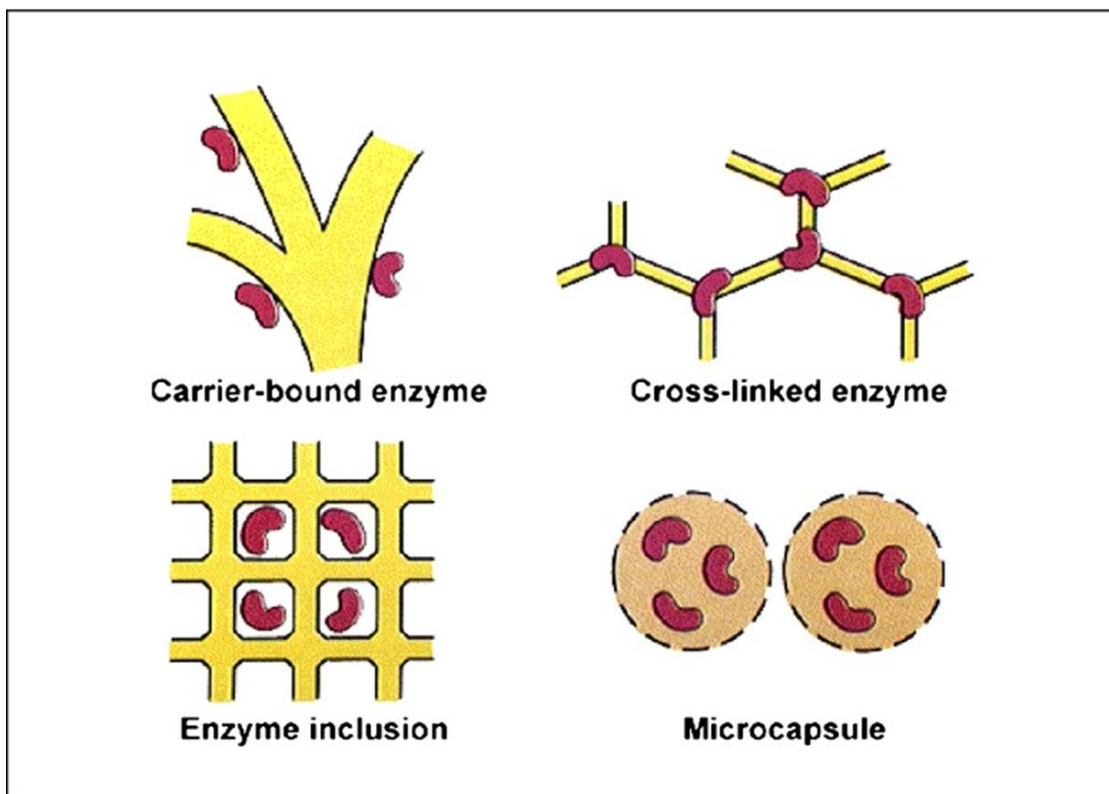


Figure 2.9 Some of the commonly used enzyme immobilization methods (Homaei et al. 2013).

Because of the different structure, physical and chemical properties, location of the active sites of the enzymes, the suitable immobilization methods show the huge difference in applications. These enzyme immobilization methods have different advantages and disadvantages (Datta et al. 2013, Nisha et al. 2012), which is shown in the following table.

Table 2.1 The categories of enzyme immobilization methods and their advantages and disadvantages

Immobilization methods	Classification	Advantages	Disadvantages
Non-covalent adsorption and deposition	Physical immobilization	Easy operation, low cost, and high efficiency	frequently reversible
Entrapment		Avoid negative influence on enzyme surface, high thermal and	diffusional is limited

		mechanical stability	
Covalent attachment	Chemical immobilization	Relatively stable to hydrolysis at neutral pH	High cost, enzyme performance is easily be affected
Cross-linking		High efficiency and durability	

### 2.3.2 Enzyme immobilization for SOD

As one of the important enzymes in the research of oxidative stress, several different immobilization methods for SOD have been studied. The most widely used methods are based on electrostatic interactions and covalent attachment.

As a high charge density cationic polymer, poly(diallyldimethylammonium chloride) was proved to adsorb SOD strongly through electrostatic and hydrophobic interactions. Figure 2.10 shows the successful self-assembly by immobilization of SOD on the titania nanosheets treated poly(diallyldimethylammonium chloride) polyelectrolyte (Rouster et al. 2018). The enzyme showed functional integrity and excellent activity.

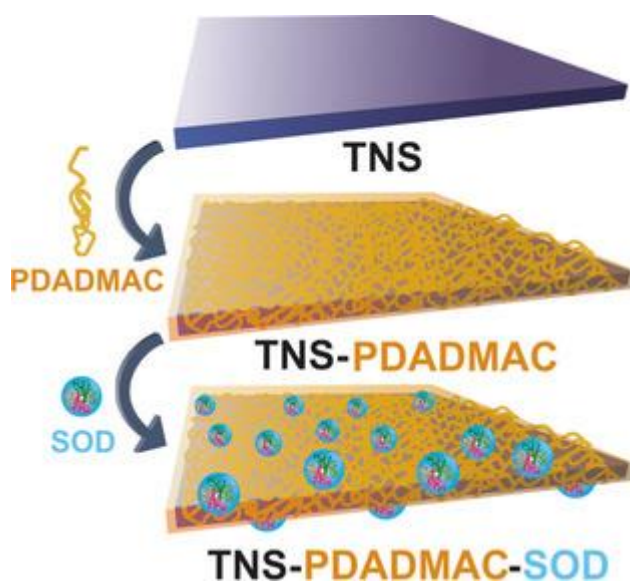


Figure 2.10 Schematic representation of SOD immobilization on PDADMAC-functionalized TNS. TNS: titania nanosheets, PDADMAC: poly(diallyldimethylammonium chloride) polyelectrolyte (Rouster et al.

2018).

It is also reported that the immobilization of SOD by cross-linking was successfully applied. Braik et al. (2016) immobilized SOD-glutaraldehyde mixed solution onto the top of the chitosan layer, which is shown in Figure 2.11. The covalent bond is achieved through the combination of the amino group from chitosan and the carboxyl group of both enzyme and glutaraldehyde.

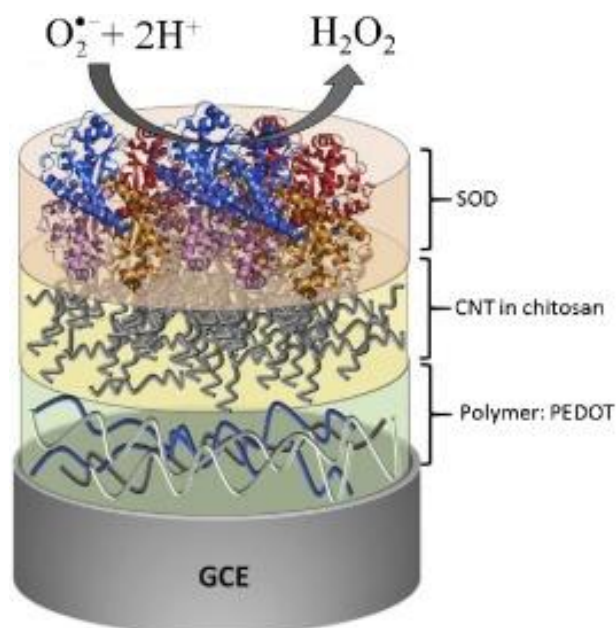


Figure 2.11 Schematic representation of SOD biosensor based on PEDOT and CNT. CNT: carbon nanotubes, PEDOT: poly(3,4-ethylenedioxythiophene). (Braik et al. 2016)

Mahlicli et al. (2015) compared the efficiency of coupled SOD/catalase which was covalently and ionically immobilized respectively (shown in Figure 2.12). Compared with electrostatic immobilization, covalent immobilization required more time for the treatment. Results showed similar rates for the enzyme catalysed reactions, but the ionically immobilized enzyme was found lost from the surface after 4 hours.

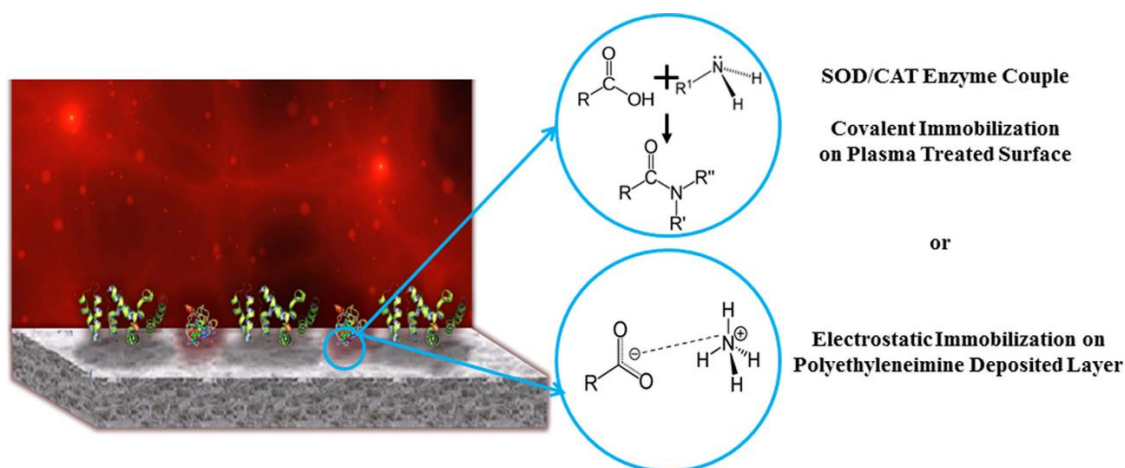


Figure 2.12 Schematic representation of SOD/CAT couple immobilization based on covalent bond and electrostatic force respectively. CAT: catalase. (Mahlicli et al. 2015)

Thus, for the long-term catalytic reactions of SOD, the covalent immobilization provides stronger bindings. Electrostatic immobilization is more advantageous for short-time detections due to the simple operation.

### 2.3.3 Enzyme immobilization for HRP

Most studies on HRP immobilization are based on chemical immobilization. Since the first discussion on the structure of HRP enzyme with carboxyl group in 1997 (Gajhede et al. 1997), the covalent attachment was widely used and developed.

Rong et al. (2019) introduced a graphene oxide composite as the support for HRP immobilization (shown in Figure 2.13). HRP was immobilized on 6arm-PEG-NH<sub>2</sub>, a polyethylene glycol derivative that is rich in amino groups, via the cross-linking agent glutaraldehyde. The loading amount and thermal stability of HRP were improved by this immobilization.

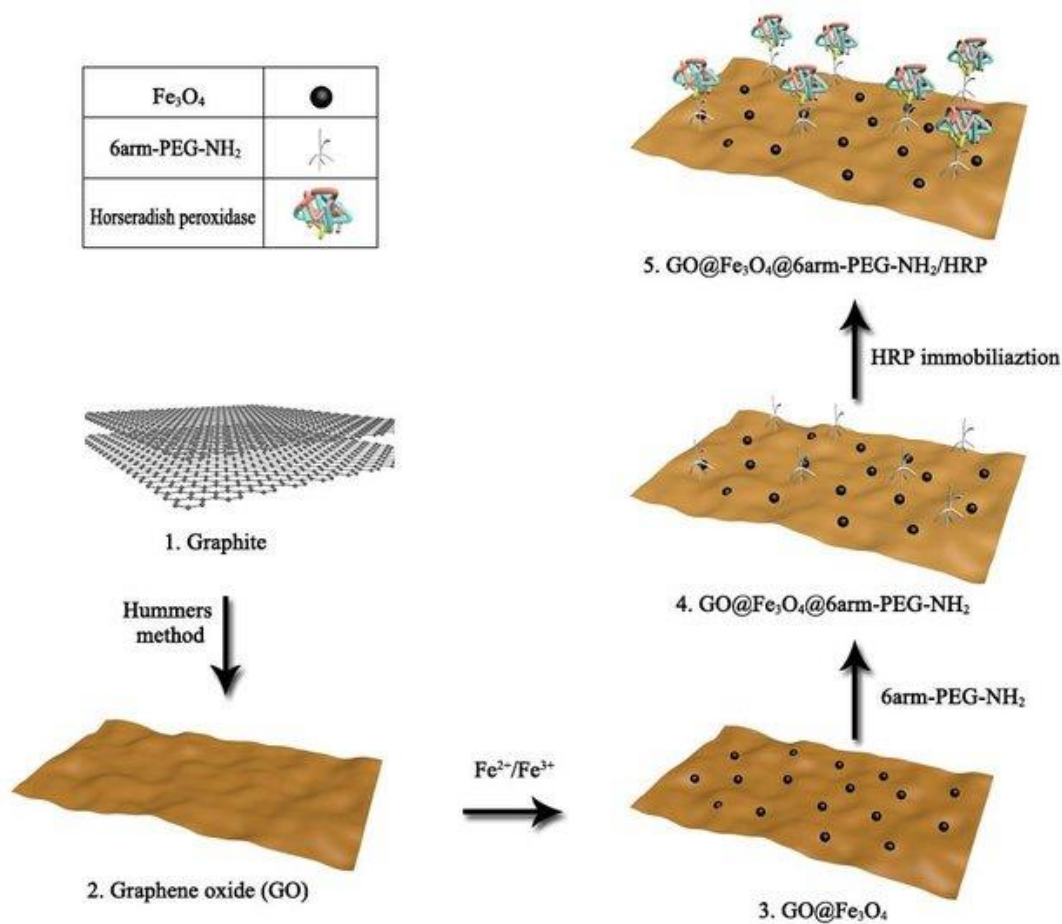


Figure 2.13 Schematic diagram of immobilization of HRP on  $\text{GO}@Fe_3O_4@6arm\text{-PEG-NH}_2$ . (Rong et al. 2019)

Şahin (2020) described a two-step HRP enzyme immobilization on single-walled nanotube coated screen-printed electrodes by using a heterobifunctional crosslinker, 1-Pyrenebutyric acid N-hydroxysuccinimide ester (shown in Figure 2.14). The HRP enzyme was proved strongly combined on the electrode based on the covalent bond and the strong  $\pi$ - $\pi$  interactions. By immobilizing HRP, the modified electrode achieved the effective and sensitive detection of  $\text{H}_2\text{O}_2$  and showed high selectivity and reproducibility.

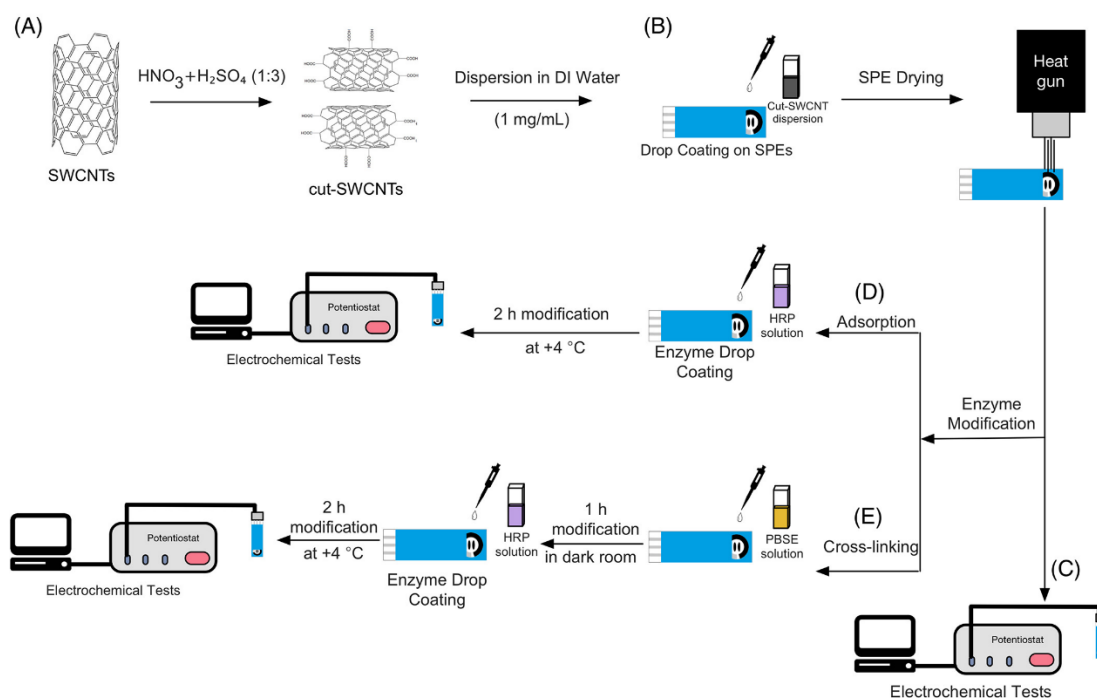


Figure 2.14 Schematic diagram of cut single-walled carbon nanotube electrode preparation. PBSE: 1-Pyrenebutyric acid N-hydroxysuccinimide ester, SPE: screen-printed electrodes. (Şahin 2020)

Except for the immobilization methods based on chemical bonds through the functional group, entrapment of HRP based on protein bind was mostly described by molecular imprinting technology. Sardarelli et al. (2021) provided an electropolymerized  $\beta$ -Cyclodextrin ( $\beta$ -CD) matrix on a glassy carbon electrode which could bind the protein of HRP by hydrogen bonding interaction of OH (shown in Figure 2.15). The excellent electro-conductivity of  $\beta$ -cyclodextrin enhanced electron transfer and the large coverage of the matrix contributed to simple and efficient re-binding towards HRP targets. This biosensor showed excellent behaviour in real samples, which provided the possibility of  $\text{H}_2\text{O}_2$  analysis in clinic studies.

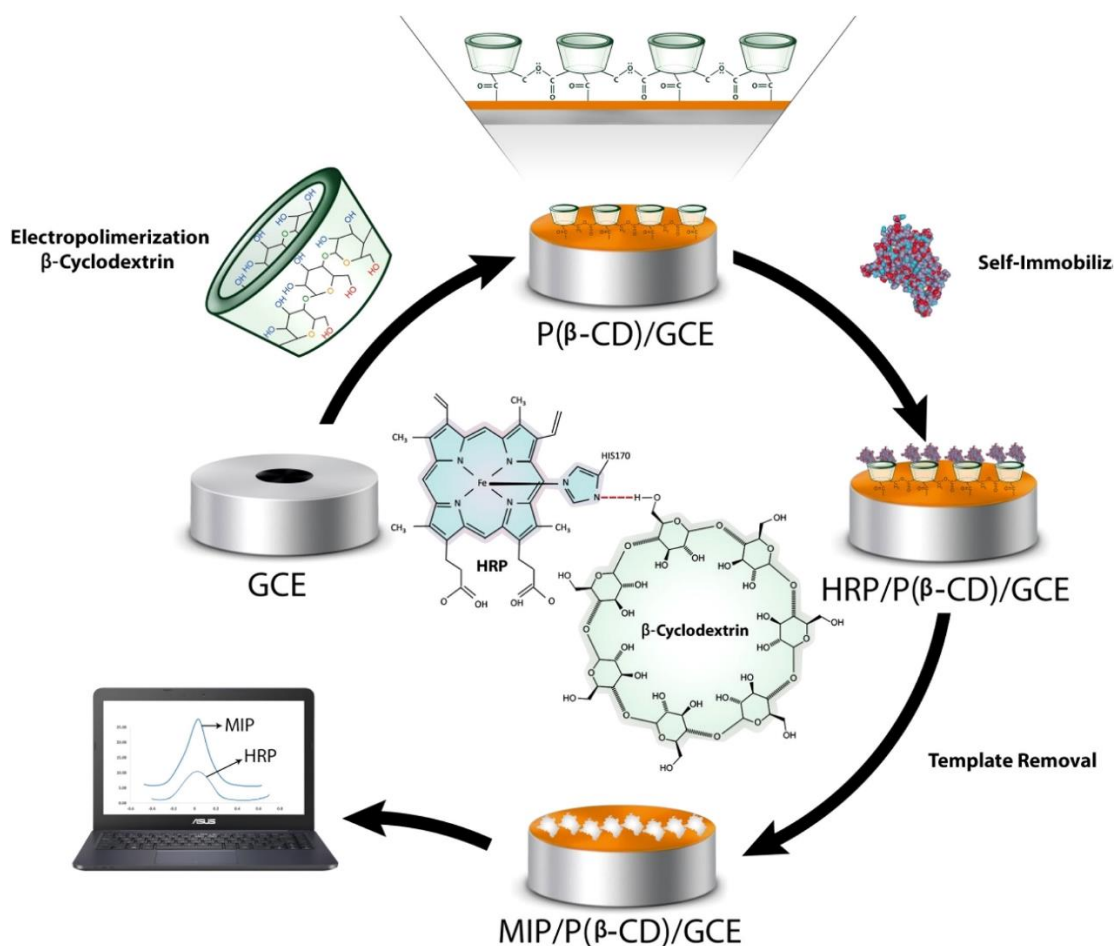


Figure 2.15 Schematic diagram of MIP/P(β-CD)/GCE (biosensor) preparation. GCE: glassy carbon electrode, MIP: molecularly imprinted polymers, P(β-CD): poly beta-cyclodextrin. (Sardaremelli et al. 2021)

## 2.4 Review of methods for analysis

### 2.4.1 Ultraviolet-visible spectroscopy

Spectroscopy is a method of analysis based on the measurement of the wavelength and intensity of emitted, absorbed or scattered radiation resulting from transitions between energy levels that occur within a substance when it interacts with electromagnetic radiation (Penner 2017). When light from a light source comes into contact with a molecule, the light energy of a certain wavelength is converted into kinetic energy causing the electrons to move to a higher excited state, thus causing excitation of the electron energy level (Gandhimathi et al. 2012).

Spectrophotometry is an important part of spectroscopy and is a method for the qualitative and quantitative analysis of a substance by measuring the absorbance or luminous intensity of the substance at a specific wavelength or within a certain wavelength range. As a commonly used method, UV-Vis spectrophotometry is a method for determining the absorbance of a substance

in the wavelength range of 190 to 800 nm for identification, impurity checking and quantitative determination (Perkampus 2013, Shinde et al. 2020, Verma and Mishra 2018).

As shown in Figure 2.16 (Mohanta 2017), the UV-Vis spectrophotometer consists of five components: 1) a light source providing a stable, continuous spectrum with sufficient output power; 2) a diffraction grating for generating high-purity monochromatic beams by breaking up the light source to produce a composite light into monochromatic light; 3) cells which holding the substances for absorbance measurement; 4) the detector and 5) the chart recorder.

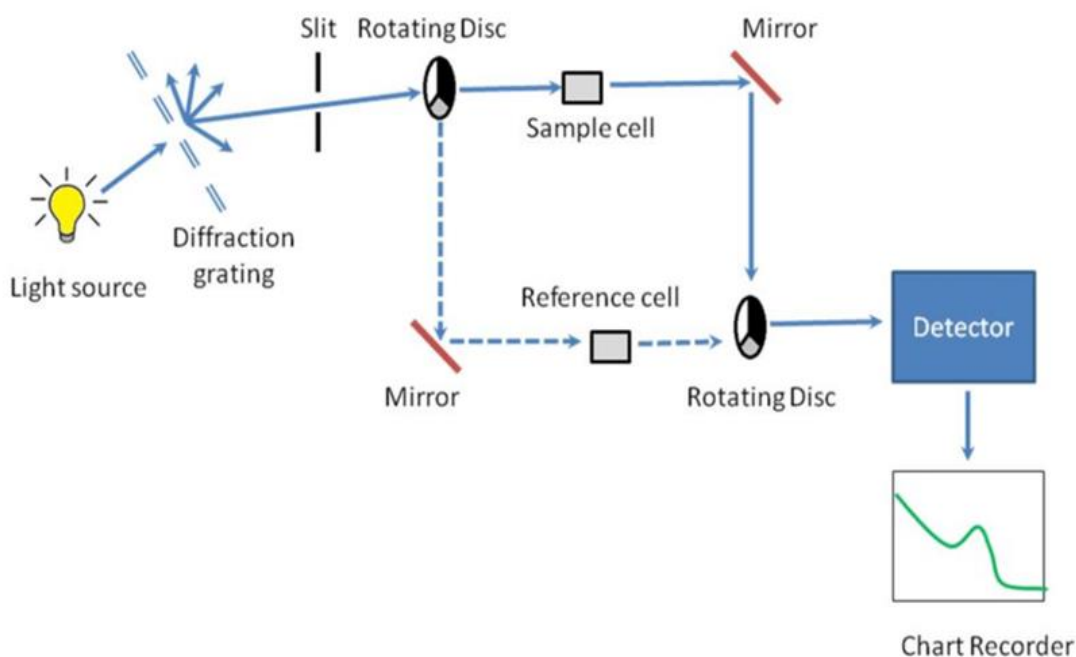


Figure 2.16 Schematic diagram of UV-vis spectrophotometer (Mohanta 2017)

Absorbance measures the light which does not pass through the samples and is decided by the extinction coefficient, the path length of the light and the concentration of samples. As known as Lambert-Beers law, absorbance is given by equation 2.8 (Mäntele and Deniz 2017, Mayerhöfer et al. 2020):

$$A = \log_{10} \frac{I_0}{I} = -\log_{10} \frac{1}{T} = \epsilon cd \quad (\text{Eq.2.8})$$

Where,  $I_0$  and  $I$  are the intensity of incident light and transmitted light,  $T$  is the transmittance,  $\epsilon$  is the molar absorption coefficient,  $c$  is the concentration of the species in the samples and  $d$  is the path length of the measuring beam in the samples. The absorbance is proportional to the concentration of the substance to be measured in the sample under the same conditions and can

therefore be used for the indirect quantification of the concentration of the substance.

#### 2.4.2 Electrochemical characterization

##### ***The electrochemical cell set-up***

To ensure that the working electrode of the electrochemical biosensor maintains a constant potential during operation, the reference electrode and the counter electrode are generally used to compose a three-electrode two-loop system (Yang 2013). The working principle of the current-type electrochemical sensor is shown in Figure 2.17, which is re-created from (Braustein 2017).

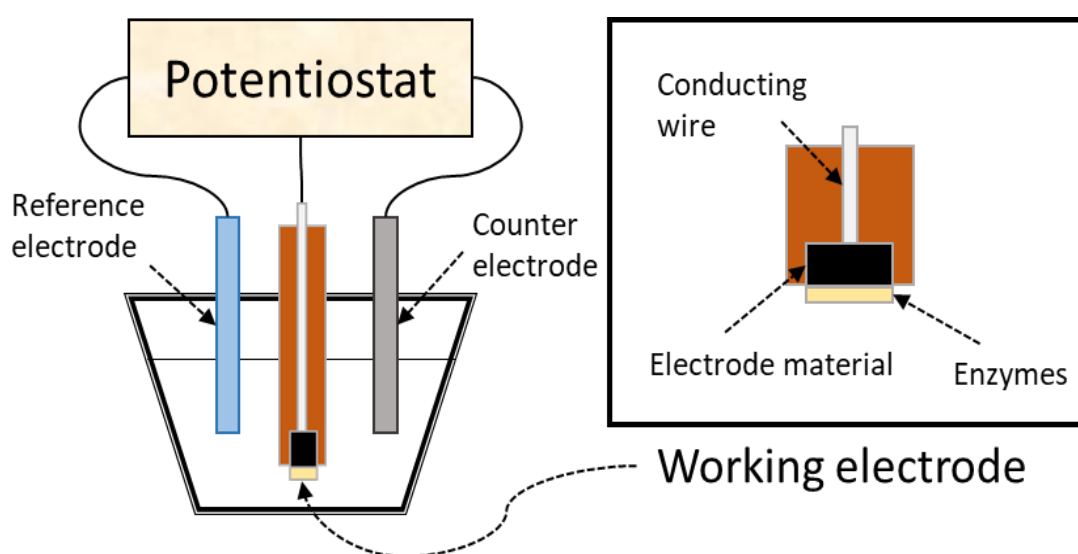


Figure 2.17 Schematic diagram of the principle of electrochemical biosensor

The current flows between the working electrode and the counter electrode, and the reference electrode is placed not far from the working electrode to keep the voltage of the working electrode constant. When the analyte is diffused to the surface of the working electrode, the redox reaction occurs at the counter electrode and the working electrode respectively to generate a current, and the concentration of the analyte is obtained by detecting the redox current (Bard and Faulkner 1983).

After being modified onto the electrode, the bio-sensitive molecule reacts with the specifically recognized molecule to selectively recognize the target analyte (Viswanathan et al. 2009). Because using bio-specific materials as bio-sensitive elements for electrochemical sensors, it has the ability to rapidly and directly capture analyte information from complex biological systems with high selectivity.

## *Voltammetry*

Voltammetry is a widely employed technique in the electrochemical analysis due to its ability to maintain dynamic current-voltage conditions, which correspond to the typical electrochemical reaction process (Patel 2021).

Cyclic voltammetry (CV) is one of the most important methods of electroanalytical chemistry that allows for the investigation of the redox behaviour of electroactive species. It is widely used in many research areas such as electrochemistry, inorganic chemistry, organic chemistry and biochemistry due to its simple instrumentation, ease of operation and intuitive analysis of the spectra (Brett et al. 1993).

The current-potential curve is recorded by controlling the electrode potential with one or more repeated scans of the triangular waveform over time at a certain rate, which is shown in Figure 2.18 (Bard and Faulkner 1983). Reduction and oxidation reactions can occur alternately at the electrode in the potential range. By cycling the potential, the technique provides information on the oxidation and reduction potentials, kinetics, and mechanism of redox processes, as well as the concentration and diffusion coefficients of the species (Elgrishi et al. 2018).

CV is commonly used for studying reversible and quasi-reversible redox processes characterized by proximate oxidation and reduction potentials (Pajkossy 2018). The positions and shapes of the current peak provide information about the thermodynamics and kinetics of the redox process. For irreversible redox processes, where the oxidation and reduction potentials are widely separated, the voltammogram exhibits a broad, featureless peak or plateau. In this case, the kinetics and mechanism of the process, as well as the diffusion coefficients of the species can still be analysed from the voltammogram.

Except the recognition of the reversible and irreversible redox reactions, CV can also be used to study the behaviour of electrode surfaces, including the adsorption and desorption of species on the surface (Yamada et al. 2022). By modifying the electrode surface with functional groups or nanoparticles, it is possible to selectively detect specific redox species or catalytic sites. Thus, CV was widely found in the applications on the characterization of electroactive materials, the development of electrochemical sensors, and the optimization of electrocatalytic processes, as well as biological systems, including the redox behaviour of enzymes and the electrochemistry of DNA and other biomolecules.

The limitation of CV is its sensitivity to experimental parameters, such as the electrolyte, scan rate and the solution temperature (Xu et al. 1999). The choice of electrolyte can affect the kinetics and mechanism of the redox process. The scan rate affects the current obtained from the redox process and can lead to distortion of the voltammogram (Zhu et al. 2020). The electrode surface could be considered to be in a steady state at slow scan rate of 5 mV/s. At slow rates the current observed can be primarily attributable to Faradaic current (no capacitive double layer current). Electrode around peak current will be under diffusion control and hence current will be proportional to redox concentration. For the more accurate results and to avoid the peak offset at a high scan rate in CV, referring to the previous group research on different scan rates towards H<sub>2</sub>O<sub>2</sub> detections (Şahin 2020), 5 mV/s was used in all procedures in this study. The slow scan is used to identify region of interest (potential where peak occurs) so device can operate at fixed potential. The solution temperature can affect the diffusion coefficients of the species, the kinetics of the redox process and the stability of the electrode material and the redox species.

From a cyclic voltammogram, some parameters are important for data analysis, including the peak cathodic and anodic current ( $i_{pc}$  and  $i_{pa}$  respectively), the cathodic peak potential ( $E_{pc}$ ) and the peak anodic potential ( $E_{pa}$ ). In an ideal system, the difference between two peak potentials is only related to the number of transferred electrons (Nicholson 1965):

$$\Delta E_p = E_{pa} - E_{pc} = \frac{57}{n} mV \quad (\text{Eq.2.9})$$

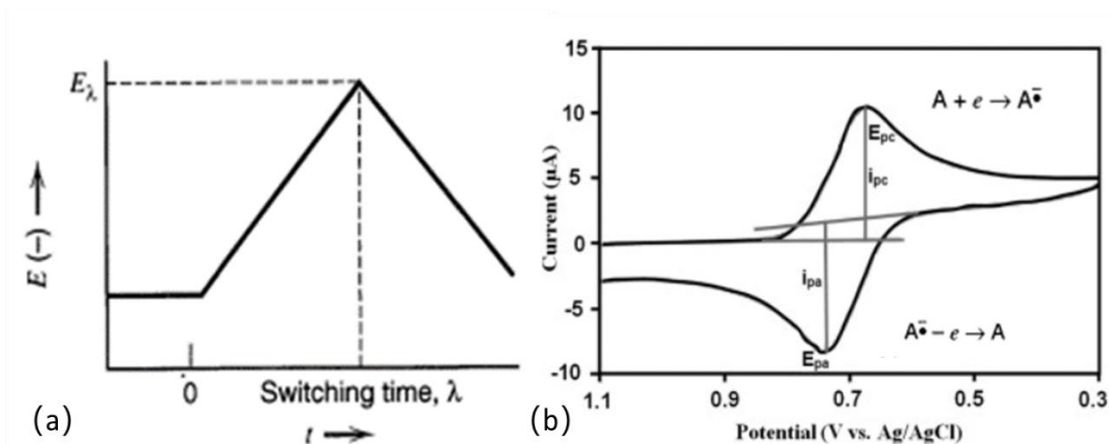


Figure 2.18 (a) CV potential sweep waveform (Bard and Faulkner 1983) and (b) typical resulting cyclic voltammogram (Zhang et al. 2013).

Linear sweep voltammetry (LSV) at a faster scan rate could be regarded as half-cycle of CV processes, which is also a detection of the current changing with the linearly changed potential. At an extremely slow scan rate, the current response of LSV could be regarded as Faradaic current, and the response curve called the steady-state polarization curve. LSV has extensive applications in various fields, primarily including the evaluation of photoelectric performance in solar cells, determination of oxygen reduction curves in fuel cells, and detection of catalytic curves in electrocatalysis (Aoki et al. 1985, Raesi-Kheirabadi et al. 2022, Rossi et al. 2020). Different from LSV, CV is primarily employed to investigate the energy storage and capacitance properties of supercapacitors, as well as to study the redox characteristics of materials on the working electrodes.

Except LSV and CV, the pulse voltammetry is also one of the commonly used electrochemical analysis technique. Pulse voltammetry involves applying regularly increasing amplitude potential pulses to the electrode, and it can be described as normal pulse voltammetry (NPV), differential pulse voltammetry (DPV) and square wave voltammetry (SWV) regarding to the applied potential, which is shown in Figure 2.19.

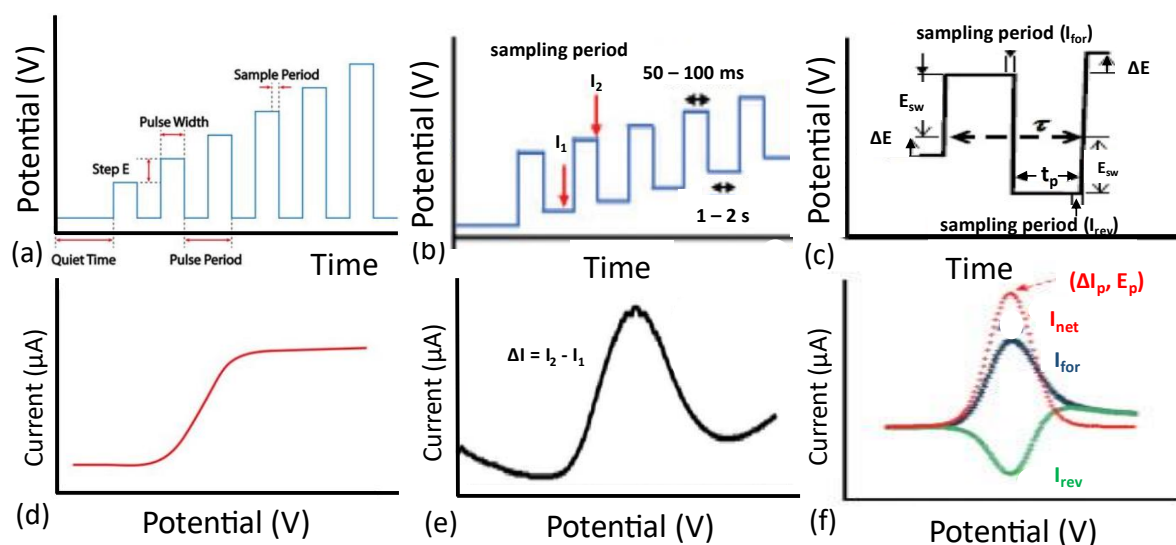


Figure 2.19 Schematic of pulse voltammetry. Applied waveform for (a) NPV, (b) DPV and (c) SWV; typical voltammogram for (d) NPV, (e) DPV and (f) SWV. Recreated from literature (Deffo et al. 2023, Simões and Xavier 2017, Venton and DiScenza 2020).

As shown in Figure 2.19 (a), the rectangular potential pulse of NPV increases by a constant amplitude with constant time intervals (Bontempelli and Toniolo 2005). In NPV, there is no Faradaic reactions until a short-time pulse applied to stimulate Faradaic reactions. Due to the absence of the previous diffusion layer, a higher diffusion flux and faradaic current would be

generated. NPV is often used to analyze low concentrations of heavy metals, organics, with the detection limit that can reach 1 to 0.1  $\mu\text{M}$  (Worsfold et al. 2019).

Different from NPV, the short amplitude potential pulses of DPV (shown in Figure 2.19(b)) are superimposed on a linear ramp. From Figure 2.19 (d) and (e), the baseline of NPV showed linear relationship with the voltage and DPV is a fixed value. This is caused by the behaviour of charging current of the electric double layer with the increasing potential pulses. Unlike NPV, the returns to its initial condition of the diffusion layer in each current sampling interval is not required in DPV (Batchelor-McAuley et al. 2015). DPV has higher detection sensitivity and lower detection limit due to the reduced background current, which enables it to be applied to occasions where the concentration is as low as about 1  $\mu\text{M}$  (1  $\mu\text{g/L}$ ) with the detection limit about  $10^{-2}$   $\mu\text{M}$  (Venton and DiScenza 2020).

SWV is the technique that combined both NPV and DPV. In SWV, as shown in Figure 2.19 (e), a waveform consisting of a balanced square wave is superimposed onto a base staircase potential and applied to the working electrode (Nambiar et al. 2023). It has both the advantages of higher current value in NPV and the benefits of higher sensitivity and no requirements of diffusion layer returns in DPV. Thus, SWV is most commonly used to amplify the electrochemical signal of the redox analyte.

### ***Chronoamperometry***

Chronoamperometry (CA) is a simple and widely used electrochemical detection technique. It works by applying a potential step between the working electrode and the reference electrode as an excitation, resulting in a time-varying response current generated by a redox reaction that flows through the working electrode and the counter electrode, with the initial value of the current being large and decreasing with time. Figure 2.20 shows the waveform for a step experiment and the typical resulting current-time curve (Bard and Faulkner 1983).

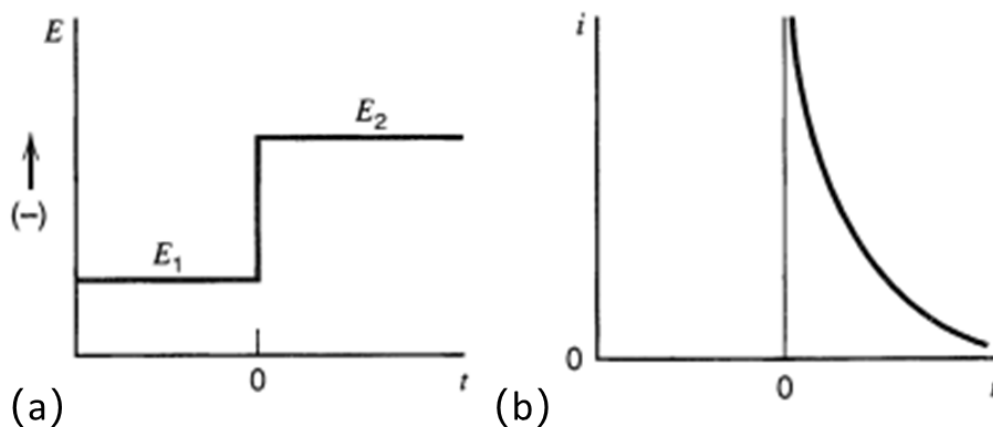


Figure 2.20 (a) Waveform for single-step experiment; (b) typical resulting current flow vs. time. (Bard and Faulkner 1983)

Comparing with the other electrochemical analysis techniques, CA has the advantage of fast detection, and the response time could down to minutes, which is suitable for the family handheld device. Besides, CA yields a superior signal-to-noise ratio when compared to other techniques due to its integration of current over relatively longer time intervals (Daws and Toney 2007). While other electrochemical methods can also provide value information and separation between kinetics and mass transport of redox processes, we focused on used on chronoamperometry as it is the simplest and cheapest to implement in handheld device as well as provide direct correlation of limiting current with target redox species concentration. To analyse the reaction activity, the CA was scanned with a fixed potential from the CV curve (the potential of the peak signal).

As a standard in  $O_2^{\cdot-}$  detection, the calibration curve would be the most important part of the biosensor. Since the current would change with the changing of  $O_2^{\cdot-}$  concentration, the calibration curve was generated by current and different  $O_2^{\cdot-}$  concentrations in the electrolyte at a fixed potential for 100 seconds.

According to the Cottrell equation, which is shown in the following equation, using the relationship between  $i(t)$  and  $c_0$  as a proportional relationship, CA can be used for quantitative analysis (Cottrell 1902, Gueshi et al. 1978, Mazloun-Ardakani et al. 2022).

$$i(t) = \frac{n F A D_0^{\frac{1}{2}} C_0}{\pi^{\frac{1}{2}} t^{\frac{1}{2}}} \quad (\text{Eq.2.10})$$

Where,  $i(t)$  is the current detected at a certain time  $t$ ,  $n$  is the number of electrons in the oxidation or reduction process,  $A$  is the surface area of the working electrode,  $D_0$  is the diffusion coefficient of the process,  $c_0$  is the bulk concentration of the substrates for the oxidation or reduction process.

To change the  $O_2^{\cdot-}$  concentration, the stock of the  $O_2^{\cdot-}$  solution was prepared first. This project chose the wide range of  $O_2^{\cdot-}$  concentration from 0.02 mM to 10 mM, so several stocks with different concentrations were prepared to reach the wide range.

For the method using  $Na_2S_2O_4$  and NaOH solution, both  $Na_2S_2O_4$  concentration and generated  $H_2O_2$  concentration are half of the concentration of  $O_2^{\cdot-}$ . The solution is 2 ml 0.1M NaOH solution. To reach the certain concentration, pipetting a certain small volume of  $Na_2S_2O_4$  solution can increase the accuracy.

For the method using xanthine and xanthine oxidase solution, xanthine concentration was changed as the control factor of the  $O_2^{\cdot-}$  and generated  $H_2O_2$  concentration. The detected  $O_2^{\cdot-}$  concentration is theoretically lower than two times xanthine concentration and higher than two times generated  $H_2O_2$  concentration due to the complex procedure of several enzymatic reactions.

#### 2.4.3 Chemiluminescence methods

As shown in Figure 2.21, luminescence is the process by which electrons in a molecule or atom absorb energy and then transits from a ground state (lower energy level) to an excited state (higher energy level), before returning to the ground state and emitting a photon (Omary and Patterson 2017). Depending on the source of energy used to form the excited state molecule luminescence can be classified as photoluminescence, thermoluminescence and chemiluminescence, etc (Guilbault 2020).

Chemiluminescence typically has a surprisingly wide wavelength range of light emitted and high sensitivity because of low ambient interferences (autofluorescence of compounds, media and cells) (Capitán-Vallvey et al. 2015, Gundermann and McCapra 2012).

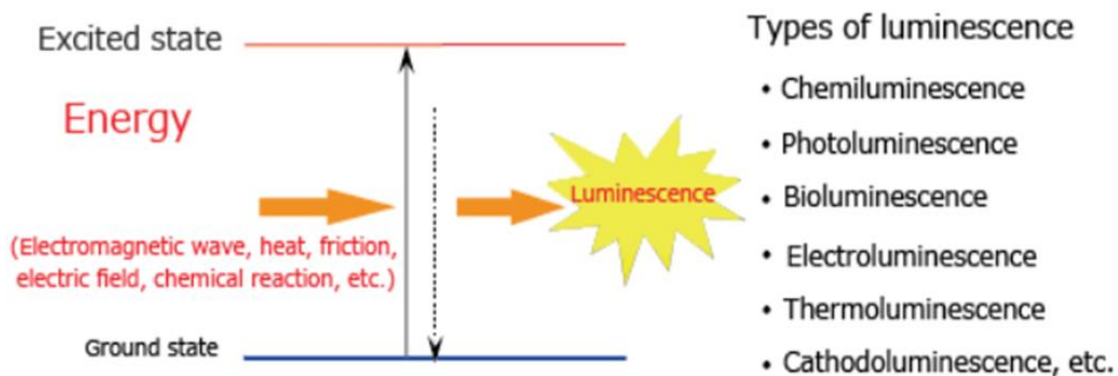


Figure 2.21 Schematic diagram of the principle and category of luminescence (Shimadzu, 2022).

Chemiluminescence analysis is based on the principle that the concentration of the substance to be measured in the detection system and the chemiluminescence intensity of the system under certain conditions in a linear quantitative relationship and determine the content of the substance by detecting the system chemiluminescence intensity.

As a typical chemiluminescence agent with high luminous efficiency (which can reach 0.01), luminol has been widely used to identify blood. Figure 2.22 shows the chemiluminescence reaction induced by luminol. Luminol can be oxidised by a number of oxidants like hydrogen peroxide under certain conditions and emits blue light with a maximum emission wavelength of 425 nm (Luminol , Bustos et al. 2001, Erdey et al. 1962).

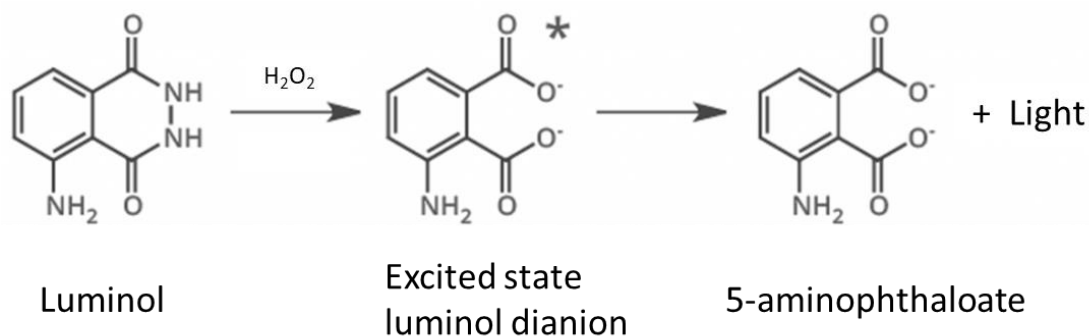


Figure 2.22 The chemiluminescence reaction of luminol (Hayashi et al. 2019).

Although chemiluminescence has the advantage of high selectivity and lower background signal leading to the high sensitivity, many chemiluminescent reactions exhibit a low quantum efficiency, resulting in the generation of faint luminescence. Some chemiluminescence systems may encounter complications due to interferences and nonlinear behaviour (Heard and Pilling 2003). Comparing with chemiluminescence, electrochemical analysis shows lower selectivity and sensitivity. However, it offers a faster signal response, typically within a minute, and does

not rely on bulky specialized instrumentation, or need for sample treatment, making it more suitable to portable detection and easier to implement. Additionally, the linear behaviour of limiting current with concentration in range of interest makes the generation of calibration curves relatively easy.

## Chapter 3 Methodology

In this chapter, the major methods and techniques used in this project were summarized. For the highest activity and accurate results, all the solutions used in this project were prepared fresh as described in this Chapter. The method for cut single-wall carbon nanotubes (cut-SWCNT) was included. The enzyme immobilization methods were introduced in detail, including the immobilization of superoxide dismutase (SOD), xanthine oxidase (XOD) using a layer-by-layer structure with poly(dimethyldiallylammonium chloride) (PDDA) and horseradish peroxidase (HRP) using a cross-linking technique with 1-pyrenebutyric acid N-hydroxysuccinimide ester (PBSE). Because the electrochemical analysis was used for the quantitative measurement of the superoxide and hydrogen peroxide, the electrodes, screen-printed electrodes, cells, and equipment (potentiostats) were introduced in detail. The main electrochemical parameters used in this project for two electrochemical characterisations, cyclic voltammetry (CV) and chronoamperometry (CA), were summarised, including scan rate, time and potential conversions. The data processing and calibrations obtained from the recorder were also mentioned.

### 3.1 Experimental preparation

All the chemicals used in this project, including  $K_2HPO_4$ ,  $KH_2PO_4$ , HCl, PDDA, PBSE, DMF,  $H_2O_2$ , xanthine, NaOH,  $H_2SO_4$ ,  $HNO_3$ , carbon nanotubes, and the enzymes including SOD, HRP and XOD were purchased from Sigma-Aldrich (Dorset, UK). The blood sample was collected fresh from the fingertip of two healthy volunteers under the help of research fellows in School of Medicine, stored in 4 °C icebox and was used within four hours. The project was collaborated with others in obtaining the necessary ethical approvals and data access. The blood collections and detections were finished with the help of Prof. Birch-Machin's group in Medical School, and followed the protocols, which were reviewed by the Newcastle university ethical committee (protocol number ET13-002).

#### 3.1.1 Solution preparation

0.1 M phosphate-buffered solution (PBS) was prepared by mixing 80.2 ml 1M  $K_2HPO_4$  and 19.8 ml 1 M  $KH_2PO_4$  and diluted to 1 liter with deionized water followed by adjusting pH to 7.4 by HCl. PDDA (20% w/w in  $H_2O$ ) was diluted to 1% with deionized water. PBSE solution was prepared by dissolving in dry DMF to 5 mM.

The enzyme (SOD and XOD) stock solutions were respectively dissolved into PBS to 0.5 g/ml, and the 3 mg/ml enzyme solutions were prepared fresh every few days from stock solutions. HRP was dissolved into PBS to prepare 10 mg/ml HRP solution and stored in a 4 °C fridge.

For a series of the detection with different concentrations of H<sub>2</sub>O<sub>2</sub> and xanthine, stock solutions (1 M H<sub>2</sub>O<sub>2</sub> in deionized water and 50 mg/ml xanthine sodium salt in 1 M NaOH) were prepared priorly and stored in a 4 °C fridge. 1 ml 10 mM and 1 mM H<sub>2</sub>O<sub>2</sub> stock solution were respectively prepared fresh before use by diluting 1 M H<sub>2</sub>O<sub>2</sub> solution with PBS. Similarly, xanthine sodium salt was respectively diluted to 10 times and 100 times solution before each series of detections.

For the blood sample tests, the freshly collected blood was diluted 20, 40, 60, 80 and 100 times with PBS and stored in an icebox filled with the crushed ice. The diluted blood sample was pipetted several times for a good mixture and detected immediately.

All the prepared solutions were stored in a 4 °C fridge when not in use, and PBS for the electrolyte was placed in the oven at 30 °C for 10 minutes to make sure the temperature reached room temperature before the detections.

### *3.1.2 Modification of carbon nanotube by acid cutting*

Single-wall carbon nanotube (SWCNT) is one of the important supporting materials and the commonly used electrical conductor in electrochemical biosensors. However, the length of the original SWCNT up to several hundred micrometers exhibits high hydrophobicity and limits its processability (Kierkowicz et al. 2018). Short and functionalized SWCNT presents a higher dispersibility, good biocompatibility and excellent transport properties for ions and electrons (Ali-Boucetta et al. 2013, Neves et al. 2012).

As one of the efficient methods to shorten the length of SWCNT, the strong oxidizing acids (sulfuric / nitric acid) mixtures with the ultrasound are usually used for cutting SWCNT on a large scale (Dai and Wang 2021). This method cuts SWCNTs by destroying the carbon bonds with oxidizing acids and breaking long SWCNTs with ultrasonication, and the formation of the carboxyl functional group at the open end of SWCNTs increases with the increasing cutting time (Ziegler et al. 2005). Under low-temperature conditions, this method reduces sidewall damage and carbon loss of SWCNTs caused by oxidation, and the high power density of ultrasound increases the cutting rate, resulting in length distribution of around 50 – 200 nm in

the cut SWCNTs (He et al. 2013, Shuba et al. 2012). The effect on the electron transport characteristics of SWCNT by acid treatment was reported to be reduced at low temperatures (below 8 °C) (Dai and Wang 2021).

To obtain aqueous nanomaterial dispersions, this project used the mixture of sulfuric acid (H<sub>2</sub>SO<sub>4</sub>, 95%) and nitric acid (HNO<sub>3</sub>, 65%) at the ratio of 3:1 as the oxidizing acid to cut the longer nanotubes into short (Liu et al. 1998, Zhang et al. 2003). 50 mg SWCNT was dissolved in 50 ml mixed acid and sonicated for 4 hours. The solution then was diluted with 100 ml deionized water followed by standing for two days. The upper solution was removed, and the lower solution was centrifuged at room temperature for 60 seconds to separate the SWCNT from the acid. The SWCNT was washed with deionized water until acid was removed completely, followed by drying in the oven at 60 °C overnight. The dried SWCNT was dissolved in deionized water to prepare 1 mg/ml SWCNT solution followed by sonicating for 3 hours. The prepared SWCNT solution was sonicated for 15 minutes each time before use to get the evenly distributed suspension.

## **3.2 Enzyme-based biosensor fabrication**

All the chemicals used in this project, including PDDA, PBSE, and the enzymes including SOD, HRP and XOD were purchased from Sigma-Aldrich (Dorset, UK). The electrodes used in this project were screen-printed electrodes (SPE). All the electrodes including screen-printed carbon electrode (C-SPE, model DRP-C110), screen-printed cobalt-phthalocyanine/carbon electrode (CPC-SPE, model DRP-410), dual screen-printed carbon electrode (duo-SPE, model DRP-C1110) and the other electrochemical analysis accessories were obtained from DropSens (Oviedo, Spain).

### *3.2.1 Layer-by-layer immobilization for SOD and XOD*

For the immobilization of SOD and XOD, the layer-by-layer self-assembly method was used in this project due to the high simplicity, good versatility and wide compatibility with various enzymes. This method is based on an electrostatic combination with two oppositely charged solutions, i.e., the positively charged PDDA is used to immobilize the negatively charged SOD and XOD enzymes. The surface of SPEs used in this project was examined using scanning electron microscopy (SEM) by previous group research (Şahin 2020), as shown in Figure 3.1, the regular grid structure was showed on the surface of SPEs, which leads to the good

conductivity for electrochemical analysis.

Some research have been suggested the structure of layer-by-layer based on electrostatic combination on screen printed carbon electrodes by characterising the multilayers with cyclic voltammetry, which is considered as a common method to follow the deposition process of multilayer composites films (Barsan and Brett 2015, Şahin et al. 2018, Sassolas et al. 2012). The multilayers usually consist of several repeated bilayers, including an enzyme layer and a polymer layer with the opposite charge to the enzyme. The voltammogram showed increasing current with the increasing number of bilayers on SPEs (Gao et al. 2011). The multilayer deposition process of bilayer containing PDDA and negative charged enzyme, e.g. SOD, was characterised by CV in previous group research.

To immobilize the SOD enzyme (shown as the first two steps in Figure 3.1), 15  $\mu\text{l}$  (for C-SPEs and CPC-SPEs, or 7  $\mu\text{l}$  for duo-SPEs) 1% PDDA was dropped onto the working electrode of SPE for 30 minutes, followed by rinsing with 15  $\mu\text{l}$  (for C-SPEs and CPC-SPEs, or 7  $\mu\text{l}$  for duo-SPEs) deionized water twice to remove the excessive PDDA. Then 15  $\mu\text{l}$  (for C-SPEs and CPC-SPEs, or 7  $\mu\text{l}$  for duo-SPEs) SOD solution (3 mg/ml in 1 M PBS, pH=7.4) was dropped onto the working electrode for 30 minutes, followed by washing with PBS twice. The immobilization of each layer was characterised by electrochemical analysis, cyclic voltammetry, which will be detailed mentioned in Chapter 5.

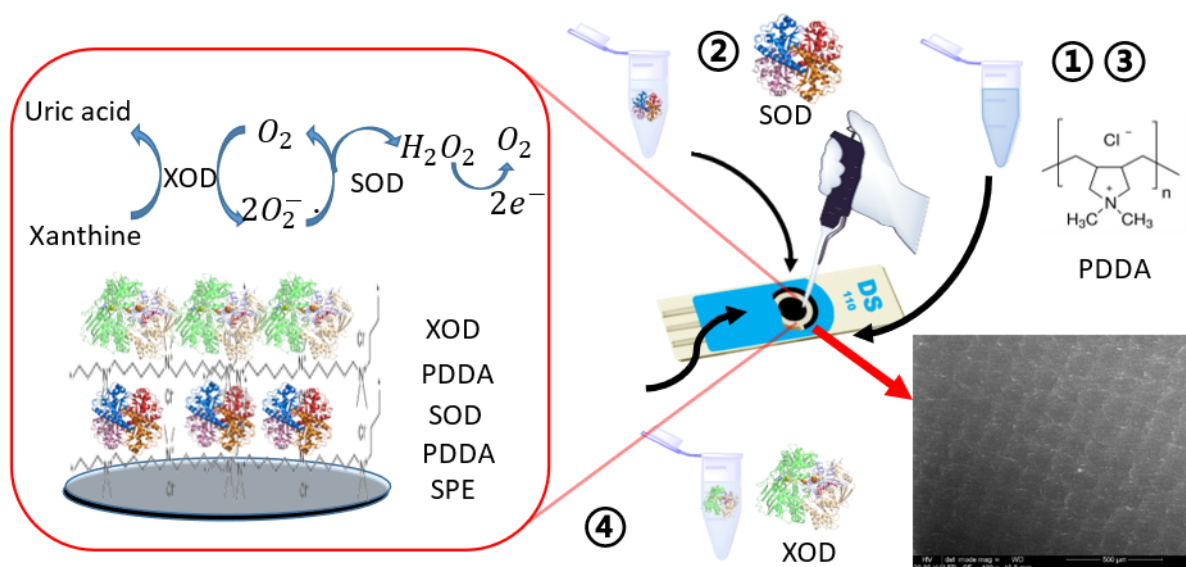


Figure 3.1 (a) Schematic reactions and the layer-by-layer structure on the working electrode of SPEs (left) and the steps of the layer-by-layer self-assembly for the biosensor (right); (b) The SEM of surface of SPE (Şahin 2020).

Superoxide preparation used in this project was the enzymatic reaction of xanthine, which required an additional enzyme layer, XOD immobilized on the top of the enzyme-modified working electrode by 1% PDDA (shown as the third and fourth steps in Figure 3.1). The XOD enzyme layer was used for the generation of the calibration curve for all the above four systems, but not in the biosensor applied for the interferences and blood tests.

### 3.2.2 *Cross-linking immobilization for HRP*

For the HRP enzyme, different from the self-assembly method which is based on an electrostatic combination with two oppositely charged solutions, a cross-linking technique based on the amide bonds was used in this project.

Since the large surface area of carbon nanomaterials leads to a fast response and high conductivity, a successful HRP immobilization by crosslinking could be the binding SWCNT with pyrene derivatives (Şahin 2020). To achieve easy operation and save time, PBSE was used in this project as the binding mediator of the HRP enzyme by cross-linking technology. PBSE contains a pyrene and an amine-reactive hydrophobic region, which could be regarded as the intermediate of pyrene and its derivatives after the treatment by EDC-NHS activation (Reuillard et al. 2014). The SWCNT coated carbon electrode connects to the pyrene side of PBSE through strong  $\pi$ - $\pi$  interactions between the sidewall of the nanotube and aromatic organic molecules (Xu et al. 2008). HRP enzyme immobilization is achieved by the reaction between its amine groups and the anchored amine-reactive hydrophobic region of PBSE to form amide bonds (Chen et al. 2001).

Referring to the work published by Samet (Şahin 2020), to immobilize HRP enzyme on the carbon working electrode by cross-linking technique, 0.15 mg/cm<sup>2</sup> SWCNT was first drip-coated on the electrode surface for better performance and easy operation, followed by drying the SWCNT coating with a hairdryer. Then 15  $\mu$ l (for C-SPEs and CPC-SPEs, or 7  $\mu$ l for duo-SPEs) 5 mM PBSE solution was dropped on the SWCNT coating as the crosslinker of HRP enzymes. The PBSE-treated electrode was stored overnight under flowing nitrogen to dry and in a box to avoid light. The HRP enzyme layer was formed by dropping 15  $\mu$ l (for C-SPEs and CPC-SPEs, or 7  $\mu$ l for duo-SPEs) HRP solution (10 mg/ml in 1 M PBS, pH=7.4) onto the PBSE-treated electrode and stored in a box at 4 °C for two days until dry. The process is outlined in Figure 3.2.

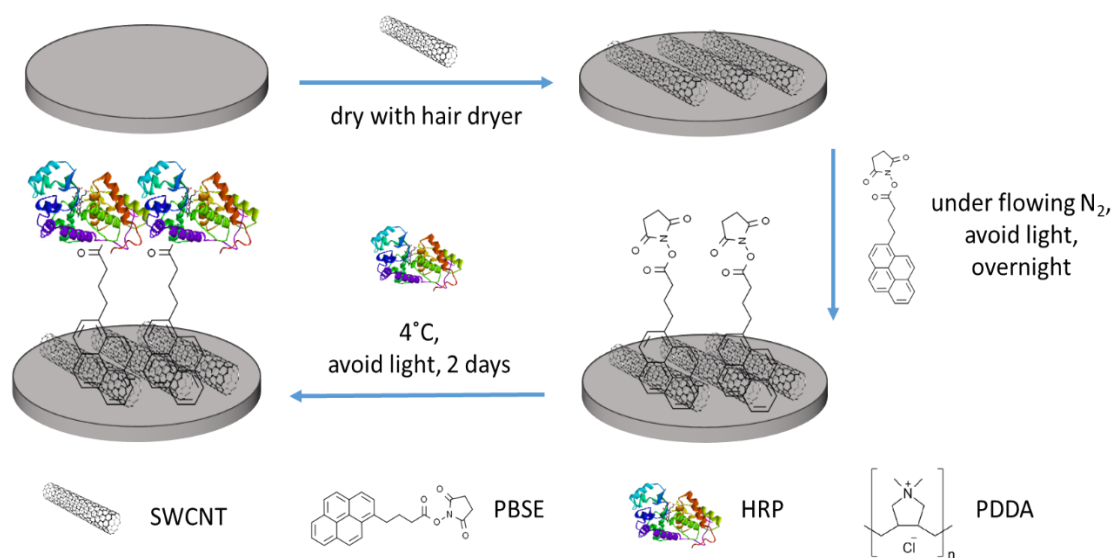


Figure 3.2 Schematic representation of crosslinking of HRP enzymes on SWCNT coated SPEs.

### 3.3 Biosensor set-up and electrochemical measurement

#### 3.3.1 Biosensor set-up

All the electrochemical reactions and measurements were carried out at ambient temperature and pressure. All the electrochemical analysis were carried out by CV and CA using a three-electrode system and a potentiostat. The electrodes for a glass cell vial, including glassy carbon electrode (GCE), counter electrode, alkaline reference electrode, Ag/AgCl reference electrode, were purchased from Alvatek Ltd. (Romsey, UK). As mentioned in Section 3.2, all the SPEs and the other electrochemical analysis accessories were obtained from DropSens (Oviedo, Spain).

For superoxide generation, the effect of dissolved oxygen on the yield of superoxide was carried out by CA using a GCE as the working electrode. The electrodes used in this project, including GCE (3 mm diameter), counter electrode (platinum wire auxiliary electrode, 7.5 cm), alkaline reference electrode (ARE, filled with 1M NaOH) for high pH solutions and an Ag/AgCl reference electrode (filled with 3 M NaCl) were shown in Figure 3.3 (a). The glass cell vial with a total size of 50 mm × 59 mm which contains 5 to 15 ml electrolyte and the Teflon cell top with three holes for fixing electrodes were shown in Figure 3.3 (b). Figure 3.3 (c) shows the electrochemical set-up carried out by Autolab potentiostat-galvanostat.



Figure 3.3 Experiment set-up for electrochemical analysis. (a) The electrodes (from left to right: Ag/AgCl reference electrode, ACE, counter electrode, GCE), (DropSens 2020) (b) the glass cell and (c) the Autolab potentiostat-galvanostat used in research (DropSens 2020).

For the electrochemical measurements and analysis of the biosensors, screen-printed electrodes (SPEs) were used in biosensor fabrication (Chapter 5 to Chapter 7) to achieve the small-volume, low-cost and highly reproducible electrochemical detection.

There were three different types of SPEs used in this project, including screen-printed carbon electrode (C-SPE, model DRP-C110), screen-printed cobalt-phthalocyanine/ carbon electrode (CPC-SPE, model DRP-410) and dual screen-printed carbon electrode (duo-SPE, model DRP-C1110), which were shown in Figure 3.4. The only difference between the SPEs is the working electrode. The size of the working electrode of both C-SPE and CPC-SPE are 4 mm diameter and 12.6 mm<sup>2</sup> of the area, while duo-SPE contains two elliptic carbon working electrodes with the size of 5.9 mm<sup>2</sup> of the area. CPC-SPE contains cobalt-phthalocyanine coatings on the carbon working electrode, while both C-SPE and duo-SPE have bare carbon working electrodes. SPEs contain a carbon counter electrode and a short silver reference electrode (~ 0.074 V vs SHE). The electric contacts are silver and the SPEs have a ceramic substrate with a size of 33 mm length × 10 mm width × 0.5 mm thick. The SPEs were stored at room temperature in a dry box away from light.

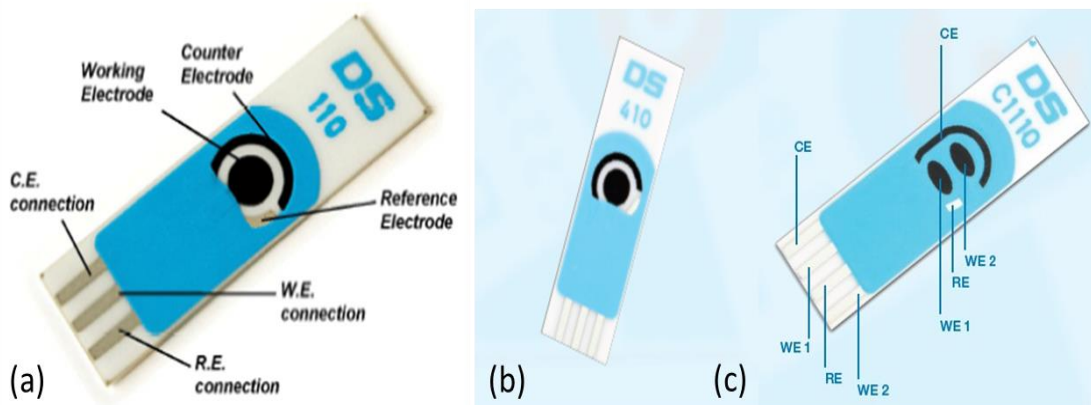


Figure 3.4 The detailed structure of (a) carbon screen-printed electrode, (b) screen-printed cobalt-phthalocyanine/ carbon electrode and (c) dual screen-printed carbon electrode (DropSens 2020)

Cable connectors for C-SPE, CPC-SPE (model CAC) and duo-SPE (model BICAC), shown respectively in Figure 3.5 (a) and (b), were purchased from DropSens (Oviedo, Spain). The red and yellow alligator clip connectors connect to the bottom working electrode (WE1) and the upper working electrode (WE2) respectively. Figure 3.5 (c) and (d) show the types of equipment used for the electrochemical analysis in this project, the Autolab potentiostat-galvanostat (multi autolab cabinet, MAC80126) and (PGSTAT204) respectively.

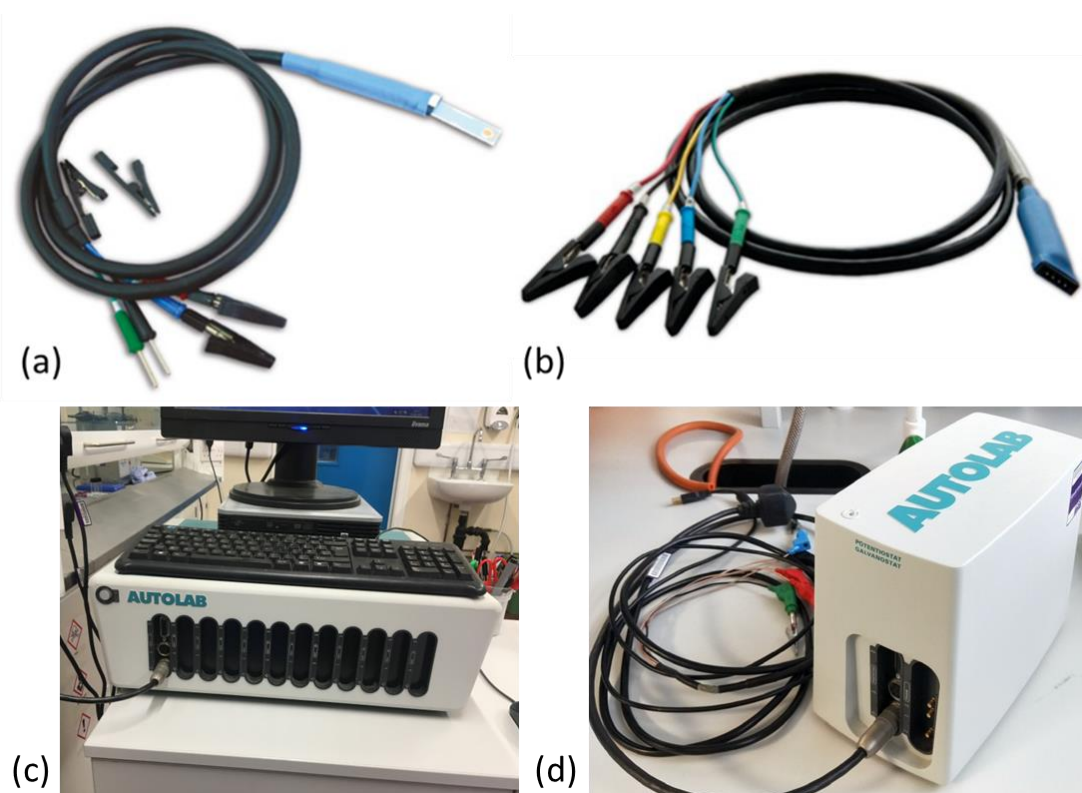


Figure 3.5 Cable connectors for (a) carbon screen-printed electrode and (b) dual screen-printed carbon electrode (DropSens 2020); and Autolab potentiostat-galvanostat (c) multi autolab cabinet, MAC80126

and (d) PGSTAT204.

The red, yellow, blue, black and green alligator clip connectors connect to working electrode 1, working electrode 2, reference electrode, counter electrode and ground respectively.

The cell used for the electrochemical analysis is a cube with a whole size of length 29 × width 29 × height 15 mm. Figure 3.6 shows the disassembled structures of the cell for SPEs, in which the cover with a circular opening and the bottom with a groove of SPE dimensions are fastened by four sets of screws, and could be assembled with the SPE as a cell with a 4 mm diameter cavity in the centre to carry 100  $\mu$ l electrolyte for the detection. A thin rubber gasket with a bit smaller hole was compacted between SPE and cell to guarantee the whole-cell tightness.

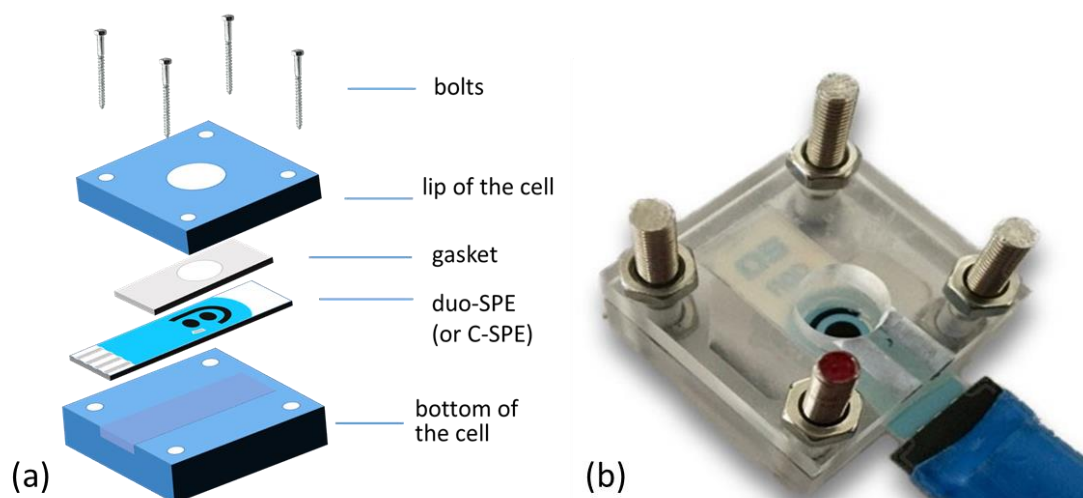


Figure 3.6 (a) The detailed disassembly diagram and (b) the assembled cell for SPEs.

### 3.3.2 Electrochemical measurement

CV is one of the most common electrochemical characterisations for the initial exploration of the electrochemical behaviour of the biosensors. In this project, all the CV scans were carried out three cycles between a potential range with the scan rate of 5 mV/s. In Chapter 5 and 6, CV was applied to determine the potential of the oxidation and reduction of hydrogen peroxide respectively.

CA is also a common electrochemical characterisation that records the current over time at the applied potential. The reaction time was set as 100 seconds for the stable results. With the different reference electrodes in different electrolytes, the applied potential should be converted.

Chapter 4 refers to the different pH of the electrolytes from different  $O_2^-$  preparing methods, so the potential used for the analysis in  $O_2^-$  generation was converted to the potential against

Reversible Hydrogen Electrode (RHE). Ag/AgCl reference electrode and ARE were used in the neutral electrolyte and strong alkaline electrolyte respectively. The potential used for CA was calculated as 1.64 V vs RHE according to equation 3.1 & 3.2:

$$E (vs RHE) = E (vs ARE) + 0.28 V + 0.0591 \times pH \quad (\text{Eq. 3.1})$$

$$E (vs RHE) = E (vs Ag / AgCl) + 0.197 V + 0.0591 \times pH \quad (\text{Eq. 3.2})$$

In Chapter 5 to 7, the potential applied to the biosensor was the potential against a silver reference electrode, which could be converted to the potential against Standard Hydrogen Electrode (SHE) according to equation 3.3:

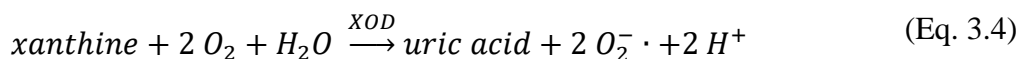
$$E (vs SHE) = E (vs Ag / Ag^+) + 0.074 V \quad (\text{Eq. 3.3})$$

The applied potential for CA to analyse and calibrate the SOD-based biosensor which determining superoxide by the oxidation of H<sub>2</sub>O<sub>2</sub> was set as 0.6 V vs Ag/Ag<sup>+</sup>, while an applying constant voltage of 0.1 V vs Ag/Ag<sup>+</sup> was used in the coupled SOD-HRP biosensor which detecting superoxide by the reduction of H<sub>2</sub>O<sub>2</sub>.

### 3.4 Calculations for the calibrations of superoxide

The electrochemical quantitative measurements were carried out by CA to record currents at a particular potential with the various concentrations of substrates (superoxide or H<sub>2</sub>O<sub>2</sub>). The calibration curves for the SOD-based and coupled SOD-HRP biosensors were generated respectively in Chapter 5 and 6. The superoxide concentration in blood samples was calculated in Chapter 7.

The calibration curve was firstly generated by measuring currents with the various certain concentrations of xanthine and H<sub>2</sub>O<sub>2</sub>. According to reaction equation 3.4 and 3.5, the concentration of superoxide in the electrolytes could be regarded as in the range of two times xanthine (maximum) and two times H<sub>2</sub>O<sub>2</sub> (minimum) concentrations.





The xanthine to H<sub>2</sub>O<sub>2</sub> conversion relationship was determined by correlating the required concentrations of xanthine (Cali. I) and H<sub>2</sub>O<sub>2</sub> (Cali. II) to produce the same current value. The closer the ratio of xanthine to H<sub>2</sub>O<sub>2</sub> is to 1, the smaller the calculated range of superoxide concentrations and the more accurate the measurements will be.

The overall calibration curve for the biosensors (Cali. sensor) was generated by plotting the range of superoxide concentrations calculated from the calibration curve (Cali. I and II) with the current value as the variable. However, for the SOD-based biosensor, the existence of the XOD layer showed positive effects on detection readings, resulting in a current calibration before the generation of the overall calibration curve.

The current calibration was carried out by recording current with various H<sub>2</sub>O<sub>2</sub> concentrations respectively in the presence and absence of XOD (Cali. III). From this result, the relationship between the currents with and without XOD (Cali. IV) was generated in the electrolyte with the same H<sub>2</sub>O<sub>2</sub> concentrations. The current without XOD represents the detected reading from the biosensor, while the current with XOD represents the calibrated current which was used to figure out superoxide concentration from the overall calibration curve (Cali. sensor).

The blood sample test was finished by recording currents corresponding to different dilutions of blood samples. The relationship between currents and dilutions of blood was generated with dilution multiples of 20, 40, 60, 80 and 100, and was used for the estimation of the current corresponding to blood sample without dilutions (I(a)). For the SOD-based biosensor, the bias due to the glucose was considered, and the current (I(a)) was calibrated to I(b) assuming a blood glucose level of 5 mM. Then the current (I(b)) was calibrated to I(c) based on the current calibration curve (Cali. IV). The concentration of superoxide was calculated based on the calibrated current I(c) and the overall calibration curve for the SOD-based biosensor (in Chapter 5). For the coupled SOD-HRP biosensor, the current does not need to be corrected, which means that the concentration of superoxide was calculated based on I(a) and the overall calibration curve for the coupled SOD-HRP biosensor (in Chapter 6).

## Chapter 4 Superoxide generation

In this chapter, the superoxide preparations by different methods were described. A chemical preparation using sodium hydroxide and sodium dithionite for the accurate concentration of superoxide and an enzymatic preparation using xanthine and xanthine oxidase for the neutral environment were compared by ultraviolet-visible spectroscopy (UV). For the single control variable, the effect of the amount of dissolved oxygen was carried out by electrochemical analysis. Since the chemical preparation required a strong alkaline environment, enzyme activity was determined between alkaline, neutral and acidic environments by using sulfuric acid to adjust pH values. The stabilities of prepared superoxide by different methods were compared in 5.5 hours. Results illustrated that enzyme had higher activity in neutral solution, and the enzymatic preparation provided more stable superoxide. Considering the better performance of the prepared superoxide, the enzymatic method was used to generate the calibration curve for superoxide biosensors.

### 4.1 Introduction

Superoxide anions distributed throughout the body usually have a longer half-life than other reactive oxygen species (Sikora et al. 2017). The electrochemical biosensors for superoxide anions detection were commonly reported due to the advantages of high sensitivity, non-destructive and easy to implement (Manning and McNeil 2011). However, superoxide is difficult to maintain in a stable state, which caused widespread concern about the generation of superoxide (Hayyan et al. 2016). The instability of superoxide anions makes their commercialisation a challenge, and the quantitative measurements of superoxide anions requires a sample at a defined concentration as a standard, so it is important to find an efficient preparation method that can determine the concentration of superoxide anions directly or indirectly.

It is reported that many methods were available, including electrochemical reduction of oxygen, photochemical and photocatalytic generations, chemical reactions and biological methods (Bielski and Arudi 1983, Hayyan et al. 2016, Sawyer 1991).

In early, electrochemical reduction of oxygen was demonstrated to be the most simple and direct method due to single putout, and the condition of oxygen reduction reaction was developed with the proper electrolyte that had low viscosity and species-adsorption (Jin et al. 2010). Sawyer and Roberts (1966) discussed the electrochemical behaviour and the electron

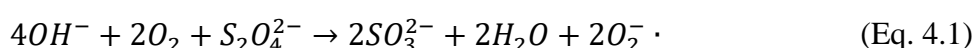
transfer between oxygen and superoxide anion by using platinum, gold and mercury electrodes respectively, provided a successful superoxide generation method in dimethyl sulfoxide (DMSO). However, the condition of no protonic and H<sub>2</sub>O was required to avoid the decomposition of produced superoxide anion (Costentin et al. 2010).

Photochemical and photocatalytic generations is also a common method especially in phytochemistry and photobiology. This method is based on the photochemically initiated electron transfer by high-energy ionizing radiations or vacuum-UV photolysis (Bielski and Arudi 1983). The prepared alkaline aqueous superoxide solutions showed long-term stability, but the thermal instability and the selection of the photocatalyst still be a challenge to this method.

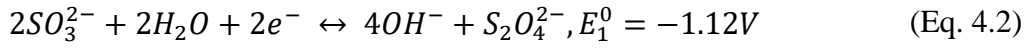
The chemical method for superoxide generation could be summarised into two different ways, the initial one is based on the synthesis of superoxide salts subsequently realising superoxide anion, and the other one is based on the redox reactions in strong alkaline environments (Chin et al. 1982).

Carter et al. (1952) first reported that the superoxide compounds could be generated by the reaction of alkali metals and oxygen at atmospheric pressure. The superoxide salts widely used in superoxide generation are potassium superoxide (KO<sub>2</sub>) or sodium superoxide (NaO<sub>2</sub>) because of the advantages of easy access to materials. However, the various admixtures in the commercial superoxide salts make the purity to be a difficult problem for further reactions and detections (Hayyan et al. 2016). Moreover, the superoxide anion is obtained from the dissolving superoxide salts which have extremely low solubility in aprotic solvents, resulting in the addition of the stimulation components like tetraalkylammonium salts (Moorcroft et al. 2003).

Lambeth and Palmer (1973) discussed the kinetics and mechanism of the electron transfer for the reaction of dithionite, which provided a possible method to generate superoxide anion in the lab environment. The reaction was based on the reduction of the O<sub>2</sub> - O<sub>2</sub><sup>•-</sup> pair and the oxidation of the SO<sub>3</sub><sup>2-</sup> - S<sub>2</sub>O<sub>4</sub><sup>2-</sup> pair in strong alkaline environment. The total reaction is as follow (Weng et al. 1989a):



The standard electrode potential (E<sup>0</sup>) of the SO<sub>3</sub><sup>2-</sup> - S<sub>2</sub>O<sub>4</sub><sup>2-</sup> and the O<sub>2</sub> - O<sub>2</sub><sup>•-</sup> pairs are:

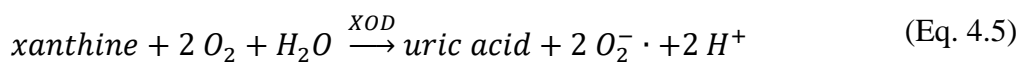


The standard electrode potential of the total reaction could be calculated as:

$$E_{total}^0 = E_2^0 - E_1^0 = -0.563V - (-1.12V) = 0.557V \quad (\text{Eq. 4.4})$$

Thus, the reaction can proceed spontaneously, and the reaction equilibrium constant (K) is calculated as  $7.6 \times 10^{18}$ . The concentration of  $OH^-$  plays an essential role in the reaction that the high concentration leads to the formation of the stable superoxide anion (Hayyan et al. 2016). Since the equilibrium constant of the reaction is large, this reaction can be considered to be completely performed in an alkaline aqueous solution saturated with oxygen, so that the concentration of  $O_2^{\cdot -}$  can be represented by the half of original concentration of  $S_2O_4^{2-}$ .

The biological method for superoxide generation is based on the enzyme-catalysed reaction by xanthine oxidase (XOD), one of the important enzymes in oxidative stress, which can be considered as the crucial source of the superoxide anion in the human body (Cos et al. 1998, Fridovich 1972, Kong et al. 2018, Rahmani et al. 2019). The reaction of the generation is as follows (Kostić et al. 2015):



However, the concentration of generated superoxide is difficult to determine by this method due to the complex reaction process. According to the above reaction equation, the concentration of the produced superoxide could be easily controlled by xanthine concentrations in solution (Kong et al. 2018). Thus, the concentration of the generated superoxide anions should be determined indirectly as a range, with the maximum concentration as the twice xanthine concentration which reacted completely. The minimum concentration of superoxide can be determined by the produced hydrogen peroxide from the disproportionation of superoxide anions, which was mentioned in Chapter 4.4.

The principle of the superoxide determination with superoxide dismutase (SOD) assay kit is

based on the colorimetric method by a UV-vis plate reader. 2-(4-Iodophenyl)-3-(4-nitrophenyl)-5-(2,4-disulfophenyl)-2H-tetrazolium, monosodium salt (WST-1, structure shown in Figure 4.1 (b)) was used as the dye by reduced to the yellow water-soluble formazan in the presence of superoxide anion (Berridge and Tan 1998, Yang et al. 2020). This is the most convenient way to directly tell the changes in the concentration of superoxide and solve the selectivity problem so that not affected by the reduced form of XOD.

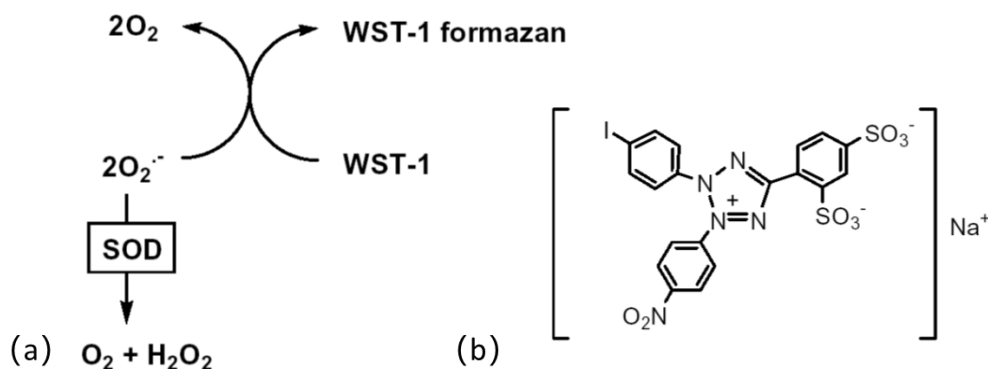


Figure 4.1 (a) The principle of the chromogenic assay for superoxide detection. (b) The structure of the dye (WST-1).

In this research, the generation of superoxide was discussed, and the chemical method based on the redox reaction in the strong alkaline environment and the biological method were compared. The pH effects and the stability of the prepared superoxide were performed by a UV plate reader.

## 4.2 Experimental

### 4.2.1 Materials

Hydrochloric acid (HCl, 37%), sodium hydroxide (NaOH, 1 M solution in H<sub>2</sub>O), sulfuric acid (H<sub>2</sub>SO<sub>4</sub>, 95.0% - 97%), sodium dithionite (Na<sub>2</sub>S<sub>2</sub>O<sub>4</sub>, powder), xanthine (≥99.5%), potassium phosphate dibasic (K<sub>2</sub>HPO<sub>4</sub>, ≥98%), potassium phosphate monobasic (KH<sub>2</sub>PO<sub>4</sub>, ≥99%), SOD (from bovine erythrocytes, ≥3,000 units/mg protein) and XOD (from bovine milk, ≥0.4 units/mg protein) and SOD Assay Kit were purchased from Sigma-Aldrich (Dorset, UK).

0.1 M phosphate-buffered solution (PBS, pH = 7.4), xanthine stock solutions and enzyme solutions were prepared fresh every few days as mentioned in Chapter 3.1.1.

#### 4.2.2 *The method of superoxide preparation*

To effectively control the concentration of superoxide in solution, the chemical reaction would be one of the methods. The simplest method is the reaction between sodium hydroxide (NaOH) and sodium dithionite ( $\text{Na}_2\text{S}_2\text{O}_4$ ) with oxygen (Weng et al. 1989b). Superoxide was prepared by adding various concentrations of  $\text{Na}_2\text{S}_2\text{O}_4$  to 2 ml 0.1M NaOH solution with air bubbling for about 10 minutes followed by standing for 30 minutes to guarantee the reaction completely.

Another method for preparing  $\text{O}_2^{\cdot-}$  is the enzymatic reaction which was carried out in the neutral environment. Superoxide was prepared from the oxidation of various concentrations of xanthine and dissolved oxygen in the solution in the presence of the XOD enzyme. The enzyme solution was centrifuged for five seconds for the homogeneous solution before the dilution with 2.5 ml 0.1M PBS (for electrochemical analysis) or dilute buffer (from SOD Assay Kit, for UV spectroscopy).

#### 4.2.3 *Ultraviolet-visible spectroscopy*

UV-vis experiments were made using a spectrometer-based absorbance microplate reader, SPECTROstar Nano (shown in Figure 4.2), which is purchased from BMG Labtech (Ortenberg, Germany). This absorbance microplate reader showed the advantages of fast speed, easy operation and the ability to store individual assay protocols for absorbance measurements.



*Figure 4.2 The spectrometer-based absorbance microplate reader used for the chromogenic assay.*

The 96 well-plate was used to compare the variety of the factors in the same conditions, a

reagent reservoir and multichannel pipette were used to guarantee the same reaction time. Since the peak of the absorbance of the water-soluble formazan dye from the absorption spectrum was at 440 nm (shown in Figure 4.3), the UV analysis can be quantified by measuring the absorbance of samples between the wavelength of 400 to 500 nm.

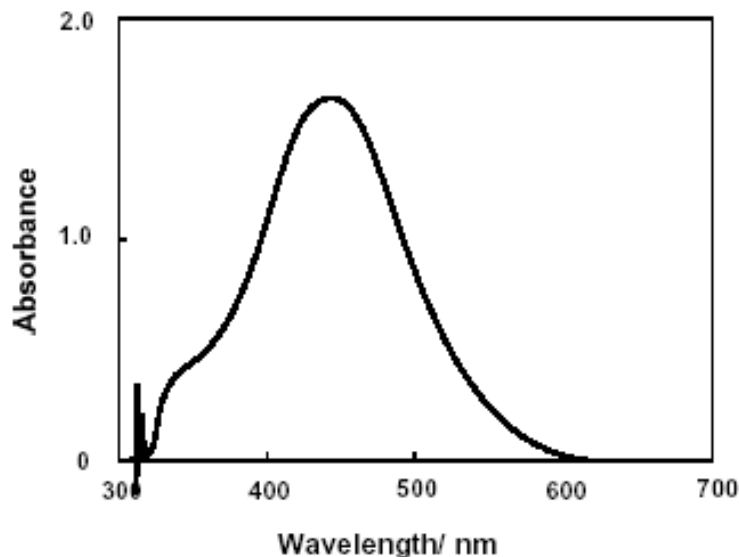


Figure 4.3 The absorption spectrum of WST-1 formazan (from Product Information of SOD Assay Kit)

#### 4.2.4 Electrochemical measurements

All the electrochemistry accessories including glassy carbon working electrode (GCE, 3 mm diameter), counter electrode (platinum wire auxiliary electrode, 7.5 cm), alkaline reference electrode (ARE, filled with 1M NaOH) for high pH solutions, Ag/AgCl reference electrode (filled with 3 M NaCl), the glass cell vial and an electrode polishing kit for GCE were purchased from Alvatek (BASi, Romsey, UK).

In electrochemical analysis, the current response and electron transfer of redox-active species can be obviously affected by the surface of the working electrode, which means the electrode polishing is essential for the reproducible results (McCreery 2008). The GCE was first polished by 1  $\mu\text{m}$  fine diamond polish on a grey grit pad and then applied to 0.3  $\mu\text{m}$  fine diamond polish on a white nylon diamond pad, followed by 0.05  $\mu\text{m}$  alumina on a tan velvet microcloth pad to obtain a mirror-finish polished surface (*Activation of Glassy Carbon Electrodes*). The GCE was rinsed thoroughly with deionized water followed by dried with nitrogen between each polishing step, and ultrasonicated in deionized water for 30 minutes to remove the residual alumina after all polishing steps finished.

The electrochemical analysis was set up as mentioned in Chapter 3.3.1, experiments were carried out by Autolab potentiostat-galvanostat (multi autolab cabinet, MAC80126) using chronoamperometry (CA) in the cell carried 5 ml electrolyte.

### 4.3 Results and discussions

#### 4.3.1 *The determination of control variable for chemical superoxide preparation*

According to the reaction of chemical superoxide preparation, the concentration of reduced superoxide in the strong alkaline solution is controlled by the concentration of  $\text{Na}_2\text{S}_2\text{O}_4$  and the dissolved oxygen in the solution. Since the easy operation of changing and determining  $\text{Na}_2\text{S}_2\text{O}_4$  concentration, the effect of dissolved oxygen in solution was carried out by CA at 1.64 V vs reversible hydrogen electrode (RHE) with 3 mg/ml SOD-immobilised GCE.

The dissolved oxygen in the electrolyte containing 0.1M NaOH was determined by a dissolved oxygen meter between every five minutes of air bubbling. Figure 4.4 (a) indicates the concentration of dissolved oxygen reaches saturation (7.5 mM approximately) after 10-minutes of air bubbling and almost doubled the concentration of dissolved oxygen without air bubbling (4 mM approximately). The data is shown in Appendix Table S1.1.

The electrochemical performance for the reaction was tested in the presence and absence of 5 mM  $\text{Na}_2\text{S}_2\text{O}_4$  respectively, comparing the current response before air bubbling and after 10-minutes air bubbling. Figure 4.4 illustrates that the current response stabilizes at about 100 seconds and increases by about 1.15  $\mu\text{A}$  because of the produced superoxide from  $\text{Na}_2\text{S}_2\text{O}_4$ . In the absence of  $\text{Na}_2\text{S}_2\text{O}_4$ , the current response of high concentration dissolved oxygen electrolyte shows a slight drop compared to lower oxygen concentration electrolyte, the reason would be the increasing concentration of oxygen inhibits the oxidation of  $\text{OH}^-$ . In the presence of  $\text{Na}_2\text{S}_2\text{O}_4$ , the current response of both the electrolyte before and after air bubbling show similar results, which represents air bubbling does not affect the reaction of superoxide preparation and the oxygen is excessive in the electrolyte. In this case, the concentration of  $\text{Na}_2\text{S}_2\text{O}_4$  (which could provide superoxide up to 10 mM) is the only control variable in 0.1 M NaOH solution.

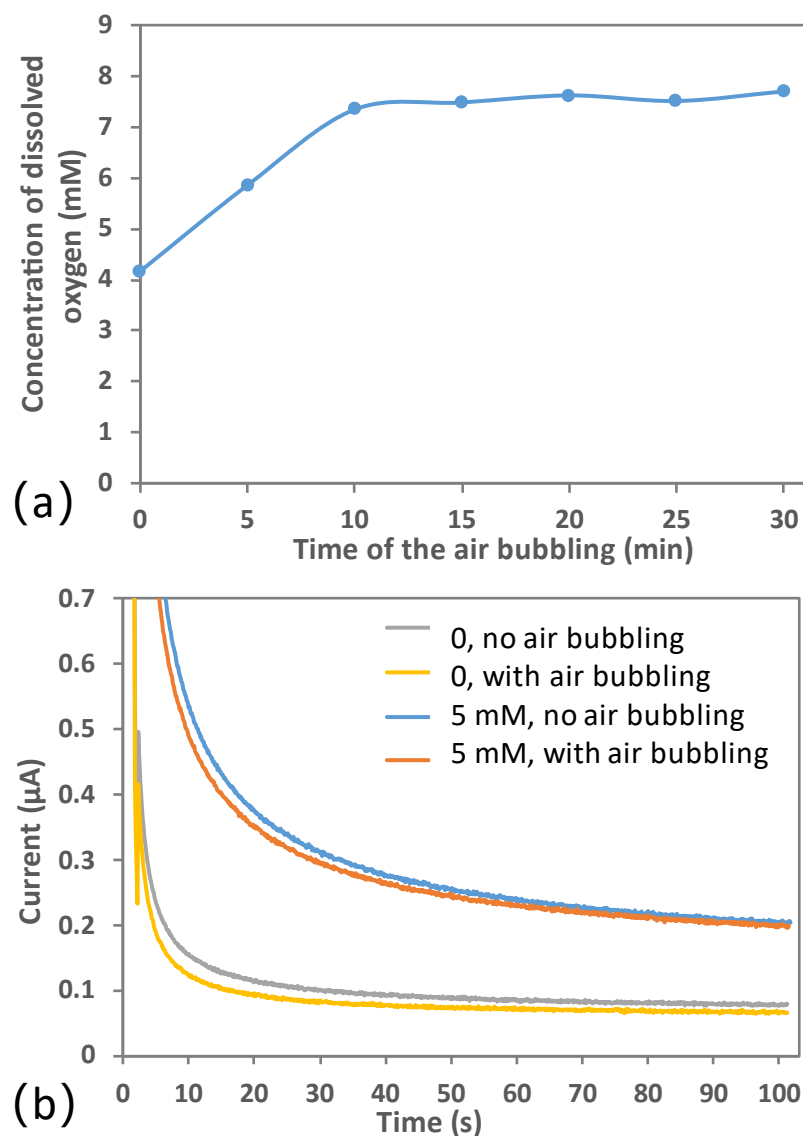


Figure 4.4 The change of concentration of dissolved oxygen with the time of air bubbling. (b) CA of the alkaline solution for superoxide preparation (0 or 5 mM  $\text{Na}_2\text{S}_2\text{O}_4$ ) at 1.64 V for 100 seconds in the presence and absence of 10-min air bubbling.

#### 4.3.2 The pH effect on SOD enzyme activity

To make sure the  $\text{Na}_2\text{S}_2\text{O}_4$  is transformed to  $\text{O}_2^-$  completely, the amount of NaOH must be excessive. Therefore, the solution prepared is a strongly alkaline solution which the pH value would up to 13. However, the activity of the SOD enzyme might be affected by the alkaline electrolyte. In this project, the activity of the SOD enzyme was performed in the strong alkaline, neutral solution and strong acid solution respectively. The alkaline solution was a solution of 0.1 M NaOH containing 5 mM  $\text{Na}_2\text{S}_2\text{O}_4$  after 30 minutes of reaction, the neutral and acid solutions were prepared by adjusting the pH of the strong alkaline solution by  $\text{H}_2\text{SO}_4$ .

The activity measurement of the SOD enzyme was carried out by UV in a 96-well microplate at the wavelength of 440 nm. The experiment set-up is shown in Table 4.1. SOD enzyme was dissolved in dilution buffer (from SOD Assay Kit) to prepare 3 mg/ml enzyme solutions. Except for the SOD enzyme and sample solutions, all other components came from SOD Assay Kit.

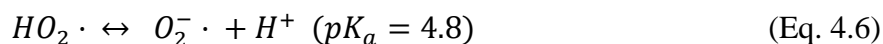
*Table 4.1 The components and the adding order (from top to bottom) for pH effect on SOD activity by UV at 37 °C (Unit:  $\mu$ L; where, O and S present the generated superoxide without and with SOD enzyme respectively)*

	Blank1	Blank2	pH13 <sub>O</sub>	pH13 <sub>S</sub>	pH7 <sub>O</sub>	pH7 <sub>S</sub>	pH3 <sub>O</sub>	pH3 <sub>S</sub>
0.1 M NaOH	20	20	--	--	--	--	--	--
Sample	--	--	20	20	20	20	20	20
Dilution buffer	20	--	20	--	20	--	20	--
SOD solution	--	20	--	20	--	20	--	20
Working solution	200	200	200	200	200	200	200	200
Mix by shaking 30 seconds								

Where O is the measurement of the actual generated superoxide, and S represents the remaining superoxide after the redox reaction in the presence of the SOD enzyme. To guarantee the high activity of the enzyme, the microplate was kept in a 37 °C incubator during the whole procedure.

Figure 4.5 (a) shows the absorbance of the different solutions which represents the concentration changes of superoxide in these solutions with different pH values. The 0.1 M NaOH solutions with and without SOD enzyme were set as the blank control to show the

absorbance of the solution with no superoxide, and the results of samples in acid environment show barely exist of superoxide at pH 3.18. The reason could be the association of superoxide with the hydrogen ion ( $H^+$ ) forms a conjugated acid of the  $HO_2^{\cdot}$  in a low pH environment (Hayyan et al. 2016).



The solution adjusted to pH 7.49 shows a similar absorbance with the samples in alkaline solution (pH 12.81), which means the produced superoxide is still stable in neutral solutions. With the addition of SOD enzymes, both alkaline and neutral solution show a significant drop of absorbance, which means superoxide is catalysed and SOD enzyme has activity in both solutions. Compared with the alkaline solution, the absorbance at pH 7.49 shows the larger drop while adding the SOD enzyme, which illustrates the higher activity of the enzyme.

The superoxide concentration and the activity of the SOD enzyme were calculated from absorbance and shown in Figure 4.5 (b) (data can be found in Appendix Table S1.2). The concentration of superoxide was calculated from the calibration curve of the absorbance changes with various concentrations of superoxide, which is shown in Appendix Figure S1.1. In the presence of the SOD enzyme, the concentration of superoxide dropped from about 10 to 6 mM in the alkaline environment and decreased from about 10 to 4 mM in neutral solution, which shows the amount of catalysed superoxide in neutral solution is 1.5 times of that in alkaline solution. The activity of the SOD enzyme (inhibition rate %) was calculated based on equation 4.7:

$$SOD \text{ activity} = \frac{(A_{sample\ 0} - A_{blank\ 1}) - (A_{sample\ S} - A_{blank\ 2})}{A_{sample\ 0} - A_{sample\ S}} \times 100 \quad (\text{Eq. 4.7})$$

Where A is the absorbance of the solutions. The results show that the activity of the SOD enzyme in neutral solution is about 10 % higher than in alkaline solution, which indicates high pH has effects on the activity of enzymes. For the higher enzyme activity and good stability of superoxide, adjusting the pH of the superoxide solution to neutral is acceptable.

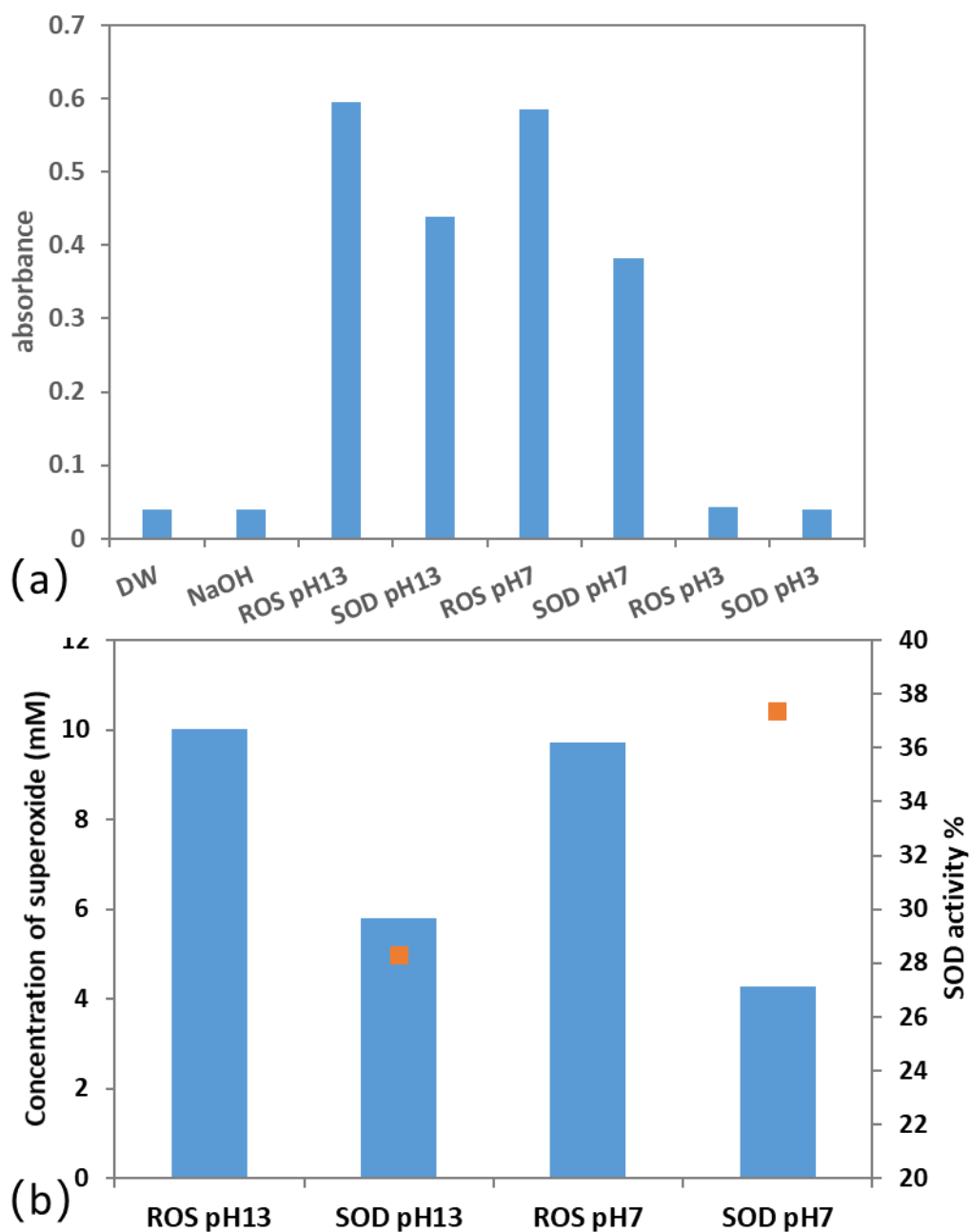


Figure 4.5 (a) Absorbance for the solutions with different pH in the presence and absence of SOD enzyme. (b) The calculated superoxide concentration and SOD activity in solutions with different pH.

#### 4.3.3 The stability of different superoxide preparations

To achieve the superoxide determination by an electrochemical biosensor, the stability of the prepared superoxide is an essential part of the calibration. Two superoxide preparation, chemical one by NaOH and  $\text{Na}_2\text{S}_2\text{O}_4$  and enzymatic one by xanthine and xanthine oxidase, were compared by measuring absorbance with some of the solutions in the SOD Assay Kit. The solution of chemical superoxide preparation (pH 12.81) and the solution been adjusted to neutral from chemical preparation (pH 7.49) were both involved in this project. The

experimental set-up was shown in Table 4.2.

*Table 4.2 The components and the adding order (from top to bottom) for the stability of the prepared superoxide by UV*

	Blank	Enzymatic method	Chem-pH13	Chem-pH7
Deionized Water	20	--	--	--
Xanthine solution	--	20	--	--
Sample	--	--	20	20
Dilution buffer	20	--	20	20
XOD enzyme solution	--	20	--	--
Working solution	200	200	200	200
Mix by shaking				

Xanthine solution was prepared as 5 mM in deionized water, the sample was prepared by 0.1 M NaOH and 5 mM Na<sub>2</sub>S<sub>2</sub>O<sub>4</sub>, and XOD enzyme solution contains 3 mg/ml XOD in dilution buffer. Dilution buffer and the working solution used in this assay were from SOD Assay Kit. All the components were mixed, kept and measured in a 37 °C incubator for the highest enzyme activity. UV scan was performed respectively after 0.5, 1.5, 3.5 and 5.5 hours at 400 to 500 nm.

Figure 4.6 shows the concentration change of superoxide by different preparation methods in several hours (data shown in Appendix Table S1.3). The prepared superoxide is about 9 to 10 mM for both two methods after the reactions and kept stable in half an hour. After 0.5 hours, the concentration of the pH-adjusted chemical-generated superoxide dropped dramatically as time went by. The chemical prepared superoxide without pH adjustment kept stable until 3.5 hours and then the concentration of that decreased rapidly. Surprisingly, the concentration of enzymatic prepared superoxide only shows a light change in 5.5 hours, which illustrates the

superoxide prepared has good stability in this preparation environment and could provide enough time for the detection procedures.

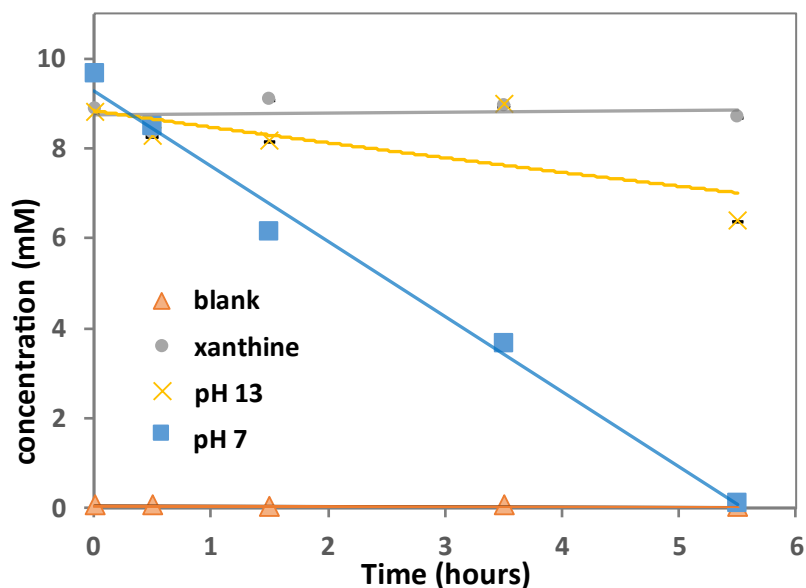


Figure 4.6 The concentration changes of superoxide anion prepared from different generations in 5.5 hours. Error bars are the sample standard deviation of measurements from repetitions ( $n = 3$ ).

#### 4.4 Conclusions

In this chapter, two methods for superoxide generation were described and compared. In order to achieve a single control variable, dissolved oxygen and NaOH was kept in excess in solution. Since the strong alkaline environment required for chemical preparation, pH effects on the activity of the SOD enzyme and the stability of superoxide were carried out by UV with SOD Assay Kit. Results show that enzyme activity in neutral solution is about 10 % higher than in alkaline solution, but superoxide becomes unstable in the acid-adjusted solution. Although it is easy to determine the concentration of prepared superoxide by chemical method, the strong alkaline shows an obvious effect on SOD enzyme activity and the acid-adjustment solution could affect the stability of superoxide. Thus, compared with the chemical preparation, the enzyme-generated method showed 10 % higher enzyme activities and good stability of generated superoxide for at least 5.5 hours, which is easier to achieve the determination of the electrochemical biosensor.

## Chapter 5 Development of the electrochemical biosensor based on oxidation reaction of hydrogen peroxide

In this chapter, the biosensor based on the oxidation reaction of  $\text{H}_2\text{O}_2$  was developed for superoxide detection and the interference tests were performed. The enzyme superoxide dismutase (SOD) used for transforming superoxide to the easy-detectable component  $\text{H}_2\text{O}_2$  and xanthine oxidase (XOD) used for superoxide preparation were immobilized on the working electrode as a layer-by-layer structure by the electrostatic forces. Electrochemical characterization of the reactions was performed in potassium phosphate-buffered solution (PBS) with different concentrations of  $\text{H}_2\text{O}_2$  or xanthine by using cyclic voltammetry (CV) and chronoamperometry (CA). Single-wall carbon nanotube (SWCNT) and screen-printed electrode (SPE) with cobalt-phthalocyanine (CP) coatings were used for enhancing the performance of the biosensor. Carbon SPE with SWCNT coating showed the increasing sensitivity and accuracy of the detection, and the calibration curve was generated based on this system. Interference tests showed the effect of some main components in blood like glucose on the detection.

### 5.1 Introduction

With the rapidly increasing serious problem of the ageing population, the prediction of age-related diseases becomes more important over years, resulting in the detection of the pathogenic factor (superoxide) of many ageing diseases being a worldwide issue (Heitzer et al. 2001). Among many analytical detection techniques for superoxide detection, such as fluorescent probes, spectrophotometry, electron spin resonance (ESR), fluorescent proteins, chemiluminescent probes and electrochemical biosensors, the electrochemical biosensor has been widely used as a quantitative monitoring method due to the advantage of simple pre-treatment processing, inexpensive instruments, fast analysis, high sensitivity, easy operation and quantitative detection (Balamurugan et al. 2018, Głód et al. 2000, Greenwald 2018, Münzel et al. 2002, Zhang et al. 2018, Zhao et al. 2005).

As a commonly used enzyme for the electrochemical biosensor to detect superoxide, unlike the non-specific catalyst Cyt. c which shows the catalytic activity to reduce oxidants including  $\text{H}_2\text{O}_2$  and ONOO, SOD has strong activity and great specificity towards the disproportionation reaction of superoxide as a catalyst. Superoxide could be rapidly disproportionated to produce  $\text{H}_2\text{O}_2$  and oxygen in the presence of SOD (Mao et al. 2008):



Although the redox reaction could be seen as two separated charge transferred reactions as mentioned in Section 1.2.2, it is accepted that the active sites of the enzymes are covered with thick insulating protein shells resulting in the difficulty of direct electron transfer between enzymes and electrodes (Carrico and Deutsch 1970). To quantitatively detect the concentration of superoxide by the electrochemical biosensor, one of the simplest ways is to detect the produced  $H_2O_2$  from SOD enzymatic reaction with the  $H_2O_2$  detection as the calibration.  $H_2O_2$  could be both oxidized and reduced at high potentials but the oxidation showed significantly more sensitivity than reduction without the catalysts (Goran et al. 2015), thus the electron transfer reaction on the working electrode could be regarded as the reaction shown in equation 5.2 (Pourbaix 1974):

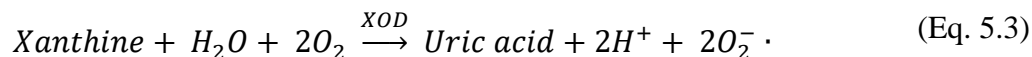


One of the most crucial aspects of the establishment of an electrochemical biosensor is the fabrication of the enzymatic electrode because the immobilized enzyme improves the reusability, stability and mechanical strength and is more suitable for the use of multi-enzyme systems (Chang 2013). To immobilize the enzymes on the working electrode, many enzyme immobilization techniques are described in enzyme engineering, such as affinity-tag binding, physical adsorption, physical entrapment, classical covalent and cross-linkage (Homaei et al. 2013). All immobilizing techniques have their specific advantages and limitations in the application.

As one of the most potential techniques for enzyme immobilization, the layer-by-layer self-assembly method has the advantages of simplicity, versatility and wide compatibility with various enzymes (Bertrand et al. 2000). The technique is based on the electrostatic force between two polyelectrolytes with opposite charges to achieve self-assembly, which could immobilize enzymes without dehydration or chemical reactions and avoid the loss of the biological activity of the enzyme (Kang et al. 2014). Since the charge of the enzyme depends on the isoelectric point and the pH of the solution, SOD has a negative charge at pH 7.4 (the isoelectric point is 4.95), so the polycation is a good binder for layer-by-layer assembly technique (Firdoz et al. 2010). As a high charge density cationic polymer,

poly(dimethyldiallylammonium chloride) (PDDA) has a good affinity to carbon nanotubes and could be well adsorbed on carbon electrodes (Alexeyeva and Tammeveski 2008).

As mentioned in Chapter 4, the instability of superoxide required another enzymatic reaction for superoxide preparation (Derkus et al. 2015, Emregül 2005):

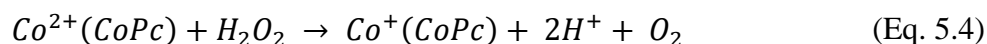


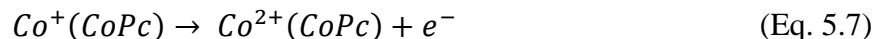
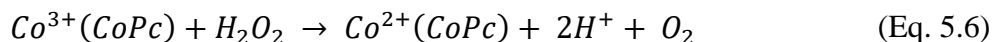
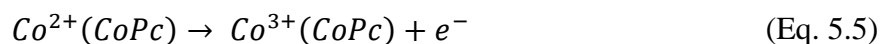
Since the isoelectric point of xanthine oxidase is 5.3 which carries a negative charge in a neutral solution (pH = 7.4), layer-by-layer immobilizing methods are available for the multi-enzyme system by PDDA.

Many researchers reported the feasibility of the XOD/SOD multi-enzyme system for superoxide detection. Song et al. (1995) introduced a superoxide biosensor using XOD/Teflon membrane/SOD/platinum working electrode for the quantitative analysis and showed the detection limit of 15  $\mu\text{M}$ . Emel (2005) described a method to determine superoxide immobilizing SOD on the platinum electrode with gelatin and using XOD and xanthine added in solution for superoxide generation with the reported detection limit of 10  $\mu\text{M}$ . Although these biosensors showed high selectivity for superoxide detection, the lack of sensitivity and accuracy were still the challenges with the untreated working electrode.

To improve the electrochemical performance of the biosensor, the development of  $\text{H}_2\text{O}_2$  detection attracts the researcher's attention. Due to the strong electrochemical catalytic activity for  $\text{H}_2\text{O}_2$  oxidation reaction, cobalt-phthalocyanine is widely used for better performance in  $\text{H}_2\text{O}_2$  detection (Ji et al. 2020, Wang et al. 2015). Kondo et al. (2008) reported a boron-doped diamond electrode modified by cobalt-phthalocyanine and proved the catalytic activity for the oxidation reaction of  $\text{H}_2\text{O}_2$ . An enzymeless and mediatorless  $\text{H}_2\text{O}_2$  sensor was described by Çeken et al. (2012) with the composite electrode modified by polyaniline and cobalt-phthalocyanine which increased the conductivity.

The reaction mechanism of the  $\text{H}_2\text{O}_2$  detection under the catalysis of cobalt-phthalocyanine is as following reactions shown as equation 5.4 to equation 5.7 (Ji et al. 2020):





Nanomaterials are also an effective way to improve the bioanalytical performance of the electrochemical biosensor due to low capacitance, high current density and large surface area. As an electrocatalytic material, SWCNT has a promising application in biological and medical research areas because of its excellent thermal, elastic, electrical and mechanical properties (Goran et al. 2015, Guerrero et al. 2020, Kim et al. 2011). Liu et al. (2014) reported a cheap, selective and sensitive H<sub>2</sub>O<sub>2</sub> biosensor by using palladium-coated carbon nanotube fibre microelectrode due to the large surface area and good mechanical strength of carbon nanotube and high electrocatalytic activity of palladium. The biosensor showed the current range of 0.002 to 1.3 mM with a sensitivity of 2 Acm<sup>-2</sup>M<sup>-1</sup> and detection limit of 2 μM. Bhattacharya et al. (2019) detected H<sub>2</sub>O<sub>2</sub> by using specific DNA-wrapped SWCNT to achieve the precisely monitor for drug therapeutic efficacy of pancreatic ductal adenocarcinoma treatment. Ren et al. (2017) introduced a directly electron-transfer H<sub>2</sub>O<sub>2</sub> biosensor by using SWCNT, horseradish peroxidase and 1-butyl-3-methylimidazolium tetrafluoroborate, and achieved high sensitivity of 4 Acm<sup>-2</sup>M<sup>-1</sup> for H<sub>2</sub>O<sub>2</sub> detection in the chemical environment.

In this research, the electrochemical biosensor based on the oxidation reaction of H<sub>2</sub>O<sub>2</sub> was established and analysed by electrochemical techniques, and the enzyme-modified electrode was developed for better performance.

## 5.2 Experimental

### 5.2.1 Materials and Equipment Used

SWCNT (powder, diam. 1.1 nm × length 0.5-100 μm), H<sub>2</sub>O<sub>2</sub> (solution, 35% wt. in H<sub>2</sub>O), H<sub>2</sub>SO<sub>4</sub> (95%), HNO<sub>3</sub> (65%), xanthine (≥99.5% (HPLC), purified by recrystallization) were purchased from Sigma-Aldrich (Dorset, UK). PDDA solution, 0.1 M phosphate-buffered solution (PBS), the enzyme solutions (both SOD and XOD), xanthine and H<sub>2</sub>O<sub>2</sub> stock solutions were prepared fresh as mentioned in Chapter 3.1.1.

SPEs used in biosensor, screen-printed carbon electrode (C-SPE, model DRP-C110) and screen-printed cobalt-phthalocyanine/carbon electrode (CPC-SPE, model DRP-410), which were mentioned in Chapter 3.3.1, were obtained from DropSens (Oviedo, Spain).

The equipment used for all the electrochemical analysis was Autolab potentiostat-galvanostat (PGSTAT204) which was mentioned in Chapter 3.3.1.

### 5.2.2 *Layer-by-layer enzyme fabrication on SPE*

For easy operation, this project used the combination of the self-assembly method and layer-by-layer electrostatic interaction (Alexeyeva and Tammeveski 2008). This method is based on an electrostatic combination with two oppositely charged solutions. As a high charge density cationic polymer, 1% PDDA was used to immobilize the enzymes (both SOD and XOD) which carried negative charge at pH 7.4.

Based on Kang's layer-by-layer immobilizing method (Kang et al. 2014), four systems of biosensors were modified for comparison (shown in Figure 5.1). For C-SPE/enzymes system and CPC-SPE/enzymes system, the fabrication simply involved dropping and rinsing PDDA or the enzyme solutions on the corresponding SPEs in the order mentioned in Chapter 3.2.1. To fabricate the C-SPE/SWCNT/enzymes system, PDDA and enzymes were immobilized on the top of the working electrode of C-SPE with  $0.15 \text{ mg/cm}^2$  SWCNT coating which was prepared by dropping 1 mg/ml SWCNT solution followed by drying under a hot-air heating gun. CPC-SPE/SWCNT/enzymes system was established by immobilizing SWCNT coating followed by PDDA and enzymes on CPC-SPE.

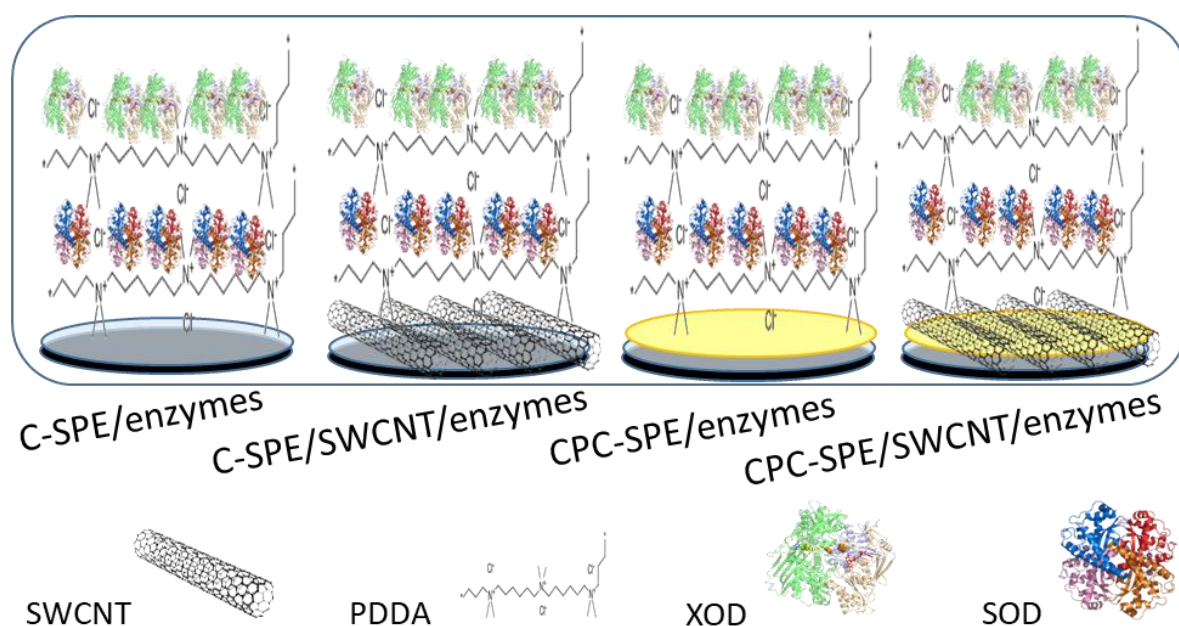


Figure 5.1 The structure of the four systems for the biosensor.

### 5.2.3 Electrochemical Measurements

The electrochemical measurements were carried out by a potentiostat-galvanostat with a small cell containing 100  $\mu\text{l}$  electrolyte. CV scans between a potential range with the scan rate of 5 mV/s and CA at 0.6 V vs Ag/Ag<sup>+</sup> for 100 seconds were used for the analysis.

The electrolytes were prepared fresh before each series of electrochemical tests. For a series of the detection with different concentrations of H<sub>2</sub>O<sub>2</sub> and xanthine, the electrolytes were prepared by adding certain amount of stock solutions (10 mM and 1 mM H<sub>2</sub>O<sub>2</sub>, 10- and 100-times diluted xanthine sodium salt, mentioned in Chapter 3.1.1) into 100  $\mu\text{l}$  PBS. For the interference tests, a certain amount of glucose, uric acid (UA), ascorbic acid (AA) (Mao et al. 2008) and bovine serum albumin (BSA) were respectively added to PBS to prepare the electrolytes in the absence of H<sub>2</sub>O<sub>2</sub>. Each series of the interference tests with various H<sub>2</sub>O<sub>2</sub> concentrations were finished by changing the amount of H<sub>2</sub>O<sub>2</sub> stock solutions being added to the electrolytes.

## 5.3 Results and discussions

### 5.3.1 Performance of SOD towards H<sub>2</sub>O<sub>2</sub> and superoxide detection

SOD and XOD immobilized C-SPE by layer-by-layer self-assembly was analysed by cyclic voltammetry electrochemical techniques in 0.1 M PBS at pH 7.4. For the confirmation of the layer immobilization, the CV scan was first carried out after each step of the electrode

modification (bare electrode, first layer of PDDA, SOD enzyme, second layer of PDDA layer, XOD enzyme in that order) (Zhang et al. 2008). The potential range was chosen a large range as -0.4 to 0.8 V vs Ag/Ag<sup>+</sup> based on the potential range of oxidation reaction of superoxide and H<sub>2</sub>O<sub>2</sub> in literature due to the high driving force of metastable H<sub>2</sub>O<sub>2</sub> for the oxidation and reduction reactions (Feng et al. 2016, Goran et al. 2015, Gulaboski et al. 2019). Figure 5.2 shows the electrochemical response with each layer immobilized on the working electrode.

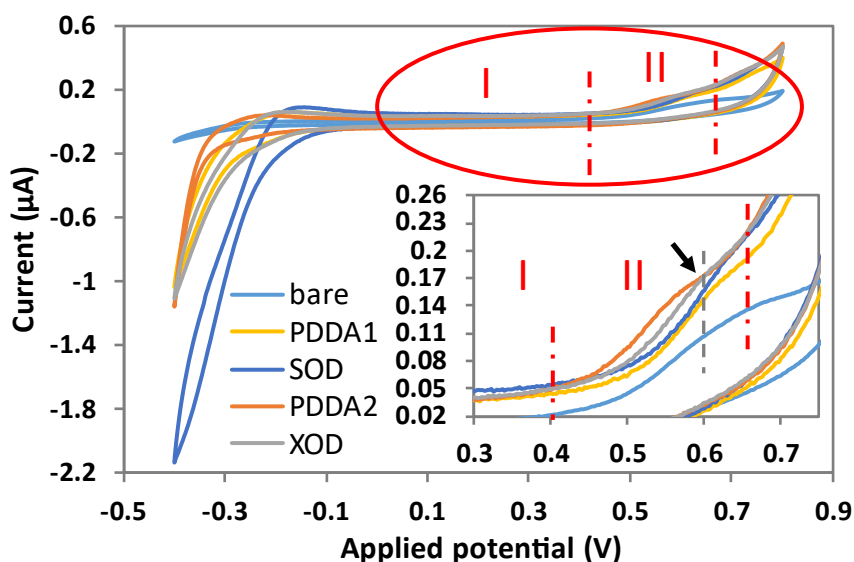


Figure 5.2 Voltammogram for the electrochemical performance of each layer immobilized by layer-by-layer enzyme self-assembly technique.

Tested in PBS (pH = 7.4) with C-SPE (Ag/Ag<sup>+</sup>, 0.074 V vs SHE, surface area of 0.126 cm<sup>2</sup>). The Figure on the right corner is the enlarged vision in the red circle at a high potential. Scan rate: 5 mV/s.

From Figure 5.2, in region I, parallel negative and positive charging current can be seen known as double layer region. The average current is around zero, where positive current is seen in positive sweep direction and negative current is seen in negative sweep direction. The double layer current or also known as capacitive current is resulting from charging the electrode and ions adsorption at interface by increasing or decreasing electrode potential and therefore doesn't involve electron transfer to reactive species or Faradic current. At the higher potential (in region II), a sharp increase in current due to the oxidation of carbon working electrode, as well as OH-adsorption starts to be detected and the rate increase with the increasing potential. At around 0.6 V vs Ag/Ag<sup>+</sup>, there is an oxidation peak which can be assigned to reversible adsorption of OH (Katsounaros et al. 2012, Marković et al. 1999, Westbroek and Temmerman 2000). From 0.65 V, the high potential provides the higher driving force for oxidation which rapidly increases the current signal. It is expected that any superoxide or H<sub>2</sub>O<sub>2</sub> present in solution would

also be oxidised in this region but given the similarity in oxidation current between PDDA1, SOD, PDDA2 and XOD, this suggests that the oxidation current seen is dominated by OH-adsorption and working electrode oxidation with current of 0.2  $\mu$ A at 0.6 V.

The reduction current on the other hand changes after each layer are immobilized on the working electrode, which means the self-assembly method works for both SOD and XOD enzymes on SPE and the current would change with the different number of layers. The first addition of PDDA both increases the oxidation and reduction currents which could be because PDDA induces the charge transfer between the electrolyte and the working electrode as a high ion conditioning polymer (Dai et al. 2020). The additional SOD layer also increased the current signal for reduction reaction or shift the onset of reduction by ca. -80 mV. This suggests that the reduction current is kinetically controlled and addition of SOD catalyst/mediator enhances the activity which is in agreement with lack of peak reduction current (Katsounaros et al. 2012). Additional layers additions of PDDA2 results in decline in reduction current activity possibly due to need of reacting species to diffuse through additional layers (Kang et al. 2014). This indicates that the additional layers required on electrode surface for superoxide preparation could have effects on the detection current and should be considered in the calibration curve.

With both SOD and XOD immobilized by self-assembly method, CV was also scanned respectively in 0.1M PBS solution with and without 0.5 mM  $H_2O_2$  for the electrochemical performance of the biosensor based on enzyme-modified C-SPE. The potential range was obtained from Figure 5.2 from region I to the oxidation peak, i.e. 0 to 0.6 V vs Ag/Ag<sup>+</sup>. The repeatability of enzyme immobilisation was tested by performing CV scans on three identically modified SPEs. The CV scans were repeated three times in PBS in the presence and absence of  $H_2O_2$ .

The result shows the activity where there was with no added  $H_2O_2$  in the solution (the blue line) reaches around 0.2  $\mu$ A at 0.6 V which is similar to Figure 5.2. The electrochemical response of the biosensor to  $H_2O_2$  (the orange line in Figure 5.3) shifts from 0.25 V which indicates the detectable oxidation reaction of  $H_2O_2$  started at 0.25 V and the current difference increased with the growth of supplied potential until reaching the largest current difference (the electric signal of 0.5 mM  $H_2O_2$ ) around 0.2  $\mu$ A at 0.6 V. For the sensitive detection, the highest potential 0.6 V was used to get the electric signal response with the different concentration of  $H_2O_2$  in solution.

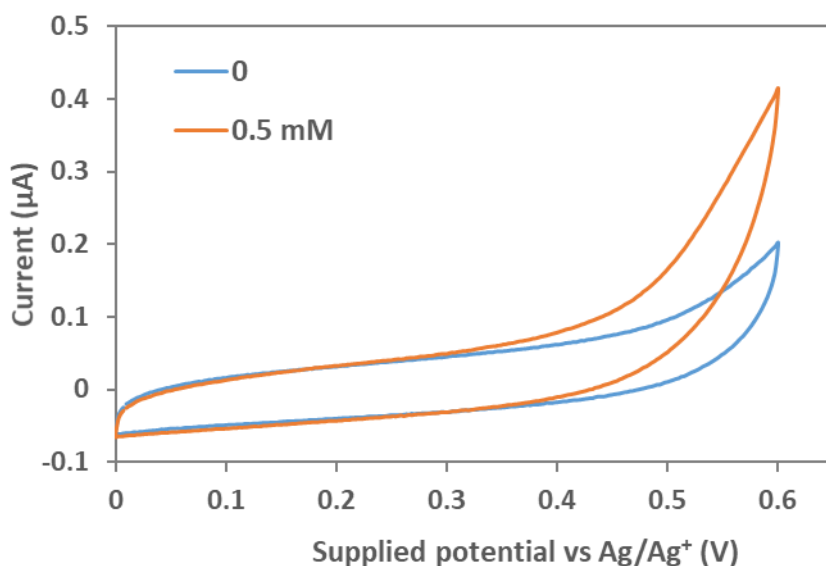


Figure 5.3 CV scans of the fully enzyme-immobilised C-SPE (containing both SOD and XOD) in PBS (pH = 7.4) with 0 mM and 0.5 mM  $\text{H}_2\text{O}_2$ .

The reference electrode is silver ( $\sim 0.074$  V vs SHE) and the surface area of the carbon working electrode is  $0.0126$   $\text{cm}^2$ . Repeating three times on different SPEs for the repeatability. Scan rate: 5 mV/s

Given that the 0.4 to 0.6 V region contains significant contributions from non-Faradaic OH-adsorption, using lower scan rates will result in lower current which should decrease significantly if fixed potential was applied. In the absence of  $\text{H}_2\text{O}_2$ , after 100s, the oxidation current from working electrode substrate and OH- adsorption current decrease to ca.  $0.08$   $\mu\text{A}$  at 0.6 V (Figure 5.4). The calibration curve for  $\text{H}_2\text{O}_2$  detection of the biosensor (Figure 5.4) is generated by a series current value corresponding to different concentrations of  $\text{H}_2\text{O}_2$  (0.01 mM to 0.5 mM in PBS) at 0.6 V vs  $\text{Ag}/\text{Ag}^+$  in the chrono amperometry diagram (Appendix Figure S2.1) at 100 s for a stable current signal. The result shows the linear relationship ( $R^2 = 0.9905$ ) between current and  $\text{H}_2\text{O}_2$  concentration when concentration is higher than 0.05 mM with the sensitivity as  $0.3493$   $\mu\text{A}/\text{mM}$ , and the limitation of concentration of this system, 0.05 mM, is higher than the expected lowest detectable range. At a lower concentration of  $\text{H}_2\text{O}_2$ , the detected current shows random results that approximate the current with no  $\text{H}_2\text{O}_2$  in the electrolyte. This result indicated the biosensor has the detecting limitation of 0.05 mM  $\text{H}_2\text{O}_2$  and/or superoxide. The error bias was obtained from the sample standard deviation of three duplications (the value could be found in Appendix Table S2.1). The large error bias at higher concentration represents the low accuracy of the biosensor on 0.1 mM to 0.5 mM  $\text{H}_2\text{O}_2$  and/or superoxide detection. The lack of accurate detection and low sensitivity of  $\text{H}_2\text{O}_2$  oxidation can be attributed to low efficiency of electron transfer, the limited number of immobilised-enzyme on working electrode, and high potential used for  $\text{H}_2\text{O}_2$  where other reactions and processes take place

including OH<sup>-</sup> adsorption, water oxidation and carbon oxidation/corrosion. Similarly, this was also seen in the literature (Huang et al. 2021, Liu et al. 2022, Wu et al. 2019), highlighting the importance of developments of other methods for H<sub>2</sub>O<sub>2</sub> detection e.g. through reduction.

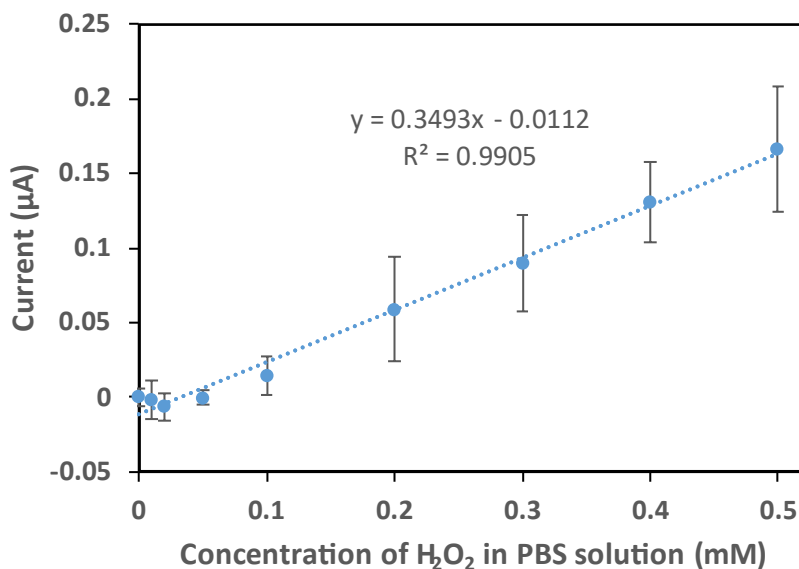


Figure 5.4 The calibration curve for H<sub>2</sub>O<sub>2</sub> detection of the biosensor with the fully enzyme-immobilised (both SOD and XOD) C-SPE (surface area of working electrode: 0.126 cm<sup>2</sup>).

The data was obtained from CA tested in PBS (pH = 7.4) with different concentration of H<sub>2</sub>O<sub>2</sub> (0, 0.01, 0.02, 0.05, 0.1, 0.2, 0.3, 0.4 and 0.5 mM) at 0.6V vs Ag/Ag<sup>+</sup> (~ 0.074 V vs SHE) at 100 s. Error bars are the sample standard deviation of measurements from repetitions (n = 3).

### 5.3.2 Comparison for four systems of biosensor for H<sub>2</sub>O<sub>2</sub> detection

For the better performance of the biosensor, two developments were used on the working electrode. To enhance the sensitivity of the biosensor and broaden the detection range, SWCNT was used to increase the surface area of the working electrode and the amount of the immobilized enzyme as well as the electrical conductivity (Şahin 2020, Zhang et al. 2003). For the ideal detection of H<sub>2</sub>O<sub>2</sub> with the lower concentration, the CPC-SPE was used to replace the C-SPE (Ceken et al. 2012, Sánchez-Calvo et al. 2020).

To improve the sensitivity and accuracy of the oxidation biosensor, three systems, C-SPE/SWCNT/ enzymes, CPC-SPE/ enzymes and CPC-SPE/ SWCNT/ enzymes, were prepared and tested for comparison. CPC-SPE is coated with Cobalt-Phthalocyanine which is an effective electrocatalyst for the H<sub>2</sub>O<sub>2</sub> oxidation reaction. SWCNT was cut into short lengths for the larger surface area and higher current response.

Four systems were compared by CV analysis respectively scanned in 100 µl 0.1 M PBS solution

with and without 0.5 mM H<sub>2</sub>O<sub>2</sub> as the electrolyte at 0 to 0.6 V vs Ag/Ag<sup>+</sup>. To control for consistency of other conditions except for electrode treatments, all four systems were immobilized with both SOD and XOD by self-assembly method as mentioned in Section 4.2.3.

Regarding the onset oxidation potential (the start potential point where the current obtained with H<sub>2</sub>O<sub>2</sub> is higher than without H<sub>2</sub>O<sub>2</sub>), that of CPC-SPE / enzymes system shown in Figure 5.5 is about 0.05 V, while that of the C-SPE/ enzymes system is 0.35 V, which illustrated cobalt-phthalocyanine shift the reaction to the lower potential because the reduction of cobalt III to cobalt II stimulates the oxidation of H<sub>2</sub>O<sub>2</sub> at a lower potential (Li et al. 2013). The peak oxidation current of the CPC-SPE / enzymes system in 0.5 mM H<sub>2</sub>O<sub>2</sub> (yellow line) can be assigned to cobalt II oxidized to cobalt III (Ji et al. 2020). The onset oxidation potential of C-SPE/ SWCNT/ enzymes and CPC-SPE/ SWCNT/ enzymes systems was approximately 0.25 V (the right one of Figure 5.5), similar to the C-SPE/ enzymes system. The reason could be SWCNT was covered over the cobalt-phthalocyanine coating on the carbon electrode so that the large beneficial difference in conductivity and the active surface area on addition of SWCNT on charge transfer is greater than that of cobalt-phthalocyanine. This can be seen from the difference in current magnitude between the right and left figures of 5.5.

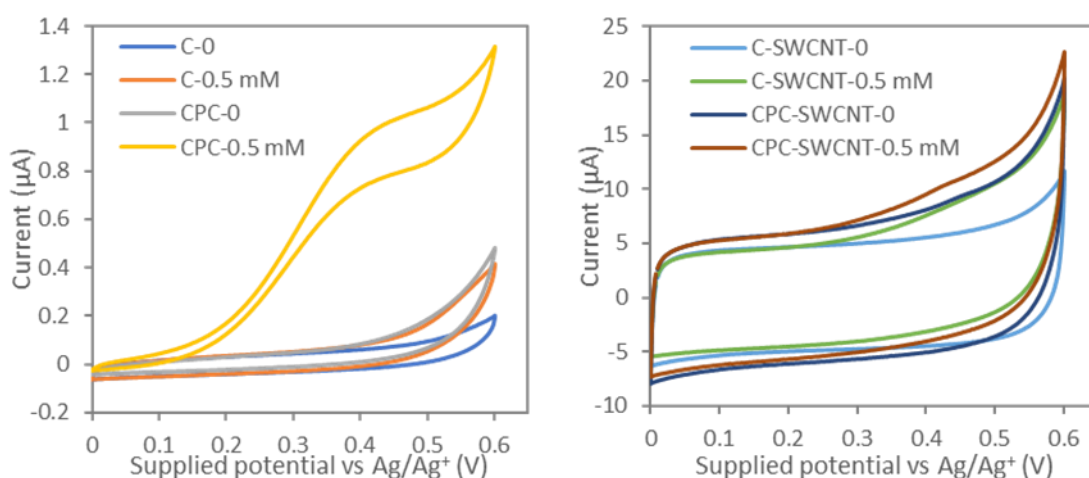


Figure 5.5 CV scans of four different systems of the biosensor (left: C-SPE/enzymes and CPC-SPE/enzymes; right: C-SPE/SWCNT/enzymes and CPC-SPE/SWCNT/enzymes) with the full enzyme immobilization (including both SOD and XOD).

Tested in PBS (pH = 7.4) with 0 mM and 0.5 mM H<sub>2</sub>O<sub>2</sub>. SWCNT loading is 0.15 mg/cm<sup>2</sup> on the working electrode with 0.0126 cm<sup>2</sup> surface area. The reference electrode is silver (~ 0.074 V vs SHE). Scan rate: 5 mV/s.

Figure 5.5 also illustrates that all the three developed systems enhanced the current response and the sensitivity of the biosensor towards the oxidation of H<sub>2</sub>O<sub>2</sub>. With the cobalt-

phthalocyanine coating, the current in PBS at 0.6V increases to 0.5  $\mu\text{A}$  and the current difference after adding 0.5 mM  $\text{H}_2\text{O}_2$  increases to 0.8  $\mu\text{A}$ . With the SWCNT coating, both the current with no  $\text{H}_2\text{O}_2$  and the current difference after adding  $\text{H}_2\text{O}_2$  at 0.6 V increases rapidly from 0.2  $\mu\text{A}$  to 10  $\mu\text{A}$ , which indicates that SWCNT could improve the sensitivity of the biosensor to a greater extent than other studied systems here. The ability of SWCNT to improve the sensitivity of biosensor was also reported in literature (Merkoçi et al. 2005, Meskher et al. 2023, Şahin 2020), because that the large surface area of SWCNT allows larger number of enzymes to be immobilised on the electrode, and its one-dimensional structure provides excellent electrical conductivity.

The calibration curve for  $\text{H}_2\text{O}_2$  detection of three developed oxidation biosensor systems compared with C-SPE/ enzymes system (Figure 5.6) was obtained from CA with different concentrations of  $\text{H}_2\text{O}_2$  (0.01 mM to 0.5 mM in PBS) at 0.6 V vs  $\text{Ag}/\text{Ag}^+$  at 100 s (the electrochemical response for a longer detection time were tested in both different concentrations of  $\text{H}_2\text{O}_2$  and xanthine solutions with the same enzyme-modified SPEs, which is shown in Appendix Figure S2.2). The result shows the electrochemical performance of the biosensors (based on the different systems) for  $\text{H}_2\text{O}_2$  detection. The sensitivity and limit of detection (LoD) (Armbruster and Pry 2008, Boqué and Heyden 2009) were calculated from the average current and sample standard deviation of repeating experiments (shown in Appendix Table S2.1 ~ 4, n = 3). C-SPE/ enzymes system has the lowest sensitivity 0.349  $\mu\text{A}/\text{mM}$  and the highest LoD 49.5  $\mu\text{M}$ . By comparison, CPC-SPE/ SWCNT combined system has the highest sensitivity 13.651  $\mu\text{A}/\text{mM}$  and the lower LoD 39.9  $\mu\text{M}$ . The sensitivity of C-SPE/ SWCNT/ enzymes and CPC-SPE/ enzymes systems are respectively 9.002  $\mu\text{A}/\text{mM}$  and 2.739  $\mu\text{A}/\text{mM}$ , and the LoD are calculated as 8.6  $\mu\text{M}$  and 31.3  $\mu\text{M}$ .

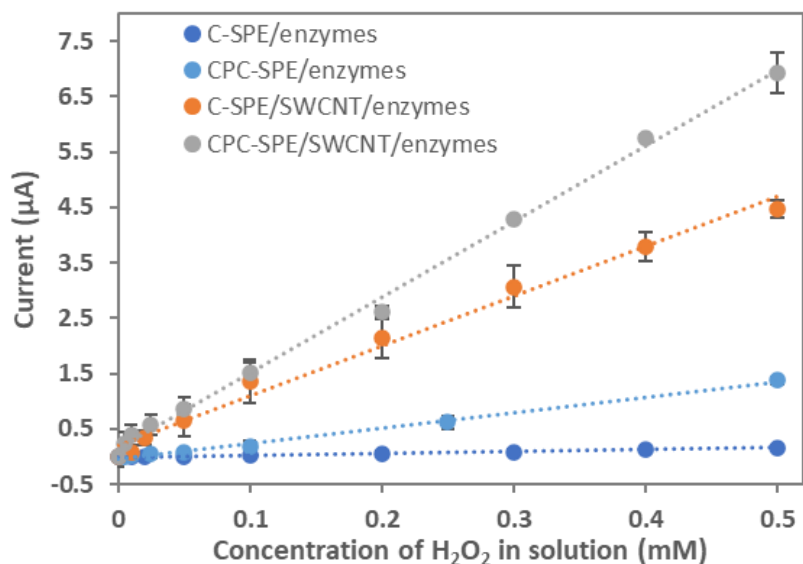


Figure 5.6 The calibration curve for H<sub>2</sub>O<sub>2</sub> detection of the four different systems of the biosensor with the fully enzyme-immobilised (both SOD and XOD).

The data was obtained from CA tested in PBS (pH = 7.4) with different concentration of H<sub>2</sub>O<sub>2</sub> (0, 0.01, 0.02, 0.05, 0.1, 0.2, 0.3, 0.4 and 0.5 mM) at 0.6V vs Ag/Ag<sup>+</sup> (~ 0.074 V vs SHE) at 100 s. The surface area of working electrode is 0.126 cm<sup>2</sup> and SWCNT loading is 0.15 mg/cm<sup>2</sup>. Error bars are the sample standard deviation of measurements from repetitions (n = 3).

The enzymes immobilized on the working electrode was used to detect superoxide in solution, these three developed systems were tested in different concentration of xanthine solution (0.01 mM to 0.5 mM) to simulate the superoxide generation in solution. The experiments has shown that dissolved oxygen had no significant effect on the current response in solution with xanthine in the studied concentration range or in other words the superoxide concentration is limited by XOD used concentration (mentioned in Chapter 4). The calibration curve for xanthine detection of three developed oxidation biosensor systems (Figure 5.7) was obtained from CA with different concentrations of xanthine in PBS at 0.6 V vs Ag/Ag<sup>+</sup> at 100 s.

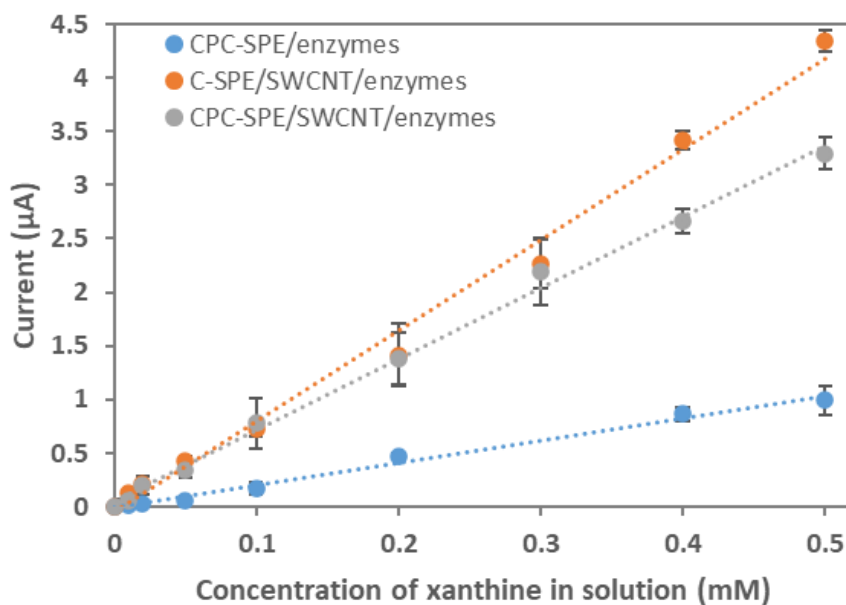


Figure 5.7 The calibration curve for superoxide detection of the three different systems of the biosensor with the fully enzyme-immobilised (both SOD and XOD).

The data was obtained from CA tested in PBS (pH = 7.4) with different concentration of xanthine (0, 0.01, 0.02, 0.05, 0.1, 0.2, 0.3, 0.4 and 0.5 mM) at 0.6V vs Ag/Ag<sup>+</sup> (~ 0.074 V vs SHE) at 100 s. The surface area of working electrode is 0.126 cm<sup>2</sup> and SWCNT loading is 0.15 mg/cm<sup>2</sup>. Error bars are the sample standard deviation of measurements from repetitions (n = 3).

The CPC-SPE/ SWCNT/ enzymes system has shown highest sensitivity for H<sub>2</sub>O<sub>2</sub> detection with C-SPE/ SWCNT/ enzymes system as second. However for superoxide detection, C-SPE/ SWCNT/ enzymes system has shown the highest sensitivity 8.459 µA/mM and lower LoD 5.6 µM followed by CPC-SPE/ SWCNT/ enzymes system, sensitivity 6.634 µA/mM and LoD 18.2 µM (calculated from three repetitions in Appendix Table S2.5 ~ 7). This result illustrated that the cobalt-phthalocyanine coating affects the enzymatic reactions for superoxide preparation and/or redox reaction of superoxide. The sensitivity of the CPC-SPE / enzymes system for xanthine (or superoxide) detection 2.089 µA/mM is less than that for H<sub>2</sub>O<sub>2</sub> detection. This lower value could suggest that the CPC layer might play a role in electrochemical H<sub>2</sub>O<sub>2</sub> oxidation, as discussed previously, giving a raise to additional oxidation current and sensitivity.

Based on the enzymatic reactions, the same concentration of H<sub>2</sub>O<sub>2</sub> and xanthine produces the same amount of electrical signal at a fixed voltage, that is, the ideal current is similar if the enzymatic reactions react completely. The linear relationship (Figure 5.8, data shown in Appendix Table S2.8) between the actual concentration of xanthine in the solution and the calculated equivalent concentration of H<sub>2</sub>O<sub>2</sub> on the working electrode is obtained based on the current response from Figure 5.6 and Figure 5.7.

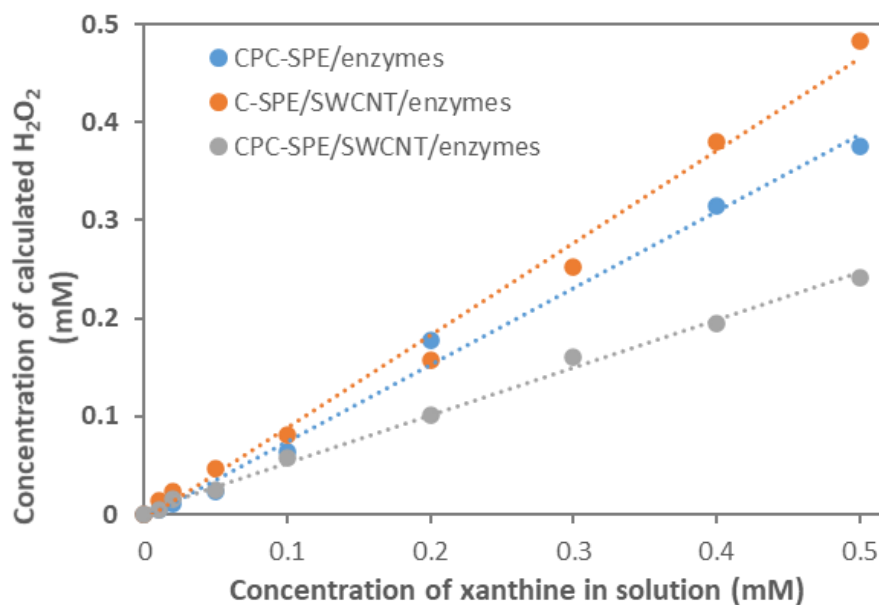


Figure 5.8 The linear relationship between the concentration of xanthine (0.01 to 0.5 mM) and the calculated  $H_2O_2$  concentration (from Figure 5.6) based on the same charge transfer (i.e. the current response in Figure 5.7).

The ratio of two components concentration in the C-SPE/ SWCNT/ enzymes system is close to the ideal ratio 1 so that the concentration of superoxide generated could be regarded as two times that of xanthine in the solution. The CPC-SPE/ SWCNT/ enzymes system showed a large difference between the ideal detection concentration and the actual detection concentration. This indicates that this system could not detect superoxide concentration effectively due to the complex structure and reactions on the working electrode.

### 5.3.3 Calibration of the biosensor based on the oxidation reaction

For the application of biosensors to detect superoxide or peroxide, XOD is not required on the working electrode as XOD purpose is to convert oxygen into superoxide or superoxide to oxygen. Additionally, as shown in Section 4.3.1, the SPE without XOD showed a lower current response for the detection than the SPE with XOD because the charge transfer was inhibited by the additional PDDA and enzyme layers. To calibrate the current value detected by biosensor (only PDDA and SOD layers on SWCNT coated C-SPE), the CA curve was scanned in the solution with different  $H_2O_2$  concentrations (0.01 mM to 0.5 mM in PBS) at 0.6 V vs  $Ag/Ag^+$  (Appendix Figure S2.3).

Figure 5.9 (a) shows the current response of the biosensor with the different concentrations of  $H_2O_2$  in the electrolyte (blue line, data in Appendix Table S2.9) compared with the results of

the biosensor with the additional PDDA and XOD enzyme layers (orange line, from Figure 5.6, data in Appendix Table S2.3). The sample standard deviation of the biosensor without XOD ( $n=3$ ) was much smaller than that of the biosensor with XOD, which illustrated that the decrease of the layers on the working electrode improved the accuracy of the detection. The reason for this could be that the additional layers increased the possibility of reversible adsorption and the inhibition of the diffusion of  $H_2O_2$  from the electrolyte to the working electrode.

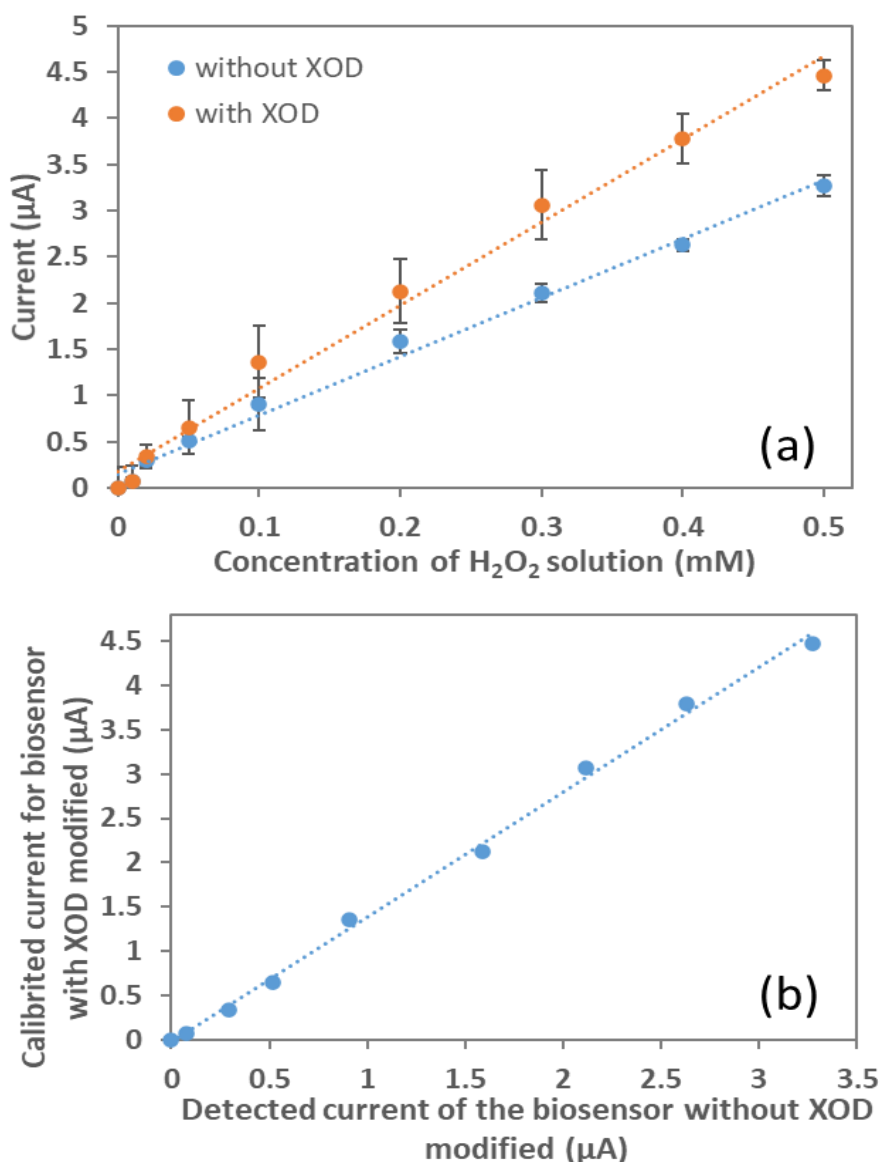


Figure 5.9 (a) The calibration curve for  $H_2O_2$  detection of the biosensor with the SOD-only and full-enzyme (SOD and XOD) immobilised on SWCNT-coated C-SPE; (b) The relationship between the detected current and the calibrated current.

The data was obtained from CA tested in PBS ( $pH = 7.4$ ) with different concentration of  $H_2O_2$  (0, 0.01, 0.02, 0.05, 0.1, 0.2, 0.3, 0.4 and 0.5 mM) at 0.6V vs  $Ag/Ag^+$  ( $\sim 0.074$  V vs SHE) at 100 s. The surface area of working electrode is  $0.126$   $cm^2$  and SWCNT loading is  $0.15$   $mg/cm^2$ . Error bars are the sample standard deviation of measurements from repetitions ( $n = 3$ ).

Based on the same concentration of  $\text{H}_2\text{O}_2$  in solutions, the relationship between the measured current in the absence of XOD (from the applied biosensor, i.e. without XOD) and the corrected current (from the biosensor for calibration, i.e. with XOD) was generated in Figure 5.9 (b) (data shown in Appendix Table S2.10). This linear relationship is used to correct the measured current from sensors containing XOD to eliminate the effect of the XOD enzyme layer on the current response.

According to the equation for the preparation of superoxide from xanthine in the presence of XOD, the ideal concentration of superoxide produced is twice the initial concentration of xanthine in the solution when all the xanthine has reacted completely. Based on the equation of disproportionation of superoxide in the presence of SOD, the ideal concentration of generated  $\text{H}_2\text{O}_2$  is half of the superoxide concentration at rest potentials. Also, if oxidative potentials applied then SOD will favor oxidation reaction converting superoxide to oxygen over its reduction to peroxide. The reactions might thus be incomplete due to complex enzymatic processes and applied potential, so the actual concentration of superoxide should be between two times the concentration of xanthine (maximum) and  $\text{H}_2\text{O}_2$  (minimum), which was shown as the error bar in the overall calibration curve.

The calculation of the superoxide concentration detected by the oxidation biosensor has three steps: 1) obtain the current values from the biosensor reading and correct the impact of XOD on current based on Figure 5.9 (b); 2) use the calibration relationship to find out corresponding  $\text{H}_2\text{O}_2$  concentration and xanthine concentration respectively based on Figure 5.6 (orange line) and Figure 5.7 (orange line); 3) superoxide concentration was estimated as a range from the concentration of xanthine and  $\text{H}_2\text{O}_2$ . The overall calibration curve of the biosensor for superoxide detection was generated in Figure 5.10 (data shown in Appendix Table S2.11).

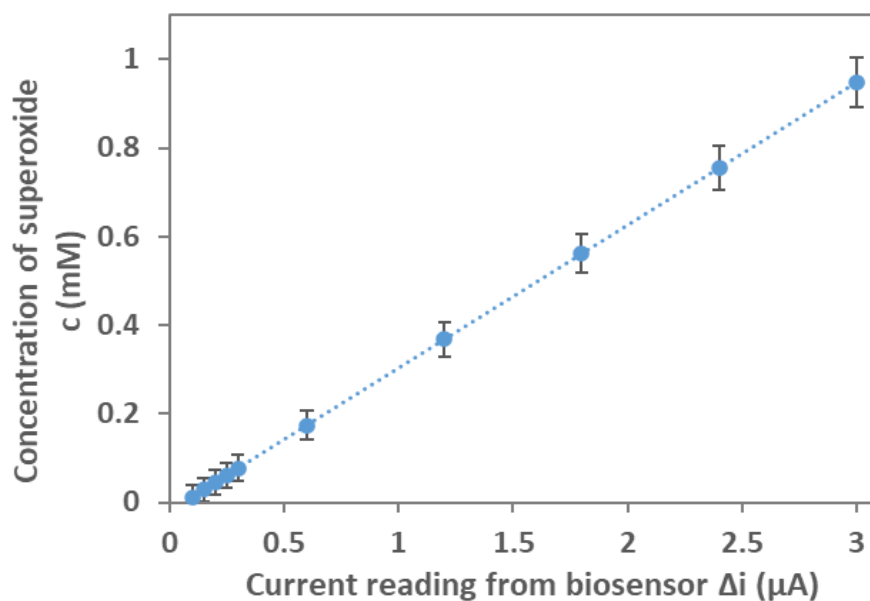


Figure 5.10 The overall calibration curve for the developed SOD-based biosensor for superoxide.

(SOD-immobilised SWCNT-coated C-SPE, the surface area of the working electrode:  $0.126 \text{ cm}^2$ , SWCNT loading:  $0.15 \text{ mg/cm}^2$ , at  $0.6V$  vs  $Ag/Ag^+$ ). The current reading should be the current response of the biosensor after being calibrated in PBS. The error bars were obtained from the calculated maximum and minimum concentrations.

This project quantified the current reading of a biosensor with the corresponding superoxide concentration within a certain range and achieved small-volume detection. The low concentration of superoxide in blood, hundreds of mM, poses a challenge for existing electrochemical blood sensors when quantitatively assessing the ROS. The biosensor developed in this project overcomes this issue, enabling detection even within low concentrations. To the best of my knowledge, there has not been reported on such work in the literature.

#### 5.3.4 Interference detection

It is known that there are many interferences in biological especially human blood samples, which requires the significant specific recognition of the biosensor without being affected by potential interferences. The selectivity of the biosensor was tested by comparing the current response at the same potential for 100 seconds of C-SPE/ SWCNT/ SOD to  $0.01 \sim 0.5 \text{ mM}$   $H_2O_2$  in PBS with interferences including UA, AA, glucose and protein (Cui et al. 2020, Moschopoulou and Kintzios 2015, Tian et al. 2002). UA and AA are two of the most main acid-based interferences for  $H_2O_2$  oxidation detection in electrochemical techniques due to their similar low oxidation potential (Sakamoto et al. 2011). The glucose and proteins are tested as other major interferences because of the high concentration in blood components. In this

research, BSA was used to simulate the protein environment as one of the interferences.

Figure 5.11 shows the selectivity results of the biosensor based on  $H_2O_2$  oxidation reaction against glucose, UA, AA and BSA according to their concentration in human blood at a normal level (data in Appendix Figure S2.12). The electrode used for the tests was SWCNT coated C-SPE with only SOD immobilized. The electrolytes had different concentration of  $H_2O_2$  (0 to 0.5 mM) in PBS with 5 mM, 400  $\mu$ M, 11.4  $\mu$ M, 4 g/l of glucose, UA, AA, BSA, respectively. The current response of UA is very close to that of the  $H_2O_2$ -only environment, while other interferences show very limited negative effects on current response, glucose have shown a large positive effect on current response.

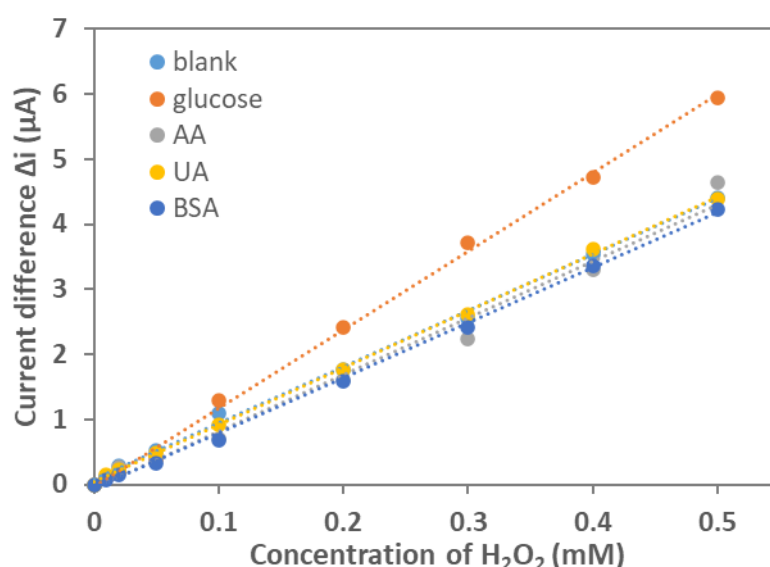


Figure 5.11 The interference tests for  $H_2O_2$  detection of the biosensor with the SOD-immobilised SWCNT-coated C-SPE.

(Surface area of working electrode:  $0.126 \text{ cm}^2$ , SWCNT loading:  $0.15 \text{ mg/cm}^2$ ). The current response was obtained from CA of different concentration of  $H_2O_2$  (0, 0.01, 0.02, 0.05, 0.1, 0.2, 0.3, 0.4 and 0.5 mM) added to PBS (pH = 7.4) respectively containing 5 mM, 400  $\mu$ M, 11.4  $\mu$ M, 4 g/l of glucose, UA, AA, BSA at 0.6V vs  $Ag/Ag^+$  ( $\sim 0.074 \text{ V vs SHE}$ ) at 100 s.

For AA and BSA, the current response at a higher concentration of interferences was tested for comparison (shown in Figure 5.12, data shown in Appendix Table S2.13). Although the concentration of interferences was increased, the current response didn't significantly change. The results illustrated that BSA and AA have an ignorable effect on biosensor oxidation detection, which is similar to the research of other electrochemical sensor for superoxide detection (Sun et al. 2023, Tian et al. 2002, Zhang et al. 2019), due to the more positive potential range of the oxidation reaction of AA, UA and BSA in an enzyme-based sensor involving electron transfer in proteins.

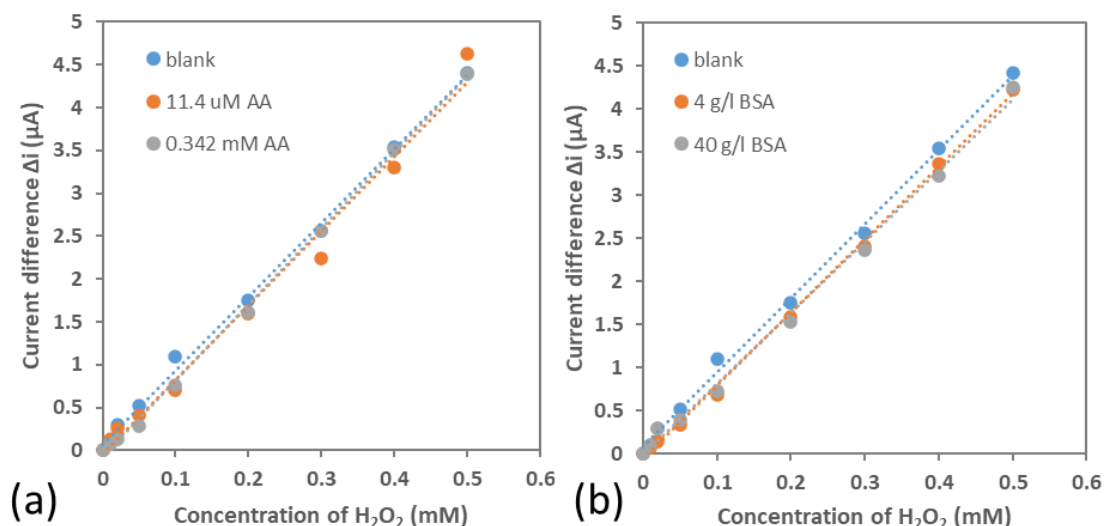


Figure 5.12 The current response of the biosensor with the SOD-immobilised SWCNT-coated C-SPE for H<sub>2</sub>O<sub>2</sub> detection against the potential interferences (a) AA and (b) BSA with a large concentration range.

The data was obtained from CA of different concentration of H<sub>2</sub>O<sub>2</sub> (0, 0.01, 0.02, 0.05, 0.1, 0.2, 0.3, 0.4 and 0.5 mM) added to PBS (pH = 7.4) respectively containing AA and BSA at 0.6V vs Ag/Ag<sup>+</sup> (~ 0.074 V vs SHE) at 100 s. The surface area of working electrode is 0.126 cm<sup>2</sup> and SWCNT loading is 0.15 mg/cm<sup>2</sup>.

The glucose shows a positive effect from Figure 5.11, this was conjectured to be caused by the oxidation of glucose due to the much higher concentration of glucose (5 mM) than H<sub>2</sub>O<sub>2</sub> (0.01 ~ 0.5 mM). Thus 0.5 mM and 5.5 mM glucose in PBS with different H<sub>2</sub>O<sub>2</sub> concentrations were tested respectively for comparison. To find out the effect of a high concentration level of glucose on the detection, 20 mM was also considered.

From Figure 5.13 (a) (data shown in Appendix Table S2.14), with the changing concentration of H<sub>2</sub>O<sub>2</sub>, the trendline of the data of 0.5 mM glucose and that of data without glucose were in parallel. This result showed that the glucose has no effects on the oxidation reaction of H<sub>2</sub>O<sub>2</sub> at the concentration of 0.5 mM glucose at the potential of 0.6 V. The current response of 5 and 5.5 mM glucose has a slight excursion compared with that of 0.5 mM glucose and the similar tendency of 5.5 mM data showed on the much higher concentration level, 20 mM of glucose. This result suggests that the excessive concentration of glucose undergoes an oxidation reaction on the surface of the working electrode resulting in additional oxidation current or additional bias affecting the current value of the biosensor which can be clearly at the intercept of x-axis (0 M H<sub>2</sub>O<sub>2</sub>). The limited change in line slope of H<sub>2</sub>O<sub>2</sub> current detection at high glucose concentration in comparison to that without glucose can suggest that the effect of glucose on the oxidation reaction of H<sub>2</sub>O<sub>2</sub> can be ignored and both process can be treated as independent.

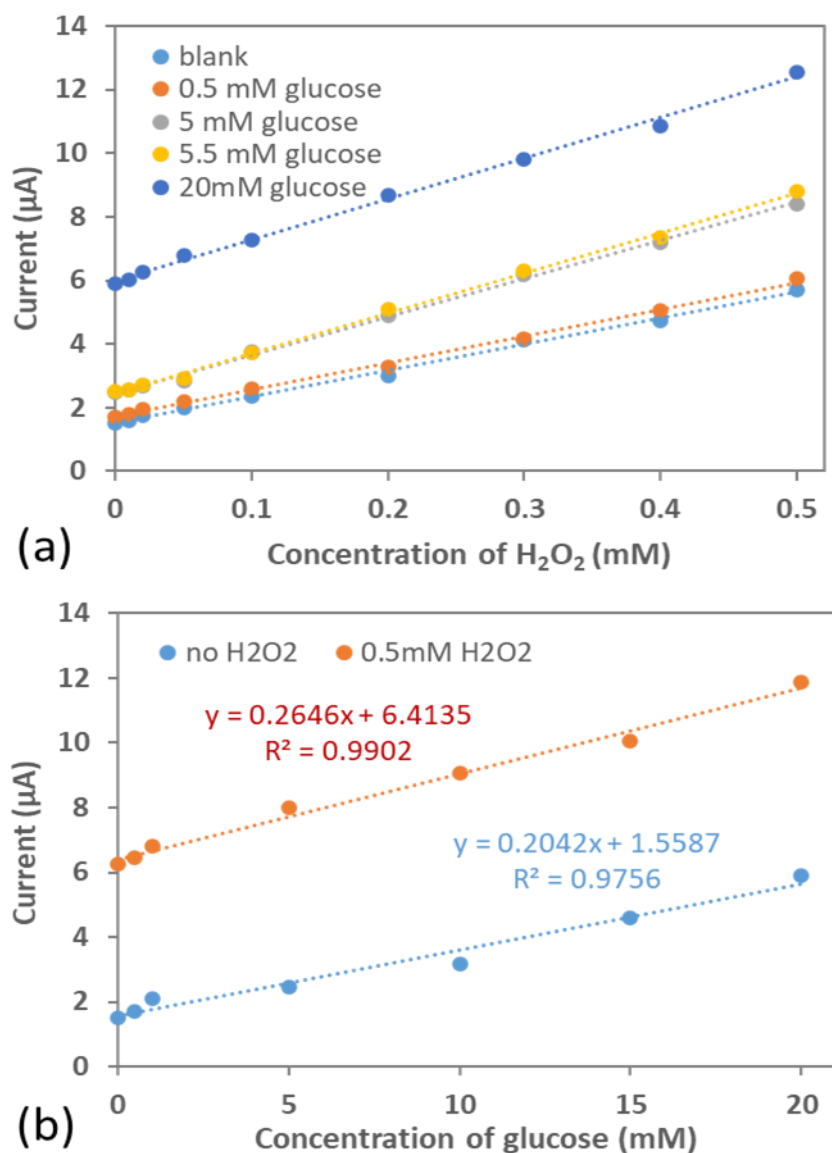


Figure 5.13 The current response of the biosensor with the SOD-immobilised SWCNT-coated C-SPE for (a)  $H_2O_2$  detection against glucose as the interference with a large concentration range and (b) oxidation detection by changing glucose concentration in the solution with and without  $H_2O_2$ .

The data was obtained from CA of different concentration of  $H_2O_2$  (0, 0.01, 0.02, 0.05, 0.1, 0.2, 0.3, 0.4 and 0.5 mM) or glucose (0, 0.5, 1, 5, 10, 15 and 20 mM) added to PBS (pH = 7.4) respectively containing 0, 0.5, 5, 5.5 mM glucose or 0, 0.5 mM  $H_2O_2$  at 0.6V vs Ag/Ag<sup>+</sup> (~ 0.074 V vs SHE) at 100 s. The surface area of working electrode is 0.126 cm<sup>2</sup> and SWCNT loading is 0.15 mg/cm<sup>2</sup>.

To further examine the influence of the concentration of glucose on the oxidation reaction of  $H_2O_2$  on the working electrode, confirmatory research was carried out by changing the concentration of glucose in the solution respectively with and without  $H_2O_2$  (Figure 5.13 (b), data shown in Appendix Table S2.15). The tendency lines of the results with and without  $H_2O_2$  are nearly parallel, which means the addition of  $H_2O_2$  has an ignorable effect on the oxidation reaction of the glucose. The current difference between two lines in the Figure represented the

detectable signal of the oxidation reaction of  $\text{H}_2\text{O}_2$ , which showed similar results with the increasing concentration of glucose. Based on these results, both the oxidation reaction of  $\text{H}_2\text{O}_2$  and glucose could be detected on the working electrode but could hardly affect each other. Thus, in the presence of a high concentration of glucose, the biosensor could still accurately measure reactive oxygen species after glucose calibration.

Considering the effect of glucose on superoxide detection, the calibration curve of the biosensor should have a positive shift of the current based on the concentration of glucose when doing blood tests. However, it should be mentioned that changes in glucose concentration in blood will affect the oxidation bias value and consequently the accuracy of superoxide detection if fixed value was used for correction.

## 5.4 Conclusions

In this chapter, the layer-by-layer self-assembly technique for enzyme immobilization (both SOD and XOD) was described and tested on C-SPE in PBS, which showed the successful assembly of each layer. The electrochemical result also showed the effect of the additional superoxide-preparation layers to that of the electrode with only SOD enzyme, on current response of the electrode resulting in the current correction/recalibration to be considered for the application of the biosensor.

Based on the oxidation reaction of  $\text{H}_2\text{O}_2$ , the electrochemical performance of the biosensor was investigated by the enzyme-immobilized electrode in PBS with different concentrations of  $\text{H}_2\text{O}_2$ . The detection potential was chosen to be 0.6 V vs  $\text{Ag}/\text{Ag}^+$  for the higher sensitivity and the detection time was 100 s for the stable current signals. The results showed the biosensor was hard to be used for application due to the lack of sensitivity ( $0.349 \mu\text{A}/\text{mM}$ ) and high limit of detection (0.05 mM).

To enhance the sensitivity and accuracy of the biosensor, SWCNT and CPC-SPE were used for the biosensor development due to their advantages of promoting performance for  $\text{H}_2\text{O}_2$  detection. The electrochemical performance of three developed systems (CPC-SPE/ enzymes, C-SPE/ SWCNT/ enzymes and CPC-SPE/ SWCNT/ enzymes) was analysed by voltammetry. Although CPC-SPE/ SWCNT/ enzymes system showed a higher sensitivity for  $\text{H}_2\text{O}_2$  detection, the effect of the enzymatic reactions prevented its application for superoxide biosensors. C-SPE/ SWCNT/ enzymes system was a successful development due to the significantly increased sensitivity and low limit of detection, respectively  $9.002 \mu\text{A}/\text{mM}$  (71.44

$\mu\text{A}/(\text{mM}\cdot\text{cm}^2)$ ) and  $8.6\ \mu\text{M}$  for  $\text{H}_2\text{O}_2$  detection and  $8.459\ \mu\text{A}/\text{mM}$  ( $67.13\ \mu\text{A}/(\text{mM}\cdot\text{cm}^2)$ ) and LoD  $5.6\ \mu\text{M}$  for superoxide detection. The results illustrated that the enzymatic reactions were nearly complete by the C-SPE/ SWCNT/ enzymes system, which means the concentration of superoxide could be determined by the concentration of  $\text{H}_2\text{O}_2$  and xanthine as a range.

For clinical application, the current response was corrected by comparing the current response of the biosensor with and without superoxide-preparation layer (i.e. XOD layer). The overall calibration curve for the developed superoxide biosensor was generated (shown in Figure 5.10).

The selectivity of the developed biosensor was tested against interferences including glucose, UA, AA and BSA (as the protein) in PBS with different concentrations of  $\text{H}_2\text{O}_2$ . UA showed no effect on the electrochemical signals, both AA and BSA had the ignorable effect even at high concentration levels. The effect of glucose on the oxidation current used for ROS detection was significant and should be considered for the blood test in clinical applications.

## Chapter 6 Development of the electrochemical biosensor based on reduction reaction of hydrogen peroxide

In this chapter, the biosensor based on the reduction reaction of  $\text{H}_2\text{O}_2$  to water was developed for superoxide detection and the interference tests were performed. The aim of the biosensor was to determine the concentration of superoxide in solution by detecting the reduction current of  $\text{H}_2\text{O}_2$  to water. The  $\text{H}_2\text{O}_2$  is produced assuming full conversion of superoxide to  $\text{H}_2\text{O}_2$  in the presence of superoxide dismutase (SOD). The enzyme horseradish peroxidase (HRP), as the electrocatalyst of the reduction reaction of  $\text{H}_2\text{O}_2$ , was immobilized on the working electrode by the cross-linking technique using 1-pyrenebutyric acid N-hydroxysuccinimide ester (PBSE). Electrochemical characterization of the reactions was performed in potassium phosphate-buffered solution (PBS) with different concentrations of  $\text{H}_2\text{O}_2$  or xanthine using cyclic voltammetry (CV) and chronoamperometry (CA). The screen-printed electrode with a dual working electrode was used to separate the redox reaction of superoxide and the reduction reaction of  $\text{H}_2\text{O}_2$ . Single-wall carbon nanotube (SWCNT) was used for improved conductivity and increasing the reaction surface area. The current signal of the biosensor showed a linear relationship with the increasing concentration of both xanthine and  $\text{H}_2\text{O}_2$ , and the calibration curve was generated based on the various concentrations of superoxide. Interference tests showed the ignorable effect of some main components in blood like uric acid (UA), ascorbic acid (AA), bovine serum albumin (BSA) and glucose on the detection.

### 6.1 Introduction

With the rapid development of the sensors, the detection of a broad range of pathogenic factors was widely studied, especially reactive oxygen species that cause several diseases (Balamurugan et al. 2018, Bayr 2005, Heitzer et al. 2001, Park et al. 2014). The electrochemical biosensors were reported by many researchers due to the advantages of fast response for analysis, simplicity and low cost, but the lack of accurate and effective detection methods for superoxide anion is still a problem that plagues researchers in the detection of reactive oxygen species (Guo et al. 2010, Sun et al. 2006, Wang et al. 2013). To achieve accurate detection, transferring the unstable superoxide anion to the easier detectable species, hydrogen peroxide ( $\text{H}_2\text{O}_2$ ), using an enzymatic pathway or reaction could be an effective way for the electrochemical analysis (Bartlett et al. 1998).

The electrochemical detection methods for  $\text{H}_2\text{O}_2$  are divided into two types: the detection based on the oxidation signal from  $\text{H}_2\text{O}_2$  to oxygen and the analysis based on the reduction of  $\text{H}_2\text{O}_2$

to water (Kosto et al. 2019, Li et al. 2011). The oxidation signal could easily be detected at a higher potential whereas the reduction signal requires the catalysts to amplify especially when the detection is down to the micromolar range (Goran et al. 2015, Wang et al. 2013). However, the electrochemical biosensor based on the oxidation reaction shows lower selectivity for the application for blood tests, and the results were affected by glucose as mentioned in Chapter 5.3.4. To avoid the effect of the oxidation from other components in blood, an electrochemical biosensor based on the reduction reaction of H<sub>2</sub>O<sub>2</sub> was established in this project.

Recently most of the reported electrochemical H<sub>2</sub>O<sub>2</sub> reduction biosensors used metal nanoparticles, mediators, nanocarbon catalysts on graphene and enzymes like horseradish peroxidase (Hrapovic et al. 2004, Sun et al. 2012). A graphene-Pt nanocomposites biosensor was described by Zhang et al. (2014) with the linear reduction range of 0.5 μM to 3.475 mM and the detection limit of 0.2 μM. Lyon and Stevenson (2006) presented an H<sub>2</sub>O<sub>2</sub> reduction biosensor utilised amplex red mediator and the performance of the biosensor showed the sensitivity as  $(2.1 \pm 0.6) \times 10^{-1} \mu\text{A}/(\mu\text{M mm}^2)$ . Zhang et al. (2017) established hybrid nanosheets with nitrogen and sulphur codoped graphene for H<sub>2</sub>O<sub>2</sub> reduction detection, and the results displayed a linear range from 0.4 μM to 33 mM with a detection limit of 26 nM. Although these enzyme-free biosensors showed the advantages like long-term operational stability and environmental stability, the enzyme still attracted research attention due to the remarkable selectivity in blood tests which contains the complex components.

HRP is isolated from horseradish roots, which is a metalloenzyme with the structure of a large alpha-helical glycoprotein. This enzyme has been widely used in biological chemical detection because of the ability that it can amplify weak signals and enhance the detectability of target molecules (Carlsson et al. 2005) by catalytic reduction of H<sub>2</sub>O<sub>2</sub>. Besides, due to the advantages of the high purity, ease of availability and low cost, the application of HRP enzyme on an electrochemical biosensor for H<sub>2</sub>O<sub>2</sub> detection has been widely discussed and analysed based on the catalyst active centre which belongs to the ferroprotoporphyrin group of peroxidases (Li et al. 2011).

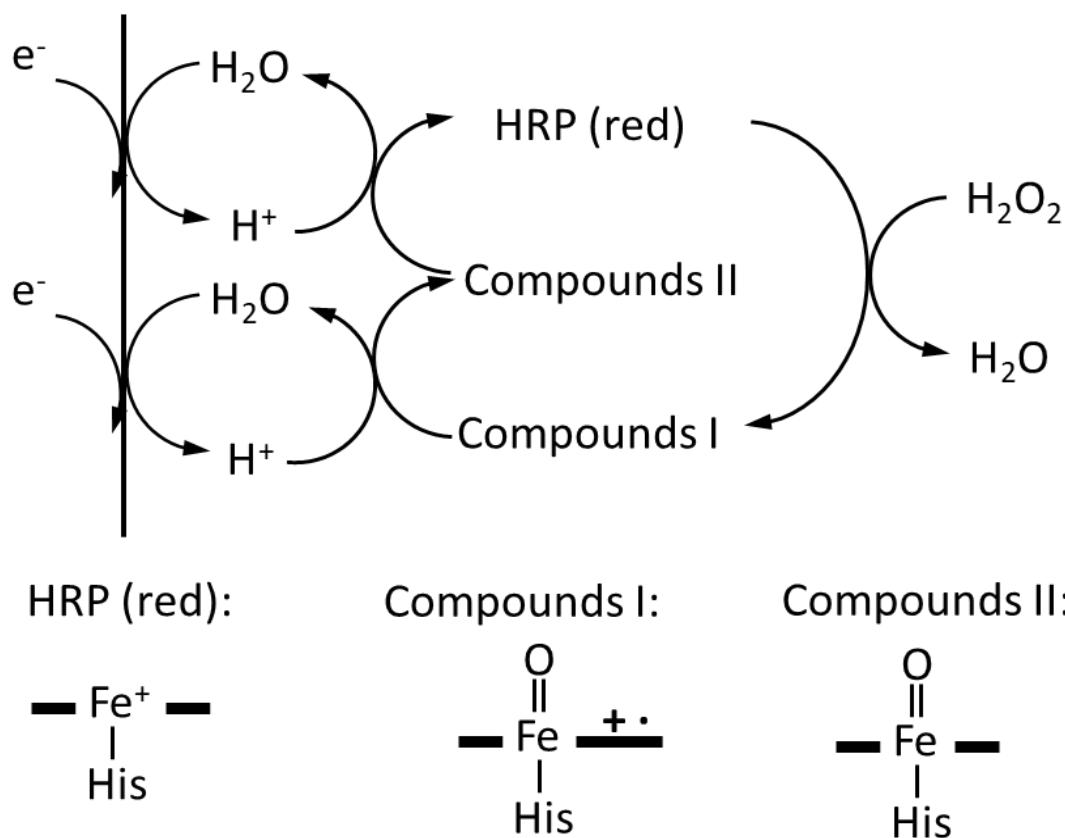
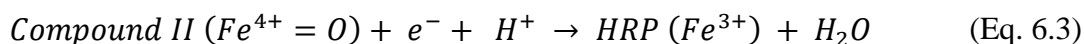
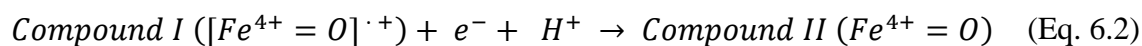


Figure 6.1 Scheme of the normal catalytic cycle for HRP enzyme in the  $\text{H}_2\text{O}_2$  reduction reaction.

HRP (red) is the ferric porphyrin of HRP, compounds I is the intermediate of the oxyferryl  $\pi$ -cation radical heme, compound II is the oxyferryl intermediate.

The principle of the reduction reaction of  $\text{H}_2\text{O}_2$  catalysed by the HRP enzyme is shown in Figure 6.1. The catalyst active centre of the HRP enzyme is the ferric porphyrin ( $\text{Fe}^{3+}$ ) which could be oxidised by free  $\text{H}_2\text{O}_2$  in solution. In this step of the catalyst process, the oxygen atom on the structure of  $\text{H}_2\text{O}_2$  transfers to the catalyst active centre of HRP, which could be regarded as a two-electrons transfer formally, and the iron formal oxidation state of the oxidised HRP (referred to as compound I, containing the active centre as the oxyferryl  $\pi$ -cation radical heme ( $[\text{Fe}^{4+}=\text{O}]^{\cdot+}$ ) is +5. The oxidised HRP obtains two electrons from the electrode and is converted back to the reduced HRP (referred to as HRP (red) which is the native ferriperoxidase, and the iron formal state is +3) through a two-step reduction reaction. In the first step of the reduction reaction of the oxidised HRP, the porphyrin radical cation of compound I is converted by a one-electron reduction to the oxyferryl intermediate compound II (the iron formal oxidation state is +4). In the second step of the reduction reaction of the oxidised HRP, with one electron from the working electrode and a proton from the electrolyte, the intermediate compound II is reduced to its native state, HRP (red), and yield water. Both compound I and compound II are the oxidized states of HRP (red).

The electrocatalytic process of the HRP enzyme could be presented as equation 6.1 to equation 6.3 (Dequaire et al. 2002, Li et al. 2011):



The overall reaction is:



As one of the new types of biosensor materials, the utilization of the nanotubes motivated the prospects of the immobilization of biomolecules on the working electrode for the electrochemical analysis (Singh 2011, Wang and Dai 2015). It is reported that an ideal miniaturized biosensor could be established by the combination of the electronic properties of nanotubes and the specific recognition properties of the immobilized enzyme systems (Daniel et al. 2007). The core of a successful biosensor is the efficient method to immobilize the enzyme onto carbon nanotubes.

In the past, several immobilization strategies for HRP enzyme have been reported for the electrochemical biosensors, such as entrapment in sol-gel, adsorption, biotin conjugate, electrode-deposition, N-ethyl-N'-(3-(dimethylamino)propyl)carbodiimide (EDC) / N-hydroxysuccinimide (NHS) binding and so on (Li et al. 2011, Wang et al. 2011). Li et al. (1996) introduced an effective enzyme immobilization based on the sol-gel technique which used immobilizing HRP enzyme on a carbon paste electrode via the silica sol-gel matrix. Sharafeldin et al. (2019) and Lei et al. (2003) respectively described an adsorption method by using chitosan-entrapped carbon electrodes with gold nanoparticle films to achieve HRP immobilization. Limoges et al. (2003) reported a biotin conjugate-based immobilization technique that successful immobilization of HRP onto the biotinylated rabbit IgG / bovine serum albumin coated carbon electrode was achieved thanks to the strong affinity for the biotin moieties. Kong et al. (2003) represented an EDC-NHS cross-linking immobilization based on

the covalent bonding between the amino group of the HRP and a carboxylic acid group of 5,2':5',2"-terthiophene-3'-carboxylic acid polymer. Tong et al. (2007) showed that using the electro-deposition technique to immobilize HRP by zirconia based on the electrostatic attraction. For the easy option, low cost, fast binding and high stability, a cross-linking method was applied, which was mentioned in Chapter 3.2.2.

In this work, the electrochemical biosensor based on the reduction reaction of  $H_2O_2$  was developed and analysed by electrochemical techniques. For better performance, the enzymatic reactions catalysed by SOD and HRP were separated into two electrodes instead of been combined together as a layer-by-layer structure on the same electrode. Both of the immobilizations were tested, and the electrochemical performance was compared by CA. For clinical applications, the calibration curve and the interference tests were represented.

## 6.2 Experimental

### 6.2.1 Materials

PBSE, dimethylformamide (DMF), AA (ACS reagent,  $\geq 99\%$ ), UA ( $\geq 99\%$ , crystalline), BSA (pH 7,  $\geq 98\%$ ) and glucose ( $\geq 99.5\%$ , powder, BioReagent, suitable for cell culture), HRP (highly stabilized, essentially salt-free, lyophilized powder, 200-300 units/mg solid) and all other enzymes were purchased from Sigma-Aldrich (Dorset, UK).

The acid-treated SWCNT, 0.1 M PBS, 1% poly(diallyldimethylammonium chloride) (PDDA),  $H_2O_2$ , xanthine, enzymes solution including SOD, HRP and xanthine oxidase (XOD) solution were purchased, stored and handled as described in Chapter 3.1.

The screen-printed electrode (SPE) used in this project including screen-printed carbon electrode (C-SPE, model DRP-C110) and dual screen-printed carbon electrode (duo-SPE, model DRP-C1110) and the cable connectors for these SPEs were obtained from DropSens (Oviedo, Spain).

### 6.2.2 The fabrication of the biosensor

To fabricate the biosensor with both two enzymes SOD and HRP on the same working electrode, the HRP enzyme was immobilized first onto the electrode and the SOD enzyme was on the top (shown in Figure 6.2) since the detection reaction of the biosensor is the reduction reaction of

H<sub>2</sub>O<sub>2</sub>. The detailed steps for SOD and HRP immobilization was mentioned in Chapter 3.2.1 and 3.2.2 respectively. In this project, the principle of the biosensor is: 1) the superoxide anion in the electrolyte first undergoes a redox reaction when passing through the SOD enzyme layer to generate H<sub>2</sub>O<sub>2</sub>; 2) then the generated H<sub>2</sub>O<sub>2</sub> is reduced to water under the action of the HRP enzyme; 3) a detectable current is formed in the measurement circuit due to the electron consumption in the reduction reaction.

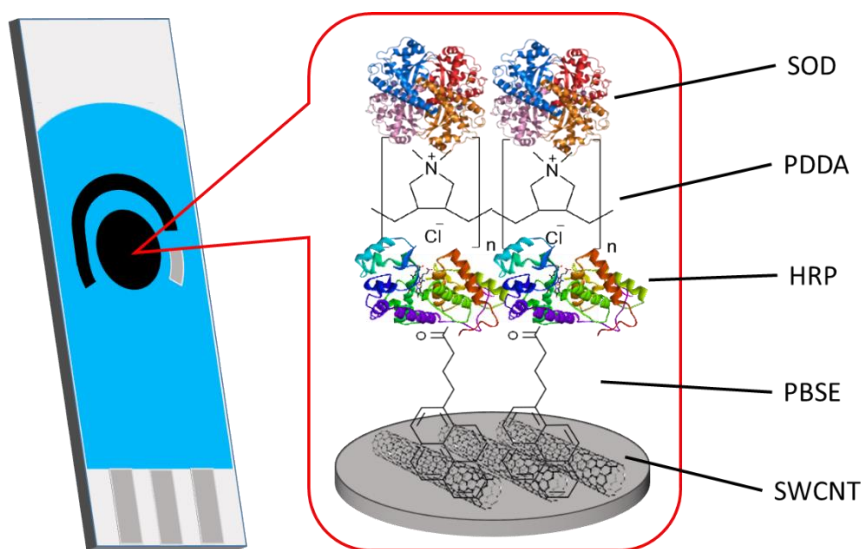


Figure 6.2 The structure of the biosensor using C-SPE with both SOD and HRP enzymes immobilized on SWCNT coated WE (XOD & SOD/HRP/SWCNT/C-SPE).

As mentioned in Chapter 5, the XOD enzyme was used for superoxide preparation due to the instability of the superoxide. Thus, the XOD enzyme was immobilized on the top of modified SPEs for the generation of the calibration curve.

For better detection performance and to avoid the influence between different reactions, the duo-SPE was used to separate the redox reaction of superoxide and the reduction reaction of H<sub>2</sub>O<sub>2</sub>. As shown in Figure 6.3, the SOD enzyme was immobilized on WE2 to fabricate a platform where H<sub>2</sub>O<sub>2</sub> was produced from the redox reaction of superoxide, and the HRP enzyme was immobilized on WE1 for the detection signal from the reduction reaction of H<sub>2</sub>O<sub>2</sub>. Both of the WEs were immersed in the electrolyte while detecting, and the pipetting mixture was applied before the signal collection to help the mass transfer of H<sub>2</sub>O<sub>2</sub> from WE2 to WE1. SWCNT was also applied to the superoxide redox reaction (WE2, subsequently immobilizing SOD and XOD) for the larger surface area and fast reaction rate of superoxide. For the same electrochemical performance, the adhesive solution and the enzyme solution should be changed due to the different surface areas of the working electrode compared with C-SPE. According to

the calculation shown as equation 6.5:

$$\frac{S_{C-SPE}}{S_{duo-SPE}} = \frac{V_{solution\ for\ C-SPE}}{V_{solution\ for\ duo-SPE}} \quad (\text{Eq. 6.5})$$

Where  $S$  is the surface area of the working electrode ( $\text{mm}^2$ ), and  $V$  is the adhesive and/or enzyme solution for enzyme immobilization ( $\mu\text{l}$ ). The solution used for enzyme immobilization on duo-SPE was calculated as  $7\ \mu\text{l}$ .

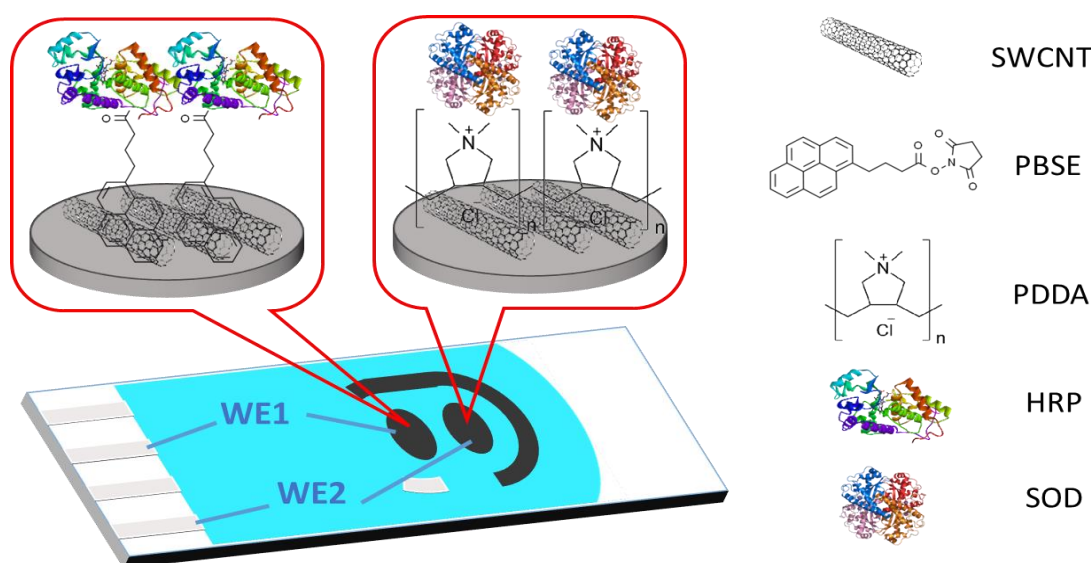


Figure 6.3 The structure of the biosensor using duo-SPE with both SOD and HRP enzymes immobilized on SWCNT coated WEs.

WE1 is for the detection signal collection and WE2 is for the redox reaction from superoxide to  $\text{H}_2\text{O}_2$ .

### 6.2.3 The design of the enzyme-fabrication box for duo-SPE

To avoid the mutual influence when processing different immobilized enzymes on the two electrodes, an enzyme-fabrication box (shown in Figure 6.4) was designed and printed by a 3D printer. The materials used in the 3D printer for the lid and bottom of the box was VeroWhitePlus™ RGD835, an organic mixture containing acrylic acid.

This enzyme-fabrication box has a channel to fix duo-SPE, and there were two elliptical holes with the same size as the working electrode on the lid of the box that corresponds to the working electrode. To guarantee the sealing between the box and two working electrodes, the lid of the enzyme-fabrication box was designed as a “pig nose” (the part around two elliptical holes is  $0.5\ \text{mm}$  protruding than other parts which look like a pig nose, shown in Figure 6.4 (b)) and a

gasket with two elliptical holes was compacted. The detailed structure and the assembled enzyme-fabrication box were shown in Figure 6.4 (a) and (c) respectively.

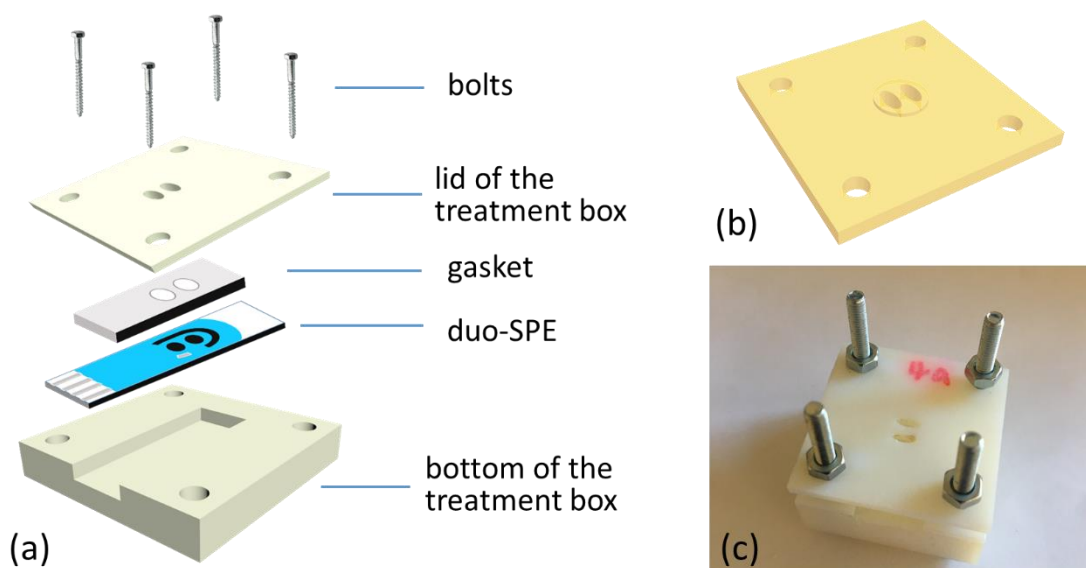


Figure 6.4 (a) The set-up for the enzyme-fabrication box; (b) the detailed structure of the lid which contains “pig nose”; (c) the assembled enzyme-fabrication box.

#### 6.2.4 Electrochemical measurements

Equipment used for all the electrochemical analysis was Autolab potentiostat-galvanostat (multi autolab cabinet, MAC80126) which was shown in Figure 6.5. All the electrochemical measurements were carried out in the cell for SPEs (mentioned in Chapter 3.3.1) covered by a box to avoid lights.

In this project, CV and CA were used for all the electrochemical analysis. CV experiments were performed at 5 mV/s of scan rate from 0 to 0.5 V vs Ag/Ag<sup>+</sup> and CA experiments were performed at an applying constant voltage 0.1 V vs Ag/Ag<sup>+</sup> which was obtained from CV curves for 100 s.

The electrolyte for electrochemical analysis using PBS containing the substrates with different concentrations. As mentioned in Chapter 3.1.1, before the electrochemical test of each modified SPEs the stock solutions including 10 mM and 1 mM H<sub>2</sub>O<sub>2</sub> or 10- and 100-times diluted xanthine sodium salt were respectively prepared fresh with PBS. For the biosensor performance tests, 100 μl PBS mixing with different volumes of fresh-prepared stock solutions was used as the electrolyte. For the interferences tests, a certain amount of glucose, uric acid (UA), ascorbic acid (AA) (Mao et al. 2008) and bovine serum albumin (BSA) in PBS were used as the

replacement of PBS.

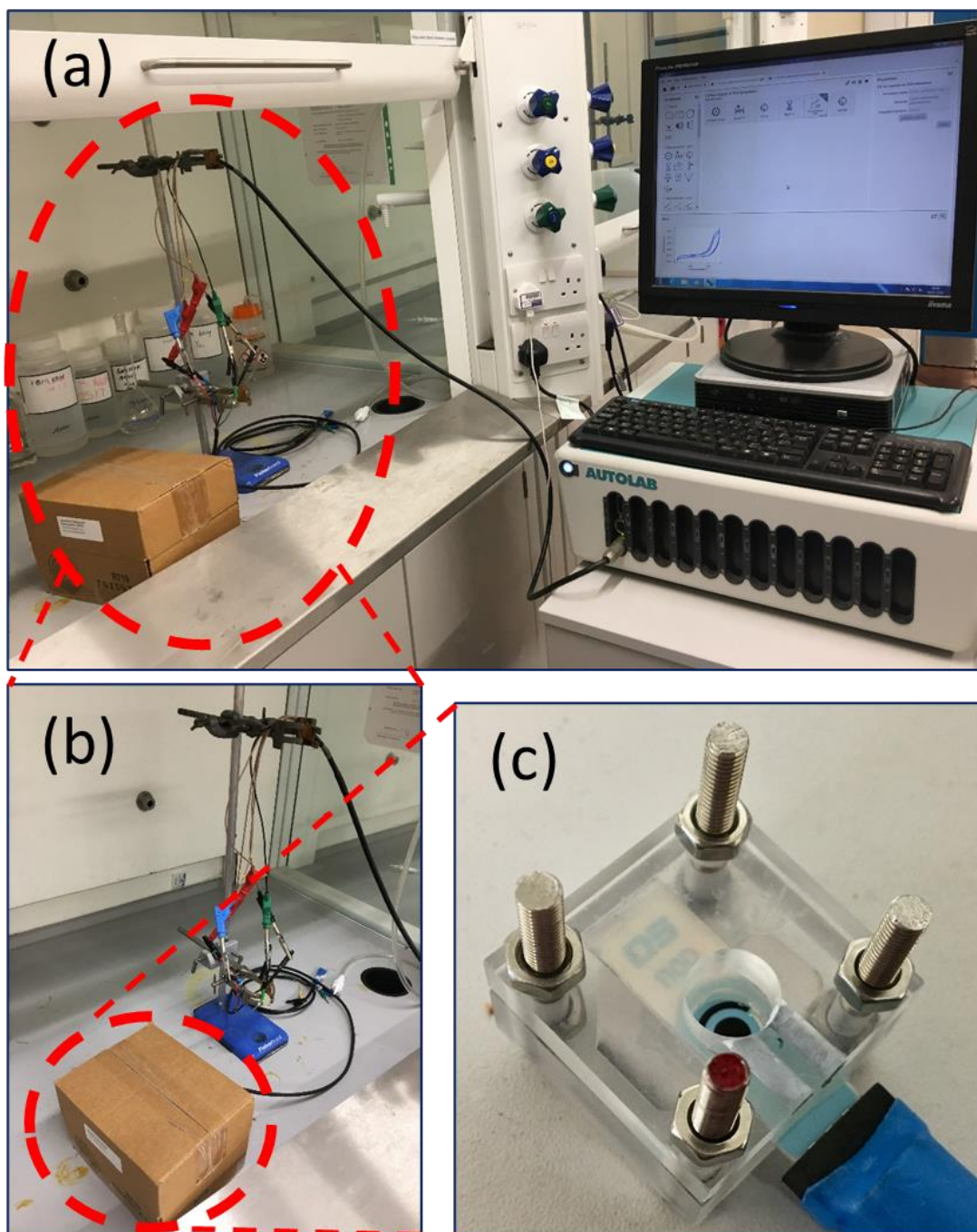


Figure 6.5 (a) & (b) Experimental set-up for electrochemical experiments; (c) the assembled cell for the electrochemical analysis.

## 6.3 Results and discussions

### 6.3.1 Performance of HRP for $H_2O_2$ detection

Before the fabrication of the electrochemical biosensor, the enzyme immobilization was analysed by cyclic voltammetry and chronoamperometry electrochemical techniques (Li et al.

2011). As mentioned in Chapter 5.3.1, SOD immobilization by the layer-by-layer self-assembly method with PDDA showed stable immobilization strength and slightly increased sensitivity of the electrode to the electric signal. Thus, HRP immobilization by cross-linking technique is the main method in this project.

For the performance of cross-linking technique based on the amide bonds and  $\pi$ - $\pi$  interactions, the CV scan was carried out after each step of the HRP immobilization in 0.1 M PBS at pH 7.4 in the presence and absence of 1 mM  $H_2O_2$  (Şahin 2020). Figure 6.6 shows the electrochemical response with each layer immobilized on the working electrode.

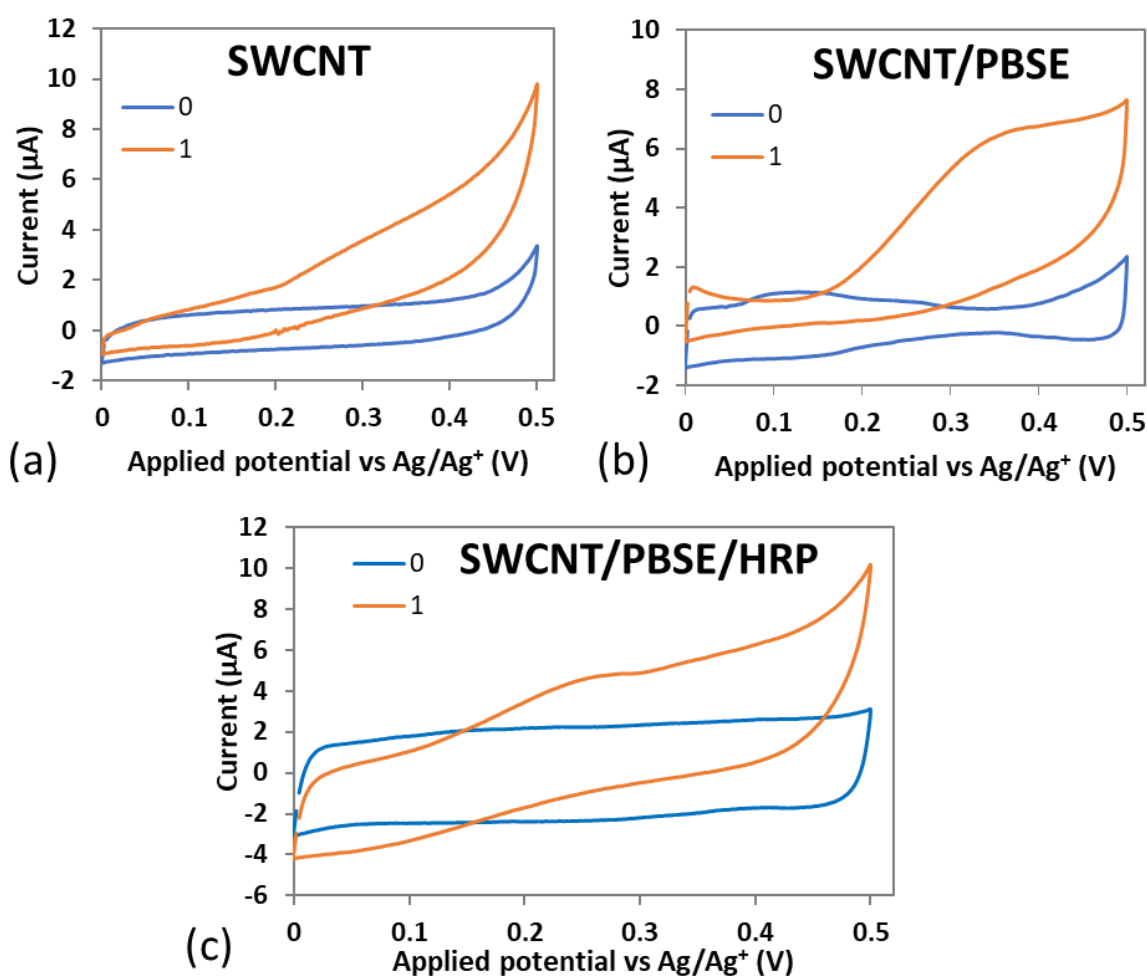


Figure 6.6 Voltammogram for the electrochemical performance of each layer immobilised by cross-linking technique: (a) SWCNT coated C-SPE; (b) PBSE / SWCNT / C-SPE; (c) HRP / PBSE / SWCNT / C-SPE. Tested in PBS (pH = 7.4) in the presence and absence of 1 mM  $H_2O_2$ . Where, 0 and 1 represent the electrolyte without and with 1 mM  $H_2O_2$  respectively. Scan rate: 50 mV/s.

The electrochemical signal changes after each layer are immobilized on the working electrode, which means the cross-linking method by PBSE works for HRP immobilization and each layer was successfully immobilized on the SWCNT-coated C-SPE. For the electrochemical

performance in the presence of PBSE in PBS without H<sub>2</sub>O<sub>2</sub>, the double layer region increased in magnitude from under 1  $\mu$ A to over 1  $\mu$ A from improved ion transfer and increased surface area. This increased further to 2  $\mu$ A upon HRP addition. For the electrochemical performance in PBS with H<sub>2</sub>O<sub>2</sub>, the oxidation current increased slightly from 3 to 5.5  $\mu$ A at 0.3 V however no reduction current or activity was seen. With the addition of HRP, oxidation activity remained similar ca. 5.5  $\mu$ A at 0.3 V however an apparent reduction current of -3.5  $\mu$ A can be seen at 0.1 V which can be assigned to reduction of H<sub>2</sub>O<sub>2</sub> to H<sub>2</sub>O.

Figure 6.6 (c) shows a reduction current response in PBS that contained 1mM H<sub>2</sub>O<sub>2</sub>. Unlike the SWCNT-coated C-SPE and PBSE / SWCNT / C-SPE, the observable reduction response starts from the range of 0.1 to 0.3 V (vs Ag/Ag<sup>+</sup>) and a slight peak at around 0.1 V (vs Ag/Ag<sup>+</sup>). This result suggests that the HRP-immobilized sensor can be used for a detection of H<sub>2</sub>O<sub>2</sub> through its reduction limiting current.

Using the HRP-immobilized sensor, the electrochemical performance for the reduction reaction of H<sub>2</sub>O<sub>2</sub> with increasing concentrations was studied by CV scans. Figure 6.7 illustrates an increasing reduction current response in the negative direction with the increasing concentration of H<sub>2</sub>O<sub>2</sub>. The clear observable reduction starts at around 0.25 V (vs Ag/Ag<sup>+</sup>) and the detectable current change starts from the voltage values of around 0.19 V (vs Ag/Ag<sup>+</sup>). The slight shift towards the negative potential is because of the acidic nature of the H<sub>2</sub>O<sub>2</sub> solution resulting in the small change of pH of the electrolyte (Jiang et al. 2009, Şahin 2020).

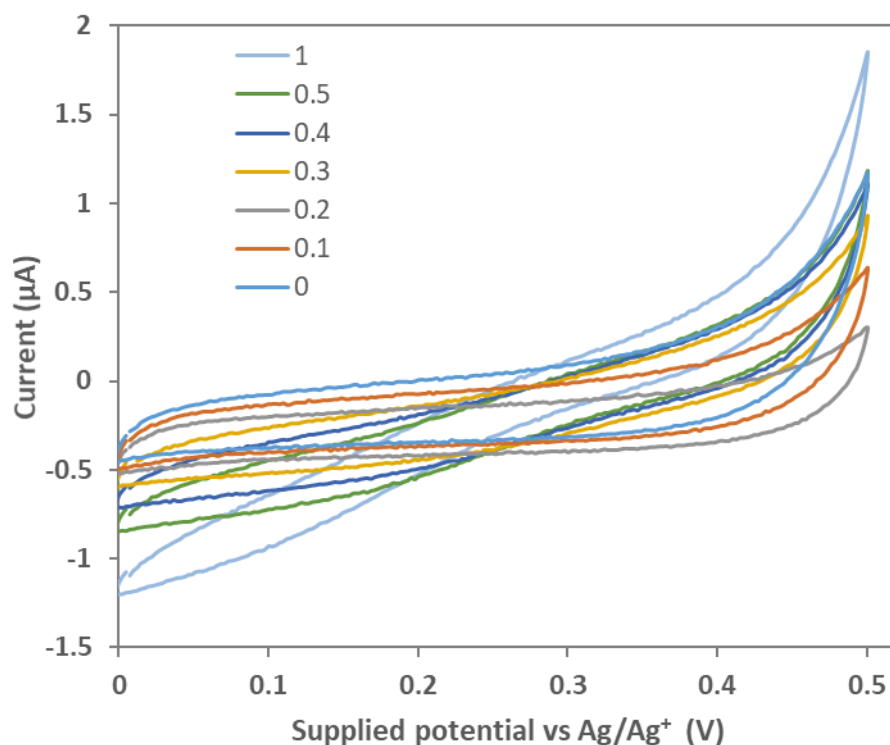


Figure 6.7 Voltammogram for the electrochemical performance of HRP-immobilised biosensor tested in PBS (pH = 7.4) which containing increasing concentration of H<sub>2</sub>O<sub>2</sub> (0, 0.1, 0.2, 0.3, 0.4, 0.5 and 1 mM). Scan rate: 5 mV/s.

The calibration curve for H<sub>2</sub>O<sub>2</sub> reduction detection (shown in Figure 6.8, data shown in Appendix Table S3.1) is generated by a series of current values corresponding to different concentrations of H<sub>2</sub>O<sub>2</sub> (0.01 mM to 0.5 mM in PBS) at 0.1 V vs Ag/Ag<sup>+</sup> from chrono amperometry at 100 s for a stable current signal. The result shows the linear relationship ( $R^2 = 0.9993$ ) between current and H<sub>2</sub>O<sub>2</sub> concentration where the reduction current (shown as negative values) increases with the consecutive addition of H<sub>2</sub>O<sub>2</sub>. The sensitivity and limit of detection (LoD) of the HRP-immobilized C-SPE for H<sub>2</sub>O<sub>2</sub> reduction detection are calculated as 3.694  $\mu\text{A}/\text{mM}$  and 26.9  $\mu\text{M}$  respectively, and the minimum detectable concentration of H<sub>2</sub>O<sub>2</sub> is recorded as 10  $\mu\text{M}$ .

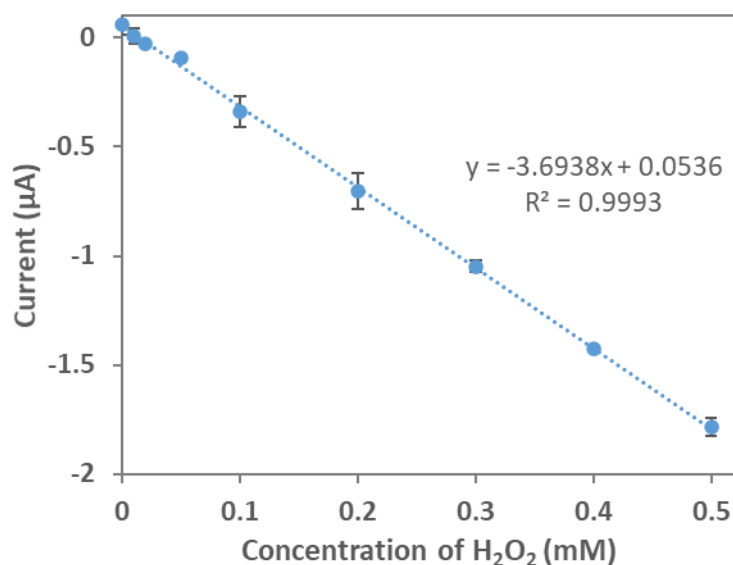


Figure 6.8 The calibration curve for H<sub>2</sub>O<sub>2</sub> reduction of the HRP-immobilized C-SPE (surface area of working electrode: 0.126 cm<sup>2</sup>).

The data was obtained from CA tested in PBS (pH = 7.4) with different concentration of H<sub>2</sub>O<sub>2</sub> (0, 0.01, 0.02, 0.05, 0.1, 0.2, 0.3, 0.4 and 0.5 mM) at 0.1V vs Ag/Ag<sup>+</sup> (~ 0.074 V vs SHE) at 100 s. Error bars are the sample standard deviation of measurements from repetitions (n = 3).

The results show that the HRP enzyme could be successfully immobilized by the cross-linking technique with SWCNT and PBSE as the crosslinker, and HRP-immobilized C-SPE using cross-linking has a quick and sensitive response on the detection of the H<sub>2</sub>O<sub>2</sub> reduction reaction, which can be used in superoxide biosensor for better performance.

### 6.3.2 Fabrication of the superoxide biosensors

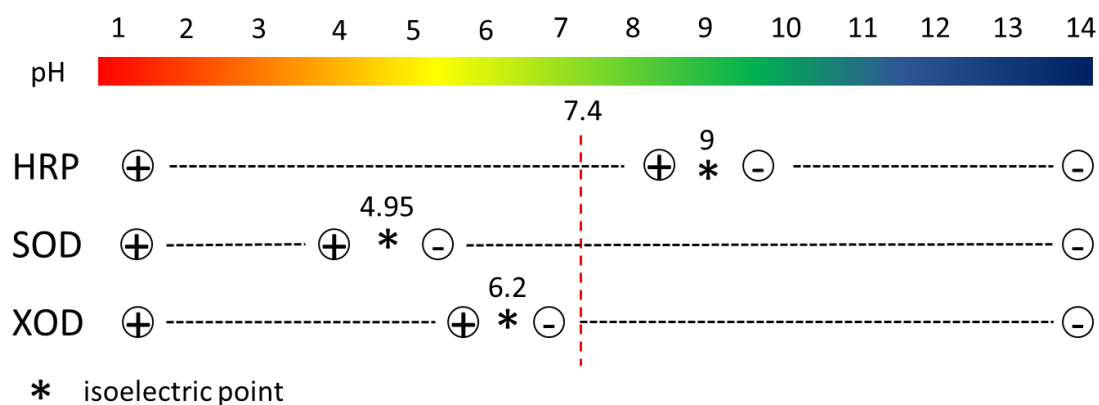
The HRP-immobilized C-SPE using cross-linking technique shows the successful electric signal response for H<sub>2</sub>O<sub>2</sub> reduction detection, and the biosensor that SOD-immobilized C-SPE by layer-by-layer self-assembly method shows the successful redox reaction from superoxide to H<sub>2</sub>O<sub>2</sub> (mentioned in Chapter 5). To fabricate the superoxide biosensor with high sensitivity and selectivity, the combination of HRP and SOD is one of the most important approaches in this project.

The simplest way to combine HRP and SOD is by directly adding the immobilized SOD onto the top of the HRP-immobilized electrode. Figure 6.9 illustrates the electrochemical performance of the biosensor which directly immobilizes both SOD and XOD on the HRP-modified C-SPE (XOD & SOD/ HRP/ SWCNT/ C-SPE, data shown in Appendix Table S3.2). The structure of this biosensor was shown in Figure 6.2, and XOD was immobilized on the top

of the biosensor by PDDA for the preparation of superoxide. The analysis was carried out by CA in PBS (pH=7.4) containing various concentration of H<sub>2</sub>O<sub>2</sub> or xanthine (0, 0.01, 0.02, 0.05, 0.1, 0.2, 0.3, 0.4 and 0.5 mM) at 0.1 V vs Ag/Ag<sup>+</sup>.

Figure 6.9 (a) shows that XOD & SOD/ HRP/ SWCNT/ C-SPE has low sensitivity for superoxide detection, and figure 6.9 (b) is the enlarge vision of the relationship between current responses and xanthine concentrations. Compared with the current response for H<sub>2</sub>O<sub>2</sub> reduction detection, the current hardly changes with the increasing concentration of xanthine. This result indicates that the reduction reaction of H<sub>2</sub>O<sub>2</sub> is still working in this biosensor while the preparation of superoxide and/or superoxide redox reaction by SOD has been affected and not proceeding. This could be due to the failure in the immobilization of SOD and/or XOD.

Table 6.1 The isoelectric point and charge carried by enzymes in solution.



Both SOD and XOD were immobilized by the layer-by-layer self-assembly method based on the electrostatic force between two opposite charges, and the charge of enzymes depends on their isoelectric point and pH value of the solution (Kang et al. 2014). From table 6.1, both SOD and XOD carry a negative charge in PBS, while HRP carries positive charges (Ball 1939, Bannister et al. 1971, Zakharova et al. 2011). Thus, SOD and XOD can be assembled steadily by PDDA, but their assembly of PDDA on top of HRP might fail. Thus, the actual structure of the immobilized enzyme could not perform well. PDDA could not form a film for enzyme immobilization. In this case, it is hard to achieve the layer-by-layer structure, which means the top of the structure was disturbed, resulting in only a limited quantity of the deposited SOD and XOD remaining on the working electrode surface.

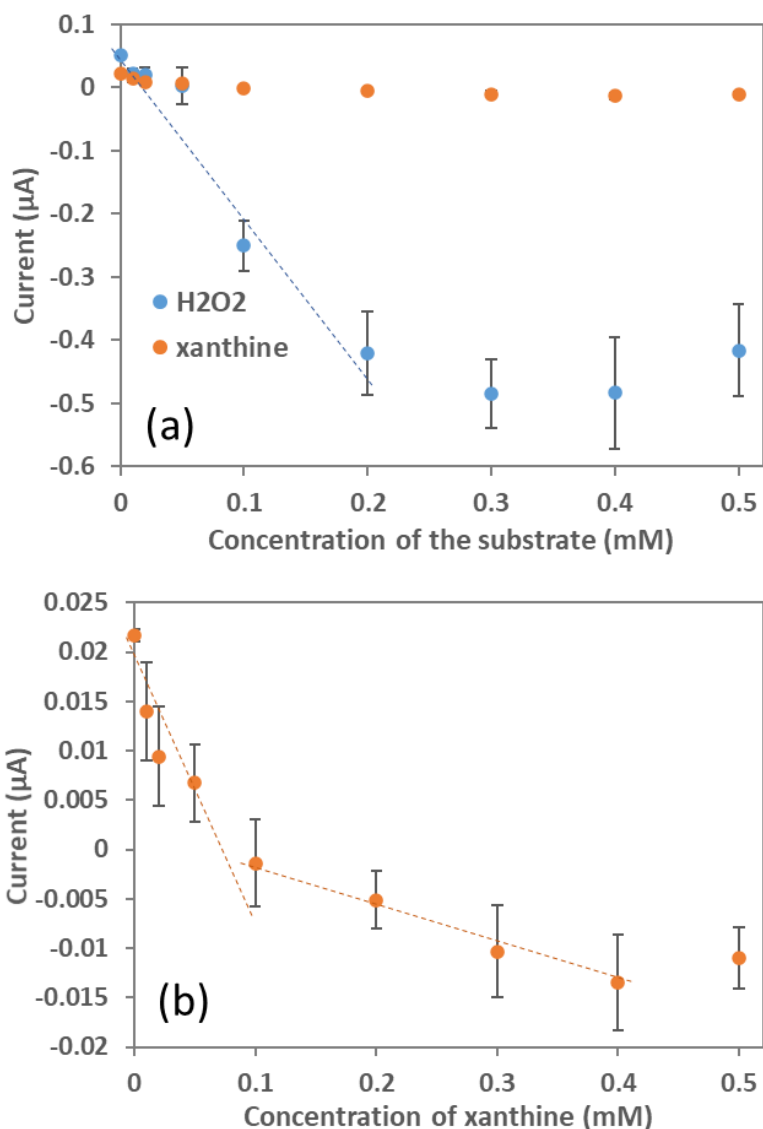


Figure 6.9 (a) The electrochemical performance for the biosensor using direct immobilization of three enzymes (HRP, SOD and XOD). (b) The enlarge vision of the current response for superoxide detection.

The data was obtained from CA tested in PBS (pH = 7.4) with different concentration (0, 0.01, 0.02, 0.05, 0.1, 0.2, 0.3, 0.4 and 0.5 mM) of H<sub>2</sub>O<sub>2</sub> (for H<sub>2</sub>O<sub>2</sub> reduction detection) or xanthine (for superoxide detection) at 0.1 V vs Ag/Ag<sup>+</sup> (~ 0.074 V vs SHE) at 100 s. The surface area of working electrode is 0.126 cm<sup>2</sup>. Error bars are the sample standard deviation of measurements from repetitions (n = 3).

Figure 6.9 also illustrates that the current response for both H<sub>2</sub>O<sub>2</sub> reduction detection and superoxide detection shows the discussed limitation. From Figure 6.9 (a), the detectable linear relationship was showed between 0 to 0.2 mM H<sub>2</sub>O<sub>2</sub> in H<sub>2</sub>O<sub>2</sub> reduction detection, and the unchanged currents were found when concentration higher than 0.2 mM. From Figure 6.9 (b), although the superoxide detection results could be separated to two linear relationships, the sensitivity of the detection between 0.1 to 0.4 mM is much lower than that between 0 to 0.1 mM xanthine, which is hardly detectable. These results illustrate that H<sub>2</sub>O<sub>2</sub> reduction is limited to a concentration lower than 0.2 mM, and the maximum limit of superoxide detection is 0.1

mM xanthine. The reason for the maximum concentration limitation could be the complex structure of the modified electrode hindered the diffusion of the substrates as well as limited amount of deposited active electrocatalyst or reagent (SOD and XOD, respectively). The current response for superoxide detection shows a linear relationship at xanthine concentration between 0.1 to 0.4 mM, but error bars illustrate the large random signal in this range, resulting in the unreliable value for the detection.

To solve this limitation of deposition compatibility, the layer-by-layer immobilized SOD and the cross-linking modified HRP were separated and deposited on two working electrodes with close proximity. The electrolyte was used to cover both of the enzyme-modified electrodes for 100 seconds to guarantee the complete reaction on both electrodes and pipette-mixed several times for less effect of mass transfer. Figure 6.10 shows the electrochemical performance for H<sub>2</sub>O<sub>2</sub> reduction and superoxide detection on enzyme-immobilized (including HRP, SOD and XOD) duo-SPE (data shown in Appendix Table S3. 3). Data were obtained in PBS containing substrates with various concentrations from 0.01 to 0.5 mM.

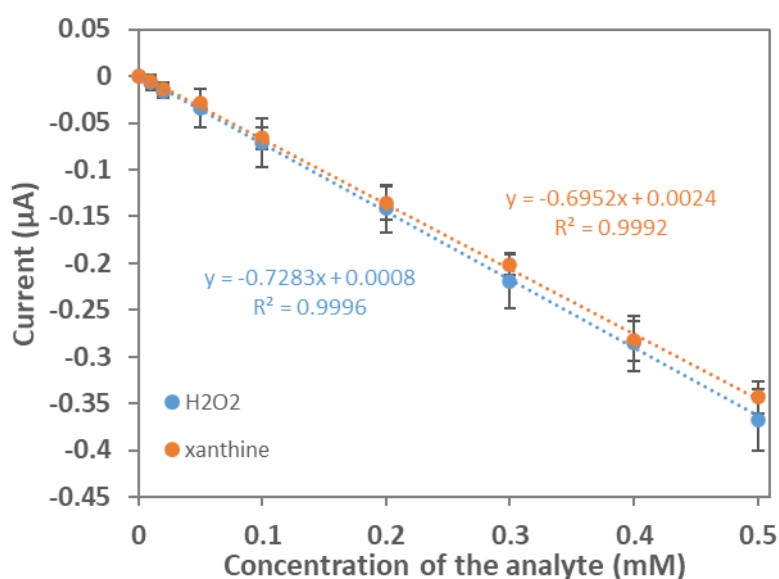


Figure 6.10 The electrochemical performance for the biosensor on enzyme-immobilized duo-SPE (containing all three enzymes: HRP, SOD and XOD).

The data was obtained from CA tested in PBS (pH = 7.4) with different concentration (0, 0.01, 0.02, 0.05, 0.1, 0.2, 0.3, 0.4 and 0.5 mM) of H<sub>2</sub>O<sub>2</sub> (for H<sub>2</sub>O<sub>2</sub> reduction detection) or xanthine (for superoxide detection) at 0.1 V vs Ag/Ag<sup>+</sup> (~ 0.074 V vs SHE) at 100 s. The surface area of working electrode is 0.059 cm<sup>2</sup>. Error bars are the sample standard deviation of measurements from repetitions (n = 3).

From Figure 6.10, a linear relationship ( $R^2 = 0.999+$ ) between the current and the concentration of substrates was obtained by CA at 0.1 V vs Ag/Ag<sup>+</sup> at 100s. The reduction current response

for superoxide detection can be seen as a bit lower than the reduction current for  $\text{H}_2\text{O}_2$  detection. The reason could be the consumption in the complex enzymatic reaction or the effect of mass transfer. The current difference between  $\text{H}_2\text{O}_2$  and superoxide detection is in the range of sample standard deviation, which illustrates that these effects could be ignored. The sensitivity of the biosensor and the LoD was calculated respectively as  $28 \mu\text{A}/(\text{mM}\cdot\text{cm}^2)$  and  $9.8 \mu\text{M}$ .

Figure 6.11 shows the linear relationship ( $R^2 = 0.9992$ ) between the actual concentration of xanthine in the solution and the calculated equivalent concentration of  $\text{H}_2\text{O}_2$  on the working electrode (data shown in Appendix Table S3.4). The data was obtained by calculating  $\text{H}_2\text{O}_2$  and xanthine concentration corresponding to the same current value from Figure 6.10. The ratio of the two concentrations was calculated as 0.9546, which is close to the ideal ratio of the reactions. This result indicates that xanthine completely reacted to produce  $\text{H}_2\text{O}_2$  and the mass transfer of  $\text{H}_2\text{O}_2$  between two working electrodes does not affect the signal.

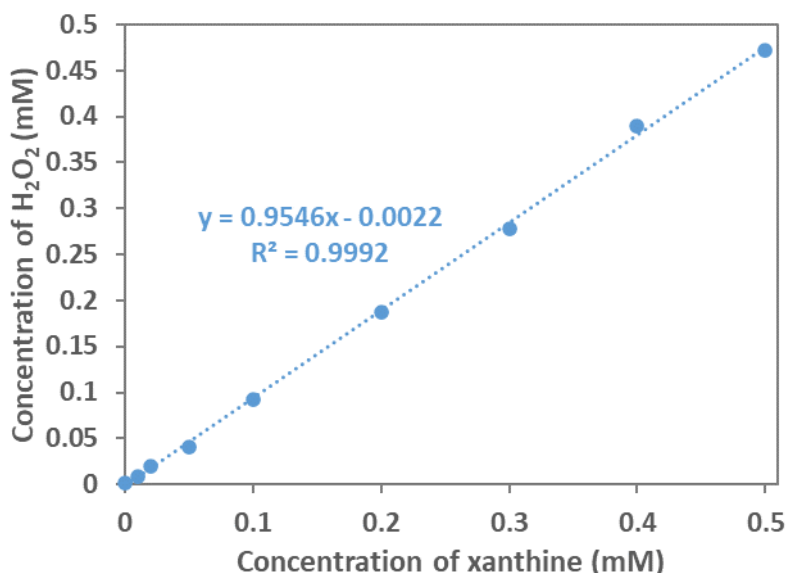


Figure 6.11 The linear relationship between the concentration of xanthine (0.01 to 0.5 mM) and the calculated  $\text{H}_2\text{O}_2$  concentration based on the same charge transfer (i.e. the current response in Figure 6.10).

### 6.3.3 Calibration of the biosensor based on the reduction reaction

In this work, the concentration of xanthine and  $\text{H}_2\text{O}_2$  is known and controlled corresponding to the detected current but the concentration of superoxide is unknown as there is not direct standard method to measure it directly. Thus, superoxide concentration was calculated as lies in the range from the known concentration of xanthine (maximum) and  $\text{H}_2\text{O}_2$  (minimum) based on the reaction from xanthine to superoxide and then to  $\text{H}_2\text{O}_2$ .

The calculation of the superoxide concentration detected by the developed SOD-HRP/ duo-SPE biosensor has two steps: 1) obtain the current values from the biosensor reading and use it to find out H<sub>2</sub>O<sub>2</sub> concentration and xanthine concentration respectively based on Figure 6.10 (blue line and orange line respectively); 2) as mentioned in Chapter 5.3.3, superoxide concentration is calculated as the average of the maximum (two times of the xanthine concentration) and the minimum (two times of the H<sub>2</sub>O<sub>2</sub> concentration).

The final calibration curve of this biosensor for superoxide detection was generated in Figure 6.12 (data shown in Appendix Table S3.5). The error bar shows the maximum and minimum values of each point. From the calibration curve, the superoxide concentration can be simply read with the current reading which represents the current drop after adding the superoxide samples in electrolytes. The sensitivity and LoD were calculated as 23.81  $\mu\text{A}/(\text{mM}\cdot\text{cm}^2)$  and 6  $\mu\text{M}$  respectively.

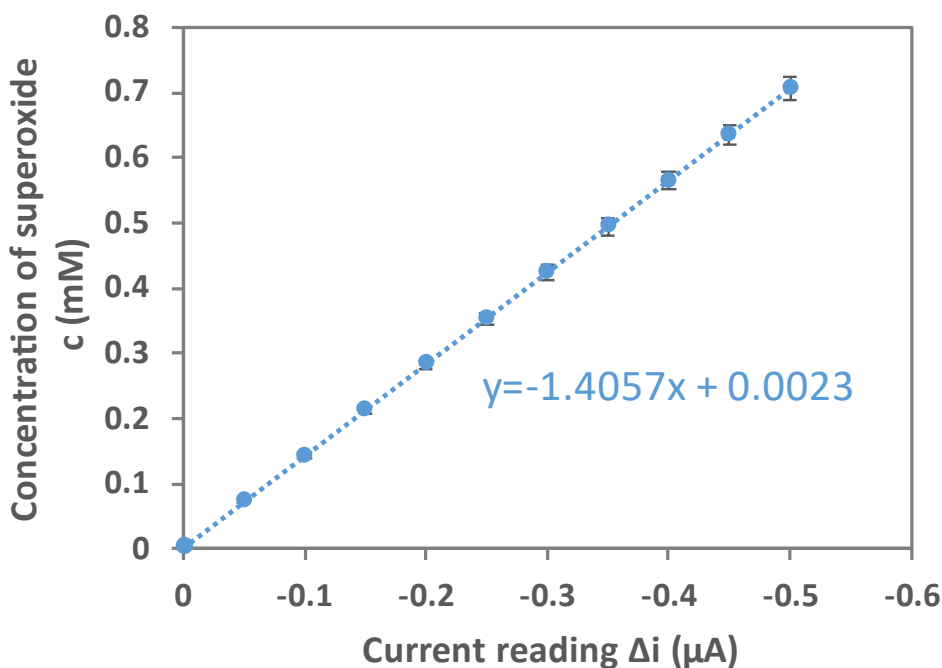


Figure 6.12 The overall calibration curve for the superoxide biosensor (enzyme-immobilized duo-SPE, the surface area of the working electrode: 0.059 cm<sup>2</sup>, SWCNT loading: 0.15 mg/cm<sup>2</sup>).

The current should be the current response of the biosensor after being calibrated in PBS. Error bars were obtained from the maximum and minimum concentrations.

This project used both SOD and HRP as a cascade system on an electrochemical biosensor, which achieves quantitative measurement for small-volume detection, making it possible to detect superoxide anions in small amounts of blood. To the best of author's knowledge, quantifying superoxide concentration by two separated working electrodes, has not yet been

reported in the literature.

### 6.3.4 Interference tests

It is reported that many interferences in human blood samples may affect the detection of  $H_2O_2$ . As the major components in blood samples, glucose, UA, AA and BSA were tested by CA analysis on enzyme-modified (HRP and SOD) duo-SPE (Chen et al. 2006, Cui et al. 2020, Moschopoulou and Kintzios 2015). Figure 6.13 shows the comparison of the current response before and after the addition of the interferences at the same potential for 100 seconds in PBS (pH=7.4) containing 0.01 ~ 0.5 mM  $H_2O_2$  (data shown in Appendix Table S3.6).

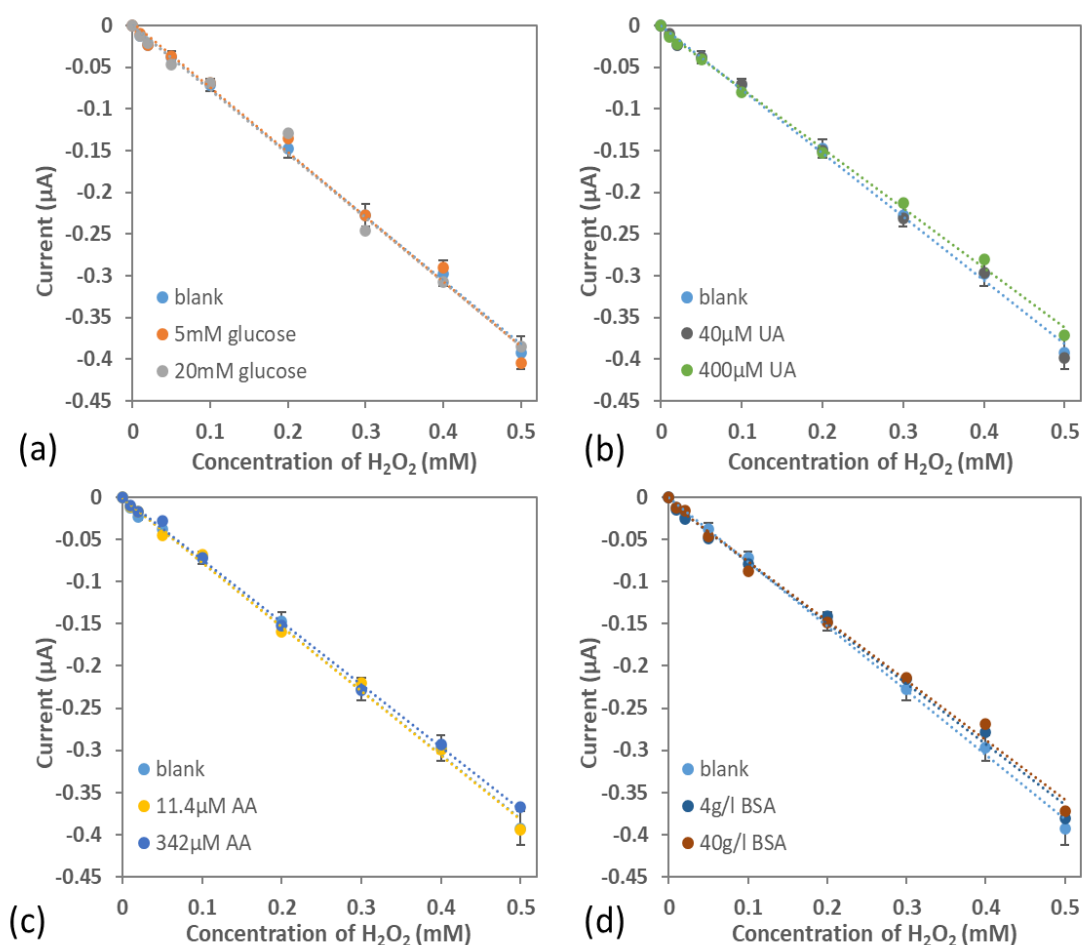


Figure 6.13 The current response of the biosensor with the SOD & HRP-immobilised duo-SPE for  $H_2O_2$  detection against (a) glucose, (b) uric acid, (c) ascorbic acid and (d) bovine serum albumin as the interference.

The data was obtained from CA of different concentration of  $H_2O_2$  (0, 0.01, 0.02, 0.05, 0.1, 0.2, 0.3, 0.4 and 0.5 mM) added to PBS (pH = 7.4) respectively containing different concentration of interferences at 0.1V vs  $Ag/Ag^+$  ( $\sim 0.074$  V vs SHE) at 100 s. Error bars are the sample standard deviation of measurements that without interferences from repetitions ( $n = 6$ ).

Figure 6.13 (a) shows the reduction current response in the presence and the absence of glucose, which illustrates that glucose has limited effect on the detection of  $\text{H}_2\text{O}_2$  reduction reaction even at high concentration levels. Figure (b), (c) and (d) respectively shows a slight shift toward the negative direction of reduction current after adding UA, AA and BSA with high concentration level. The reason for the slight shift could be that these compounds may affect the electric signal by reacting with the intermediary of HRP which is shown as the oxidised form, consuming  $\text{H}_2\text{O}_2$ , inhibiting the activity of the HRP enzyme or by reducing local  $\text{H}_2\text{O}_2$  concentration by competitive adsorption (Vojinović et al. 2004). However, this slight effect can be ignored because all the measured current is in the range of sample standard deviations, which means the effect from these interferences on the detection of  $\text{H}_2\text{O}_2$  reduction are ignorable due to the low potential (Ren et al. 2020, Yamamoto et al. 2003).

## 6.4 Conclusions

In this chapter, the cross-linking technique for HRP enzyme immobilization using SWCNT and PBSE based on  $\pi$ - $\pi$  interaction and the amide bonds was described and tested on C-SPE, which showed the successful assembly of the enzyme.

The electrochemical performance for  $\text{H}_2\text{O}_2$  detection was investigated by HRP-immobilized C-SPE in PBS with different concentrations of  $\text{H}_2\text{O}_2$  at 0.1 V vs  $\text{Ag}/\text{Ag}^+$ . The results showed good performance as high sensitivity of  $3.6938 \mu\text{A}/\text{mM}$  and the large detectable range.

For the fabrication of the superoxide biosensor, SOD was first directly immobilized on the HRP-modified C-SPE by PDDA, which shows the limited detection of  $\text{H}_2\text{O}_2$  at higher concentration and low sensitivity for superoxide detection. To separate the redox reaction of superoxide and the reduction reaction of  $\text{H}_2\text{O}_2$  on the different electrodes, enzyme-modified duo-SPE was prepared subsequently. The overall calibration curve for the superoxide biosensor was generated by enzyme-modified duo-SPE (shown in Figure 6.12). The sensitivity of the biosensor and the LoD was calculated respectively as  $23.81 \mu\text{A}/(\text{mM}\cdot\text{cm}^2)$  and  $6 \mu\text{M}$ .

The selectivity of the biosensor was tested against interferences including glucose, UA, AA and BSA in PBS with different concentrations of  $\text{H}_2\text{O}_2$ . Glucose showed no effect on the electrochemical signals, while UA, AA and BSA had the ignorable effect even at high concentration levels.

## Chapter 7 Application of biosensor in blood tests

In this chapter, the performance of both the biosensor based on the oxidation reaction of  $\text{H}_2\text{O}_2$  (SOD-based biosensor, mentioned in Chapter 5) and the biosensor based on the reduction reaction of  $\text{H}_2\text{O}_2$  (coupled SOD-HRP biosensor, mentioned in Chapter 6) were evaluated for superoxide detection in human blood samples. Electrochemical characterization of these two biosensors was performed in potassium phosphate-buffered solution (PBS) with different dilutions of human blood samples by using chronoamperometry (CA). The chemiluminescence (CL) technique with Luminol as the CL probe was used for comparison. Prior to the blood samples, various concentrations of hydrogen peroxide were detected by CL for the calibration standard. The results showed the electrochemical biosensor had better performance as the quick response, high selectivity and sensitivity for superoxide detection in blood samples while compared with the chemiluminescence technique. Both SOD-based biosensor and coupled SOD-HRP biosensor showed linear relationship between the current signal and the ratio of diluted blood in the electrolyte. Considering the interferences and electric signal deviations (especially for the SOD-based biosensor), the concentration of superoxide in human blood samples was calculated via electrochemical biosensors.

### 7.1 Introduction

Chemiluminescence can be defined as a light emission phenomenon caused by a chemical reaction. The energy released from a chemical reaction causes the decay of an electronically excited state to a lower energy level, resulting in the emission of light (Jimenez and Navas 2002).

Chemiluminescence assay is an efficient analytic method for low concentration detection, which is widely used in clinical chemistry. Chemiluminescent methods have many advantages, such as the low cellular toxicity, simple techniques, no requirement of background light, high sensitivity (Christodouleas et al. 2015).

There are different probes used for superoxide detections, including lucigenin probe, luminol probe and fluorescence probe. The fluorescence-based assay is semiquantitative, so that usually be used to provide the location of superoxide in the vessel wall in cultured cells and in sections of vascular tissues (Münzel et al. 2002). Compared with lucigenin probe, luminol-based chemiluminescence is more commonly used for superoxide detection, because it can detect both extracellular and intracellular deoxygenation products, while lucigenin probe can only detect

the extracellular radicals (Agarwal et al. 2004).

As a redox-sensitive compound, luminol emits blue light when mixed with oxidising agents. With the catalyst of different enzymes, including catalase, xanthine oxidase, cytochrome c and horseradish peroxidase, luminol-based chemiluminescence could achieve the flexible detection of superoxide anion and hydrogen peroxide (Bedouhène et al. 2017).

## 7.2 Experimental

### 7.2.1 Chemiluminescence spectroscopy

Glucose ( $\geq 99.5\%$ , powder, BioReagent, suitable for cell culture), magnesium chloride ( $\text{MgCl}_2$ ), calcium chloride ( $\text{CaCl}_2$ ), Bovine Serum Albumin (BSA, pH 7,  $\geq 98\%$ ), phorbol 12-myristate 13-acetate (PMA,  $\geq 99\%$ , powder), luminol and dimethyl sulfoxide (DMSO, ACS reagent,  $\geq 99.9\%$ ), were purchased from Sigma-Aldrich (Dorset, UK). 0.1 M potassium phosphate buffer (PBS) was purchased, prepared and stored as described in Chapter 3.1.1.

The buffer for blood was prepared fresh every few days by PBS containing 5mM glucose, 1mM  $\text{MgCl}_2$ , 0.5mM  $\text{CaCl}_2$  and 0.05% BSA. The 100 $\times$  stocks of glucose (500mM),  $\text{MgCl}_2$  (100mM),  $\text{CaCl}_2$  (50mM) and BSA (5%, g/ml) were prepared priorly in ultrapure water and freeze in aliquots at  $-20\text{ }^\circ\text{C}$  (Yamazaki et al. 2011).

To detect the maximum level of superoxide generated by white blood cells in blood samples, PMA assay was used to activate protein kinase C and consequently, superoxide was produced by phagocytes in blood samples (Caldefie-Chézet et al. 2002). The stock for the PMA assay was prepared as 1 mg/ml in DMSO and stored in aliquots at  $-20\text{ }^\circ\text{C}$ , and the working solution for the PMA assay was prepared fresh before detection by diluting 1  $\mu\text{l}$  PMA stock in 499  $\mu\text{l}$  buffer. The stock of luminol was prepared as 100 mM in DMSO and luminol assay buffer was made by diluting luminol stocks to 1 mM in the buffer.

The chemiluminescence performance was carried out in a 96-well microplate by Tecan infinite<sup>®</sup> 200 multifunctional microplate reader (Tecan Austria GmbH, Austria), which is shown in Figure 7.1.



Figure 7.1 The equipment used for chemiluminescence: Tecan infinite<sup>®</sup> 200 multifunctional microplate reader

### 7.2.2 Electrochemical measurements

The screen-printed electrode (SPE) used in biosensor, screen-printed carbon electrode (C-SPE, model DRP-C110) and dual screen-printed carbon electrode (duo-SPE, model DRP-C1110), mentioned in Chapter 5 and 6, were obtained from DropSens (Oviedo, Spain). The SPEs were stored at room temperature in a dry box away from light.

The SOD-based biosensor for superoxide detection in blood samples was fabricated by the layer-by-layer self-assembly enzyme-immobilization to form the structure of C-SPE/ SWCNT/ PDDA/ SOD, as mentioned in Chapter 5. The coupled SOD-HRP biosensor used dual-SPE to separate two enzymatic reactions, as mentioned in Chapter 6, with the structure of C-SPE/ SWCNT/ PBSE/ HRP as the H<sub>2</sub>O<sub>2</sub> detecting electrode and C-SPE/ SWCNT/ PDDA/ SOD as the superoxide reacting electrode.

Equipment used for all the electrochemical analysis was Autolab potentiostat-galvanostat (multi autolab cabinet, MAC80126, mentioned in Chapter 3.3.1). All the electrochemical measurements were carried out by chronoamperometry (CA) in the cell for SPEs covered by a box to avoid lights. The cell used for the electrochemical analysis can hold 100  $\mu$ l of various

times PBS-diluted blood samples as the electrolyte.

### 7.3 Results and discussions

The blood sample tests were carried out with the support of researchers in the Faculty of Medical Science. The chemiluminescence method was used for comparison. Both the chemiluminescence technique and the electrochemical biosensor detected the blood sample from the same volunteer with the same concentration (volume ratio i.e., v/v in buffer solution).

#### 7.3.1 *The calibration of chemiluminescence for superoxide detection*

Prior to the superoxide detection in real samples, the various concentrations of superoxide generated from xanthine in the presence of XOD were detected for the calibration curve. The superoxide level was detected by using luminol (100 mM in dimethyl sulfoxide, diluted to 1 mM with PBS buffer) in a luminometer for over a period of 25 minutes to allow time for the reaction to take place, with a 96-well plate read once per minute (Vessey et al. 2014).

The superoxide anion solution was prepared fresh before chemiluminescence analysis. As mentioned before in Chapter 4, the concentration of generated superoxide was controlled by the concentration of xanthine in PBS buffer which contains 3 mg/ml XOD. Each individual detection solution contained 20  $\mu$ l of superoxide-generation solutions and 200  $\mu$ l of luminol buffer.

The chemiluminescence signal shows the extremely unstable results for superoxide detection (Figure 7.2, data shown in Appendix Table S4.1). Compared with the result of detection in the absence of superoxide anion, the chemiluminescence response started from 18 minutes and increased continuously until 25 minutes. The signal for the xanthine concentration range of 0.05 mM to 5 mM could hardly be recognized separately, and all signals were maintained around the value of the start point during the whole detection procedure. The reason for the results could be low concentration beyond the limit of detection.

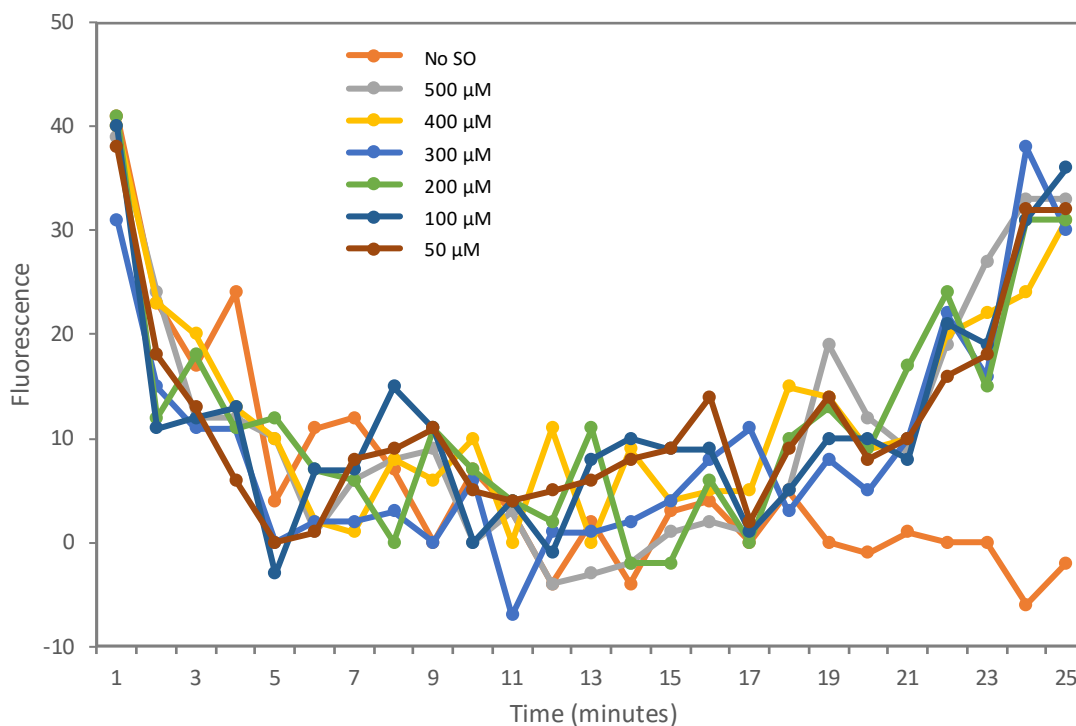


Figure 7.2 Results of chemiluminescence technique for superoxide detection with different concentration of xanthine from 0.05 mM to 0.5 mM in buffer. SO: superoxide produced from xanthine in the presence of xanthine oxidase.

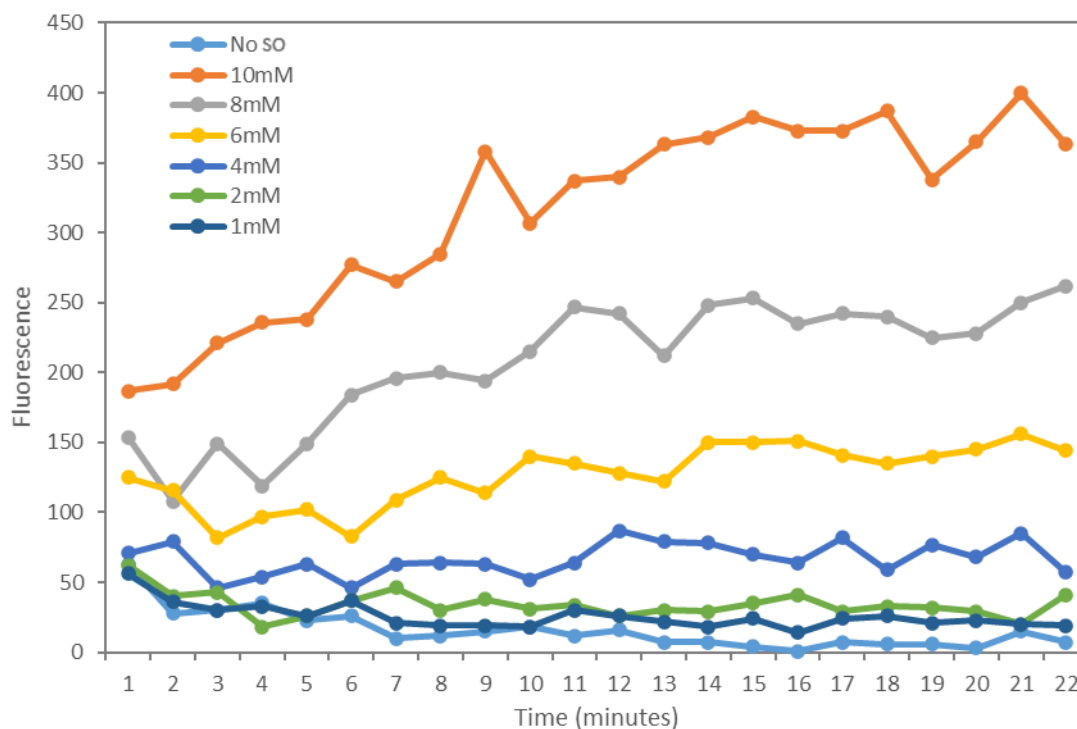


Figure 7.3 Results of chemiluminescence technique for superoxide detection with various high concentration level in buffer. SO: superoxide produced from xanthine in the presence of xanthine oxidase.

To find the limit of detection for the chemiluminescence methods, the signal was measured in

buffer with the various high-level concentrations of superoxide (Figure 7.3, data shown in Appendix Table S4.2). The signal increases in the first 10 minutes and reached a relatively stable state at 14 minutes, which could be regarded as the minimum detecting time. The calibration curve for chemiluminescence analysis was generated based on the relationship between the concentration of xanthine and the corrected fluorescence value. The value was obtained by the following two steps:

(1) the sample fluorescence was corrected by removing the background of the blank test (fluorescence of solution without xanthine), which is shown in equation 7.1 (Szkola et al. 2013).

$$\text{fluorescence}_{corrected} = \text{fluorescence}_{sample} - \text{fluorescence}_{blank} \quad (\text{Eq. 7.1})$$

(2) the average value was calculated from 15 to 22 min due to the slight changes in their stable state.

The corrected fluorescence shows a linear increase at a high concentration level (2 mM or higher), which indicates the successful detection of superoxide (data shown in Appendix Table S4.3). The limit of detection was calculated as 3.5 mM from the Figure 7.4. For the samples with a low concentration of superoxide, the luminol-base chemiluminescence could only achieve the recognition but not quantitative measurement. These results represent that luminal-based chemiluminescence is lack efficiency and sensitivity for low-concentration detections.

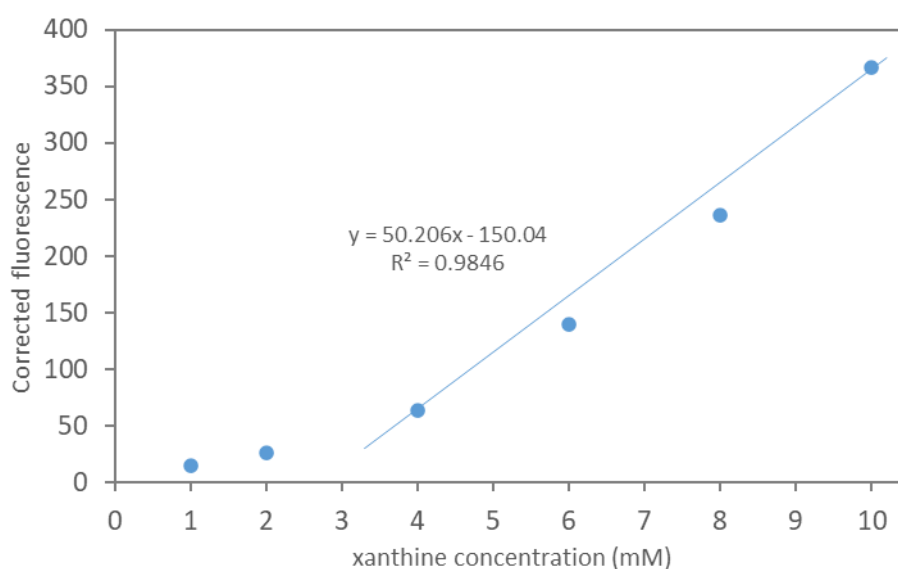


Figure 7.4 Calibration curve for high concentration detection of superoxide.

### 7.3.2 The blood sample tests by chemiluminescence

The chemiluminescence for the blood sample detection was carried out in the maximum oxidative stress environment. The blood sample were diluted by 20, 40, 60, 80 and 100 times in blood buffer which contained 5 mM glucose, 1 mM MgCl<sub>2</sub>, 0.5 mM CaCl<sub>2</sub> and 0.05% BSA (0.05 g/ml in deionized water) in PBS.

PMA (1 mg/ml in dimethyl sulfoxide, diluted to 0.4% v/v in blood buffer) is added to the blood sample for the maximum level of oxidative stress detection due to the stimulation of PMA on the activation of protein kinase C resulting in the produced superoxide by phagocytes (Yamazaki et al. 2011). The PMA assay for the detection includes 40 µl of diluted blood, 20 µl of PMA solution and 200 µl of luminol buffer in each sample solution.

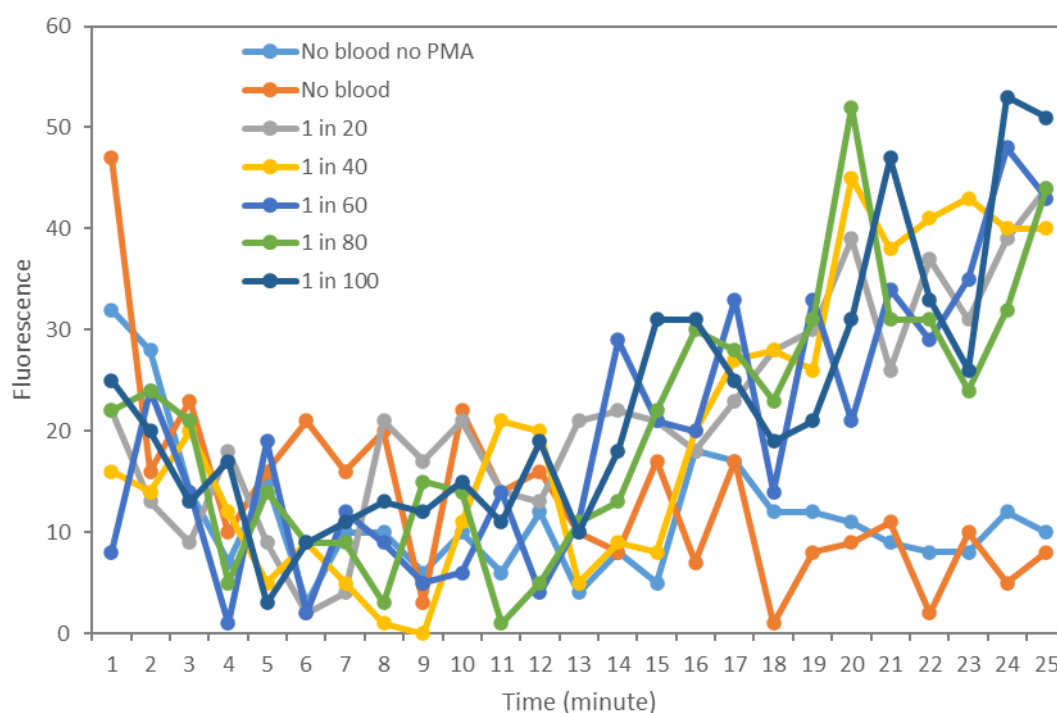


Figure 7.5 Results of chemiluminescence technique for superoxide detection in blood samples diluted with blood buffer.

1 in 20 (40/60/80/100) is 1 volume of blood diluted to 20 (40/60/80/ 100) volume of solution with blood buffer.

Figure 7.5 (data shown in Appendix Table S4.4) represents the result of the chemiluminescence method for superoxide detection in the blood sample with different dilutions. The detection is available from 16 ~ 19 minutes and the fluorescence of those blood samples increases with time, which showed similar behaviour in low-concentration detection.

The chemiluminescence could easily detect the difference between blood and buffer samples and was not affected by some blood other components e.g. glucose. But chemiluminescence could not detect the effect of dilution and drop in superoxide concentration in the blood sample, which means the method lacks quantitative measurement for superoxide in blood tests at the studied concentrations.

Instead of detecting superoxide, the luminol-drive chemiluminescence is generic ROS detection method, since it could be affected by a variety of other oxygen species, such as hydroxyl radical, peroxynitrite, etc. (Münzel et al. 2002).

### 7.3.3 The blood sample tests by electrochemical biosensor

The electrochemical biosensor for the blood sample detection was carried out by the enzyme-immobilized system which was respectively mentioned in Chapter 5 and Chapter 6. The blood sample from the same resource as the chemiluminescence technique was diluted by 20, 40, 60, 80 and 100 times in PBS (pH = 7.4) as the electrolyte.

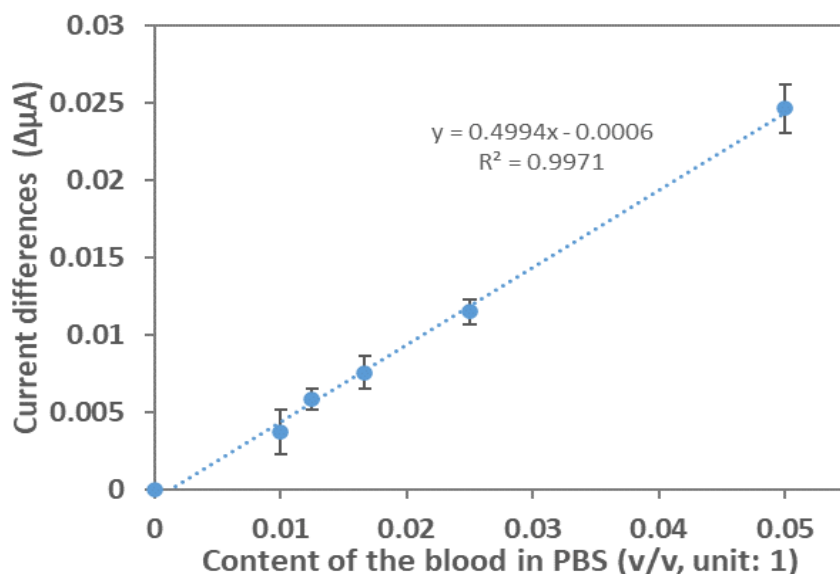


Figure 7.6 Results of the blood test for superoxide detection by the developed SOD-based biosensor

(SOD-immobilised SWCNT-coated C-SPE, the surface area of the working electrode: 0.126 cm<sup>2</sup>, SWCNT loading: 0.15 mg/cm<sup>2</sup>). v/v is the volume ratio of blood to the electrolyte (blood dilutions by PBS, pH 7.4). Error bars are the sample standard deviation of measurements from repetitions (n = 3).

Figure 7.6 (data shown in Appendix Table S4.5) shows the average current response of three repetitions (CA at 0.6 V vs Ag/Ag<sup>+</sup> at 100 s) to the testing of the blood sample with different dilutions. The relationship between blood dilutions and current response shows good linearity

( $R^2 = 0.9971$ ), which means the developed SOD-based electrochemical biosensor has good sensitivity and selectivity toward superoxide detection in blood. The relatively smaller deviation confirms the good reproducibility and the accuracy of the biosensor. The sensitivity of this detection was calculated as  $3.96 \mu\text{A}/(\text{mM}\cdot\text{cm}^2)$ . As mentioned in Chapter 3.4, considering the glucose effect on the current response, the superoxide concentration of this blood sample was calculated as  $0.258 \pm 0.031 \text{ mM}$  based on the calibration curve (Figure 5.10) of the developed SOD-based biosensor.

The quantitative measurement for superoxide in blood samples was also performed by the coupled SOD-HRP biosensor. The electrochemical performance for the diluted blood samples is shown in Figure 7.7 (data shown in Appendix Table S4.6). Data was obtained from three repetitions of each measurement using CA at  $0.1 \text{ V}$  vs  $\text{Ag}/\text{Ag}^+$  at  $100 \text{ s}$ . Very good linearity ( $R^2 = 0.9978$ ) between blood dilutions and current response was seen confirming the high accuracy and selectivity of the developed biosensor with coupled SOD-HRP system toward superoxide detection and its successful application in blood tests. The sensitivity of this detection was calculated as  $1.33 \mu\text{A}/(\text{mM}\cdot\text{cm}^2)$ . With the calculation steps mentioned in Chapter 3.4, the superoxide concentration of the blood sample was calculated as  $0.217 \pm 0.018 \text{ mM}$  based on the calibration curve (Figure 6.12) of the coupled SOD-HRP biosensor.

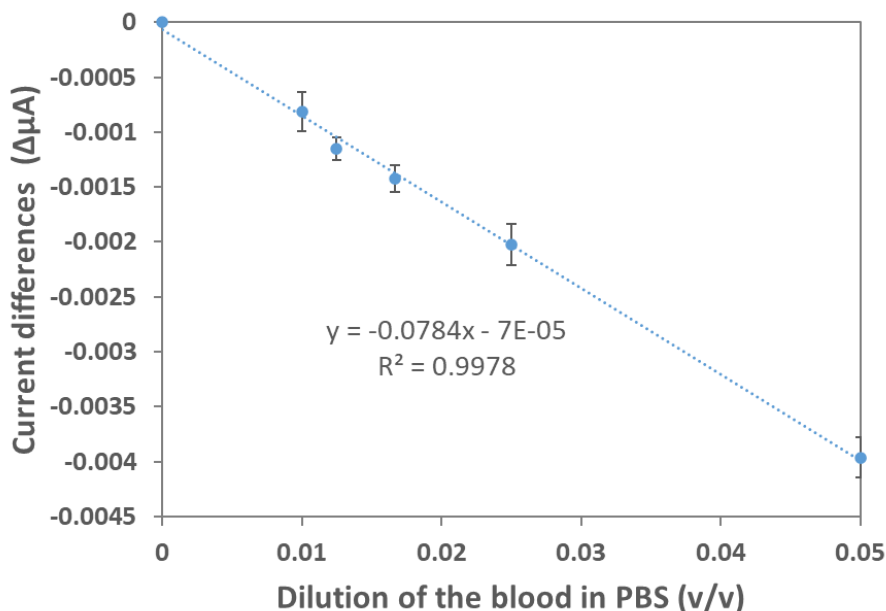


Figure 7.7 Results of the blood test for superoxide detection by the developed coupled SOD-HRP biosensor.

(Surface area of the working electrode:  $0.059 \text{ cm}^2$ , SWCNT loading:  $0.15 \text{ mg}/\text{cm}^2$ ). v/v is the volume ratio of blood to the electrolyte (blood dilutions by PBS, pH 7.4). Error bars are the sample standard

*deviation of measurements from repetitions (n = 3).*

Compared with the SOD-based biosensor, the current signal of coupled SOD-HRP biosensor shows a small value, and the current density is also smaller than the SOD-based biosensor. Because of the difference in detection mechanism, the rate of electron transfer is different, as indicated by differences in current and current density. The SOD-based biosensor detects superoxide based on the direct oxidation reaction of  $\text{H}_2\text{O}_2$  on the working electrode, while coupled SOD-HRP biosensor is based on the enzymatic-catalysed reduction reaction of  $\text{H}_2\text{O}_2$  (Malomo et al. 2011). The electron transfer of coupled SOD-HRP biosensor depends on the amount and activity of the immobilized HRP and might be affected by the local exceed oxygen molecules and  $\text{H}_2\text{O}_2$  (Vlasits et al. 2010). For the accurate detection of superoxide, coupled SOD-HRP biosensor is better than SOD-based biosensor as it is not susceptible to large effect of glucose and does not require measurement or knowledge of glucose concentration for correction.

Reactive oxygen species in blood, e.g., superoxide, can degrade or undergo chemical changes over time, especially been exposed to air or light. Thus, the detections required fresh blood samples to ensure the concentration of superoxide remaining stable during testing, and providing more accurate and consistent results. Due to time constraints and the impact of COVID-19, some challenges, e.g., a lack of volunteers, and sample availability from the School of Medicine, were found in this project, resulting in only two blood samples were obtained via a finger prick method.

The samples were assigned to their respective biosensor, and to increase number of test samples and examine detection level and accuracy of measurement a dilution series was completed for each of the two samples. Chemiluminescence data were also obtained from the same samples for comparison. A promising result was obtained from the existing data. The linear plot obtained from the dilution series, shown in Figure 7.6 for SOD-based biosensor and Figure 7.7 for coupled SOD-HRP biosensor, showed the accuracy of detection in low concentrations, and the feasibility of blood dilutions when doing the measurements. The blood dilution with buffer solution can be effective in reducing the amount of cell debris present in the samples during the detections and consequently the fouling of electrode surface (Pradhan et al. 2022). However, this requires pre-treatment of sample which is not desired. Other approach could be to add selective membrane or coating to restrict deposition of cell debris while allowing ROS diffusion, or to implement a flow system by continuously flowing the sample over the sensor to minimize the contact time and the possibilities of fouling.

The results from different blood samples obtained respectively from two biosensors were similar, around 0.2 mM. This result provides some validation of the consistency of the two sensors for blood measurements, although more samples are still needed to eliminate the potential for incidental results of an individual testing.

## 7.4 Conclusions

Compared with the chemiluminescence method, the electrochemical biosensor shows better performance for superoxide detection in human blood. For detection time, chemiluminescence spent 16 to 19 minutes to recognize the blood sample and the reactions lasted for up to 25 minutes, while biosensors used only 100 seconds for the stable current response. For the selectivity, chemiluminescence detected the maximum level of superoxide due to the catalysis of PMA, while the biosensor focused on the concentration of existing superoxide in blood. For the sensitive and accurate detection, chemiluminescence could hardly tell the difference of the blood sample with different dilutions, while biosensors showed the superoxide concentration in human blood based on the calibration curve.

Both the SOD-based biosensor and the coupled SOD-HRP biosensor were proved as high-selectivity and accurate biosensors which could successfully be applied in human blood detections. Comparing two biosensors, the SOD-based biosensor showed the higher current density and higher sensitivity of  $3.96 \mu\text{A}/(\text{mM}\cdot\text{cm}^2)$  while  $1.33 \mu\text{A}/(\text{mM}\cdot\text{cm}^2)$  for the coupled SOD-HRP biosensor, which was contributed to the direct electron transfer on working electrode. However, the detection results of the SOD-based biosensor were affected by glucose concentration in blood samples, which means that the coupled SOD-HRP biosensor has the higher accuracy of detections. To consider the bias from glucose on the detections, the superoxide concentration detected by the SOD-based biosensor was calculated assuming blood glucose level of 5 mM. The calculated superoxide concentration for two biosensors were both around 0.2 mM.

## Chapter 8 Conclusion and recommendations for future work

### 8.1 Conclusion

The incidence of aging diseases caused by the high-level concentration of reactive oxygen species, especially superoxide in the human body increased by years and reached its highest level nowadays, and the biosensor, as an analytical device, is one of the most common ways to detect superoxide. To address the lack of easy-operation, high-selectivity, and quick-response of existing biosensors, the aim of this project was to develop a superoxide biosensor that could fit in a hand-held device to provide quick and accurate results.

This project firstly worked on the generation methods of superoxide anion because of its characteristics of poor stability. For easy operation, low cost and less requirement of the aqueous environment, the chemical generation in NaOH solution and biological method using xanthine oxidase enzyme were compared. Since the requirement of strong alkaline for chemical generation, the effect of pH on enzyme activity was investigated. Although the superoxide concentration can be confirmed by chemical generation, the high pH of the solution was proved to affect the enzyme activity. When adjusting pH to neutral, the generated superoxide showed instability and decreased in concentration with time. The biological method which using xanthine and xanthine oxidase enzyme (XOD) for superoxide preparation resulted in 10 % higher activity than the chemical generation by sodium hydroxide and dithionite, and the produced superoxide showed excellent stability in more than five hours. Thus, the biological method was then chosen to generate superoxide for subsequent biosensor analysis because of its better performance.

The superoxide dismutase (SOD)-based biosensor was focused on in this project due to the high selectivity for detection of superoxide anion. The quantitative measurement was based on the determination of oxidation of hydrogen peroxide produced from the superoxide disproportionation reaction on SOD. For easy operation, the immobilization of the enzyme was achieved using layer-by-layer self-assembly by poly(diallyldimethylammonium chloride) (PDDA) on the working electrode, where the single-wall carbon nanotube (SWCNT) was used to enhance the sensitivity of the biosensor. Results showed this developed SOD-based biosensor having high sensitivity of  $71.44 \mu\text{A}/(\text{mM}\cdot\text{cm}^2)$  and low limit of detection (LoD) as  $8.6 \mu\text{M}$ , which meets the requirements of low-concentration detection in blood. The effect of interferences on the electrochemical performance of biosensor was tested, uric acid, ascorbic acid and bovine serum albumin hardly affected the detection and the bias from glucose was

considered into the calibration curve for this SOD-based biosensor.

Horseradish peroxidase (HRP) was then studied for the biosensor based on the detection of reduction reaction of hydrogen peroxide to improve the accuracy of the superoxide biosensor by decreasing the detecting potential and avoiding the oxidation reaction from other components in blood. A coupled-enzyme biosensor was established with both SOD and HRP as a cascade system. Two enzymes were separated on different electrodes of a two-electrode system for better electrochemical performance, where SOD was immobilized with PDDA by layer-by-layer adsorption and HRP was immobilized with 1-pyrenebutyric acid N-hydroxysuccinimide ester (PBSE) and carbon nanotubes by  $\pi$ - $\pi$  interaction and the amide bonds. This coupled SOD-HRP biosensor showed the sensitivity of  $23.8 \mu\text{A}/(\text{mM}\cdot\text{cm}^2)$  and LoD as  $6 \mu\text{M}$ , which also meet the requirements of low-concentration detection in blood. The interferences were proved no effect on the superoxide detection and the calibration curve was subsequently generated.

Comparing with the SOD-based biosensor, coupled SOD-HRP biosensor showed lower current response and similar limit of detection, but it had higher sensitivity because that the current signal not being affected by interferences. The accurate detection by SOD-based biosensor requires the known concentration of glucose to eliminate the bias, while coupled SOD-HRP could directly obtained superoxide concentrations.

Both SOD-based biosensor and coupled SOD-HRP biosensor successfully finished the superoxide detection in blood samples. The blood sample was diluted at different multiples to demonstrate the high stability and accuracy of the biosensors. Chemiluminescence (CL) method for reactive oxygen species detection was also studied for comparison. Compared with the CL method, the biosensors showed the advantages of quick response, high selectivity and successful quantitative measurement of superoxide with low concentration. The superoxide concentration in the human blood sample was calculated as  $0.258 \pm 0.031 \text{ mM}$  and  $0.217 \pm 0.018 \text{ mM}$  respectively by these two biosensors. Considering the accuracy of the biosensor for the quantitative detection of superoxide anions, coupled SOD-HRP biosensor is better than SOD-based biosensor because it avoids large effect of high-concentration glucose and does not need to measure or know glucose concentration in blood samples for correction. Unfortunately, there is no efficient way reported to date to validate this data in real blood samples.

In summary, this project successfully established the biosensors for the quantitative measurements of superoxide anion in low concentration, which is down to  $\mu\text{M}$ , with the limit

of detection of 6  $\mu\text{M}$ , and achieved the simple modification, easy operation, one-minute fast response, high sensitivity of 23.8  $\mu\text{A}/(\text{mM}\cdot\text{cm}^2)$ , and high selectivity without being affected by interferences in small volume detections. These advantages making it suitable applied to a handheld device for family use. The quantitative detection was also used for small volume blood tests and showed similar results by two biosensors, which is barely reported in the literature.

## 8.2 Recommendations for future work

The detection of reactive oxygen species especially in small-volume blood has attracted increasing attention and research interests. Although the quantitative measurement by electrochemical biosensor was achieved, further development of the biosensor is still challenging as some issues should be considered, such as the environmental instability of enzymes, new fabrication materials with better performance, and simultaneous detection of different reactive oxygen species.

### 8.2.1 Biosensor optimisation and refinement

This project has finished most part of the superoxide biosensor establishment and development, and has been successfully achieved the detection of a single blood sample. However, there are still works to be completed before viable device is developed.

The blood sample tests by electrochemical biosensors require testing on large number of patients and volunteers. This project only finished two volunteers blood samples by two types of biosensors, even the calculated detection readings obtained from different biosensors were similar, the results might still subject to variability and randomness. Thus, two to four blood samples from different volunteers should be detected by each of biosensors to consolidate the results.

Besides, the detection of superoxide concentration in blood samples still lack verifications by other methods. The more accurate quantitative measurement might be achieved by developing chemiluminescence techniques, such as changing the luminol probe to CLA-based (2-methyl-6-phenyl-3, 7-dihydroimidazo[1-2-a]pyrazin-3-one) probe, involving nanomaterials to chemiluminescence system, or using advanced enhancers (Chen et al. 2023, Teng et al. 2023, Yu and Zhao 2021).

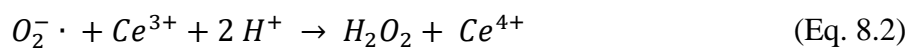
Another challenge is the deposition of cell debris on the electrode surface. This topic required the determination of reproducible amount for blood detections and the choice of coating which can stop fouling of cell debris or other proteins. A dense polymer film resistant to fouling by various foulants was reported, which was formed by attaching individual polymer chains to the electrode surface, and was successfully applied in glucose sensor (Dornhof et al. 2022, Hanssen et al. 2016). The sensitivity of sensor could be adjusted by varying the height of the membrane. However, the addition of barrier layer may affect sensitivity and accuracy of the sensor, which requires more research on the development of enzyme immobilisations.

To apply the lab-scale biosensors to a handheld device, the calibration and the calculation equations should be confirmed, listed and programmed. By following the equations, the current signal which obtained from electrochemical processor should automatically transferred to the concentration readings.

### 8.2.2 *Biomimic materials instead of enzymes*

Considering the disadvantages of enzymes such as high cost, instability and complicated immobilization, the sensor based on functional nanocomposites was discussed in the literature for reactive oxygen species (Wang et al. 2013).

Cerium nanoparticles (CeNPs) were reported to be developed SOD-mimetic activity due to the catalytic activity towards superoxide anion and showed better catalytic activity than native Cu/Zn SOD, which achieves the feasibility of nanoparticle alternatives (Singh 2019, Zhao et al. 2020). The dismutation of superoxide anion is shown as equation 8.1 & 8.2:



For the alternatives of horseradish peroxidase, Pt nanoparticle has been demonstrated as an excellent catalyst for the reduction of H<sub>2</sub>O<sub>2</sub> (Sun et al. 2012, Tang et al. 2011, Xu et al. 2011). Pt and its alloy nanoparticles showed decreases of H<sub>2</sub>O<sub>2</sub> oxidation and reduction overvoltage and enhanced catalytic performance for the reduction reaction of H<sub>2</sub>O<sub>2</sub>. A graphene-Pt nanocomposite decorated sensor was reported to perform high peak current and low overpotential and successfully applied on the detection of living cells with good electrocatalytic

activity and stability in the detection range of 0.5M to 3.475 mM (Figure 8.1 (a)) (Zhang et al. 2014). Figure 8.1 (b) shows a representation of PtPd–Fe<sub>3</sub>O<sub>4</sub> Nanoparticles based sensor which was reported to detect H<sub>2</sub>O<sub>2</sub> from mouse leukemic monocyte macrophage with the limit of detection of 5 nM (Sun et al. 2012).

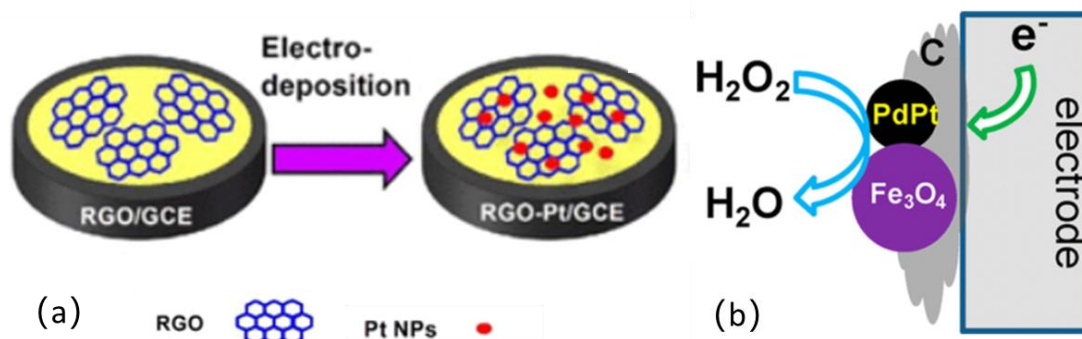


Figure 8.1 Schematic diagram of (a) RGO-Pt modified GCE for oxygen reduction (Zhang et al. 2014) and (b) dumbbell-like PtPd–Fe<sub>3</sub>O<sub>4</sub> nanoparticles for enhanced electrochemical detection of H<sub>2</sub>O<sub>2</sub> (Sun et al. 2012). Where RGO is reduced graphene oxide and GCE is the glassy carbon electrode.

Except nanomaterials mentioned above, researchers found that molybdenum disulfide (MoS<sub>2</sub>) nanosheets show multienzyme-like activity in the physiological environment, which could efficiently scavenge both superoxide anion and H<sub>2</sub>O<sub>2</sub> (Chen et al. 2018, Hille et al. 2014).

### 8.2.3 Materials for Electrode Fabrication

Graphene was demonstrated as a popular supporting material in electrochemical biosensors because of its large surface area, high mechanical conductivity and simple functionalization (Babadi et al. 2016). Compared with the random network of one-dimensional carbon nanotubes (CNTs), two-dimensional graphene shows the higher reproducibility of electrochemical sensing and easier surface modification of biomolecules, which endows high potential of applications of graphene on electrochemical biosensors (Liu et al. 2011, Pumera et al. 2010).

Lalaoui et al. (2015) described a graphene-multi-walled CNTs assembly for oxygen reduction and proved the highly efficient electrocatalytic performance. Figure 8.2 shows the structure of the assembly, CNT was used for the stable deposition of graphene and avoided the aggregation of graphene nanosheets.

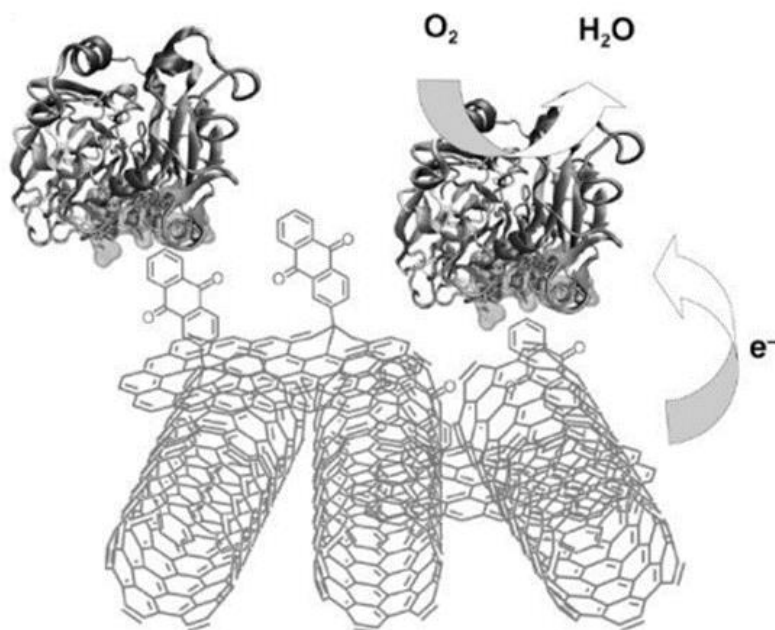


Figure 8.2 Schematic diagram of the structure of graphene-multi-walled CNTs for oxygen reduction by laccase (Lalaoui et al. 2015).

#### 8.2.4 “Superoxide anion + hydrogen peroxide” detection

Both superoxide detection and  $\text{H}_2\text{O}_2$  detection were achieved by the electrochemical biosensor, but the actual value it detects is the sum of the concentrations of  $\text{H}_2\text{O}_2$  and superoxide anion in the electrolyte environment. Although it is easy to determine the concentration of  $\text{H}_2\text{O}_2$ , the biosensor which could separately and simultaneously detect both  $\text{H}_2\text{O}_2$  and superoxide in the same procedure could be a challenge. Since the direct electron transfer of SOD could be promoted by the cysteine molecule (Tian et al. 2002), this issue might be solved by multi-channel detecting the electrons transfer of  $\text{H}_2\text{O}_2$  reduction and direct electron transfer of SOD.

## Appendix

### Appendix A

Table S1. 1 The concentration changes of dissolved oxygen (DO) in solution with air bubbling in 30 minutes.

Time (min)	0	5	10	15	20	25	30
Concentration of DO (mM)	4.15	5.85	7.35	7.49	7.63	7.52	7.71

Table S1. 2 The data of absorbance, calibrated superoxide concentration and calculated SOD activity in superoxide chemical-generation solutions with different pH in the absence and presence of SOD enzyme.

	Absorbance	Concentration of superoxide (mM)	SOD activity (%)
DDW	0.039233	--	--
NaOH	0.040133	--	--
ROS pH13	0.5947	10.00538	28.2825
SOD pH13	0.4385	5.806452	
ROS pH7	0.5843	9.725806	37.3716
SOD pH7	0.3815	4.274194	
ROS pH3	0.043	--	--
SOD pH3	0.038767	--	

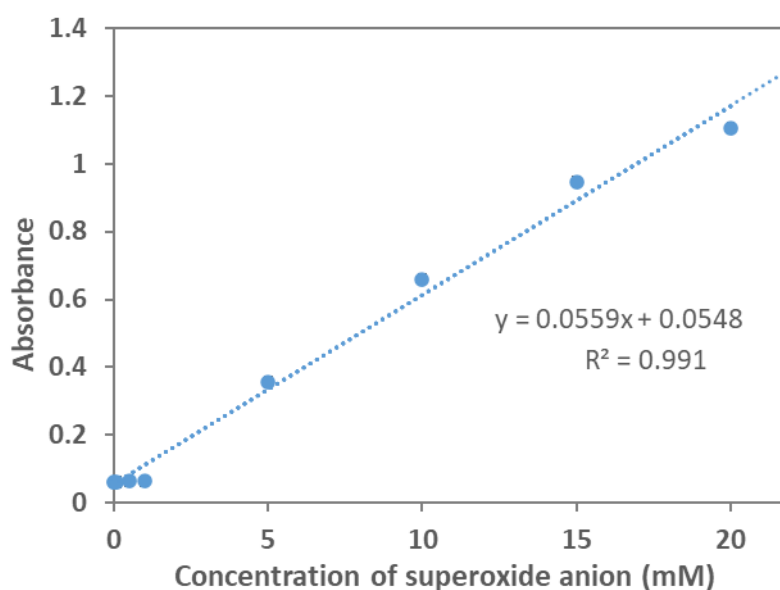


Figure S1. 1 The calibration curve for absorbance changes with various concentrations of superoxide (0, 0.1, 0.5, 1, 5, 10, 15, 20 mM).

Table S1. 3 The superoxide concentration changes with time by different preparation methods in different pH.

	Concentration of superoxide (mM)
--	----------------------------------

Time (hours)	blank	Enzymatic method	Chemical method (pH 13)	Chemical method (pH 7)
0	0.048387097	8.870967742	8.801075269	9.668011
0.5	0.066263441	8.350806452	8.25672043	8.473562
1.5	0.036290323	9.107526882	8.166666667	6.125901
3.5	0.048790323	8.946236559	8.998387097	3.656815
5.5	0.046639785	8.712365591	6.374556452	0.099019

## Appendix B

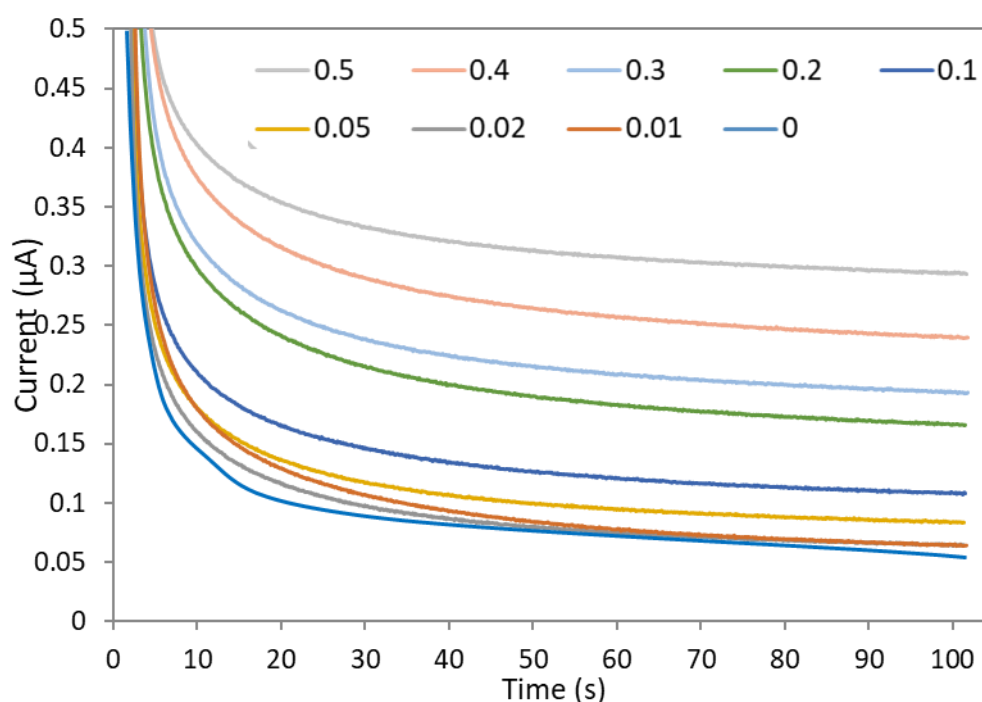


Figure S2. 1 The amperometry diagram for H<sub>2</sub>O<sub>2</sub> detection of the XOD/ PDDA/ SOD/ PDDA/ C-SPE at 0.6V vs Ag/Ag<sup>+</sup> (~ 0.074 V vs SHE) at 100 s.

Table S2. 1 The data for three repeats of the current responses with various H<sub>2</sub>O<sub>2</sub> concentrations on XOD/ PDDA/ SOD/ PDDA/ C-SPE by CA at 0.6V vs Ag/Ag<sup>+</sup> at 100 s.

Concentration of H <sub>2</sub> O <sub>2</sub> (mM)	Current (µA)				Sample standard deviation
	Sample 1	Sample 2	Sample 3	Average	
0	0.07486	0.086365	0.081116	0.08078	0.00576
0.01	0.086639	0.085907	0.06366	0.078735	0.013061
0.02	0.076569	0.082184	0.064209	0.07432	0.009196
0.05	0.082306	0.074707	0.083923	0.080312	0.004921

0.1	0.095734	0.082306	0.107513	0.095184	0.012613
0.2	0.152802	0.100128	0.165894	0.139608	0.034812
0.3	0.184418	0.134094	0.193695	0.170736	0.03207
0.4	0.210236	0.185394	0.239502	0.211711	0.027084
0.5	0.234955	0.212494	0.29364	0.24703	0.041899

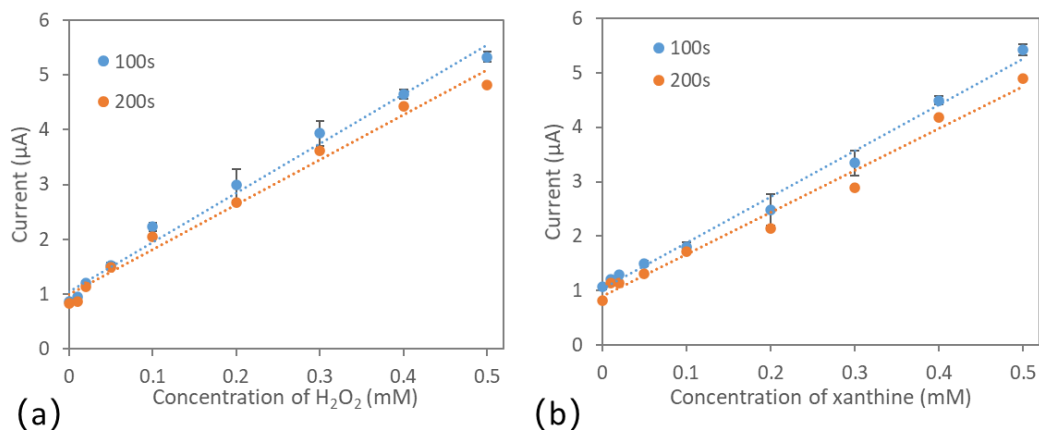


Figure S2. 2 The electrochemical responses for different detection time in different concentration of  $H_2O_2$  and xanthine solutions on XOD & SOD/PDDA/SWCNT/C-SPE by CA at 0.6V vs Ag/Ag<sup>+</sup> at 100 s.

Table S2. 2 The data for three repeats of the current responses with various  $H_2O_2$  concentrations on XOD & SOD/PDDA/CPC-SPE by CA at 0.6V vs Ag/Ag<sup>+</sup> at 100 s.

Concentration of $H_2O_2$ (mM)	Current ( $\mu A$ )				Sample standard deviation
	Sample 1	Sample 2	Sample 3	Average	
0	0.128815	0.087555	0.142456	0.11960863	0.02858497
0.005	0.127319	0.108246	0.145386	0.12698366	0.01857227
0.01	0.213867	0.112213	0.145905	0.15732833	0.05178082
0.025	0.239807	0.112366	0.155151	0.169108	0.06485676
0.05	0.269714	0.147949	0.179504	0.19905566	0.06319319
0.1	0.393982	0.318719	0.212769	0.30849	0.09103852
0.25	0.870972	0.643835	0.694098	0.73630166	0.11930493
0.5	1.44318	1.4776	1.56366	1.49481333	0.06205708

Table S2. 3 The data for three repeats of the current responses with various  $H_2O_2$  concentrations on XOD & SOD/PDDA/SWCNT/C-SPE by CA at 0.6V vs Ag/Ag<sup>+</sup> at 100 s.

Concentration of $H_2O_2$ (mM)	Current ( $\mu A$ )				Sample standard deviation
	Sample 1	Sample 2	Sample 3	Average	
0	0.840857	0.89283	0.865784	0.866490333	0.025993699

0.01	0.91638	0.98275	0.931091	0.943407	0.034856952
0.02	1.23438	1.32416	1.06232	1.206953333	0.133057179
0.05	1.46956	1.26318	1.83502	1.522586667	0.289584387
0.1	1.79285	2.36938	2.52777	2.23	0.386777636
0.2	2.71796	3.3905	2.883	2.997153333	0.350500714
0.3	4.34875	3.81165	3.63373	3.931376667	0.372242201
0.4	4.72443	4.35669	4.87732	4.652813333	0.267601587
0.5	5.31006	5.49921	5.18799	5.33242	0.156810233

Table S2. 4 The data for three repeats of the current responses with various  $H_2O_2$  concentrations on XOD & SOD/ PDDA/ SWCNT/ CPC-SPE by CA at 0.6V vs Ag/Ag<sup>+</sup> at 100 s.

Concentration of $H_2O_2$ (mM)	Current ( $\mu$ A)				Sample standard deviation
	Sample 1	Sample 2	Sample 3	Average	
0	1.078613	0.79077	0.74264	0.870674333	0.181681015
0.005	1.123474	0.88812	1.29706	1.102884667	0.205246002
0.01	1.196716	1.13623	1.47986	1.270935333	0.183444205
0.025	1.335571	1.33672	1.66724	1.446510333	0.191158362
0.05	1.58185	1.6358	1.98218	1.733276667	0.217237894
0.1	2.25537	2.27606	2.59955	2.376993333	0.193017153
0.2	3.57587	3.51843	3.38507	3.493123333	0.097885037
0.3	5.162535	5.14319	5.18188	5.162535	0.019345
0.4	6.613645	6.66296	6.56433	6.613645	0.049315
0.5	7.53125	8.21228	7.63245	7.791993333	0.367479281

Table S2. 5 The data for three repeats of the current responses with various xanthine concentrations on XOD & SOD/ PDDA/ CPC-SPE by CA at 0.6V vs Ag/Ag<sup>+</sup> at 100 s.

Concentration of xanthine (mM)	Current ( $\mu$ A)				Sample standard deviation
	Sample 1	Sample 2	Sample 3	Average	
0	0.115845	0.139923	0.113525	0.123098	0.014617267
0.01	0.120911	0.149933	0.136383	0.135742	0.014521603
0.02	0.136688	0.168671	0.15509	0.153483	0.016051944
0.05	0.160278	0.19693	0.202759	0.186656	0.023028901
0.1	0.367126	0.273315	0.248474	0.296305	0.062577786
0.2	0.568542	0.622754	0.5901	0.593799	0.027294603

0.4	0.927892	0.982104	1.04945	0.986482	0.060897143
0.5	0.963135	1.15479	1.22527	1.114398	0.135655094

Table S2. 6 The data for three repeats of the current responses with various xanthine concentrations on XOD & SOD/ PDDA/ SWCNT/ C-SPE by CA at 0.6V vs Ag/Ag<sup>+</sup> at 100 s.

Concentration of xanthine (mM)	Current (µA)				Sample standard deviation
	Sample 1	Sample 2	Sample 3	Average	
0	1.05402	1.03357	1.03145	1.03968	0.01246396
0.01	1.19177	1.20061	1.22375	1.205377	0.016514265
0.02	1.29169	1.31669	1.25641	1.288263	0.030285741
0.05	1.54407	1.44495	1.49628	1.4951	0.049570535
0.1	1.7796	1.88942	1.73645	1.801823	0.078869276
0.2	2.15016	2.67191	2.63397	2.485347	0.290899359
0.3	3.35277	3.5604	3.10883	3.340667	0.226028171
0.4	4.40088	4.56361	4.51965	4.494713	0.084182191
0.5	5.30797	5.4693	5.48096	5.41941	4.346396667

Table S2. 7 The data for three repeats of the current responses with various xanthine concentrations on XOD & SOD/ PDDA/ SWCNT/ CPC-SPE by CA at 0.6V vs Ag/Ag<sup>+</sup> at 100 s.

Concentration of xanthine (mM)	Current (µA)				Sample standard deviation
	Sample 1	Sample 2	Sample 3	Average	
0	1.67542	1.82289	1.77784	1.758717	0.075571996
0.01	1.77756	1.84302	1.84784	1.822807	0.039258805
0.02	1.89435	1.94178	2.05841	1.964847	0.084427331
0.05	2.02043	2.15173	2.12494	2.099033	0.069377871
0.1	2.28284	2.59949	2.74414	2.542157	0.235933795
0.2	3.14954	2.89886	3.37585	3.141417	0.238598735
0.3	4.05457	3.59802	4.20503	3.95254	0.316105798
0.4	4.53827	4.31549	4.40277	4.418843	0.112256386
0.5	4.87701	5.12651	5.16008	5.054533	0.154653279

Table S2. 8 The data for the concentration of H<sub>2</sub>O<sub>2</sub> calculated from the current detected with various concentrations of xanthine based on the current-concentration(H<sub>2</sub>O<sub>2</sub>) curve for SOD-based biosensor.

	The calculation of the concentration of H <sub>2</sub> O <sub>2</sub> from current (mM)
--	---

Conc. of xanthine (mM)	CPC-SPE/enzymes		C-SPE/SWCNT/enzymes		CPC-SPE/SWCNT/enzymes	
	$y=2.7385x-0.0274$		$y=9.002x+0.1846$		$y=13.651x+0.145$	
0	0.1227	0.0548	1.0730	0.0986	1.7587	0.1182
0.01	0.1351	0.0593	1.20537	0.1133	1.82280	0.1229
0.02	0.1537	0.0661	1.2882	0.1226	1.96484	0.1333
0.05	0.18820	0.07873	1.4951	0.14557876	2.09903	0.143142
0.1	0.29630	0.118205	1.80182	0.1796515	2.54215666	0.17560300
0.2	0.60909	0.232424	2.48534	0.25558172	3.14141666	0.21950162
0.3	0.98648	0.37023	3.34066	0.35059616	3.95254	0.27892022
0.4	1.15158	0.430520	4.49471	0.47879508	4.41884333	0.31307914
0.5	0.12271	0.054816	5.41941	0.58151633	5.05453333	0.35964642

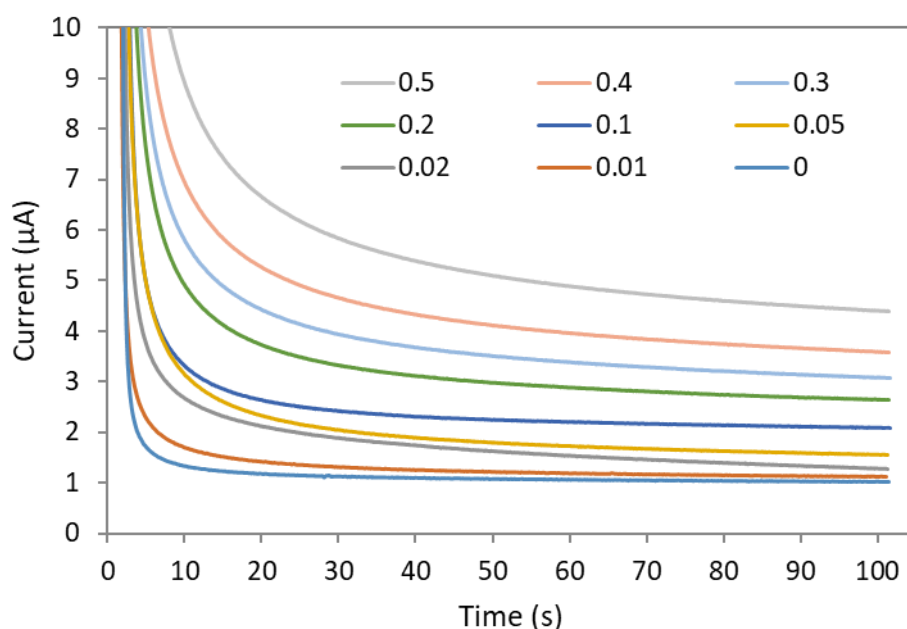


Figure S2. 3 The amperometry diagram for  $H_2O_2$  detection of the SOD/ PDDA/ SWCNT/ C-SPE at 0.6V vs  $Ag/Ag^+$  at 100 s.

Table S2. 9 The data for three repeats of the current responses with various  $H_2O_2$  concentrations on SOD/ PDDA/ SWCNT/ C-SPE by CA at 0.6V vs  $Ag/Ag^+$  at 100 s.

Concentration of $H_2O_2$ (mM)	Current ( $\mu A$ )				Sample standard deviation
	Sample 1	Sample 2	Sample 3	Average	
0	0.769043	1.21887	1.02345	1.003788	0.225557
0.01	0.903931	1.22681	1.11816	1.082967	0.164291
0.02	1.24969	1.37848	1.27244	1.300203	0.068737

0.05	1.53381	1.47644	1.55533	1.52186	0.04078
0.1	2.06566	1.586	2.07639	1.90935	0.280081
0.2	2.68097	2.45209	2.63933	2.590797	0.121914
0.3	3.2309	3.05328	3.06638	3.116853	0.098984
0.4	3.65692	3.68744	3.56576	3.636707	0.063308
0.5	4.3045	4.14948	4.37836	4.277447	0.116814

Table S2. 10 Summary of the current response changes of SOD/ PDDA/ SWCNT/ C-SPE and XOD & SOD/ PDDA/ SWCNT/ C-SPE with various H<sub>2</sub>O<sub>2</sub> concentrations by CA at 0.6V vs Ag/Ag<sup>+</sup> at 100 s.

Concentration of H <sub>2</sub> O <sub>2</sub> (mM)	Current changes after adding H <sub>2</sub> O <sub>2</sub> (μA)	
	Without XOD	With XOD
0	0	0
0.01	0.079179333	0.076916667
0.02	0.296415667	0.340463
0.05	0.518072333	0.656096333
0.1	0.905562333	1.363509667
0.2	1.587009	2.130663
0.3	2.113065667	3.064886333
0.4	2.632919	3.786323
0.5	3.273659	4.465929667

Table S2. 11 The data for the calculated concentration of superoxide from current reading from SOD/ PDDA/ SWCNT/ C-SPE.

Current reading from biosensor (μA)	Calibrated current (with XOD) (μA)	Concentration of superoxide (mM)			Sample standard deviation
		Maximum	Minimum	Average	
0.1	0.12122	0.039656	-0.01408	0.012787	0.026869
0.15	0.19163	0.056304	0.001562	0.028933	0.027371
0.2	0.26204	0.072952	0.017205	0.045079	0.027874
0.25	0.33245	0.0896	0.032848	0.061224	0.028376
0.3	0.40286	0.106248	0.048491	0.07737	0.028878
0.6	0.82532	0.206136	0.142351	0.174243	0.031893
1.2	1.67024	0.405911	0.330069	0.36799	0.037921
1.8	2.51516	0.605686	0.517787	0.561737	0.04395
2.4	3.36008	0.805462	0.705505	0.755484	0.049978

3	4.205	1.005237	0.893224	0.94923	0.056007
---	-------	----------	----------	---------	----------

Table S2. 12 The data for current changes with different concentration of H<sub>2</sub>O<sub>2</sub> on SOD/ PDDA/ SWCNT/ C-SPE in the presence of additional interferences.

Concentration of H <sub>2</sub> O <sub>2</sub> (mM)	Current responses (μA)				
	Blank	Glucose	Ascorbic acid	Uric acid	Bovine serum albumin
0	0	0	0	0	0
0.01	0.103824	0.091192	0.132842	0.14984	0.076641
0.02	0.295442	0.185612	0.2623	0.227748	0.145396
0.05	0.515473	0.383052	0.408706	0.486692	0.329016
0.1	1.099945	1.288206	0.704921	0.91217	0.681253
0.2	1.755384	2.418426	1.598345	1.76693	1.579106
0.3	2.561997	3.723564	2.243563	2.61607	2.408074
0.4	3.545954	4.713906	3.297234	3.611103	3.358962
0.5	4.412781	5.940458	4.635472	4.383371	4.225723

Table S2. 13 The data for current changes with different concentrations of H<sub>2</sub>O<sub>2</sub> on SOD/ PDDA/ SWCNT/ C-SPE in the presence of the additional various concentrations of interferences (ascorbic acid and bovine serum albumin).

Concentration of H <sub>2</sub> O <sub>2</sub> (mM)	Current responses (μA)				
	Blank	Ascorbic acid		Bovine serum albumin	
		11.4 μM	0.342 mM	4 g/l	40 g/l
0	0	0	0	0	0
0.01	0.103824	0.13284215	0.0777561	0.076641022	0.095398
0.02	0.295442	0.26230015	0.1294532	0.145395574	0.2925722
0.05	0.515473	0.40870568	0.2804773	0.329016384	0.391235
0.1	1.099945	0.70492065	0.7639058	0.681252828	0.7219553
0.2	1.7553844	1.59834535	1.6136905	1.579105708	1.5257264
0.3	2.5619965	2.24356335	2.5590594	2.408074364	2.3666530
0.4	3.5459544	3.29723415	3.5173992	3.358962125	3.2298473
0.5	4.4127807	4.63547175	4.3977864	4.225722883	4.2499505

Table S2. 14 The data for current responses with different concentrations of H<sub>2</sub>O<sub>2</sub> and additional glucose on SOD/ PDDA/ SWCNT/ C-SPE.

Concentration of H <sub>2</sub> O <sub>2</sub> (mM)	Current responses (μA)				
	Blank	Concentration of glucose (mM)			
		0.5	5	5.5	20
0	1.49994	1.69403	2.47681	2.5	5.89875
0.01	1.591727	1.8019	2.568002	2.577406	6.00663
0.02	1.769889	1.948639	2.662422	2.722366	6.2613
0.05	2.002434	2.190186	2.859862	2.924603	6.80451
0.1	2.350149	2.590973	3.765016	3.73844	7.273111
0.2	3.012625	3.298684	4.895236	5.108833	8.672678
0.3	4.12627	4.167205	6.200374	6.299168	9.820646
0.4	4.717978	5.045957	7.190716	7.354089	10.87577
0.5	5.711965	6.049746	8.417268	8.792047	12.56852

Table S2. 15 The data for current responses with different concentrations of glucose on SOD/ PDDA/ SWCNT/ C-SPE in the absence and presence of 0.5 mM H<sub>2</sub>O<sub>2</sub>.

Concentration of glucose (mM)	Current responses (μA)	
	Without H <sub>2</sub> O <sub>2</sub>	With 0.5 mM H <sub>2</sub> O <sub>2</sub>
0	1.49994	6.2744
0.5	1.69403	6.4458
1	2.10999	6.7998
5	2.47681	8.012727
10	3.17001	9.052261
15	4.57626	10.05539
20	5.89875	11.88374

## Appendix C

Table S3. 1 The data for three repeats of the current responses with various H<sub>2</sub>O<sub>2</sub> concentrations on HRP/ PBSE/ SWCNT/ C-SPE by CA at 0.1V vs Ag/Ag<sup>+</sup> at 100 s.

Concentration of H <sub>2</sub> O <sub>2</sub> (mM)	Current (μA)				Sample standard deviation
	Sample 1	Sample 2	Sample 3	Average	
0	0.0059938	0.0063872	0.0060785	0.0061905	0.031967
0.01	-0.01913	0.031949	0.005789	0.006407	0.025542
0.02	-0.03058	-0.01789	-0.02543	-0.02424	0.006343

0.05	-0.08847	-0.09885	-0.09399	-0.09366	0.005188
0.1	-0.29056	-0.39017	-0.34765	-0.34036	0.049804
0.2	-0.64606	-0.75928	-0.69783	-0.70267	0.05661
0.3	-1.06689	-1.02957	-1.04783	-1.04823	0.018663
0.4	-1.43097	-1.42027	-1.42476	-1.42562	0.00535
0.5	-1.81647	-1.75774	-1.79836	-1.78711	0.029365

Table S3. 2 The data for the current responses with various  $H_2O_2$  or xanthine concentrations on three enzymes-immobilized C-SPE by CA at 0.1V vs Ag/Ag<sup>+</sup> at 100 s ( $n = 3$  repeats).

Concentration of $H_2O_2$ (mM)	Current response ( $\mu A$ )	Sample standard deviation	Concentration of xanthine (mM)	Current response ( $\mu A$ )	Sample standard deviation
0	0.05146	0.001332	0	0.021683	0.000669
0.01	0.022682	0.007	0.01	0.014008	0.004951
0.02	0.021049	0.011194	0.02	0.00943	0.005038
0.05	0.0028	0.028334	0.05	0.006755	0.00389
0.1	-0.25037	0.039769	0.1	-0.00136	0.004383
0.2	-0.41962	0.066033	0.2	-0.00509	0.002892
0.3	-0.48431	0.054811	0.3	-0.01031	0.004654
0.4	-0.48309	0.087955	0.4	-0.01348	0.004834
0.5	-0.41603	0.072742	0.5	-0.01099	0.003056

Table S3. 3 The data for the current responses with various  $H_2O_2$  or xanthine concentrations on three enzymes-immobilized duo-SPE by CA at 0.1V vs Ag/Ag<sup>+</sup> at 100 s ( $n = 3$  repeats).

Concentration of $H_2O_2$ (mM)	Current response ( $\mu A$ )	Sample standard deviation	Concentration of xanthine (mM)	Current response ( $\mu A$ )	Sample standard deviation
0	0	0.003105	0	0	0.00228
0.01	-0.00661	0.007629	0.01	-0.00577	0.00601
0.02	-0.01651	0.006625	0.02	-0.01334	0.007145
0.05	-0.03434	0.021015	0.05	-0.02873	0.00285
0.1	-0.07154	0.026262	0.1	-0.06601	0.011816
0.2	-0.14177	0.025604	0.2	-0.13545	0.018329
0.3	-0.21929	0.028545	0.3	-0.20129	0.011564
0.4	-0.28552	0.029579	0.4	-0.28296	0.021039
0.5	-0.36766	0.032479	0.5	-0.34329	0.017656

Table S3. 4 The data for the calculated concentration of superoxide from the current reading for coupled SOD-HRP biosensor.

Concentration of xanthine (mM)	Current response ( $\mu\text{A}$ )	The calculation of the concentration of $\text{H}_2\text{O}_2$ from current (mM)
0	0	0.001098
0.01	-0.00577	0.009018
0.02	-0.01334	0.01941
0.05	-0.02873	0.04055
0.1	-0.06601	0.091734
0.2	-0.13545	0.187076
0.3	-0.20129	0.277487
0.4	-0.28296	0.389618
0.5	-0.34329	0.472459

Table S3. 5 The data for three repeats of the current responses in the absence and presence of XOD with various  $\text{H}_2\text{O}_2$  concentrations on three enzymes-immobilized duo-SPE by CA at 0.1V vs Ag/Ag<sup>+</sup> at 100 s.

Current reading from biosensor ( $\mu\text{A}$ )	Concentration of superoxide (mM)			Sample standard deviation
	Maximum	Minimum	Average	
-0.05	0.075374	0.069751	0.072563	0.002811
-0.1	0.147296	0.138405	0.14285	0.004446
-0.15	0.219217	0.207058	0.213138	0.00608
-0.2	0.291139	0.275711	0.283425	0.007714
-0.25	0.363061	0.344364	0.353712	0.009349
-0.3	0.434983	0.413017	0.424	0.010983
-0.35	0.506904	0.48167	0.494287	0.012617
-0.4	0.578826	0.550323	0.564574	0.014252
-0.45	0.650748	0.618976	0.634862	0.015886
-0.5	0.72267	0.687629	0.705149	0.017521

Table S3. 6 The data for current changes with different concentration of  $\text{H}_2\text{O}_2$  on three enzymes-immobilized duo-SPE by CA at 0.1V vs Ag/Ag<sup>+</sup> in the presence of additional interference.

Concentration of $\text{H}_2\text{O}_2$ (mM)	Current responses ( $\mu\text{A}$ )				
	Blank	Glucose		Uric acid	
		5 mM	20 mM	40 $\mu\text{M}$	400 $\mu\text{M}$
0	0	0	0	0	0

0.01	-0.0127564	-0.0097518	-0.0125793	-0.01002	-0.013425
0.02	-0.0238342	-0.0230728	-0.0215515	-0.02355	-0.021689
0.05	-0.0380065	-0.0369125	-0.0471558	-0.03799	-0.040888
0.1	-0.0714418	-0.0686966	-0.0684265	-0.06978	-0.080057
0.2	-0.1476748	-0.1354691	-0.1290343	-0.15049	-0.152592
0.3	-0.2272641	-0.2278150	-0.2454705	-0.23149	-0.212854
0.4	-0.2973022	-0.2905900	-0.3079617	-0.29587	-0.280252
0.5	-0.3921816	-0.4044691	-0.3852147	-0.39864	-0.37089
Concentration of H <sub>2</sub> O <sub>2</sub> (mM)	Current responses (μA)				
	Blank	Ascorbic acid		Bovine serum albumin	
		11.4 μM	0.342 mM	4 g/l	40 g/l
0	0	0	0	0	0
0.01	-0.0127564	-0.0108093	-0.010037	-0.01473	-0.01193
0.02	-0.0238342	-0.0169434	-0.017056	-0.0262	-0.01646
0.05	-0.0380065	-0.0457579	-0.027676	-0.04931	-0.0467
0.1	-0.0714418	-0.0687867	-0.072415	-0.07961	-0.08785
0.2	-0.1476748	-0.1589659	-0.152524	-0.14131	-0.14821
0.3	-0.2272641	-0.2202819	-0.228573	-0.21542	-0.21373
0.4	-0.2973022	-0.2986663	-0.292997	-0.27889	-0.26914
0.5	-0.3921816	-0.3933774	-0.367062	-0.38039	-0.37209

## Appendix D

Table S4. 1 The fluorescence changes with time in solutions with different concentrations of superoxide, (SO: superoxide anion).

Time (min)	Fluorescence						
	No SO	500 μM	400 μM	300 μM	200 μM	100 μM	50 μM
1	41	39	40	31	41	40	38
2	23	24	23	15	12	11	18
3	17	12	20	11	18	12	13
4	24	12	13	11	11	13	6
5	4	10	10	0	12	-3	0
6	11	1	2	2	7	7	1

7	12	6	1	2	6	7	8
8	7	8	8	3	0	15	9
9	0	9	6	0	11	11	11
10	7	0	10	6	7	0	5
11	3	3	0	-7	4	4	4
12	-4	-4	11	1	2	-1	5
13	2	-3	0	1	11	8	6
14	-4	-2	9	2	-2	10	8
15	3	1	4	4	-2	9	9
16	4	2	5	8	6	9	14
17	0	1	5	11	0	1	2
18	5	5	15	3	10	5	9
19	0	19	14	8	13	10	14
20	-1	12	9	5	9	10	8
21	1	9	10	10	17	8	10
22	0	19	20	22	24	21	16
23	0	27	22	16	15	19	18
24	-6	33	24	38	31	31	32
25	-2	33	31	30	31	36	32

*Table S4. 2 The fluorescence changes with time in solutions with the different high-level concentrations of superoxide, (SO: superoxide anion).*

Time (min)	Fluorescence						
	No SO	10 mM	8 mM	6 mM	4 mM	2 mM	1 mM
1	63	187	154	125	71	62	56
2	28	192	108	116	79	40	36
3	30	221	149	82	46	43	30
4	35	236	119	97	54	18	33
5	23	238	149	102	63	26	26
6	26	277	184	83	46	37	37
7	10	265	196	109	63	46	21
8	12	285	200	125	64	30	19
9	15	358	194	114	63	38	19

10	18	307	215	140	52	31	18
11	12	337	247	135	64	34	30
12	16	340	242	128	87	26	26
13	7	363	212	122	79	30	22
14	7	368	248	150	78	29	18
15	4	383	253	150	70	35	24
16	1	373	235	151	64	41	14
17	7	373	242	141	82	29	24
18	6	387	240	135	59	33	26
19	6	338	225	140	77	32	21
20	3	365	228	145	68	29	23
21	15	400	250	156	85	20	20
22	7	363	262	144	57	41	19

Table S4. 3 The corrected fluorescence at detection time of 15 ~ 22 minutes with different concentrations of superoxide in solution.

Concentration of xanthine (mM)	Corrected fluorescence
1	7
2	22.5
4	62.5
6	139.5
8	227.5
10	358.5

Table S4. 4 The fluorescence changes with time in the blood which was diluted at different multiples for superoxide detection by chemiluminescence method.

Time (min)	Fluorescence						
	No blood no PMA	No blood	Blood dilution at different multiples				
			1 in 20	1 in 40	1 in 60	1 in 80	1 in 100
1	32	47	22	16	8	22	25
2	28	16	13	14	24	24	20
3	14	23	9	20	14	21	13
4	7	10	18	12	1	5	17

5	15	16	9	5	19	14	3
6	3	21	2	9	2	9	9
7	10	16	4	5	12	9	11
8	10	20	21	1	9	3	13
9	6	3	17	0	5	15	12
10	10	22	21	11	6	14	15
11	6	14	14	21	14	1	11
12	12	16	13	20	4	5	19
13	4	10	21	5	11	11	10
14	8	8	22	9	29	13	18
15	5	17	21	8	21	22	31
16	18	7	18	20	20	30	31
17	17	17	23	27	33	28	25
18	12	1	28	28	14	23	19
19	12	8	30	26	33	31	21
20	11	9	39	45	21	52	31
21	9	11	26	38	34	31	47
22	8	2	37	41	29	31	33
23	8	10	31	43	35	24	26
24	12	5	39	40	48	32	53
25	10	8	44	40	43	44	51

Table S4. 5 The current responses of the blood at different dilution levels for superoxide detection by the developed SOD-based biosensor.

Content of blood in PBS (v/v, unit: 1)	Current responses ( $\mu\text{A}$ )				Sample standard deviation
	Sample 1	Sample 2	Sample 3	Average	
0	0	0	0	0	0
0.01 (1 in 100)	0.005356	0.003021	0.002821	0.003733	0.001409
0.0125 (1 in 80)	0.006646	0.00531	0.005629	0.005861	0.000697
0.016667 (1 in 60)	0.008291	0.006336	0.008125	0.007584	0.001084
0.025 (1 in 40)	0.012464	0.010962	0.011076	0.011501	0.000836
0.05 (1 in 20)	0.025894	0.022906	0.025164	0.024655	0.001558

Table S4. 6 The current responses of the blood at different dilution levels for superoxide detection by coupled SOD-HRP biosensor.

Content of blood in PBS (v/v, unit: 1)	Current responses ( $\mu\text{A}$ )				Sample standard deviation
	Sample 1	Sample 2	Sample 3	Average	
0	0	0	0	0	0
0.01 (1 in 100)	-0.00086	-0.00096	-0.00062	-0.00081	0.000175
0.0125 (1 in 80)	-0.0012	-0.00123	-0.00103	-0.00115	0.000105
0.016667 (1 in 60)	-0.00149	-0.00128	-0.0015	-0.00142	0.000123
0.025 (1 in 40)	-0.00202	-0.00184	-0.00222	-0.00203	0.000187
0.05 (1 in 20)	-0.00414	-0.00396	-0.00378	-0.00396	0.000183

## References

- Abel, S., Waks, M. and Marchi, M. (2010) Molecular dynamics simulations of cytochrome c unfolding in AOT reverse micelles: The first steps. *The European Physical Journal E*, 32(4), pp. 399-409.
- Activation of Glassy Carbon Electrodes*, Available: <https://chem.libretexts.org/@go/page/61023> [Accessed 2021/12/18/].
- Agarwal, A., Allamaneni, S. S. and Said, T. M. (2004) Chemiluminescence technique for measuring reactive oxygen species. *Reproductive BioMedicine Online*, 9(4), pp. 466-468.
- Akkara, J. A., Senecal, K. J. and Kaplan, D. L. (1991) Synthesis and characterization of polymers produced by horseradish peroxidase in dioxane. *Journal of Polymer Science Part A: Polymer Chemistry*, 29(11), pp. 1561-1574.
- Alexeyeva, N. and Tammeveski, K. (2008) Electroreduction of oxygen on gold nanoparticle/PDDA-MWCNT nanocomposites in acid solution. *Analytica Chimica Acta*, 618(2), pp. 140-146.
- Ali-Boucetta, H., Nunes, A., Sainz, R., Herrero, M. A., Tian, B., Prato, M., Bianco, A. and Kostarelos, K. (2013) Asbestos-like pathogenicity of long carbon nanotubes alleviated by chemical functionalization. *Angewandte Chemie International Edition*, 52(8), pp. 2274-2278.
- Ambarsari, L. and Lindawati, E. (2017) Isolation, Fractionation and Characterization of Catalase from *Neurospora crassa* (InaCC F226). in *IOP Conference Series: Earth and Environmental Science*: IOP Publishing. pp. 012068.
- Anne (2017) *Reactive Oxygen Species (ROS) Responsive Polymers - A Review - Advanced Science News*, Available: <http://www.materialsvIEWS.com/reactive-oxygen-species-ros-responsive-polymers-review/> [Accessed December 2017].
- Ansari, A. A., Alhoshan, M., Alsalhi, M. and Aldwayyan, A. (2010) Nanostructured metal oxides based enzymatic electrochemical biosensors. in *Biosensors*: InTech.

- Aoki, K., Honda, K., Tokuda, K. and Matsuda, H. (1985) Voltammetry at microcylinder electrodes: Part I. Linear sweep voltammetry. *Journal of Electroanalytical Chemistry and Interfacial Electrochemistry*, 182(2), pp. 267-279.
- Armbruster, D. A. and Pry, T. (2008) Limit of blank, limit of detection and limit of quantitation. *The clinical biochemist reviews*, 29(Suppl 1), pp. S49.
- Babadi, A. A., Bagheri, S. and Hamid, S. B. A. (2016) Progress on implantable biofuel cell: Nano-carbon functionalization for enzyme immobilization enhancement. *Biosensors and Bioelectronics*, 79, pp. 850-860.
- Balamurugan, M., Santharaman, P., Madasamy, T., Rajesh, S., Sethy, N. K., Bhargava, K., Kotamraju, S. and Karunakaran, C. (2018) Recent trends in electrochemical biosensors of superoxide dismutases. *Biosensors and Bioelectronics*.
- Ball, E. G. (1939) Xanthine oxidase: Purification and properties. *Journal of Biological Chemistry*, 128, pp. 51-67.
- Bannister, J., Bannister, W. and WOOD, E. (1971) Bovine Erythrocyte Cupro-Zinc Protein: 1. Isolation and General Characterization. *European journal of Biochemistry*, 18(2), pp. 178-186.
- Bard, A. J. and Faulkner, L. R. (1983) Electrochemical Methods: Fundamentals and Applications. *Surface Technology*, 20(1), pp. 91-92.
- Barsan, M. M. and Brett, C. (2015) GRAPHENE AND CARBON NANOTUBE NANOMATERIALS IN LAYER-BY-LAYER STRUCTURED ELECTROCHEMICAL ENZYMATIc BIOSENSORS: A REVIEW. *Studia Universitatis Babes-Bolyai, Chemia*, 60(3).
- Bartlett, P. N., Birkin, P. R., Wang, J. H., Palmisano, F. and De Benedetto, G. (1998) An enzyme switch employing direct electrochemical communication between horseradish peroxidase and a poly (aniline) film. *Analytical chemistry*, 70(17), pp. 3685-3694.

- Basso, A. and Serban, S. (2019) Industrial applications of immobilized enzymes—A review. *Molecular Catalysis*, 479(4), pp. 110607.
- Batchelor-McAuley, C., Kätelhön, E., Barnes, E. O., Compton, R. G., Laborda, E. and Molina, A. (2015) Recent advances in voltammetry. *ChemistryOpen*, 4(3), pp. 224-260.
- Bayr, H. (2005) Reactive oxygen species. *Critical Care Medicine*, 33(12), pp. S498-S501.
- Bedouhène, S., Moulti-Mati, F., Hurtado-Nedelec, M., Dang, P. M.-C. and El-Benna, J. (2017) Luminol-amplified chemiluminescence detects mainly superoxide anion produced by human neutrophils. *American journal of blood research*, 7(4), pp. 41.
- Berridge, M. and Tan, A. (1998) Trans-plasma membrane electron transport: a cellular assay for NADH-and NADPH-oxidase based on extracellular, superoxide-mediated reduction of the sulfonated tetrazolium salt WST-1. *Protoplasma*, 205(1), pp. 74-82.
- Bertrand, P., Jonas, A., Laschewsky, A. and Legras, R. (2000) Ultrathin polymer coatings by complexation of polyelectrolytes at interfaces: suitable materials, structure and properties. *Macromolecular rapid communications*, 21(7), pp. 319-348.
- Bhattacharya, S., Gong, X., Wang, E., Dutta, S. K., Caplette, J. R., Son, M., Nguyen, F. T., Strano, M. S. and Mukhopadhyay, D. (2019) DNA–SWCNT Biosensors Allow Real-Time Monitoring of Therapeutic Responses in Pancreatic Ductal Adenocarcinoma. *Cancer research*, 79(17), pp. 4515-4523.
- Bielski, B. H. and Arudi, R. L. (1983) Preparation and stabilization of aqueous/ethanolic superoxide solutions. *Analytical Biochemistry*, 133(1), pp. 170-178.
- Bontempelli, G. and Toniolo, R. (2005) Voltammetry-Linear sweep and cyclic.
- Boqué, R. and Heyden, Y. V. (2009) The limit of detection. *LCGC Europe*, 22(2), pp. 82-85.
- Braik, M., Barsan, M. M., Dridi, C., Ben Ali, M. and Brett, C. M. A. (2016) Highly sensitive

amperometric enzyme biosensor for detection of superoxide based on conducting polymer/CNT modified electrodes and superoxide dismutase. *Sensors and Actuators B: Chemical*, 236, pp. 574-582.

Braustein (2017) *Biosensors*, Available:  
<https://www.slideshare.net/DrHaroldBraustein/biosensors-39756753> [Accessed  
December 2017].

Brett, C. M., Brett, O. and Electrochemistry, A. (1993) Principles, methods and applications.

Bustos, C., Salgado, G. and López, C. (2001) The Oxidation of Luminol an Experiment to Maximize the Efficiency of Chemiluminescence from Luminol. *The Chemical Educator*, 6(2), pp. 97-99.

Byrne, B., Stack, E., Gilmartin, N. and O’Kennedy, R. (2009) Antibody-based sensors: principles, problems and potential for detection of pathogens and associated toxins. *Sensors*, 9(6), pp. 4407-4445.

Caldefie-Chézet, F., Walrand, S., Moinard, C., Tridon, A., Chassagne, J. and Vasson, M.-P. (2002) Is the neutrophil reactive oxygen species production measured by luminol and lucigenin chemiluminescence intra or extracellular? Comparison with DCFH-DA flow cytometry and cytochrome c reduction. *Clinica Chimica Acta*, 319(1), pp. 9-17.

Campanella, L., Favero, G. and Tomassetti, M. (1997) A modified amperometric electrode for the determination of free radicals. *Sensors and Actuators B: Chemical*, 44(1-3), pp. 559-565.

Cao, L. (2005) Introduction: Immobilized enzymes: Past, present and prospects. *Carrier-bound immobilized enzymes: principles, application and design*, 1, pp. 1-52.

Capitán-Vallvey, L. F., Lopez-Ruiz, N., Martinez-Olmos, A., Erenas, M. M. and Palma, A. J. (2015) Recent developments in computer vision-based analytical chemistry: A tutorial review. *Analytica Chimica Acta*, 899, pp. 23-56.

Carlsson, G. H., Nicholls, P., Svistunenko, D., Berglund, G. I. and Hajdu, J. (2005) Complexes

of horseradish peroxidase with formate, acetate, and carbon monoxide. *Biochemistry*, 44(2), pp. 635-642.

Carrico, R. and Deutsch, H. F. (1970) The presence of zinc in human cytochrome c and some properties of the apoprotein. *Journal of Biological Chemistry*, 245(4), pp. 723-727.

Carter, G., Margrave, J. and Templeton, D. (1952) A high-temperature crystal modification of K<sub>2</sub>O. *Acta Crystallographica*, 5(6), pp. 851-851.

Ceken, B., Kandaz, M. and Koca, A. (2012) Electrochemical hydrogen peroxide sensor based on cobalt phthalocyanine captured in polyaniline film on a glassy carbon electrode. *Journal of Porphyrins and Phthalocyanines*, 16(04), pp. 380-389.

Centre for Ageing Better (2022) *Summary | The State of Ageing 2022*, Available: <https://ageing-better.org.uk/summary-state-ageing-2022> [Accessed May 2023].

Chang, T. M. S. (2013) *Biomedical Applications of Immobilized Enzymes and Proteins: Volume 1*, Springer Science & Business Media.

Chen, F., Zhang, Y., Li, T., Peng, D., Qi, Z., Song, J., Deng, T. and Liu, F. (2023) Discovering ester and ether derivatives of luminol as advanced chemiluminescence probes. *Chinese Chemical Letters*, 34(3), pp. 1074-96.

Chen, J., Wollenberger, U., Lisdat, F., Ge, B. and Scheller, F. W. (2000) Superoxide sensor based on hemin modified electrode. *Sensors and Actuators B: Chemical*, 70(1-3), pp. 115-120.

Chen, R. J., Zhang, Y., Wang, D. and Dai, H. (2001) Noncovalent Sidewall Functionalization of Single-Walled Carbon Nanotubes for Protein Immobilization. *Journal of the American Chemical Society*, 123(16), pp. 3838-3839.

Chen, S., Yuan, R., Chai, Y., Xu, L., Wang, N., Li, X. and Zhang, L. (2006) Amperometric Hydrogen Peroxide Biosensor Based on the Immobilization of Horseradish Peroxidase (HRP) on the Layer-by-Layer Assembly Films of Gold Colloidal Nanoparticles and Toluidine Blue. *Electroanalysis: An International Journal Devoted to Fundamental and*

*Practical Aspects of Electroanalysis*, 18(5), pp. 471-477.

- Chen, T., Zou, H., Wu, X., Liu, C., Situ, B., Zheng, L. and Yang, G. (2018) Nanozymatic antioxidant system based on MoS<sub>2</sub> nanosheets. *ACS applied materials & interfaces*, 10(15), pp. 12453-12462.
- Chen, X., Fu, C., Wang, Y., Yang, W. and Evans, D. G. (2008) Direct electrochemistry and electrocatalysis based on a film of horseradish peroxidase intercalated into Ni–Al layered double hydroxide nanosheets. *Biosensors and Bioelectronics*, 24(3), pp. 356-361.
- Chen, X. J., West, A. C., Cropek, D. M. and Banta, S. (2008) Detection of the superoxide radical anion using various alkanethiol monolayers and immobilized cytochrome c. *Analytical chemistry*, 80(24), pp. 9622-9629.
- Chin, D. H., Chiericato Jr, G., Nanni Jr, E. J. and Sawyer, D. T. (1982) Proton-induced disproportionation of superoxide ion in aprotic media. *Journal of the American Chemical Society*, 104(5), pp. 1296-1299.
- Christodouleas, D. C., Giokas, D. L., Garyfali, V., Papadopoulos, K. and Calokerinos, A. C. (2015) An automatic FIA-CL method for the determination of antioxidant activity of edible oils based on peroxyoxalate chemiluminescence. *Microchemical Journal*, 118, pp. 73-79.
- Cos, P., Ying, L., Calomme, M., Hu, J. P., Cimanga, K., Van Poel, B., Pieters, L., Vlietinck, A. J. and Berghe, D. V. (1998) Structure–Activity Relationship and Classification of Flavonoids as Inhibitors of Xanthine Oxidase and Superoxide Scavengers. *Journal of Natural Products*, 61(1), pp. 71-76.
- Costentin, C., Robert, M. and Savéant, J.-M. (2010) Concerted proton– electron transfers: Electrochemical and related approaches. *Accounts of chemical research*, 43(7), pp. 1019-1029.
- Cottrell, F. (1902) Application of the Cottrell equation to chronoamperometry. *Z Physik Chem*, 42, pp. 385.

- Cui, M., Ren, J., Wen, X., Li, N., Xing, Y., Zhang, C., Han, Y. and Ji, X. (2020) Electrochemical detection of superoxide anion released by living cells by manganese (III) tetraphenyl porphine as superoxide dismutase mimic. *Chemical Research in Chinese Universities*, 36(5), pp. 774-780.
- Dai, W. and Wang, D. (2021) Cutting Methods and Perspectives of Carbon Nanotubes. *The journal of physical chemistry C*, 125(18), pp. 9593-9617.
- Dai, Y., Gao, P., Wang, X., Wang, P., Gao, D. and Luo, C. (2020) Enhanced Water Oxidation of CoP/CNTs via Interfacial Charge Transfer Induced by Poly Dimethyl Diallyl Ammonium Chloride. *New Journal of Chemistry*.
- Daniel, S., Rao, T. P., Rao, K. S., Rani, S. U., Naidu, G., Lee, H.-Y. and Kawai, T. (2007) A review of DNA functionalized/grafted carbon nanotubes and their characterization. *Sensors and Actuators B: Chemical*, 122(2), pp. 672-682.
- Datta, S., Christena, L. R. and Rajaram, Y. R. S. (2013) Enzyme immobilization: an overview on techniques and support materials. *3 Biotech*, 3(1), pp. 1-9.
- Daws, L. C. and Toney, G. M. (2007) High-speed chronoamperometry to study kinetics and mechanisms for serotonin clearance in vivo. *Electrochemical methods for neuroscience*.
- Deffo, G., Nde Tene, T. F., Medonbou Dongmo, L., Zambou Jiokeng, S. L. and Tonleu Temgoua, R. C. (2023) Differential pulse and square-wave voltammetry as sensitive methods for electroanalysis applications. in *Reference Module in Chemistry, Molecular Sciences and Chemical Engineering*: Elsevier.
- Dequaire, M., Limoges, B., Moiroux, J. and Savéant, J.-M. (2002) Mediated electrochemistry of horseradish peroxidase. Catalysis and inhibition. *Journal of the American Chemical Society*, 124(2), pp. 240-253.
- Derkus, B., Emregul, E. and Emregul, K. C. (2015) Copper–zinc alloy nanoparticle based enzyme-free superoxide radical sensing on a screen-printed electrode. *Talanta*, 134, pp. 206-214.

- Di, J., Peng, S., Shen, C., Gao, Y. and Tu, Y. (2007) One-step method embedding superoxide dismutase and gold nanoparticles in silica sol-gel network in the presence of cysteine for construction of third-generation biosensor. *Biosensors and Bioelectronics*, 23(1), pp. 88-94.
- Dornhof, J., Kieninger, J., Muralidharan, H., Maurer, J., Urban, G. A. and Weltin, A. (2022) Microfluidic organ-on-chip system for multi-analyte monitoring of metabolites in 3D cell cultures. *Lab on a Chip*, 22(2), pp. 225-239.
- DropSens (2020) *Screen-printed electrodes*, Available: [http://www.dropsens.com/en/screen\\_printed\\_electrodes\\_pag.html](http://www.dropsens.com/en/screen_printed_electrodes_pag.html) [Accessed 11 October 2020].
- Elgrishi, N., Rountree, K. J., McCarthy, B. D., Rountree, E. S., Eisenhart, T. T. and Dempsey, J. L. (2018) A Practical Beginner's Guide to Cyclic Voltammetry. *Journal of Chemical Education*, 95(2), pp. 197-206.
- Emregül, E. (2005) Development of a new biosensor for superoxide radicals. *Analytical and Bioanalytical Chemistry*, 383(6), pp. 947-954.
- Emregul, E., Kocabay, O., Derkus, B., Yumak, T., Emregul, K. C., Sinag, A. and Polat, K. (2013) A novel carboxymethylcellulose-gelatin-titanium dioxide-superoxide dismutase biosensor; electrochemical properties of carboxymethylcellulose-gelatin-titanium dioxide-superoxide dismutase. *Bioelectrochemistry*, 90, pp. 8-17.
- Endo, K., Miyasaka, T., Mochizuki, S., Aoyagi, S., Himi, N., Asahara, H., Tsujioka, K. and Sakai, K. (2002) Development of a superoxide sensor by immobilization of superoxide dismutase. *Sensors and Actuators B: Chemical*, 83(1), pp. 30-34.
- Enomoto, J., Matharu, Z. and Revzin, A. (2013) Electrochemical biosensors for on-chip detection of oxidative stress from cells. *Method Enzymol*, 526, pp. 107-121.
- Erdey, L., Pickering, W. and Wilson, C. (1962) Chemiluminescence of luminol and haemin. *Talanta*, 9(8), pp. 653-659.

- Feng, D., Li, X., Wang, B., Li, D. and Liu, Z. (2011) Determination of hydrogen peroxide in beer by horseradish peroxidase biosensor. *Brewing Technology*, 12, pp. 37-39.
- Feng, L., Wang, R., Shi, Y., Wang, H., Yang, J., Zhu, J., Chen, Y. and Yuan, N. (2016) Electrochemical study of hydrogen peroxide detection on MnO<sub>2</sub> micromaterials. *Int J Electrochem Sci*, 11, pp. 5962-5972.
- Ferapontova, E. E., Grigorenko, V. G., Egorov, A. M., Borchers, T., Ruzgas, T. and Gorton, L. (2001) Mediatorless biosensor for H<sub>2</sub>O<sub>2</sub> based on recombinant forms of horseradish peroxidase directly adsorbed on polycrystalline gold. *Biosensors and Bioelectronics*, 16(3), pp. 147-157.
- Firdoz, S., Ma, F., Yue, X., Dai, Z., Kumar, A. and Jiang, B. (2010) A novel amperometric biosensor based on single walled carbon nanotubes with acetylcholine esterase for the detection of carbaryl pesticide in water. *Talanta*, 83(1), pp. 269-273.
- Fridovich, I. (1972) Superoxide radical and superoxide dismutase. *Accounts of chemical research*, 5(10), pp. 321-326.
- Gaikwad, R., Thangaraj, P. and Sen, A. (2021) Direct and rapid measurement of hydrogen peroxide in human blood using a microfluidic device. *Scientific Reports*, 11(1), pp. 2960.
- Gajhede, M., Schuller, D. J., Henriksen, A., Smith, A. T. and Poulos, T. L. (1997) Crystal structure of horseradish peroxidase C at 2.15 Å resolution. *Nature structural biology*, 4(12), pp. 1032-1038.
- Gandhimathi, R., Vijayaraj, S. and Jyothirmaie, M. (2012) Analytical process of drugs by ultraviolet (UV) spectroscopy—a review. *International Journal of Pharmaceutical Research & Analysis*, 2(2), pp. 72-78.
- Gao, Q., Guo, Y., Zhang, W., Qi, H. and Zhang, C. (2011) An amperometric glucose biosensor based on layer-by-layer GOx-SWCNT conjugate/redox polymer multilayer on a screen-printed carbon electrode. *Sensors and Actuators B: Chemical*, 153(1), pp. 219-225.
- Ge, B. and Lisdat, F. (2002) Superoxide sensor based on cytochrome c immobilized on mixed-

thiol SAM with a new calibration method. *Analytica Chimica Acta*, 454(1), pp. 53-64.

Głód, B. K., Czapski, G. A. and Haddad, P. R. (2000) Application of high-performance liquid chromatography to the investigation of free radical reactions in biological systems. *TrAC Trends in Analytical Chemistry*, 19(8), pp. 492-497.

Goran, J. M., Phan, E. N., Favela, C. A. and Stevenson, K. J. (2015) H<sub>2</sub>O<sub>2</sub> detection at carbon nanotubes and nitrogen-doped carbon nanotubes: oxidation, reduction, or disproportionation? *Analytical chemistry*, 87(12), pp. 5989-5996.

Greenwald, R. A. (2018) *Handbook methods for oxygen radical research*, CRC press.

Grieshaber, D., MacKenzie, R., Voeroes, J. and Reimhult, E. (2008) Electrochemical biosensors-sensor principles and architectures. *Sensors*, 8(3), pp. 1400-1458.

Guerrero, L. A., Fernández, L., González, G., Montero-Jiménez, M., Uribe, R., Díaz Barrios, A. and Espinoza-Montero, P. J. (2020) Peroxide Electrochemical Sensor and Biosensor Based on Nanocomposite of TiO<sub>2</sub> Nanoparticle/Multi-Walled Carbon Nanotube Modified Glassy Carbon Electrode. *Nanomaterials*, 10(1), pp. 64.

Gueshi, T., Tokuda, K. and Matsuda, H. (1978) Voltammetry at partially covered electrodes: Part I. Chronopotentiometry and chronoamperometry at model electrodes. *Journal of Electroanalytical Chemistry and Interfacial Electrochemistry*, 89(2), pp. 247-260.

Guilbault, G. G. (2020) *Practical fluorescence*, CRC Press.

Gulaboski, R., Mirčeski, V., Kappl, R., Hoth, M. and Bozem, M. (2019) Quantification of hydrogen peroxide by electrochemical methods and electron spin resonance spectroscopy. *Journal of The Electrochemical Society*, 166(8), pp. G82.

Gundermann, K.-D. and McCapra, F. (2012) *Chemiluminescence in organic chemistry*, Springer Science & Business Media.

- Guo, S., Wen, D., Zhai, Y., Dong, S. and Wang, E. (2010) Platinum nanoparticle ensemble-on-graphene hybrid nanosheet: one-pot, rapid synthesis, and used as new electrode material for electrochemical sensing. *Acs Nano*, 4(7), pp. 3959-3968.
- Hanssen, B. L., Siraj, S. and Wong, D. K. (2016) Recent strategies to minimise fouling in electrochemical detection systems. *Reviews in Analytical Chemistry*, 35(1), pp. 1-28.
- Hayyan, M., Hashim, M. A. and AlNashef, I. M. (2016) Superoxide Ion: Generation and Chemical Implications. *Chemical Reviews*, 116(5), pp. 3029-3085.
- He, R., Pei, X., Pan, L., Tian, L., Luo, F., Sui, L., Wan, Q. and Wang, J. (2013) Effects of ultrasonic radiation intensity on the oxidation of single-walled carbon nanotubes in a mixture of sulfuric and nitric acids. *Nano*, 8(04), pp. 1350040.
- He, W., Liu, Y., Wamer, W. G. and Yin, J.-J. (2014) Electron spin resonance spectroscopy for the study of nanomaterial-mediated generation of reactive oxygen species. *Journal of food and drug analysis*, 22(1), pp. 49-63.
- Health | The State of Ageing 2020. (2021) *Centre for Ageing Better*.
- Heard, D. E. and Pilling, M. J. (2003) Measurement of OH and HO<sub>2</sub> in the troposphere. *Chemical Reviews*, 103(12), pp. 5163-5198.
- Heitzer, T., Schlinzig, T., Krohn, K., Meinertz, T. and Münzel, T. (2001) Endothelial dysfunction, oxidative stress, and risk of cardiovascular events in patients with coronary artery disease. *Circulation*, 104(22), pp. 2673-2678.
- Held, P. (2012) An introduction to reactive oxygen species: measurement of ROS in cells (white paper).
- Hille, R., Hall, J. and Basu, P. (2014) The mononuclear molybdenum enzymes. *Chemical Reviews*, 114(7), pp. 3963-4038.

- Homaei, A. A., Sariri, R., Vianello, F. and Stevanato, R. (2013) Enzyme immobilization: an update. *Journal of chemical biology*, 6(4), pp. 185-205.
- Hrapovic, S., Liu, Y., Male, K. B. and Luong, J. H. (2004) Electrochemical biosensing platforms using platinum nanoparticles and carbon nanotubes. *Analytical chemistry*, 76(4), pp. 1083-1088.
- Huang, S., Zhang, L., Dai, L., Wang, Y. and Tian, Y. (2021) Nonenzymatic Electrochemical Sensor with Ratiometric Signal Output for Selective Determination of Superoxide Anion in Rat Brain. *Analytical chemistry*, 93(13), pp. 5570-5576.
- Ji, J., Chung, Y. and Kwon, Y. (2020) The effects of cobalt phthalocyanine and polyacrylic acid on the reactivity of hydrogen peroxide oxidation reaction and the performance of hydrogen peroxide fuel cell. *Journal of Power Sources*, 480, pp. 228860.
- Jia, F., Narasimhan, B. and Mallapragada, S. (2014) Materials -based strategies for multi-enzyme immobilization and co - localization: a review. *Biotechnology and bioengineering*, 111(2), pp. 209-222.
- Jiang, H., Du, C., Zou, Z., Li, X., Akins, D. L. and Yang, H. (2009) A biosensing platform based on horseradish peroxidase immobilized onto chitosan-wrapped single-walled carbon nanotubes. *Journal of Solid State Electrochemistry*, 13(5), pp. 791-798.
- Jie, Z., Liu, J., Shu, M., Ying, Y. and Yang, H. (2022) Detection strategies for superoxide anion: A review. *Talanta*, 236, pp. 122892.
- Jimenez, A. and Navas, M. (2002) Chemiluminescence methods (present and future). *Grasas y Aceites*, 53(1), pp. 64-75.
- Jin, W., Du, H., Zheng, S., Xu, H. and Zhang, Y. (2010) Comparison of the oxygen reduction reaction between NaOH and KOH solutions on a Pt electrode: the electrolyte-dependent effect. *The Journal of Physical Chemistry B*, 114(19), pp. 6542-6548.
- Kang, J., Hussain, A. T., Catt, M., Trenell, M., Haggett, B. and Yu, E. H. (2014) Electrochemical detection of non-esterified fatty acid by layer-by-layer assembled

enzyme electrodes. *Sensors and Actuators B: Chemical*, 190, pp. 535-541.

Kangralkar, V., Patil, S. D. and Bandivadekar, R. (2010) Oxidative stress and diabetes: a review. *Int J Pharm Appl*, 1(1), pp. 38-45.

Katsounaros, I., Schneider, W. B., Meier, J. C., Benedikt, U., Biedermann, P. U., Auer, A. A. and Mayrhofer, K. J. (2012) Hydrogen peroxide electrochemistry on platinum: towards understanding the oxygen reduction reaction mechanism. *Physical Chemistry Chemical Physics*, 14(20), pp. 7384-7391.

Kierkowicz, M., Pach, E., Santidrián, A., Sandoval, S., Gonçalves, G., Tobías-Rossell, E., Kalbáč, M., Ballesteros, B. and Tobias, G. (2018) Comparative study of shortening and cutting strategies of single-walled and multi-walled carbon nanotubes assessed by scanning electron microscopy. *Carbon*, 139, pp. 922-932.

Kim, J.-H., Patra, C. R., Arkalgud, J. R., Boghossian, A. A., Zhang, J., Han, J.-H., Reuel, N. F., Ahn, J.-H., Mukhopadhyay, D. and Strano, M. S. (2011) Single-molecule detection of H<sub>2</sub>O<sub>2</sub> mediating angiogenic redox signaling on fluorescent single-walled carbon nanotube array. *Acs Nano*, 5(10), pp. 7848-7857.

Kitada, M., Xu, J., Ogura, Y., Monno, I. and Koya, D. (2020) Manganese Superoxide Dismutase Dysfunction and the Pathogenesis of Kidney Disease. *Frontiers in Physiology*, 11.

Kondo, T., Tamura, A., Fujishima, A. and Kawai, T. (2008) High sensitivity electrochemical detection of hydrogen peroxide at a cobalt phthalocyanine-modified boron-doped diamond electrode. *ECS Transactions*, 16(11), pp. 465.

Kong, Y.-T., Boopathi, M. and Shim, Y.-B. (2003) Direct electrochemistry of horseradish peroxidase bonded on a conducting polymer modified glassy carbon electrode. *Biosensors and Bioelectronics*, 19(3), pp. 227-232.

Kong, Y., Li, X., Zhang, N., Miao, Y., Feng, H., Wu, T. and Cheng, Z. (2018) Improved bioautographic assay on TLC layers for qualitative and quantitative estimation of xanthine oxidase inhibitors and superoxide scavengers. *Journal of pharmaceutical and biomedical analysis*, 150, pp. 87-94.

- Kostić, D. A., Dimitrijević, D. S., Stojanović, G. S., Palić, I. R., Đorđević, A. S. and Ickovski, J. D. (2015) Xanthine Oxidase: Isolation, Assays of Activity, and Inhibition. *Journal of Chemistry*, 2015, pp. 294858.
- Kosto, Y., Zanut, A., Franchi, S., Yakovlev, Y., Khalakhan, I., Matolin, V., Prince, K. C., Valenti, G., Paolucci, F. and Tsud, N. (2019) Electrochemical activity of the polycrystalline cerium oxide films for hydrogen peroxide detection. *Applied Surface Science*, 488, pp. 351-359.
- Lalaoui, N., Le Goff, A., Holzinger, M., Mermoux, M. and Cosnier, S. (2015) Wiring Laccase on Covalently Modified Graphene: Carbon Nanotube Assemblies for the Direct Bioelectrocatalytic Reduction of Oxygen. *Chemistry—A European Journal*, 21(8), pp. 3198-3201.
- Lambeth, D. O. and Palmer, G. (1973) The Kinetics and Mechanism of Reduction of Electron Transfer Proteins and Other Compounds of Biological Interest by Dithionite. *Journal of Biological Chemistry*, 248(17), pp. 6095-6103.
- Lei, C.-X., Hu, S.-Q., Shen, G.-L. and Yu, R.-Q. (2003) Immobilization of horseradish peroxidase to a nano-Au monolayer modified chitosan-entrapped carbon paste electrode for the detection of hydrogen peroxide. *Talanta*, 59(5), pp. 981-988.
- Li, J., Tan, S. N. and Ge, H. (1996) Silica sol-gel immobilized amperometric biosensor for hydrogen peroxide. *Analytica Chimica Acta*, 335(1), pp. 137-145.
- Li, M., Xu, S., Tang, M., Liu, L., Gao, F. and Wang, Y. (2011) Direct electrochemistry of horseradish peroxidase on graphene-modified electrode for electrocatalytic reduction towards H<sub>2</sub>O<sub>2</sub>. *Electrochimica Acta*, 56(3), pp. 1144-1149.
- Li, Y. and Dai, Y. (2004) The Analytical Application and Developing Tendency of Biosensors. *Journal of Yunyang Teachers College*, 24 (3), pp. 42-45.
- Li, Z.-H., Guedri, H., Viguier, B., Sun, S.-G. and Marty, J.-L. (2013) Optimization of hydrogen peroxide detection for a methyl mercaptan biosensor. *Sensors*, 13(4), pp. 5028-5039.

- Limoges, B., Savéant, J.-M. and Yazidi, D. (2003) Quantitative Analysis of Catalysis and Inhibition at Horseradish Peroxidase Monolayers Immobilized on an Electrode Surface. *Journal of the American Chemical Society*, 125(30), pp. 9192-9203.
- Liu, F., Choi, K. S., Park, T. J., Lee, S. Y. and Seo, T. S. (2011) Graphene-based electrochemical biosensor for pathogenic virus detection. *BioChip Journal*, 5(2), pp. 123-128.
- Liu, F., Yu, R., Wei, H., Wu, J., He, N. and Liu, X. (2022) Construction of a novel electrochemical sensing platform to investigate the effect of temperature on superoxide anions from cells and superoxide dismutase enzyme activity. *Analytica Chimica Acta*, 1198, pp. 339561.
- Liu, J., Rinzler, A. G., Dai, H., Hafner, J. H., Bradley, R. K., Boul, P. J., Lu, A., Iverson, T., Shelimov, K., Huffman, C. B., Rodriguez-Macias, F., Shon, Y.-S., Lee, T. R., Colbert, D. T. and Smalley, R. E. (1998) Fullerene Pipes. *Science*, 280(5367), pp. 1253.
- Liu, Y., Sun, G., Jiang, C., Zheng, X. T., Zheng, L. and Li, C. M. (2014) Highly sensitive detection of hydrogen peroxide at a carbon nanotube fiber microelectrode coated with palladium nanoparticles. *Microchimica Acta*, 181(1), pp. 63-70.
- Lu, Y. (2016) Present status and application of biosensors. *Chemistry of life*, 36 (1), pp. 7-12.
- Luminol*, Available: <https://chem.libretexts.org/@go/page/76102> [Accessed 2022/2/18/].
- Lvovich, V. and Scheeline, A. (1997) Amperometric Sensors for Simultaneous Superoxide and Hydrogen Peroxide Detection. *Analytical chemistry*, 69(3), pp. 454-462.
- Lyon, J. L. and Stevenson, K. J. (2006) Picomolar peroxide detection using a chemically activated redox mediator and square wave voltammetry. *Analytical chemistry*, 78(24), pp. 8518-8525.
- Mäntele, W. and Deniz, E. (2017) UV–VIS absorption spectroscopy: Lambert-Beer reloaded.

in: Elsevier. pp. 965-968.

- Mahlicli, F. Y., Şen, Y., Mutlu, M. and Altinkaya, S. A. (2015) Immobilization of superoxide dismutase/catalase onto polysulfone membranes to suppress hemodialysis-induced oxidative stress: A comparison of two immobilization methods. *Journal of Membrane Science*, 479, pp. 175-189.
- Malomo, S., Adeoye, R., Babatunde, L., Ibraheem, S., Iniaghe, O. and Olorunniyi, F. (2011) Suicide inactivation of horseradish peroxidase by excess hydrogen peroxide: The effects of reaction pH, buffer ion concentration, and redox mediation. *Biokemistri*, 23.
- Manickam, P., Kaushik, A., Karunakaran, C. and Bhansali, S. (2017) Recent advances in cytochrome c biosensing technologies. *Biosensors and Bioelectronics*, 87, pp. 654-668.
- Manning, P. and McNeil, C. J. (2011) Electrochemical and optical sensing of reactive oxygen species: pathway to an integrated intracellular and extracellular measurement platform. *Biochemical Society Transactions*, 39(5), pp. 1288-1292.
- Mao, B., Han, G., Ma, L., Liu, B., Gao, X., Li, G. and Liu, G. (2009) Fundamentals and progresses of DNA electrochemical biosensor. *chemical sensors*, 29 (1), pp. 9-15.
- Mao, L., Tian, Y. and Ohsaka, T. (2008) CHAPTER 6 - Superoxide electrochemical sensors and biosensors: principles, development and applications. in Zhang, X., Ju, H. and Wang, J., (eds.) *Electrochemical Sensors, Biosensors and their Biomedical Applications*, San Diego: Academic Press. pp. 145-185.
- Marković, N., Gasteiger, H., Grgur, B. and Ross, P. (1999) Oxygen reduction reaction on Pt (111): effects of bromide. *Journal of Electroanalytical Chemistry*, 467(1-2), pp. 157-163.
- Mayerhöfer, T. G., Pahlow, S. and Popp, J. (2020) The Bouguer-Beer-Lambert law: Shining light on the obscure. *ChemPhysChem*, 21(18), pp. 2029-2046.
- Mazloum-Ardakani, M., Kalantari, A. A., Alizadeh, Z., Mohamadian-Sarcheshmeh, H. and Banitaba, H. (2022) Electrochemical Investigation for Sensitive Determination of

Metoclopramide Based on Ytterbium Oxide Nanoparticles Supported on Graphene. *Analytical and Bioanalytical Chemistry Research*, 9(3), pp. 299-307.

McCord, J. M. and Fridovich, I. (1969) Superoxide dismutase: an enzymic function for erythrocyte hemocuprein (hemocuprein). *Journal of Biological Chemistry*, 244(22), pp. 6049-6055.

McCreery, R. L. (2008) Advanced Carbon Electrode Materials for Molecular Electrochemistry. *Chemical Reviews*, 108(7), pp. 2646-2687.

Melo, A., Monteiro, L., Lima, R. M., de Oliveira, D. M., de Cerqueira, M. D. and El-Bachá, R. S. (2011) Oxidative stress in neurodegenerative diseases: mechanisms and therapeutic perspectives. *Oxidative medicine and cellular longevity*, 2011.

Merkoçi, A., Pumera, M., Llopis, X., Pérez, B., del Valle, M. and Alegret, S. (2005) New materials for electrochemical sensing VI: Carbon nanotubes. *TrAC Trends in Analytical Chemistry*, 24(9), pp. 826-838.

Meskher, H., Ragdi, T., Thakur, A. K., Ha, S., Khelifaoui, I., Sathyamurthy, R., Sharshir, S. W., Pandey, A., Saidur, R. and Singh, P. (2023) A review on CNTs-based electrochemical sensors and biosensors: unique properties and potential applications. *Critical Reviews in Analytical Chemistry*, pp. 1-24.

Mohanta, D. (2017) *A DETAILED STUDY ON OPTICAL AND PHYSICAL PROPERTIES OF RICE AND ITS BY-PRODUCTS*. Unpublished, Tezpur University.

Moorcroft, M. J., Hahn, C. E. and Compton, R. G. (2003) Electrochemical studies of the anaesthetic agent enflurane (2-chloro-1, 1, 2-trifluoroethyl difluoromethyl ether) in the presence of oxygen: reaction with electrogenerated superoxide. *Journal of Electroanalytical Chemistry*, 541, pp. 117-131.

Moschopoulou, G. and Kintzios, S. (2015) Noninvasive superoxide monitoring of in vitro neuronal differentiation using a cell-based biosensor. *Journal of Sensors*, 2015.

Münzel, T., Afanas' ev, I. B., Kleschyov, A. L. and Harrison, D. G. (2002) Detection of

superoxide in vascular tissue. *Arteriosclerosis, thrombosis, and vascular biology*, 22(11), pp. 1761-1768.

Nauseef, W. M. (2014) Detection of superoxide anion and hydrogen peroxide production by cellular NADPH oxidases. *Biochimica et Biophysica Acta (BBA) - General Subjects*, 1840(2), pp. 757-767.

Neves, V., Heister, E., Costa, S., Tilmaciu, C., Flahaut, E., Soula, B., Coley, H. M., Mcfadden, J. and Silva, S. R. P. (2012) Design of double-walled carbon nanotubes for biomedical applications. *Nanotechnology*, 23(36), pp. 365102.

Nicholson, R. S. (1965) Theory and application of cyclic voltammetry for measurement of electrode reaction kinetics. *Analytical chemistry*, 37(11), pp. 1351-1355.

Nisha, S., Karthick, S. A. and Gobi, N. (2012) A review on methods, application and properties of immobilized enzyme. *Chemical Science Review and Letters*, 1(3), pp. 148-155.

Omary, M. A. and Patterson, H. H. (2017) Luminescence, theory.

Organization, W. H. (2001) Men, ageing and health: Achieving health across the life span.

Organization, W. H. (2012) World Health Day 2012: ageing and health: toolkit for event organizers.

Pajkossy, T. (2018) Analysis of quasi-reversible cyclic voltammograms: Transformation to scan-rate independent form. *Electrochemistry Communications*, 90, pp. 69-72.

Park, J. W., Park, S. J., Kwon, O. S., Lee, C. and Jang, J. (2014) Polypyrrole nanotube embedded reduced graphene oxide transducer for field-effect transistor-type H<sub>2</sub>O<sub>2</sub> biosensor. *Analytical chemistry*, 86(3), pp. 1822-1828.

Pastor, I., Esquembre, R., Micol, V., Mallavia, R. and Mateo, C. R. (2004) A ready-to-use fluorimetric biosensor for superoxide radical using superoxide dismutase and

peroxidase immobilized in sol-gel glasses. *Analytical Biochemistry*, 334(2), pp. 335-343.

Patel, B. A. (2021) *Electrochemistry for bioanalysis*, Elsevier.

Penner, M. H. (2017) Basic principles of spectroscopy. in *Food analysis*: Springer. pp. 79-88.

Perkampus, H.-H. (2013) *UV-VIS Spectroscopy and its Applications*, Springer Science & Business Media.

Pourbaix, M. (1974) Atlas of electrochemical equilibria in aqueous solution. *NACE*, 307.

Pradhan, S., Albin, S., Heise, R. L. and Yadavalli, V. K. (2022) Portable, disposable, biomimetic electrochemical sensors for analyte detection in a single drop of whole blood. *Chemosensors*, 10(7), pp. 263.

Pumera, M., Ambrosi, A., Bonanni, A., Chng, E. L. K. and Poh, H. L. (2010) Graphene for electrochemical sensing and biosensing. *TrAC Trends in Analytical Chemistry*, 29(9), pp. 954-965.

Qin, L., Li, X., Kang, S.-Z. and Mu, J. (2015) Gold nanoparticles conjugated dopamine as sensing platform for SERS detection. *Colloids and Surfaces B: Biointerfaces*, 126, pp. 210-216.

Raeisi-Kheirabadi, N., Nezamzadeh-Ejhih, A. and Aghaei, H. (2022) Cyclic and linear sweep voltammetric studies of a modified carbon paste electrode with nickel oxide nanoparticles toward tamoxifen: effects of surface modification on electrode response kinetics. *ACS omega*, 7(35), pp. 31413-31423.

Rahmani, H., Ghavamipour, F. and Sajedi, R. H. (2019) Bioluminescence detection of superoxide anion using aequorin. *Analytical chemistry*, 91(20), pp. 12768-12774.

Razola, S. S., Ruiz, B. L., Diez, N. M., Mark, H. B. and Kauffmann, J. M. (2002) Hydrogen

peroxide sensitive amperometric biosensor based on horseradish peroxidase entrapped in a polypyrrole electrode. *Biosensors and Bioelectronics*, 17(11), pp. 921-928.

Ren, Q.-Q., Wu, J., Zhang, W.-C., Wang, C., Qin, X., Liu, G.-C., Li, Z.-X. and Yu, Y. (2017) Real-time in vitro detection of cellular H<sub>2</sub>O<sub>2</sub> under camptothecin stress using horseradish peroxidase, ionic liquid, and carbon nanotube-modified carbon fiber ultramicroelectrode. *Sensors and Actuators B: Chemical*, 245, pp. 615-621.

Ren, Q.-Q., Yang, F., Ren, W., Wang, C., Jiang, W.-S., Zhao, Z.-Y., Chen, J., Lu, X.-Y. and Yu, Y. (2020) Amperometric Biosensor Based on Coimmobilization of Multiwalled Carbon Nanotubes and Horseradish Peroxidase-Gold Nanocluster Bioconjugates for Detecting H<sub>2</sub>O<sub>2</sub>. *Journal of Nanomaterials*, 2020.

Reuillard, B., Le Goff, A., Holzinger, M. and Cosnier, S. (2014) Non-covalent functionalization of carbon nanotubes with boronic acids for the wiring of glycosylated redox enzymes in oxygen-reducing biocathodes. *Journal of Materials Chemistry B*, 2(16), pp. 2228-2232.

Rong, J., Zhou, Z., Wang, Y., Han, J., Li, C., Zhang, W. and Ni, L. (2019) Immobilization of horseradish peroxidase on multi-armed magnetic graphene oxide composite: Improvement of loading amount and catalytic activity. *Food technology and biotechnology*, 57(2), pp. 260.

Rossi, R., Pant, D. and Logan, B. E. (2020) Chronoamperometry and linear sweep voltammetry reveals the adverse impact of high carbonate buffer concentrations on anode performance in microbial fuel cells. *Journal of Power Sources*, 476, pp. 228715.

Rother, C. and Nidetzky, B. (2009) Enzyme immobilization by microencapsulation: methods, materials, and technological applications. *Encyclopedia of Industrial Biotechnology: Bioprocess, Bioseparation, and Cell Technology*, pp. 1-21.

Rouster, P., Pavlovic, M. and Szilagyi, I. (2018) Immobilization of Superoxide Dismutase on Polyelectrolyte-Functionalized Titania Nanosheets. *ChemBioChem*, 19(4), pp. 404-410.

Sánchez-Calvo, A., Costa-García, A. and Blanco-López, M. C. (2020) Paper-based electrodes modified with cobalt phthalocyanine colloid for the determination of hydrogen peroxide and glucose. *Analyst*, 145(7), pp. 2716-2724.

- Şahin, S. (2020) A simple and sensitive hydrogen peroxide detection with horseradish peroxidase immobilized on pyrene modified acid - treated single - walled carbon nanotubes. *Journal of Chemical Technology & Biotechnology*, 95(4), pp. 1093-1099.
- Şahin, S., Merotra, J., Kang, J., Trenell, M., Catt, M. and Yu, E. H. (2018) Simultaneous electrochemical detection of glucose and non-esterified fatty acids (NEFAs) for diabetes management. *IEEE Sensors Journal*, 18(22), pp. 9075-9080.
- Sakamoto, H., Hatsuda, R., Miyamura, K., Shiraishi, H. and Sugiyama, S. (2011) Electrochemical Selective Detection of Uric Acid Using a Copper-modified Carbon Electrode. *Analytical Sciences*, 27(3), pp. 333-333.
- Sanders, C., Turkarlan, S., Lee, D.-W. and Daldal, F. (2010) Cytochrome c biogenesis: the Ccm system. *Trends in Microbiology*, 18(6), pp. 266-274.
- Sardarelli, S., Hasanzadeh, M. and Razmi, H. (2021) Chemical binding of horseradish peroxidase enzyme with poly beta-cyclodextrin and its application as molecularly imprinted polymer for the monitoring of H<sub>2</sub>O<sub>2</sub> in human plasma samples. *Journal of Molecular Recognition*, 34(5), pp. e2884.
- Sassolas, A., Blum, L. J. and Leca-Bouvier, B. D. (2012) Immobilization strategies to develop enzymatic biosensors. *Biotechnology advances*, 30(3), pp. 489-511.
- Sawyer, D. T. (1991) *Oxygen chemistry*, Oxford university press.
- Sawyer, D. T. and Roberts, J. L. (1966) Electrochemistry of oxygen and superoxide ion in dimethylsulfoxide at platinum, gold and mercury electrodes. *Journal of Electroanalytical Chemistry (1959)*, 12(2), pp. 90-101.
- Sebastiani, P., Thyagarajan, B., Sun, F., Schupf, N., Newman, A. B., Montano, M. and Perls, T. T. (2017) Biomarker signatures of aging. *Aging cell*, 16(2), pp. 329-338.
- Shah, K., Kumar, R. G., Verma, S. and Dubey, R. (2001) Effect of cadmium on lipid

peroxidation, superoxide anion generation and activities of antioxidant enzymes in growing rice seedlings. *Plant Science*, 161(6), pp. 1135-1144.

Sharafeldin, M., McCaffrey, K. and Rusling, J. F. (2019) Influence of antibody immobilization strategy on carbon electrode immunoarrays. *Analyst*, 144(17), pp. 5108-5116.

Sheng, Y., Abreu, I. A., Cabelli, D. E., Maroney, M. J., Miller, A.-F., Teixeira, M. and Valentine, J. S. (2014) Superoxide dismutases and superoxide reductases. *Chemical Reviews*, 114(7), pp. 3854-3918.

Shin, J.-H., Lee, M.-J., Choi, J.-H., Song, J.-a., Kim, T.-H. and Oh, B.-K. (2020) Electrochemical H<sub>2</sub>O<sub>2</sub> biosensor based on horseradish peroxidase encapsulated protein nanoparticles with reduced graphene oxide-modified gold electrode. *Nano Convergence*, 7(1), pp. 1-8.

Shinde, G., Godage, R., Jadhav, R., Manoj, B. and Aniket, B. (2020) A Review on Advances in UV Spectroscopy. *Research Journal of Science and Technology*, 12(1), pp. 47-51.

Shu, M., Ying, Y. and Yang, H. (2021) Reactive strategy-based SERS determination of O<sub>2</sub><sup>•-</sup> generated from sunscreen. *Chemical Communications*, 57(8), pp. 1018-1021.

Shuba, M., Paddubskaya, A., Kuzhir, P., Maksimenko, S., Ksenevich, V., Niaura, G., Seliuta, D., Kasalynas, I. and Valusis, G. (2012) Soft cutting of single-wall carbon nanotubes by low temperature ultrasonication in a mixture of sulfuric and nitric acids. *Nanotechnology*, 23(49), pp. 495714.

Sikora, A., Michalski, R., Hardy, M., Ouari, O., Adamus, J., Marcinek, A., Zielonka, J. and Kalyanaraman, B. (2017) N, NN', N'-tetramethylhydroethidine (TMHE)-in search for better probes for the detection of superoxide radical anion. *Free Radical Biology and Medicine*, 108, pp. S38.

Simões, F. R. and Xavier, M. G. (2017) Electrochemical sensors. *Nanoscience and its Applications*, 1, pp. 155-178.

Singh, R. P. (2011) Prospects of Nanobiomaterials for Biosensing. *International Journal of*

*Electrochemistry*, 2011, pp. 125487.

- Singh, S. (2019) Nanomaterials exhibiting enzyme-like properties (nanozymes): current advances and future perspectives. *Frontiers in chemistry*, 7, pp. 46.
- Song, L., LI, R., Qiao, Z., Tan, J., Mao, R. and Wang, X. (2005) Healthy Aging and Community Geriatric Nursing Research Progress. *JJ. Pediatr Nurs*, 31(2).
- Song, M. I., Bier, F. F. and Scheller, F. W. (1995) A method to detect superoxide radicals using Teflon membrane and superoxide dismutase. *Bioelectrochemistry and bioenergetics*, 38(2), pp. 419-422.
- Sun, C., Li, H., Ping, H., Wang, E., Zhang, M. and Liu, J. (2011) Determination of Organophosphorus Pesticides by AuNPs / Sol-gel Composite Membrane Assay with Acetylcholinesterase Biosensor. *Acta Chimica Sinica*, 32(11), pp. 2533-2538.
- Sun, N., Guan, L., Shi, Z., Li, N., Gu, Z., Zhu, Z., Li, M. and Shao, Y. (2006) Ferrocene peapod modified electrodes: preparation, characterization, and mediation of H<sub>2</sub>O<sub>2</sub>. *Analytical chemistry*, 78(17), pp. 6050-6057.
- Sun, X., Guo, S., Liu, Y. and Sun, S. (2012) Dumbbell-like PtPd-Fe<sub>3</sub>O<sub>4</sub> nanoparticles for enhanced electrochemical detection of H<sub>2</sub>O<sub>2</sub>. *Nano letters*, 12(9), pp. 4859-4863.
- Sun, Z., Zhao, H., Chen, K., Zhou, F. and Lan, M. (2023) Fabrication of dendrite PtPd bimetallic nanocomposites modified carbon fiber microelectrodes for detecting superoxide anion released from living cells. *Microchemical Journal*, 191, pp. 108855.
- Szkola, A., Campbell, K., Elliott, C. T., Niessner, R. and Seidel, M. (2013) Automated, high performance, flow-through chemiluminescence microarray for the multiplexed detection of phycotoxins. *Analytica Chimica Acta*, 787, pp. 211-218.
- Tainer, J. A., Getzoff, E. D., Richardson, J. S. and Richardson, D. C. (1983) Structure and mechanism of copper, zinc superoxide dismutase. *Nature*, 306(5940), pp. 284-287.

- Tang, Y., Kotchey, G. P., Vedala, H. and Star, A. (2011) Electrochemical Detection with Platinum Decorated Carbon Nanomaterials. *Electroanalysis*, 23(4), pp. 870-877.
- Teng, X., Qi, L., Liu, T., Li, L. and Lu, C. (2023) Nanomaterial-based chemiluminescence systems for tracing of reactive oxygen species in biosensors. *TrAC Trends in Analytical Chemistry*, 162, pp. 117020.
- Theyagarajan, K. and Kim, Y.-J. (2023) Recent Developments in the Design and Fabrication of Electrochemical Biosensors Using Functional Materials and Molecules. *Biosensors*, 13(4), pp. 424.
- Tian, Y., Mao, L. and Ohsaka, T. (2006) Electrochemical biosensors for superoxide anion. *Current Analytical Chemistry*, 2(1), pp. 51-58.
- Tian, Y., Mao, L., Okajima, T. and Ohsaka, T. (2002) Superoxide Dismutase-Based Third-Generation Biosensor for Superoxide Anion. *Analytical chemistry*, 74(10), pp. 2428-2434.
- Tian, Y., Mao, L., Okajima, T. and Ohsaka, T. (2004) Electrochemistry and electrocatalytic activities of superoxide dismutases at gold electrodes modified with a self-assembled monolayer. *Analytical chemistry*, 76(14), pp. 4162-4168.
- Tong, Z., Yuan, R., Chai, Y., Xie, Y. and Chen, S. (2007) A novel and simple biomolecules immobilization method: Electro-deposition ZrO<sub>2</sub> doped with HRP for fabrication of hydrogen peroxide biosensor. *Journal of Biotechnology*, 128(3), pp. 567-575.
- United Nations (2018) Ageing.
- Vargas-Bernal, R., Rodríguez-Miranda, E. and Herrera-Pérez, G. (2012) Evolution and expectations of enzymatic biosensors for pesticides. *Pesticides-Advances in Chemical and Botanical Pesticides*, pp. 331-354.
- Veitch, N. C. (2004) Horseradish peroxidase: a modern view of a classic enzyme. *Phytochemistry*, 65(3), pp. 249-259.

- Venton, B. J. and DiScenza, D. J. (2020) Voltammetry. *Electrochemistry for Bioanalysis*, pp. 27-50.
- Verma, G. and Mishra, M. (2018) Development and optimization of UV-Vis spectroscopy-a review. *World Journal of Pharmaceutical Research*, 7(11), pp. 1170-1180.
- Vessey, W., Perez-Miranda, A., Macfarquhar, R., Agarwal, A. and Homa, S. (2014) Reactive oxygen species in human semen: validation and qualification of a chemiluminescence assay. *Fertility and sterility*, 102(6), pp. 1576-1583. e4.
- Vijayalakshmi, S., Anand, M. and Ranjitha, J. (2020) Microalgae-Based Biofuel Production Using Low-Cost Nanobiocatalysts. in *Microalgae Cultivation for Biofuels Production*: Elsevier. pp. 251-263.
- Viswanathan, S., Radecka, H. and Radecki, J. (2009) Electrochemical biosensors for food analysis. *Monatshefte für Chemie-Chemical Monthly*, 140(8), pp. 891.
- Vlasits, J., Jakopitsch, C., Bernroither, M., Zamocky, M., Furtmüller, P. G. and Obinger, C. (2010) Mechanisms of catalase activity of heme peroxidases. *Archives of Biochemistry and Biophysics*, 500(1), pp. 74-81.
- Vojinović, V., Azevedo, A., Martins, V., Cabral, J., Gibson, T. and Fonseca, L. (2004) Assay of H<sub>2</sub>O<sub>2</sub> by HRP catalysed co-oxidation of phenol-4-sulphonic acid and 4-aminoantipyrine: characterisation and optimisation. *Journal of molecular catalysis B: enzymatic*, 28(2-3), pp. 129-135.
- Wang, C., Yan, Q., Liu, H.-B., Zhou, X.-H. and Xiao, S.-J. (2011) Different EDC/NHS Activation Mechanisms between PAA and PMAA Brushes and the Following Amidation Reactions. *Langmuir*, 27(19), pp. 12058-12068.
- Wang, D., Thu, M. K., Firdhaosh, M. and Susanto, A. P. (2006) Superoxide Detection by Chemiluminescence, Fluorescence, and Spectrophotometry Methods. in *2006 International Conference on Biomedical and Pharmaceutical Engineering*. pp. 537-540.

- Wang, H., Bu, Y., Dai, W., Li, K., Wang, H. and Zuo, X. (2015) Well-dispersed cobalt phthalocyanine nanorods on graphene for the electrochemical detection of hydrogen peroxide and glucose sensing. *Sensors and Actuators B: Chemical*, 216, pp. 298-306.
- Wang, T., Zhu, H., Zhuo, J., Zhu, Z., Papakonstantinou, P., Lubarsky, G., Lin, J. and Li, M. (2013) Biosensor based on ultrasmall MoS<sub>2</sub> nanoparticles for electrochemical detection of H<sub>2</sub>O<sub>2</sub> released by cells at the nanomolar level. *Analytical chemistry*, 85(21), pp. 10289-10295.
- Wang, Z. and Dai, Z. (2015) Carbon nanomaterial-based electrochemical biosensors: an overview. *Nanoscale*, 7(15), pp. 6420-6431.
- Warwar, N., Mor, A., Fluhr, R., Pandian, R. P., Kuppusamy, P. and Blank, A. (2011) Detection and imaging of superoxide in roots by an electron spin resonance spin-probe method. *Biophysical Journal*, 101(6), pp. 1529-1538.
- Weng, Y., Huang, S. and Weng, N. (1989a) Using Alkaline Sodium Dithionite Solution to Generate Superoxide Anion. *Biochemistry and Biophysical Progress*, 16 (3), pp. 209.
- Weng, Y., Huang, S. and Weng, N. (1989b) Using Alkaline Sodium Dithionite Solution to Generate Superoxide Anion. *Biochemistry and Biophysical Progress*, 16 (3), pp. 209.
- Westbroek, P. and Temmerman, E. (2000) Mechanism of hydrogen peroxide oxidation reaction at a glassy carbon electrode in alkaline solution. *Journal of Electroanalytical Chemistry*, 482(1), pp. 40-47.
- Worsfold, P., Townshend, A., Poole, C. F. and Miró, M. (2019) *Encyclopedia of analytical science*, Elsevier.
- Wu, B., Zhang, G., Gao, C. and Shuang, S. (2004) Application and Development of Biosensors. *China Biotechnology*, 24 (7), pp. 65-69.
- Wu, P., Cai, Z., Chen, J., Zhang, H. and Cai, C. (2011) Electrochemical measurement of the flux of hydrogen peroxide releasing from RAW 264.7 macrophage cells based on enzyme-attapulgite clay nanohybrids. *Biosensors and Bioelectronics*, 26(10), pp. 4012-

- Wu, T., Li, L., Song, G., Ran, M., Lu, X. and Liu, X. (2019) An ultrasensitive electrochemical sensor based on cotton carbon fiber composites for the determination of superoxide anion release from cells. *Microchimica Acta*, 186(3), pp. 198.
- Xu, F., Sun, Y., Zhang, Y., Shi, Y., Wen, Z. and Li, Z. (2011) Graphene–Pt nanocomposite for nonenzymatic detection of hydrogen peroxide with enhanced sensitivity. *Electrochemistry Communications*, 13(10), pp. 1131-1134.
- Xu, K., Ding, S. P. and Jow, T. R. (1999) Toward reliable values of electrochemical stability limits for electrolytes. *Journal of The Electrochemical Society*, 146(11), pp. 4172.
- Xu, K., Liu, X. and Tang, B. (2007) A phosphinate-based red fluorescent probe for imaging the superoxide radical anion generated by RAW264. 7 macrophages. *ChemBioChem*, 8(4), pp. 453-458.
- Xu, Y., Bai, H., Lu, G., Li, C. and Shi, G. (2008) Flexible graphene films via the filtration of water-soluble noncovalent functionalized graphene sheets. *Journal of the American Chemical Society*, 130(18), pp. 5856-5857.
- Yamada, H., Yoshii, K., Asahi, M., Chiku, M. and Kitazumi, Y. (2022) Cyclic Voltammetry Part 2: Surface Adsorption, Electric Double Layer, and Diffusion Layer. *Electrochemistry*, 90(10), pp. 102006-102006.
- Yamamoto, K., Shi, G., Zhou, T., Xu, F., Xu, J., Kato, T., Jin, J.-Y. and Jin, L. (2003) Study of carbon nanotubes–HRP modified electrode and its application for novel on-line biosensors. *Analyst*, 128(3), pp. 249-254.
- Yamazaki, T., Kawai, C., Yamauchi, A. and Kuribayashi, F. (2011) A highly sensitive chemiluminescence assay for superoxide detection and chronic granulomatous disease diagnosis. *Tropical medicine and health*, 39(2), pp. 41-45.
- Yang, J., Cao, Y. and Zhang, N. (2020) Spectrophotometric method for superoxide anion radical detection in a visible light (400–780 nm) system. *Spectrochimica Acta Part A:*

*Molecular and Biomolecular Spectroscopy*, pp. 118556.

Yang, Y. (2013) *Study on Several Electrochemical Sensors for Reactive oxygen species and DNA*. Unpublished PhD, Hunan University.

Yasui, K. and Baba, A. (2006) Therapeutic potential of superoxide dismutase (SOD) for resolution of inflammation. *Inflammation Research*, 55(9), pp. 359-363.

Ye, Q., Li, W., Wang, Z., Zhang, L., Tan, X. and Tian, Y. (2014) Direct electrochemistry of superoxide dismutases (Mn-, Fe-, and Ni-) from human pathogen *Clostridium difficile*: Toward application to superoxide biosensor. *Journal of Electroanalytical Chemistry*, 729, pp. 21-26.

Yogranjan, L. M., Satpute, G. and Srivastava, A. (2017) Plant Stress Signaling Through Corresponding Nanobiotechnology.

Younus, H. (2018) Therapeutic potentials of superoxide dismutase. *International journal of health sciences*, 12(3), pp. 88-93.

Yu, W. and Zhao, L. (2021) Chemiluminescence detection of reactive oxygen species generation and potential environmental applications. *TrAC Trends in Analytical Chemistry*, 136, pp. 116197.

Zakharova, G., Uporov, I. and Tishkov, V. (2011) Horseradish peroxidase: modulation of properties by chemical modification of protein and heme. *Biochemistry (Moscow)*, 76(13), pp. 1391-1401.

Zhang, C. and Xing, X. H. (2011) 2.23 - Enzyme Bioreactors. in Moo-Young, M., (ed.) *Comprehensive Biotechnology (Second Edition)*, Burlington: Academic Press. pp. 319-329.

Zhang, H., Cai, X., Zhao, H., Sun, W., Wang, Z. and Lan, M. (2019) Enzyme-free electrochemical sensor based on ZIF-67 for the detection of superoxide anion radical released from SK-BR-3 cells. *Journal of Electroanalytical Chemistry*, 855, pp. 113653.

Zhang, J. and Pantelelis, N. G. (2011) Iterative learning control of a reactive polymer composite moulding process using batch-wise updated linearised models. *Computer Aided Chemical Engineering*, 29, pp. 1613-1617.

Zhang, J., Wu, J., Zhang, H. and Zhang, J. (2013) *PEM fuel cell testing and diagnosis*, Newnes.

Zhang, J., Zou, H., Qing, Q., Yang, Y., Li, Q., Liu, Z., Guo, X. and Du, Z. (2003) Effect of Chemical Oxidation on the Structure of Single-Walled Carbon Nanotubes. *The Journal of Physical Chemistry B*, 107(16), pp. 3712-3718.

Zhang, L., Gong, W., Pan, Y. and Zhang, Y. (2008) Fabrication of multilayer-film-modified gold electrode composed of myoglobin, chitosan, and polyelectrolyte-wrapped multi-wall carbon nanotubes by layer-by-layer assembled technique and electrochemical catalysis for hydrogen peroxide and trichloroacetic acid. *Russian Journal of Electrochemistry*, 44(11), pp. 1271-1279.

Zhang, T., Gu, Y., Li, C., Yan, X., Lu, N., Liu, H., Zhang, Z. and Zhang, H. (2017) Fabrication of novel electrochemical biosensor based on graphene nanohybrid to detect H<sub>2</sub>O<sub>2</sub> released from living cells with ultrahigh performance. *ACS applied materials & interfaces*, 9(43), pp. 37991-37999.

Zhang, Y., Bai, X., Wang, X., Shiu, K.-K., Zhu, Y. and Jiang, H. (2014) Highly sensitive graphene–Pt nanocomposites amperometric biosensor and its application in living cell H<sub>2</sub>O<sub>2</sub> detection. *Analytical chemistry*, 86(19), pp. 9459-9465.

Zhang, Y., Dai, M. and Yuan, Z. (2018) Methods for the detection of reactive oxygen species. *Analytical Methods*, 10(38), pp. 4625-4638.

Zhao, H., Joseph, J., Fales, H. M., Sokoloski, E. A., Levine, R. L., Vasquez-Vivar, J. and Kalyanaraman, B. (2005) Detection and characterization of the product of hydroethidine and intracellular superoxide by HPLC and limitations of fluorescence. *Proceedings of the National Academy of Sciences of the United States of America*, 102(16), pp. 5727.

Zhao, L., Lu, L., Wang, A., Zhang, H., Huang, M., Wu, H., Xing, B., Wang, Z. and Ji, R. (2020) Nano-biotechnology in agriculture: use of nanomaterials to promote plant growth and

stress tolerance. *Journal of agricultural and food chemistry*, 68(7), pp. 1935-1947.

Zhu, H., Li, Y., Song, Y., Zhao, G., Wu, W., Zhou, S., Wang, D. and Xiao, W. (2020) Effects of cyclic voltammetric scan rates, scan time, temperatures and carbon addition on sulphation of Pb disc electrodes in aqueous H<sub>2</sub>SO<sub>4</sub>. *Materials technology*, 35(3), pp. 135-140.

Ziech, D., Franco, R., Georgakilas, A. G., Georgakila, S., Malamou-Mitsi, V., Schoneveld, O., Pappa, A. and Panayiotidis, M. I. (2010) The role of reactive oxygen species and oxidative stress in environmental carcinogenesis and biomarker development. *Chemico-biological interactions*, 188(2), pp. 334-339.

Ziegler, K. J., Gu, Z., Peng, H., Flor, E. L., Hauge, R. H. and Smalley, R. E. (2005) Controlled Oxidative Cutting of Single-Walled Carbon Nanotubes. *Journal of the American Chemical Society*, 127(5), pp. 1541-1547.